Pavement-Watering in Cities for Urban Heat Island Mitigation and Climate Change Adaptation

Martin Hendel

Université Paris.Diderot (Paris 7) Sorbonne Paris Cité

Ecole Doctorale de Physique en Ile-de-France ED 564
Laboratoire Matière et Systèmes Complexes UMR 7057

Doctorat
Sciences Pour l'Ingénieur

Pavement-Watering in Cities for Urban Heat Island Mitigation and Climate Change Adaptation

A Study of its Cooling Effects and Water Consumption in Paris

L'arrosage urbain comme moyen de limitation des îlots de chaleur urbains et d'adaptation au changement climatique

Etude de ses effets rafraîchissants et de sa consommation d'eau à Paris

Thèse dirigée par Laurent ROYON

Soutenue par **Martin HENDEL**

le vendredi 16 octobre 2015

Jury

M. Hassan Peerhossaini	Président
M. Mat Santamouris	Rapporteur
M. Valéry Masson	Rapporteur
M. Hervé Andrieu	Examinateur
Mme Morgane Colombert	Invitée, Encadrante
M. Dominique Coutart	Invité, Encadrant
M. Youssef Diab	Invité, Co-directeur
M. Laurent Royon	Invité, Directeur

Abstract

This dissertation examines pavement-watering as a cooling strategy for cities seeking to reduce the intensity of their urban heat island (UHI) and/or as an adaptation tool against increasing heat wave frequency and intensity resulting from climate change. This research is based on measurements obtained from a field experiment of pavement-watering conducted at two sites in Paris, France over the summers of 2013 and 2014.

First, an analysis method was developed to determine the method's microclimatic effects in the field. Air temperature, relative humidity and mean radiant temperature effects were investigated as well as pedestrian thermal comfort using the Universal Thermal Climate Index and UHI-mitigation. Second, the thermal effects of pavement-watering were determined, including surface temperature as well as pavement heat flux and temperature 5 cm deep. Finally, the water footprint of pavement-watering was determined based on a linear relationship found between pavement heat flux and solar irradiance. In addition, possible improvements for the watering method were determined and discussed.

The research provides useful information for decision-makers considering pavement-watering as part of their heat-wave adaptation and/or UHI-mitigation strategy. Future work should focus on the effects of different materials and street configurations on pavement-watering cooling as well as cumulative effects arising from watering large areas rather than a single street portion. Certain methodological aspects also require further investigation and may be improved.

Keywords: Pavement-watering; urban heat island; urban cooling; climate change adaptation; urban field measurements; evaporative cooling

Résumé

Ce manuscrit s'intéresse à l'arrosage urbain en tant que stratégie de rafraîchissement pour les villes souhaitant réduire l'intensité de leur îlot de chaleur urbain (ICU) et/ou en tant qu'outil d'adaptation aux canicules, amenées à devenir plus fréquentes et intenses en raison du changement climatique. Cette recherche s'appuie sur une expérimentation d'arrosage réalisée à Paris (France) sur deux sites pendant les étés 2013 et 2014.

D'abord, une méthode d'analyse a été mise au point afin de déterminer les effets micro-climatiques de l'arrosage sur le terrain. La température de l'air, l'humidité relative et la température moyenne de rayonnement ont été examinées ainsi que le confort thermique du piéton grâce au Universal Thermal Climate Index et le pouvoir d'atténuation de l'ICU. Ensuite, les effets thermiques ont été quantifiés, comprenant les effets sur la température de surface ainsi que le flux de chaleur et la température à 5 cm de profondeur. Enfin, la consommation d'eau de l'arrosage a été estimée à partir d'une relation linéaire trouvée entre le flux de chaleur à 5 cm de profondeur et le rayonnement solaire incident pendant la période d'ensoleillement direct. Par ailleurs, des améliorations de la méthode d'arrosage ont été déterminées et discutées.

Les analyses conduites ici fournissent des informations essentielles pour les décideurs intéressés par l'arrosage urbain comme volet de leur stratégie de réduction des ICUs et/ou d'adaptation aux canicules. Les recherches à venir devraient s'orienter sur l'impact d'autres matériaux et configurations urbaines sur l'arrosage ainsi que les effets cumulés atteints lorsqu'un quartier entier est arrosé plutôt qu'une portion de rue. Certaines modifications de la méthode méritent également d'être étudiées.

Mots-clés : Arrosage urbain; îlot de chaleur urbain; rafraîchissement urbain; adaptation; changement climatique; mesures de terrain; rafraîchissement évaporatif

Remerciements

Je commencerai ces remerciements par quelques mots sur le long parcours de genèse de cette thèse. Je me suis efforcé de le résumer tout en veillant à remercier tous ceux qui m'auront accompagné et demande pardon à ceux que j'aurais oublié.

Au commencement, il a fallu imaginer qu'une thèse était un choix de carrière possible. Je dois cette idée à Olivier Mirgaux que je remercie pour ses conseils donnés un vendredi matin fin 2008 pendant un cour d'introduction à l'analyse de cycle de vie aux Mines de Nancy. Malgré ses très bons conseils, il aura fallu attendre mon retour à Paris début 2011 pour que j'envoie mes premières candidatures.

En attendant d'être retenu par une équipe, j'ai été recruté à La Caféothèque en tant que barista-sommelier en café, période rebaptisée plus tard "Pause Café" par Gloria Montenegro Chirouze. Je tiens à remercier ici Bernard, Gloria et Christina Chirouze pour leur accueil chaleureux et le temps passé ensemble à la Caféothèque ainsi qu'à mes collègues devenus très bons amis Gérald, Laura et Pierre-Jacques.

En parallèle, je candidatais à des offres de thèse et c'est ainsi que j'ai pris contact avec Morgane Colombert pour la première fois. Ma première candidature n'ayant pas été retenue (merci Etienne !), elle m'a invité à répondre à une deuxième offre, une thèse CIFRE avec la Ville de Paris sur le rôle de l'eau en ville. Très sceptique initialement, j'ai suivi son conseil. En sortant de l'entretien quelques jours plus tard, j'étais entièrement convaincu par ce sujet qui était non seulement passionnant, mais correspondait parfaitement à mes attentes.

Je remercie ici Morgane de m'avoir suggéré cet autre sujet qui s'est révélé infiniment plus intéressant que ce j'ai pu imaginer au départ. Je la remercie à nouveau ainsi que Laurent Royon, Youssef Diab et Dominique Coutart de m'avoir suivi et surtout soutenu pendant la longue période d'incertitude qui a suivi.

En effet, il aura fallu 18 mois de plus pour que toutes les conditions soient réunies pour démarrer mon contrat CIFRE : candidature ANRT, validation par celle-ci puis vote final par le Conseil de Paris. Pendant ce temps, j'ai prolongé mon séjour à La Caféothèque, rejoint les rangs de l'EIVP en tant qu'ingénieur d'études puis ceux de la Ville de Paris en tant que saisonnier. Début janvier 2013, ma thèse a enfin pu démarrer.

Je souhaite faire part de ma reconnaissance profonde envers l'équipe qui m'a encadré pendant ce travail. Merci à mon directeur, Laurent Royon, pour ces trois années de collaboration et de réflexion communes très riches. Merci de tes conseils et commentaires qui m'ont aidé à améliorer la qualité de mes travaux et merci pour ton soutien au-delà de la thèse (vacations d'enseignement, poste d'ATER, etc.). J'adresse également mes remerciements à Dominique Coutart pour son soutien aussi bien logistique et administratif que managérial qui s'est révélé extrêmement précieux dans le cadre des nombreuses négociations et discussions nécessaires pour préparer les expérimentations in situ décrites dans ces pages. Merci aussi à Youssef et Morgane pour leur confiance et leur accompagnement tout au long de ce projet.

Je souhaite remercier mes rapporteurs Mat Santamouris et Valéry Masson ainsi

que mes examinateurs Hervé Andrieu et Hassan Peerhossaini pour leur travail de lecture et de critique constructive. Merci d'avoir accepté de faire partie de mon jury de thèse et pour les échanges très intéressants que nous avons pu avoir.

J'adresse également mes remerciements aux nombreuses équipes de la Mairie de Paris qui se sont mobilisées pour m'aider à mener ce projet à bien : SPE qui m'a accueilli tout d'abord, mais aussi la SAP, notamment les circonscriptions Ouest et Est ainsi que l'atelier Deleusseux, DSR, DEI, DII, STPP, SCGIQ, AEU, DVD... Je tiens aussi à saluer les participants du groupe de travail "Expérimentation de rafraîchissement de l'espace public par arrosage" que j'ai piloté à la Ville pendant mes trois années de thèse. Un très grand merci à Jérôme et à Damien du LEM pour notre étroite collaboration qui se poursuit, ainsi qu'à Anne, Jean-Marc et Claude sans qui mes essais au LEM n'auraient pas pu se dérouler dans d'aussi bonnes conditions. Merci à Julien de l'APUR pour notre collaboration qui se poursuit au-delà de la thèse.

Je tiens à remercier mes anciens et nouveaux collègues de l'EIVP pour le temps passé ensemble, pour les nombreuses et longues discussions scientifiques ou non, les dîners, godets, craquages, fous rires et dégustations en tout genre : Charlotte, Etienne, Marie T, Angel, Fatiha, Alberto, Claire, Brice, Jeanne, Samuel, Marie B, Joffrey, Serge et Antoine. Je souhaite bon courage à ceux qui poursuivent ou démarrent à peine leur thèse. Merci encore à Etienne pour sa mise en page amplement exploitée dans ce mémoire, dommage qu'elle ne t'ait finalement pas servi. Merci également aux collègues de la Ville de Paris pour leur accueil chaleureux et les bons moments passés ensemble au 5^{e}, 4^{e} et 1er étages. Merci à Maxime, Arnaud et Mathieu du laboratoire MSC pour nos discussions et échanges également.

Je salue également Carolina, Noushig, Abood, Karina et Florine pour nos collaborations et échanges, ainsi que Brice Tréméac et Mathieu Guilhot pour leur accueil chaleureux au CNAM et à l'IUT de Marne-la-Vallée en tant que vacataire.

Je souhaite également remercier tous mes amis, tout particulièrement ceux qui ont participé de près ou de loin à certains projets ou discussions : soirée thermographique avec Marie et Julien, analyses statistiques avec Guti, déjeuners Chez Prune avec Simon(s), Alex, JB, Jérém', Guti et Manon. Je remercie Charlotte, Olivier et Thomas pour leur aide précieuse pendant la préparation de la soutenance. Merci à celles et à ceux qui ont participé au buffet.

Merci à l'ensemble de ma famille pour leur soutien et nos discussions, à Isa, Fifi et Zab pour leurs relectures très utiles et à Antoine pour sa participation à une des balades thermographiques. Merci à Marc V de m'avoir soutenu et encouragé pendant le montage, long et stressant, de ce projet. Je suis bien triste de ne pas pouvoir partagé son aboutissement avec toi. Je pense que tu en serais fier.

Enfin, je dédie ce mémoire à Sophie que je remercie du fond du cœur pour son soutien sans faille depuis plus de 10 ans. Ensemble, nous aurons réussi à mener à bien plusieurs projets en parallèle : voyages, achat et travaux d'appartement, thèse de doctorat, etc. J'espère que nous continuerons encore longtemps à réaliser nos projets ensemble. Je t'aime.

Contents

Contents v

List of Figures ix

List of Tables xii

Acronyms and Abbreviations xv

List of Symbols xvii

1 Introduction 1

2 Scientific Background 5
- 2.1 Urban Climate and the urban heat island (UHI) Effect 5
- 2.2 UHI Countermeasures 7
  - Reflective Materials 8
  - Urban Greening 9
  - Other Materials 9
- 2.3 Expected Cooling Effects 10
- 2.4 Conclusion 11

3 Literature Review of Pavement-watering 13
- 3.1 Brief Description and Methodology 14
  - Brief Description 14
  - Watering Method 15
  - Analysis Method 18
- 3.2 Cooling Effects of Pavement-Watering 19
  - Micro-climatic Indicators 19
  - Thermal Indicators 24
- 3.3 Conclusion 26

4 Knowledge Gaps and Remaining Research Questions 29

1 Micro-climatic Effects of Pavement-Watering **31**

5 Introduction to Part 1 **33**

6 Methodology **35**
6.1 Location . . . 35
6.2 Watering Method . . . 37
Weather conditions . . . 38
Water Sprinkling Technique . . . 39
6.3 Instruments . . . 40
6.4 UHI Mitigation Potential . . . 42
6.5 Thermal Comfort Evaluation . . . 42
6.6 Heat Transfer Analysis . . . 42
6.7 Data Series . . . 43
6.8 Interpretation of Micro-climatic Effects . . . 44

7 Direct Case-Control Comparison **45**
7.1 Results . . . 45
7.2 Interstation Profile on Reference Days . . . 48
7.3 24-hour Average Differences . . . 49
7.4 Conclusion . . . 50

8 Interstation Behavior on Reference and Watered Days **51**
8.1 Statistical Analysis Method . . . 51
8.2 Results . . . 52
8.3 Discussion . . . 56
8.4 Conclusion . . . 61

9 Conclusion of Part 1 **63**

2 Thermal Effects of Pavement-Watering **67**

10 Introduction to Part 2 **69**

11 Methodology **71**
11.1 Instruments . . . 71
11.2 Pavement Zones . . . 73
11.3 Pavement Heat Balance . . . 75
11.4 Data Analysis . . . 76
Pavement Heat Flux . . . 77
Surface Temperature . . . 77
Pavement Temperature . . . 77
11.5 Deriving Pavement Solar Irradiance . . . 77

12 Pavement Heat Flux Effects **79**
12.1 Results . . . 79
Reference days . . . 79
Watered days . . . 80
12.2 Discussion . . . 82
12.3 Conclusion . . . 83

13 Surface Temperature Effects **85**
13.1 Results . . . 85
13.2 Discussion . . . 88
13.3 Conclusion . . . 88

14 Pavement Temperature Effects **89**
14.1 Results . . . 89
14.2 Discussion . . . 91
14.3 Conclusion . . . 92

15 Conclusion of Part 2 **93**

3 Improving the Water Use of Pavement-Watering **95**

16 Introduction to Part 3 **97**

17 Methodology **101**
17.1 Heat Transfer Analysis . . . 101
17.2 Optimization Goals . . . 104

18 Cooling Flux Φ: Determining the Evaporation Rate **107**
18.1 Results . . . 107
18.2 Confrontation with Mass Convection Transport Problem . . . 111
18.3 Discussion . . . 112
18.4 Conclusion . . . 113

19 Watering Frequency Optimization **115**
19.1 Results . . . 115
Pavement Heat Flux . . . 115
Surface Temperatures . . . 116
5 cm Pavement Temperatures . . . 118
19.2 Discussion . . . 118
Pavement Heat Flux . . . 119
Surface Temperatures . . . 120
5 cm Pavement Temperatures . . . 121
19.3 Conclusion . . . 121

20 Watering Rate Optimization **123**
20.1 Pavement Cooling Flux Φ 123
20.2 Pavement Surface Temperatures 125
20.3 Conclusion 125

21 Conclusion of Part 3 **127**

22 Conclusion **131**
22.1 Results 131
22.2 Future Research 133

Bibliography **137**

A Congrès Français de Thermique 2015 : Thermique de l'Habitat et de la Ville **145**

B XII^{ème} Colloque Interuniversitaire Franco-Québécois sur la Thermique des Systèmes **155**

C 9th International Conference on Urban Climate jointly with 12th Symposium on the Urban Environment **163**

Résumé détaillé en français **171**

List of Figures

2.1 Heat budget of a pavement surface (Hendel et al., 2015). 7

3.1 Diagram of the watering methods used in the surveyed articles. 16

6.1 Position of Experimental Sites in Paris 36
6.2 Station Positions at the Louvre (left) and Belleville (right) Sites . . . 37
6.3 Solar irradiance at Louvre (left) and Belleville (right) on July 14th 2013 38
6.4 Diagram describing the applied watering method at both sites. 39
6.5 Watering on rue du Louvre (left, from Hendel et al. (2014)) and rue Lesage (right) 39
6.6 Weather station design and instrumentation (rue du Louvre). 40
6.7 Photographs of watered and control weather stations *in situ*. From left to right: watered and control Louvre stations, watered and control Belleville stations (Hendel et al., 2015). 41
6.8 Diagram of pavement heat budget at surface (Hendel et al., 2015). . 42

7.1 Differences between Louvre case and control stations from July 2nd to 19th, 2013 (top to bottom) for T_a and relative humidity (RH) at 1.5 m (left) and 4 m (right) height and mean radiant temperature (MRT) (bottom left) and Universal Thermal Climate Index (UTCI) (bottom right). Watered days are in blue, reference days are in red. Days with uncomparable weather conditions are in grey (Hendel et al., 2015). . . 46
7.2 Differences between Belleville case and control stations from July 2nd to 19th, 2013 (top to bottom) for T_a and RH at 1.5 m (left) and 4 m (right) height and MRT (bottom left) and UTCI (bottom right). Watered days are in blue, reference days are in red. Days with uncomparable weather conditions are in grey. 47

8.1 Average watering effect at Louvre over the summers of 2013 and 2014 (top to bottom) for T_a and RH at 1.5 m (left) and 4 m (right) above ground level (a.g.l.) and MRT (bottom left) and UTCI (bottom right). Average effects are solid blue, confidence intervals are dashed red (Hendel et al., 2015). 53

8.2 Average watering effect at Belleville over the summers of 2013 and 2014 (top to bottom) for T_a and RH at 1.5 m (left) and 4 m (right) a.g.l. and MRT (bottom left) and UTCI (bottom right). Average effects are solid blue, confidence intervals are dashed red (Hendel et al., 2015). 54
8.3 Average watering effect at Louvre detected using the Belleville control stations over the summers of 2013 and 2014 (top to bottom) for T_a and RH at 1.5 m (left) and 4 m (right) height and MRT (bottom left) and UTCI (bottom right). Average effects are solid blue, confidence intervals are dashed red (Hendel et al., 2015). 59

11.1 Top view of pavement sensor (Hendel et al., 2015a). 72
11.2 Cross-section detail of pavement sensor filling materials (Hendel et al., 2015a). 73
11.3 Surface temperature measurement zones (left) and corresponding night-time corrected infrared photograph on July 22nd at 3:20 am (right). Temperature scale is in degrees Celsius. Sp2: pavement zone 1; Sp1: pavement zone 2; Sp3: sidewalk zone (Hendel et al., 2014). 74
11.4 Diagram of pavement heat budget at surface (Hendel et al., 2015a). . 76
11.5 Solar irradiance measured on July 8th and 22nd (Hendel et al., 2014). 76
11.6 G (left) and S' (right) measured on July 11th (Hendel et al., 2014) . 78

12.1 Pavement heat flux G (left) and shortwave (0.3-3 µm) (SW) radiation S (right) on control days (Hendel et al., 2014). 80
12.2 Pavement heat flux G and SW radiation S on watered days: a) and d) July 8th; b) and e) July 22nd; c) and f) July 10th (Hendel et al., 2015a). 81

13.1 Pavement directional radiometric temperature on reference days: a) July 20th and b) July 21st; and on watered days: c) July 8th and d) July 22nd (Hendel et al., 2014). 86

14.1 Pavement temperature on reference days: a) July 7th, b) July 20th and c) July 11th; and on watered days : d) July 8th, e) July 22nd and f) July 10th (Hendel and Royon, 2015). 90

17.1 Diagram of pavement heat budget at surface (Hendel et al., 2015a). . 101

18.1 G as a function of S on control and watered days. a) July 11th, b) July 14th, c) July 20th, d) July 8th, e) July 22nd, f) July 10th, 2013 (Hendel et al., 2015a). 108

19.1 Watering cycles and pavement heat flux on a) July 8th, b) July 10th and c) July 22nd, 2013. 116

19.2 Surface temperature and watering cycles on watered days: a) July 8th and b) July 22nd. 117

20.1 Pavement cooling Φ (left) and watering rate to pavement cooling ratio $\frac{V_S}{\Phi t_0}$ (right) according to the applied watering rate (Hendel et al., 2015a). 124

1 Diagram of the watering methods used in the surveyed articles. 176
2 Plan des stations des sites de Louvre (gauche) et de Belleville (droite). 177
3 Schéma et instrumentation des stations météorologiques (rue du Louvre). 178
4 Méthode d'arrosage pour Louvre et Belleville. 178

List of Tables

3.1 Reported air temperature effects. . . . 19
3.2 Reported air humidity effects. . . . 20
3.3 Reported effects on the radiative environment. . . . 21
3.4 UHI-mitigation effects. . . . 22
3.5 Reported thermal comfort effects. . . . 23
3.6 Reported pavement surface temperature effects. . . . 24
3.7 Reported pavement temperature effects. . . . 25
3.8 Reported latent heat flows. . . . 25
3.9 Reported pavement heat flux effects. . . . 26
3.10 Literature review summary. . . . 28

6.1 Weather conditions required for pavement-watering and heat-wave warnings (Hendel et al., 2015a) . . . 38
6.2 Type, height and uncertainty of meteorological instruments. Adapted from Hendel et al. (2015). . . . 41

7.1 Average case-control difference on reference days over the summers of 2013 and 2014 (Hendel et al., 2015). . . . 48
7.2 Daily interstation difference on watered days and variation from reference days over the summers of 2013 and 2014. Adapted from Hendel et al. (2015). . . . 49

8.1 Duration, mean and maximum values of statistically significant (stat. sign.) effects for Louvre over the summers of 2013 and 2014 (Hendel et al., 2015). . . . 55
8.2 Duration, mean and maximum values of stat. sign. effects for Belleville over the summers of 2013 and 2014 (Hendel et al., 2015). . . . 55
8.3 p-value and average stat. sign. (CI: 0.95) effect at Louvre and Belleville over the summers of 2013 and 2014 (Hendel et al., 2015). . . . 57
8.4 p-value and average stat. sign. (CI: 0.95) effect at Louvre using the Belleville control station over the summers of 2013 and 2014 (Hendel et al., 2015). . . . 60
8.5 Duration, mean and maximum values of stat. sign. effects for Louvre, using the Belleville control station (Hendel et al., 2015). . . . 60

11.1 Type, height and uncertainty of thermal instruments. Adapted from Hendel et al. (2014, 2015a,b). 71
11.2 Parameters used to correct apparent surface temperature (Hendel et al., 2014) 73
11.3 Pavement structure in each zone (Hendel et al., 2014). 75

12.1 Actual watering method on considered watered days (Hendel et al., 2015a). 80
12.2 Average heat flux density reduction in W/m^2 on watered days (Hendel et al., 2015a). 82

13.1 Average temperature reductions observed on July 22nd (watered) compared to average control day temperatures (July 20th and 21st) (Hendel et al., 2014). 87

14.1 Daily low, high, and temperature amplitude on July 7th, 8th, 10th, 11th, 20th and 22nd, 2013 (Hendel and Royon, 2015). 91

18.1 β and R^2 on reference days (Hendel et al., 2015a). 109
18.2 β, R^2 and G_0 (W/m^2) on watered days. The value of G_0 was input by the user (Hendel et al., 2015a). 109
18.3 Average value of meteorological parameters on July 22nd, and 10th, 2013 between 3 pm and 6:30 pm and corresponding solutions to equation 17.18 (Hendel et al., 2015a). 111
18.4 Solutions to equation 17.18 obtained with $h = 3.5\ W/m^2.K$ (Hendel et al., 2015a). 112

1 Résumé de l'état de l'art. 175
2 Conditions météorologiques nécessaires pour le déclenchement de l'arrosage urbain et conditions caniculaires pour Paris. 179

Acronyms and Abbreviations

a.g.l. above ground level.

exp. experimental.

HIP heat island potential.

IR infrared.

LW longwave (3-100 µm).

MRT mean radiant temperature.

NA not available.
NiR near infrared (1-3 µm).
NR not relevant.
num. numeric.

PCM phase change material.
PET Physiological Equivalent Temperature.
PM particulate matter.
PT Perceived Temperature.

RH relative humidity.

stat. sign. statistically significant.
SW shortwave (0.3-3 µm).

TEB Town Energy Balance.

UHI urban heat island.
UHII urban heat island intensity.
UTCI Universal Thermal Climate Index.

WBGT Wet-Bulb Globe Temperature.

List of Symbols

α Albedo and/or shortwave reflectivity, $[-]$.

β Conversion coefficient of solar irradiance to 5 cm pavement heat flux density, $[-]$.
BMI_{Max} Three-day averaged maximum daily air temperature, $[^oC]$.
BMI_{Min} Three-day averaged minimum daily air temperature, $[^oC]$.

c_p Specific heat of water, $1,000\,[J.g^{-1}.K^{-1}]$.

ΔQ Sensible heat absorption flux, $[W.m^{-2}]$.

E Evaporation rate, $[g.s^{-1}]$.
ϵ Material emissivity, $[-]$.

G Pavement heat flux 5 cm deep, $[W.m^{-2}]$.

H Upwards convective heat flux, $[W.m^{-2}]$.
h Convective heat transfer coefficient, $[W.m^{-2}.K^{-1}]$.
H/W Canyon aspect ratio, $[-]$.

L Longwave radiation, $[W.m^{-2}]$.
l Water latent heat of vaporization, $2,260\,[J.kg^{-1}]$.

p_0 Total air pressure, $[Pa]$.
Φ Pavement-watering cooling flux, $[W.m^{-2}]$.
Φ_{adv} Pavement-watering advective cooling flux, $[W.m^{-2}]$.
Φ_{lat} Pavement-watering latent cooling flux, $[W.m^{-2}]$.
p_s Saturation vapor pressure at water film temperature, $[Pa]$.
p_v Partial vapor pressure at water film temperature, $[Pa]$.

ρ Volumetric mass, $[kg.m^{-3}]$.
R_n Net radiation, $[W.m^{-2}]$.

S Shortwave radiation, $[W.m^{-2}]$.
S' Shortwave radiation, measured by station pyranometer 4 m a.g.l., $[W.m^{-2}]$.
σ Stefan-Boltzman constant, $5.67\,10^{-8}[W.m^2.K^{-4}]$.

T Temperature, $[^oC]$.
T_a Air temperature, $[^oC]$.
t_0 Time between two watering cycles, $[s]$.
T_g Globe temperature, $[^oC]$.
T_{mrt} Mean radiant temperature, $[^oC]$.
T_n Minimum daily air temperature, $[^oC]$.
T_x Maximum daily air temperature, $[^oC]$.

V Downwards conductive heat flux, $[W.m^{-2}]$.
v Wind speed, $[m.s^{-1}]$.
V_S Dispersed water volume per watering cycle, $[L.m^{-2}]$.

CHAPTER 1

Introduction

The maharajas of the Thar Desert in Rajasthan ruled over one of the driest and hottest areas in the Indian sub-continent. In the sweltering hot summer, no means were spared to improve thermal comfort, including sprinkling rose-perfumed water on the palace walls. Many other areas across the globe have developed similar practices such as "Uchimizu" in Japan. Indeed, watering ground surfaces during the hot and humid Japanese summers has been a local tradition for centuries and continues up to this day (Japan Water Forum, 2015).

Paris' strong hygienist movement during the 19th Century led to the development of its dual water supply. Originally designed to supply Paris with potable water, the Ourcq Canal quickly became the main source for the city's non-potable water network, the Seine currently providing approximately 20% of its water. Street cleaning has since relied on the use of non-potable water. Until the mid-20th Century, streets could be watered up to five times on hot summer days to prevent dust clouds from forming, as described by Girard (1923). According to the author's reports, many inhabitants at the time also believed the watering provided cooling to the city. As mechanized cleaning was generalized and dust clouds were no longer a problem, these practices were lost and nearly forgotten over time.

Today, pavement-watering is seen as a potential tool to improve thermal comfort in cities during periods of intense heat. Scientific work in Japan began in the 1990's with the use of preexisting pavement-watering installations in Nagaoka City (Kinouchi and Kanda, 1997, 1998; Takahashi et al., 2010) or block-scale demonstrators in Tokyo (Yamagata et al., 2008) as well as simulations applied to Kawasaki City (Nakayama and Fujita, 2010; Nakayama et al., 2012). More recently, the city services of Paris or Lyon have conducted their own field studies with the use of cleaning trucks or watering infrastructure prototypes (Bouvier et al., 2013; Maillard et al., 2014) (see Chapter 3 for details). In France and especially in Paris, the predicted increases in heat-wave intensity and frequency due to climate change (Lemonsu et al., 2013), combined with the high sensitiv-

ity of dense cities to such episodes (Robine et al., 2008; Li and Bou-Zeid, 2013), have focused efforts on the development of appropriate adaptation tools, including urban greening, reflective materials and pavement-watering.

Paris' interest in pavement-watering was marked with the unanimous passing of its Blue Paper in 2012 by the City Council (Paris City Council, 2012a). The Paper defined the city's strategy for the development and improvement of its water and sanitation utilities. After more than two decades of semi-abandonment, the Blue Paper officially recognized the potential of the non-potable water network for sustainable urban water use. To initiate its redevelopment, three tasks were assigned to the relevant city services. The first consisted of replacing municipal uses of potable water with non-potable water where feasible, e.g. for park irrigation. A study of solutions to diversify the network's water supply with other sustainable sources was also requested to reduce the network's environmental footprint further. Finally, the services were tasked with studying the potential of the network to be used as the backbone of a pavement-watering infrastructure to cool the city in the event of heat-waves and to tackle its worsening UHI.

The Water and Sanitation Department of Paris therefore set out to determine what the feasability of a city-wide pavement-watering strategy might be in a city such as Paris, by first identifying the method's costs and benefits.

This dissertation aims to provide answers to this question, however the words "cost" and "benefit" are not very specific and can refer to a large number of different aspects.

To help downsize the number of possibilities, we turn to the language associated with pavement-watering in the city's Blue Paper. The Paper lists several aims for pavement-watering such as to: "reduce air temperatures during intense heat events", "fight urban heat islands", "[improve] urban thermoregulation" and "provide cooling [...] during heat events" (Paris City Council, 2012a). The benefits therefore clearly refer to the method's measurable cooling effects, with a special focus on air temperature and UHI-mitigation, particularly during heat-wave events. The special importance given to heat-wave events echoes the impact that the 2003 heat-wave has had on public awareness in France. This facet should therefore not be overlooked.

The Blue Paper identifies only one cost associated with pavement-watering: its water footprint. Indeed, "to limit the impact on the Seine and Ourcq Canal which supply the non-potable water network, alternative water sources could be used [...]" While efforts are being made to diversify the non-potable networks supply, the water consumption of pavement-watering is of special importance.

This brings a close to the costs and benefits identified by the Blue Paper, however many other ones are overlooked by this list. Other positive effects include improved air quality or street cleanliness as a side-effect of pavement-watering (Amato et al., 2010), reduced sewer obstruction as a consequence of pavement-watering runoff or, as mentioned by Girard (1923), the positive social effects of perceived cooling by pedestrians. Other potential costs are economic or environmental in nature, including the financial cost of a pavement-watering infrastruc-

ture or environmental impacts other than the water footprint, such as greenhouse gas emissions or energy use. While these aspects are all important, we choose to limit ourselves to those identified in the Blue Paper.

Our research problem can therefore be summarized with the following question: what cooling effects, including air temperature and UHI-mitigation effects, can be expected of pavement-watering during heat-wave events and in exchange for what water footprint in dense urban areas?

Before attempting to answer the question on our own, we first conduct a literature review on the topic of pavement-watering. Beforehand, a brief scientific background of urban climate, the UHI effect and its countermeasures will be provided.

CHAPTER 2

Scientific Background

Having provided some historical and political perspective on the motivations behind our research topic, we now present the scientific background and context that pavement-watering falls into as a potential UHI and heat-wave mitigation tool. We begin by describing the urban climate and the UHI effect.

2.1 Urban Climate and the UHI Effect

Urban areas, through a combination of radiative trapping, increased heat storage, wind obstruction, low vegetation presence, low surface permeability, as well as high concentrations of human activity, create a localized warming effect known as the UHI effect (Oke, 1982; Grimmond, 2007). The UHI effect takes the form of increased urban air and surface temperatures with regards to surrounding rural areas, in the order of 1°-3°C on average (Akbari et al., 2001). The resulting air temperature difference, measured as that of the urban area minus that of the rural area, is known as the urban heat island intensity (UHII).

For millennia, urban climatology has been taken into account in urban design, but published scientific work remained scarce until the 1950's (Yoshino, 1990). The mid-20th Century marks a turning point with a significant increase in the number of publications over the following decades and studies gradually more dedicated to the UHI effect and its possible countermeasures.

Since then, knowledge and understanding of the UHI phenomenon has gradually shifted from empirical descriptions and predictions (Oke, 1973), towards a finer understanding of the physical processes involved (Oke, 1982). In short, sky and wind obstruction by urban morphology reduce radiative and convective exchanges and the absence of vegetation reduces latent exchanges at the city-scale, while strong heat gains occur within cities due to anthropogenic heat release.

During this period, the positive relation between city size and UHII was observed by Oke (1973). In addition, several studies identified links between radia-

tive trapping and street geometry, synthesized by the canyon aspect ratio H/W (building height-to-street width), with the help of scale models and computer simulations (Oke, 1973, 1981; Arnfield, 1990; Spronken-Smith and Oke, 1999). Indeed, a decreasing linear relationship was found by Oke (1981) between maximum UHII and sky view factor, in other words open urban designs experience lower UHII. Oke (1988) confirmed this by identifying an empirical relationship linking high aspect ratios (H/W) with higher maximum UHII from observations in European, North American and Australasian cities. More recently, investigations have helped better quantify the importance of anthropogenic heat releases (Pigeon et al., 2007), or the creation of climate-vulnerability maps of cities

By the end of the 20th and beginning of the 21st Centuries, several urban canopy models had been developed such as the Noah land surface model developed by Kusaka et al. (2001), the Town Energy Balance (TEB) model by Masson (2000), or the University of Athens (NKUA) model by Dandou et al. (2005). Over the years, some of these were refined to be able to include low-level vegetation (Lemonsu et al., 2012), green roofs (De Munck et al., 2013) and trees (Redon et al., 2014).

In 2011, the results of an international urban energy balance model comparison study (PILPS-urban) benchmarking 32 of these models against one another were published (Grimmond et al., 2011). Some of these models have since been used for sensitivity analyses of urban climate to the different urban parameters (Colombert et al., 2011), thus helping urban planners and designers target their anti-UHI measures more efficiently, depending on the urban configuration. In the past few years, urban canopy models have even been combined with other social or economic models capable for example of simulating future urban development (Masson et al., 2014).

In parallel to this work on the fundamentals of the UHI effect and its modelling and simulation, studies have also been carried out on ways of reducing UHII. UHII varies with time and local weather conditions. Typically, high wind speeds and cloud cover tend to lower it, while clear skies and low winds amplify it (Cantat, 2004). On nights with clear skies and calm winds, UHII can reach as much as 12°C (Oke, 1973). These conditions are typically reached during heat-waves. For example, during the 2003 heat-wave in Paris, UHII reached 8°C (Paris City Council, 2007).

While UHI may reduce building energy consumption during winter, the opposite is true in the summer during which cooling demand is increased (Hassid et al., 2000). For Athens, Greece for example, building cooling energy has been found to double when UHII reaches 10°C, while peak cooling electricity demand is tripled (Santamouris et al., 2001).

In addition to negative effects on energy use, UHIs also tend to exacerbate ozone and smog pollution (Rosenfeld et al., 1998) as well as the intensity of heat-waves (Li and Bou-Zeid, 2013). As a result, their health impacts are increased, making heat-waves of particular concern for dense urban areas with intense UHIs. This helps explain that the Île-de-France region was one of the worst hit in Europe

during the 2003 heat-wave which caused a two-fold increase in mortality over the first two weeks of August 2003 (Robine et al., 2008). This event created strong heat-wave awareness in France. As a result, predicted increases in heat-wave frequency and intensity (Lemonsu et al., 2013) are at the heart of climate change adaptation efforts for Paris under its 2007 Climate Plan (Paris City Council, 2007). In 2012, the Plan was updated and now includes measures addressing the UHI effect (Paris City Council, 2012b).

We now present some of the UHI countermeasures that have been studied to this day.

2.2 UHI Countermeasures

UHI countermeasures aim to reduce or compensate for the phenomena responsible for urban warming. Among these radiative trapping and low vegetation presence are often addressed.

The role of radiative trapping on UHII is based on the higher absorption of solar energy by urban surfaces. Indeed, the generally low SW reflectivity (a.k.a. albedo) of roofs, walls and pavements combined with the multiple intra-canyon reflections and emissions which occur result in increased solar absorption by urban canyons. As solar energy is absorbed in the form of sensible heat, material temperatures increase, consequently increasing convection, thus raising the ambient air temperature. Figure 2.1 illustrates the heat budget of a pavement surface but can be generalized to building walls and roofs.

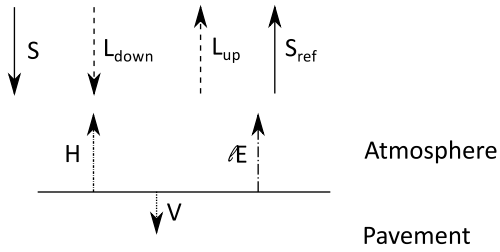

Figure 2.1 – Heat budget of a pavement surface (Hendel et al., 2015).

S and L_{down} respectfully designate incident SW and longwave (3-100 µm) (LW) radiation, while S_{ref} and L_{up} represent upwards SW (reflected only) and LW (reflected and emitted) radiation. H and lE respectfully represent the convective and latent heat fluxes towards the atmosphere, while V is the conductive heat flux into the pavement.

Therefore, two approaches can be proposed to reduce radiative trapping. The first consists of favoring open urban designs with low H/W. By increasing the sky view factor of canyon surfaces, intra-canyon reflection and emission is reduced, resulting in more energy being radiated out of the street canyon (Oke, 1988). However, this approach is only applicable to new developments and is incompatible

with dense urban designs which help limit transportation energy and urban sprawl (Newman and Kenworthy, 1989).

The second approach consists of so-called "cool materials", which can be used in new buildings and developments or to retrofit existing ones.

Reflective Materials

Cool materials have modified properties compared to standard ones in order to lower their surface temperature. As the convective flux at an urban surface depends on the surface-air temperature difference, reduced surface temperatures result in lower atmospheric warming.

Depending on the technology used, more or less feedback is available on the application of these materials. Several recent literature reviews on their use are available in the literature (Santamouris et al., 2011; Santamouris, 2013).

Originally, cool materials mostly consisted of white-coatings or materials. Their goal is to reflect SW solar radiation out of the urban canyon and back into space. As SW reflectivity is referred to as albedo, such materials are also called high-albedo. The potential for high-albedo roofing materials to reduce UHII has been studied for decades (Akbari and Taha, 1992; Taha, 1997; Akbari et al., 2001). More recently, cool-colored materials have been developed which are highly reflective in the near infrared (1-3 µm) (NiR) band. This allows for a wide variety of colors while still providing cooling performance (Santamouris et al., 2011). In addition to reducing urban temperatures, SW reflective materials create a negative radiative forcing that effectively counters the effects of increasing green house gas concentrations (Akbari and Matthews, 2012).

In the case where materials have low emissivity (e.g. Paris' zinc roofs) high emissivity coatings can be used to increase LW radiant cooling (Météo France and CSTB, 2012).

Some of the limits to the use of these materials include material aging and associated performance degradation (Bretz and Akbari, 1997). This is particularly true for pavement materials which are exposed to very intense urban pollution and to high levels of abrasive wear associated with road traffic (Rosado et al., 2014). Thus, recent work has focused on developing accelerated aging methods to determine the evolution of cool material performance over time (Takebayashi et al., 2014; Sleiman et al., 2014). Another limit to the use of these cool materials is their impact on winter conditions. Indeed, although it is only to a lesser extent, cooling observed in the summer also occurs in the winter, thus potentially increasing building heating demand. Recent work seems to indicate that the benefits in summer are not offset by winter penalties for cold climates (Akbari, 2014). Finally, in certain situations the increase in reflected radiation caused by high-albedo materials can have negative net impacts on pedestrian thermal comfort, thus defeating their purpose (Erell et al., 2013).

More recently, thermochromic coatings, which change color with increasing temperatures, are being developed and studied in the lab. These can be designed

to increase their albedo above a certain temperature and remain dark below it. These coating offer a chance to enjoy the cooling properties of high albedo in the summer without affecting energy demand in the winter (Santamouris et al., 2011).

To date, cool materials have mainly been studied in the lab, while large scale effects have been studied numerically, with little or no large-scale field testing of micro-climatic effects.

Urban Greening

Unlike cool materials, urban greening seeks to reintroduce evapotranspiration into the urban scene. Evapotranspiration consists of the combination of evaporation from the soil and plant transpiration through the process of photosynthesis. If vegetation is tall enough, pedestrians and buildings may also enjoy the added benefits of shading. Modern urban greening solutions exist and can be applied to roof, wall or street surfaces and rely on the use of trees, parks, lawns as well as green walls and roofs (Akbari et al., 2001; Ng et al., 2012; Wong et al., 2009). Indeed, while the benefits of lawns, parks and trees have been studied and promoted for several decades (Jauregui, 1990; Taha, 1997), the more recent green facades and roofs make it possible to green both horizontal and vertical building surfaces (Jaffal et al., 2012; Djedjig et al., 2013; Musy et al., 2014).

In addition to atmospheric cooling and shading, urban vegetation has other benefits such as promoting urban biodiversity. Furthermore, green facades and roofs can provide added thermal and in some cases acoustic insulation to their host buildings (Musy et al., 2014; Morille et al., 2014).

One of the main limits to urban greening is that evapotranspiration requires irrigation to create cooling (Météo France and CSTB, 2012; Musy et al., 2014). In addition, green facades and roofs may be costly and difficult to implement in retrofit projects for structural reasons.

Other Materials

Even in the absence of vegetation, bare soil still provides a relatively constant amount of evaporative cooling over the course of the day as long as it contains sufficient moisture to do so (Camuffo and Bernardi, 1982). For surfaces which cannot be vegetated for practical reasons such as high traffic, permeable paving materials have been developed (Kubo et al., 2006; Haselbach et al., 2011; Li et al., 2013). These mainly consist of concrete or asphalt concrete with high void content which allows water to drain into the sublayers of the pavement (Li et al., 2013).

While these materials may offset rainwater runoff flows into sewer systems, they are not very efficient at providing evaporative cooling. Indeed, only water stored close enough to the surface is warm enough to evaporate rapidly. Water-retaining materials make up for this by relying on capillary action to keep moisture

present at or near the pavement surface where evaporation can occur. This is clearly demonstrated by Kubo et al. (2006) who compare water-retaining pavements with porous ones.

Another way to decrease the surface temperature of urban materials is to combine the latent heat storage properties of a phase change material (PCM) with the radiative properties of cool colored materials. By incorporating PCM into existing cool colored materials, their thermal inertia is effectively increased (Santamouris et al., 2011).

2.3 Expected Cooling Effects

To date, cool and green materials have been thoroughly studied in the lab or on small-scale prototypes (Kubo et al., 2006; Levinson et al., 2007; Takebayashi and Moriyama, 2007, 2009; Karlessi et al., 2011; Li et al., 2013). Results indicate that surface temperatures are significantly reduced compared to standard materials. This is expected to result in lower atmospheric heating as sensible heat flows are reduced with urban surface temperatures. Equivalent work on green spaces has mostly focused on existing parks (Jauregui, 1990; Ca et al., 1998), though smaller scale testing has also been conducted (Spronken-Smith and Oke, 1999). Parks have been found to be up to a few degrees cooler than their surroundings through the combined effects of evapotranspiration and shading. However, field evaluations and monitoring of large-scale applications of cool materials or new urban green spaces are scarce (Santamouris, 2013; Bowler et al., 2010). Indeed, large-scale micro-climatic effects have been almost exclusively studied with the help of computer simulations (Akbari et al., 2001; Nakayama et al., 2012; Météo France and CSTB, 2012; Wei and He, 2013; Musy et al., 2014).

Pavement-watering stands out as an exception and has been studied in the field via several independent studies (Kinouchi and Kanda, 1997, 1998; Yamagata et al., 2008; Takahashi et al., 2010; Bouvier et al., 2013; Maillard et al., 2014). This technique, consisting of spraying water onto an impervious or a permeable pavement surface, is viewed as an efficient means of reducing UHI intensity.

In contrast with high albedo pavements, this is accomplished without compromising pedestrian comfort as the radiant heat fluxes are not increased by watering. Indeed, surface wetting tends to decrease pavement albedo, thus lowering reflected SW radiation (Lekner and Dorf, 1988). On the other hand, the expected increase in air humidity caused by watering could negatively affect pedestrian comfort.

The effects of different adaptation strategies for Paris were studied in the framework of the EPICEA Project (Etude Pluridiscplinaire des Impacts du Changement climatique à l'Echelle de l'Agglomération parisienne) conducted from 2008 to 2012 (Météo France and CSTB, 2012). This study was conducted using the TEB model developed by Masson (2000) and provides useful information on the micro-climatic effects that can be expected for Paris for each of these strategies. The study had three main goals, the last of which consisted of determining the

impact of four different adaptation scenarios on 2 m a.g.l. air temperatures during the August 2003 heat-wave. These four scenarios are city-wide and include: 1) reflective and emissive building materials, 2) urban greening with and without irrigation, 3) pavement-watering and 4) the combination of scenarios 1), 2) and 3).

Météo France and CSTB (2012) found that scenario 1) created 2 m a.g.l. temperature reductions in the order of 1°C both day and night, reaching up to 4°C during the day. Scenario 2) with irrigation showed up to 5°C of cooling during the day with average effects in the order of 1°C. Without irrigation, scenario 2) had a negligible impact in the city center. Scenario 3) demonstrated average cooling of approximately 0.5°C and maximum effects of 1°-2°C during the day. UHII mitigation was measured as the change in 2 m a.g.l. air temperature between 3 am and 6 am local daylight savings time (UTC+2). In this regard, scenario 1) created a spatially-uniform 1°C reduction in UHII. In areas with substantial urban greening, scenario 2) with irrigation was found responsible for a 0.5° to 1°C reduction in UHII. Finally, scenario 3) caused reductions of 0.25° to 0.5°C of UHII in the most central urban areas. Finally, the combination of these scenarios yielded the highest results with average cooling of 2.3°C and maximum cooling of 6°C 2 m a.g.l.. UHI mitigation effects reached 1.25°C.

Overall, these results agree well with the studies previously cited and thus provide an order of magnitude for the cooling effects that can be expected from reflective and green materials as well as pavement-watering.

2.4 Conclusion

In this chapter, we have described the fundamentals behind the UHI effect. Characterized by the temperature difference between urban and rural areas (UHII), UHIs form as a result of radiative trapping, reduced evapotranspiration, wind obstruction and high concentrations of anthropogenic heat sources. These phenomena are linked to urban morphology, urban materials, lack of natural soils and green spaces and energy inefficiency.

To reduce UHII, UHI countermeasures may address one or several of these aspects. Significant work has been carried out to date on the design of cool urban materials which aim to maintain low surface temperatures. This is generally achieved by increasing material albedo. In turn, urban greening seeks to compensate for the lack of evapotranspiration by either increasing the share of green areas within cities with new parks or by adding greenery to building and street surfaces. Given their long lifespans of several years, these measures can be considered as permanent.

In principle, pavement-watering achieves the same goal as cool materials of lowering urban surface temperatures by creating additional latent and non-atmospheric sensible heat flows. These flows are obtained by the evaporation of the sprinkled water film and its sensible heat absorption. If sprinkling is sufficient

to create runoff, the sensible heat flux is an advective transfer. In addition, surface wetting also reduces its SW reflectivity (Lekner and Dorf, 1988). As the pavement surface is cooled, its convective (H), emitted (Stefan-Boltzmann's $\epsilon\sigma T_{surf}^4$) and reflected radiation flows decline, resulting in a cooler atmosphere and reduced radiosity.

In order to identify preexisting answers to our research problem, we will now proceed with a description of the state of the art of pavement-watering. In the process, the literature review will identify knowledge gaps and/or needs for further evidence. Information on the method's cooling effects, particularly in terms of air temperature and UHI mitigation during heat-waves, and the water footprint of the applied watering methods are the focus points of the review. A brief description of the selected studies and their analysis method will also be provided.

CHAPTER 3

Literature Review of Pavement-watering

The following literature review will focus on identifying answers to our problem which may already exist in the literature. Certain aspects may have been insufficiently studied and require further research. We consequently turn our attention to findings on the cooling effects of pavement-watering, in particular air temperature and UHI-mitigation effects during heat-waves, and its water footprint in the hope of finding information relevant for dense cities such as Paris, France.

The articles selected for our review describe experiments or computer simulations of watering pavement surfaces at laboratory, street or greater scales. Findings on the benefits of permeable pavements, with or without water-retention, are included when wet and dry performance is compared. Studies of building surface watering are not included unless pavement-watering is part of the watering scheme. Analyses of building-only watering may however provide a useful basis for comparison of certain aspects of our analyses conducted later on.

Several studies answering these criteria have been found and can be split into two major groups: numerical studies (Nakayama and Fujita, 2010; Nakayama et al., 2012; Météo France and CSTB, 2012; Wei and He, 2013) and field studies (Kinouchi and Kanda, 1997, 1998; Yamagata et al., 2008; Takahashi et al., 2010; Li et al., 2013; Bouvier et al., 2013; Maillard et al., 2014), with Kubo et al. (2006) and Nakayama and Fujita (2010) combining both approaches.

These articles were published between 1997 and 2014, reporting results from experiments conducted from 1993 to 2012 (Kinouchi and Kanda, 1997, 1998; Kubo et al., 2006; Yamagata et al., 2008; Nakayama and Fujita, 2010; Takahashi et al., 2010; Bouvier et al., 2013; Maillard et al., 2014), as well as from simulations conducted at the laboratory-, street-, district- or city-scale (Kubo et al., 2006; Nakayama and Fujita, 2010; Nakayama et al., 2012; Météo France and CSTB, 2012; Wei and He, 2013).

It should be noted that the articles by Bouvier et al. (2013) and Maillard et al. (2014) are published in the French professional journal *Techniques, Sciences et Méthodes (TSM)*. Although its peer-review process is not as rigourous as most scientific journals cited in this manuscript, these articles provide recent examples of pavement-watering field trials conducted in two French cities. In addition, certain articles are conference papers (Kinouchi and Kanda, 1998).

In order to make the diversity and differences between the considered studies clearly apparent, we will compare each study by thematic. We will first describe the selected articles and their methodologies. We will then focus on reported cooling effects and the indicators used to quantify them, including micro-climatic, thermal and outdoor comfort parameters.

Tables will be used to facilitate the comparisons, though some information may be not available (NA) or not relevant (NR).

3.1 Brief Description and Methodology

We first provide a brief description of the selected studies as well as of the watering and analysis methods used.

Brief Description

A brief description of each study will now be presented and grouped according to the scale at which cooling effects are investigated.

It should be noted that the articles by Kinouchi and Kanda (1998) and Kubo et al. (2006) can be divided into two parts. First, Kinouchi and Kanda (1998) begin by presenting results published in a previous paper also included in this review (Kinouchi and Kanda, 1997). The second part of the article presents findings on watering a permeable pavement slab which will be discussed in this review. In their article, Kubo et al. (2006) first focus on laboratory findings on different kinds of pavement, while their second approach is a numerical simulation.

Firstly, three studies investigate small scale cooling effects in the lab. This is the case of Kinouchi and Kanda (1998), Kubo et al. (2006), Nakayama and Fujita (2010) and of Li et al. (2013). These studies focus on the effects of watering permeable pavements, though Kubo et al. (2006) also compares pervious pavements with water retaining ones. Both are set in wide open areas with little or no masks. Kubo et al. (2006) use their findings in the lab to conduct a simplified simulation at the street scale in the second part of their article. Nakayama and Fujita (2010) develop and validate a numerical model of the water-retaining pavement material against their observations.

Next, several authors study the effects of street scale cooling. This is namely the case of the simulation conducted by Kubo et al. (2006) as well as the field work conducted by Kinouchi and Kanda (1997, 1998), Yamagata et al. (2008), Takahashi et al. (2010), Bouvier et al. (2013), and Maillard et al. (2014). Kinouchi and Kanda (1997, 1998) and Takahashi et al. (2010) are set in Nagaoka City in

Niigata Prefecture on the West coast of Japan, while the second part of Kubo et al. (2006) and Yamagata et al. (2008) describe watering in Tokyo. Bouvier et al. (2013) and Maillard et al. (2014) respectively take place in Paris and Lyon, France. Both present pavement-watering as a countermeasure for heat-waves. All studies conduct watering on standard impervious pavement surfaces except for Kinouchi and Kanda (1998) and Yamagata et al. (2008) which respectively water permeable and water-retaining pavements. Where solar irradiance data is provided or can be derived, it is apparent that solar masks are low, except for Yamagata et al. (2008) and Maillard et al. (2014).

Finally, three studies analyze cooling effects at the district or city scale (Nakayama et al., 2012; Météo France and CSTB, 2012; Wei and He, 2013). Nakayama et al. (2012) use an urban canopy model of Kawasaki City to simulate the effects of water-retaining pavements combined with urban greening. Météo France and CSTB (2012) study pavement-watering of all of Paris' 2,550 ha of streets and sidewalks using the TEB model, while Wei and He (2013) conduct pavement- and building-watering of a Tokyo district, simulated with their own 3D-CAD model. No changes in material properties are considered in the former, while the latter considers building walls and slanted roofs with a reflective and hydrophilic TiO_2 coating and water-retaining pavement blocks.

As can be seen, most studies found focus on street-scale effects.

Watering Method

Pavement-watering implies the choice of a watering method. The first step involves the choice of a target area. Once it has been defined, every watering method can be characterized by three parameters: the watering period, the watering rate and the watering frequency.

The first outlines the period(s) of each day during which pavement-watering is conducted in order to keep the pavement wet. The second is the average amount of water delivered per unit area and per unit time (expressed in mm/h, equivalent to $L/m^2.h$), averaged over the watering period. Finally, the last indicates the frequency of the watering cycles in the case of discontinuous watering. Of these parameters, the watering rate and period are the ones that define the method's water consumption. Different watering methods are used in the numerical and experimental studies described here.

The different watering methods are summarized graphically in Figure 3.1 based on the information provided by the authors in their articles. We first describe watering conducted in experimental studies.

Kinouchi and Kanda (1997) and Takahashi et al. (2010) use the same snowmelting infrastructure to water an impervious pavement surface. This snowmelting infrastructure consists of watering pipes already present in the streets of Nagaoka City. They are used in winter to melt away accumulated snow and rely on underground water whose temperature is approximately 15°C all year. Kinouchi and

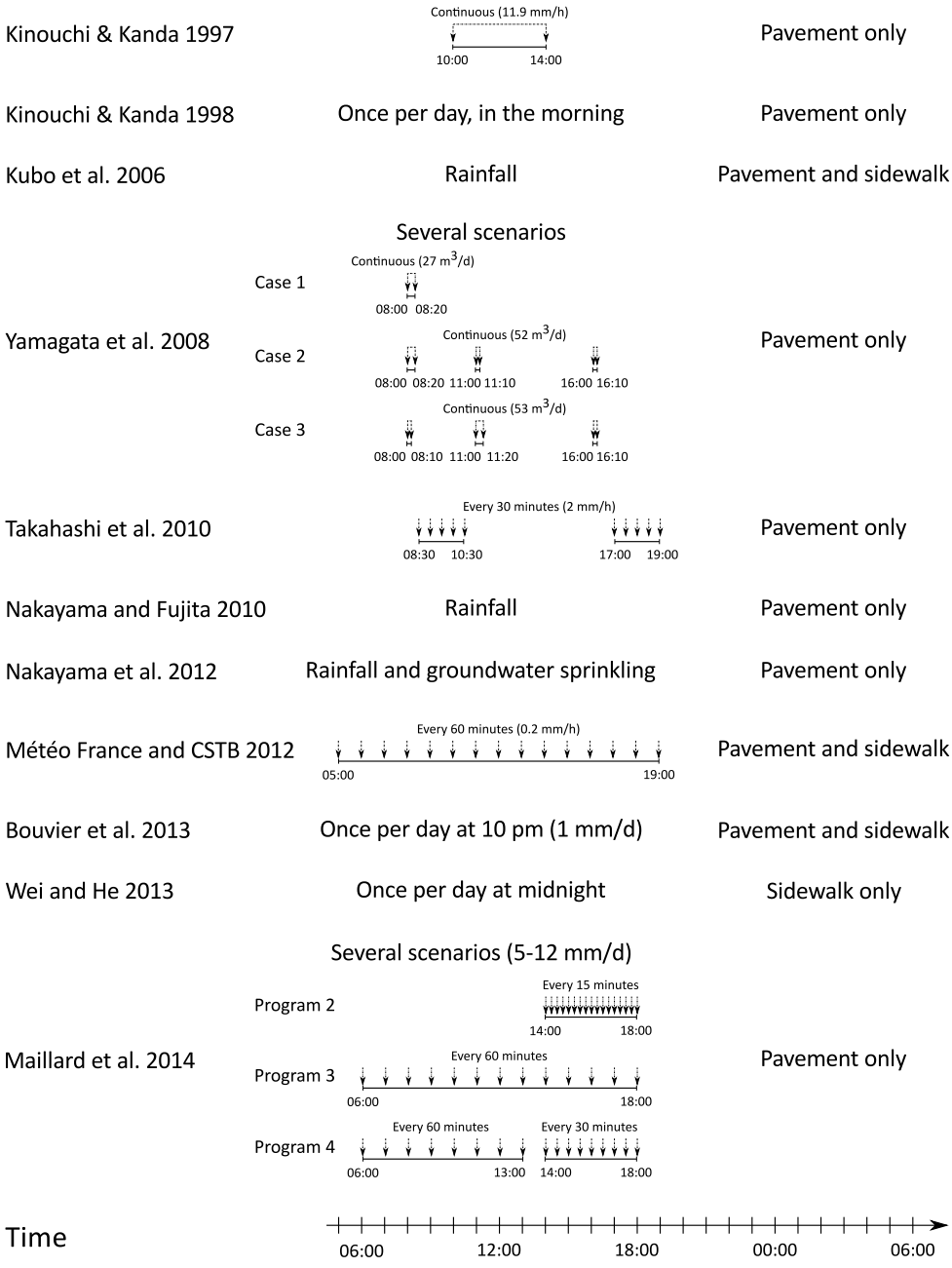

Figure 3.1 – Diagram of the watering methods used in the surveyed articles.

Kanda (1997) run the system continuously at an average rate of 11.9 mm/h, while Takahashi et al. (2010) run it intermittently at an average rate of 2 mm/h.

For the second half of their study, Kinouchi and Kanda (1998) water a porous pavement once a day. Judging from their graphical indications, watering occurs approximately at 9 am. Watered volumes are not known.

For their experimental data, Kubo et al. (2006) and Nakayama and Fujita (2010) rely on rainfall to water their pavement slabs.

Yamagata et al. (2008) install temporary watering pipes in a central road planter to water a water-retaining pavement. The system is run continuously from 10-20 minutes at a time up to three times a day between 6:30 am and 4:10 pm. Total water consumption is provided, but the watered surface area is unknown.

Li et al. (2013) consider impervious and pervious pavement slabs measuring 4 x 4 m. Over an investigation period of 15 days, the pervious pavements are watered once with 0.2 mm after six days.

Bouvier et al. (2013) relies on a cleaning truck and manual operator to water impervious pavement and sidewalk surfaces once at approximately 10 pm. The watering cycle deposits 1 mm of water and is activated if certain weather conditions are met, similar to but less strict than heat-wave conditions for Paris.

Maillard et al. (2014) describe a watering infrastructure integrated into the sidewalk edge. Nozzles connected to the city's potable water network are used to sprinkle the pavement only. The system is operated intermittently following three watering scenarios at different frequencies which vary from every 15 minutes to every 60 minutes. The watering period also varies according to the scenario and occurs between 6 am and 6 pm. The watering rate ranges from 5 mm/d to 12 mm/d.

For their numerical simulation, Kubo et al. (2006) conduct no watering but use the results from their experimental data. More details on their analysis method will be given in the next Subsection.

Nakayama et al. (2012) rely on rainfall and groundwater sprinkling to saturate the water-retaining pavements. No information on the amount of water involved or the watering mechanism is given.

Météo France and CSTB (2012) use a hypothetical infrastructure relying on the Paris' non potable water network to sprinkle 0.2 mm/h every hour from 5 am to 7 pm on pavement and sidewalk.

Wei and He (2013) conduct continuous watering of building walls and roofs between 9 am and 6 pm at a rate of 12 kg/m^2.h. Pavement-watering of the sidewalk is conducted once until saturation at midnight the day before, but applied water volumes are unknown.

As can be seen, varying levels of information are provided. Kinouchi and Kanda (1997), Takahashi et al. (2010) and Météo France and CSTB (2012) for example provide sufficient information to be able to determine all of the watering parameters, while Yamagata et al. (2008), Nakayama et al. (2012) and Maillard et al. (2014) only provide partial data. Finally, Kubo et al. (2006) and Nakayama

and Fujita (2010) use rain events to determine the surface temperature effects of water-retaining permeable pavements in the lab. Only two studies water the sidewalk in addition to the pavement surface (Bouvier et al., 2013; Météo France and CSTB, 2012), while Wei and He (2013) also waters building walls and slanted roofs. Although Yamagata et al. (2008) and Maillard et al. (2014) consider several watering methods, they do not compare the obtained results in these articles.

Of these papers, only Takahashi et al. (2010) and Météo France and CSTB (2012) describe attempts to optimize the watering method. Takahashi et al. (2010) optimize both watering rate and frequency based on surface and 90 cm air temperature observations over a period of one hour after watering. On this basis, it was found that each watering cycle should deliver 1 mm. Their analysis then led them to conclude that watering during the day, between 11 am and 3 pm, was ineffective as no temperature difference could be detected. Finally, the watering frequency was designed to water the pavement as soon as it became completely dry. This resulted in watering roughly every 30 minutes. Météo France and CSTB (2012) base their own optimization on findings from Takahashi et al. (2010) with the hypothesis of a pavement water-holding capacity of 1 mm. They optimize the watering rate based on 2 m a.g.l. air temperature simulations with a one-hour time step. Watering rates are deemed optimal if increasing them further only marginally increases cooling. It should be noted that these analyses are only briefly described in both papers and make no mention of explicit optimization targets or goals.

Analysis Method

We now describe the different methods used to determine the effects of pavement-watering in the selected literature.

Numerical Studies First, it should be noted that Kubo et al. (2006) only indirectly simulate watering effects. Indeed, water evaporation or advection are not integrated into their model, which only includes air flows and sensible heat exchanges. The effects of watering are accounted for in the form of surface temperature reductions, as they were observed in the experimental portion of their study. They therefore simulate the atmospheric effects of a 10°C reduction in pavement and sidewalk temperatures. On the contrary, Nakayama et al. (2012), Météo France and CSTB (2012) and Wei and He (2013) simulate water evaporation in their studies.

All of the numerical studies considered compare a single area in two states: with and without watering. As a result, any difference in the considered indicators can be unquestionably attributed to their watering strategy.

Experimental Studies Laboratory-scale studies directly compare the same pavement area in dry and wet conditions, accounting for significant changes in solar irradiance from one day to the next (Kinouchi and Kanda, 1998; Nakayama and

Fujita, 2010; Kubo et al., 2006; Li et al., 2013). No studies basing their analyses on comparisons of a control slab with a watered one were found.

In all of the considered field trials at the street scale, the methodology applied to determine micro-climatic effects is a direct comparison between case and control site measurements. Indeed, Kinouchi and Kanda (1997), Yamagata et al. (2008), Bouvier et al. (2013) and Maillard et al. (2014) base their analyses on the differences observed between a watered area and an unwatered one. Takahashi et al. (2010), though they use average observations from several watered and unwatered weather stations, proceed in the same manner. In all cases, the observed difference between watered and control sites is interpreted as the effect of pavement-watering. Since this method does not account for preexisting differences between sites, site pairs must be chosen carefully.

3.2 Cooling Effects of Pavement-Watering

We now proceed to present the cooling effects reported in the selected literature. The cooling effects of pavement-watering are measured using a variety of indicators to quantify micro-climatic and thermal effects.

Micro-climatic Indicators

Micro-climatic parameters used to study the effects of pavement-watering include air temperature, relative humidity, globe temperature and MRT. In addition, thermal comfort and UHI-mitigation indicators are also used.

In terms of frequency, air temperature is used most often, while globe temperature and MRT are least represented, though they are often included in the calculation of thermal comfort indexes.

Air Temperature Air temperature is widely used in the articles we have selected. Table 3.1 provides a summary of the air temperature effects provided as well as the instrument type and measurement height used, when indicated.

Table 3.1 – Reported air temperature effects.

Author	Instrument	Height	Max
Kinouchi and Kanda (1997)	Pt resistance	1 m	-1°C
Yamagata et al. (2008)	NA	0.5 m	-2.5°C
Takahashi et al. (2010)	NA	0.9 m	-4°C
Bouvier et al. (2013)	NA	2 m	-0.4°C
Kubo et al. (2006)	numeric	1.5 m	-0.73°C
Kubo et al. (2006)	numeric	0.5 m	-2.13°C
Nakayama et al. (2012)	numeric	1.5 m	-5°C
Météo France and CSTB (2012)	numeric	2 m	-2°C

As can be seen, reported maximum effects span from -0.4°C to -5°C. Only Bouvier et al. (2013) indicate that cooling lasts up to one hour after watering. No other papers provide information on the duration of the effects or on their average intensity.

Among experimental studies, only Kinouchi and Kanda (1997) describe the instrument used to measure air temperature and its properties. Information on its uncertainty, height and measurement frequency as well as manufacturer and model is provided. When relevant information is available (description, photograph, ...), it is clear that the instruments used in the selected papers are sheltered.

In addition to a wide variety of reported air temperature effects, very few studies have comparable measurement heights, making it difficult to compare findings from one study to the next. It is therefore not possible for us to determine a general trend for the air temperature effects of pavement-watering.

Air Humidity Air humidity is not as widely represented in the literature as air temperature. It is considered by Kinouchi and Kanda (1997), Bouvier et al. (2013) and Météo France and CSTB (2012) who investigate changes in RH. Their findings are presented in Table 3.2.

Table 3.2 – Reported air humidity effects.

Author	Instrument	Height	Max
Kinouchi and Kanda (1997)	capacitive hygrometer	1 m	+4%
Bouvier et al. (2013)	NA	2 m	+4%
Météo France and CSTB (2012)	numeric	2 m	a few %

As was the case for air temperature, only Kinouchi and Kanda (1997) provide details on the instrument used. Similarly, available information indicates that instruments are sheltered.

The two experimental studies report identical results despite significant differences in measurement height. This may be attributable to differences in watering method (see Section 3.1).

All three papers indicate that pavement-watering results in an increase in RH in the order of a few percentage points.

Radiative Environment Apart from air temperature and humidity, indicators representative of the radiative environment have also been used to quantify the effects of pavement-watering, such as MRT and globe temperature. Only two studies include these parameters (Kinouchi and Kanda, 1997; Wei and He, 2013). Their results are presented in Table 3.3.

Unlike the cases of air temperature and humidity measurements, Kinouchi and Kanda (1997) do not specify what kind of globe thermometer is used.

Table 3.3 – Reported effects on the radiative environment.

Author	Parameter	Height	Max
Kinouchi and Kanda (1997)	globe temperature	1 m	-4°C
Wei and He (2013)	MRT	1.5 m	-6°C

As globe temperature (T_g) is determined by the balance between radiative heat gains and radiative and convective heat losses, the latter depending on air temperature (T_a) and wind speed (v). Therefore, air temperature and wind speed measurements at the same height as the globe thermometer permit the calculation of MRT from globe temperature. The standard formula is given by ASHRAE (2001), as described by Thorsson et al. (2007), with D being the diameter (in mm) of the globe:

$$T_{mrt} = \left((T_g + 273.15)^4 + \frac{1.1 \times 10^8 v^{0.6}}{\epsilon D^{0.4}} \times (T_g - T_a) \right)^{0.25} - 273.15 \quad (3.1)$$

Following this method, globe temperature is measured by a globe thermometer made of a matte black-painted copper globe 150 mm in diameter, 0.4 mm in thickness and instrumented with a Pt100 resistance thermometer in its center. This sensor has a 20 minute response time after which isothermal conditions inside the globe are obtained.

Alternative designs with shorter response times involve replacing the copper globe with a ping pong ball which are 40 mm in diameter (formerly 38 mm) and made of acrylic. In addition, the ratio of convective-to-radiative exchanges is deemed more representative of a human and therefore more appropriate (Wang and Li, 2015). The reliability of ping pong balls as globe thermometers have been investigated by de Dear (1987), as cited by Thorsson et al. (2007) and Wang and Li (2015). In principle, the equation 3.1 remains valid accounting for the change in diameter.

Another alternative design is the so-called grey globe developed by Thorsson et al. (2007) which also uses a ping pong ball and whose albedo is deemed more representative of that of a clothed pedestrian. To achieve this, the ping pong ball is simply painted flat grey. An accompanying modified formula is proposed by Thorsson et al. (2007) to calculate MRT from the grey ping pong globe thermometer:

$$T_{mrt} = \left((T_g + 273.15)^4 + \frac{1.335 \times 10^8 v^{0.71}}{\epsilon D^{0.4}} \times (T_g - T_a) \right)^{0.25} - 273.15 \quad (3.2)$$

This design has caught the attention of many researchers interested in quantifying outdoor thermal comfort. Indeed, one can note more than 90 references to their article by other authors according to Scopus as of June 6th, 2015.

However, the choice of plastic or other low conductivity materials as a globe material has been called into question recently in regards to their poor performance under asymmetric radiation (Fontana, 2010; Wang and Li, 2015). Wang and Li (2015) compare two 40 mm black globe thermometers, one copper and the other acrylic in identical conditions which include asymmetrical radiation. Their findings reveal the serious shortcomings of acrylic globes in comparison to copper ones. These are mainly associated with acrylic's poor thermal conductivity and its poor opacity, even when painted. These issues undermine the hypothesis of isothermal conditions inside the globe and expose the Pt100 resistance thermometer to transmitted radiation.

Indicators of UHI-Mitigation Effects Another micro-climatic indicator used in the selected articles is that of UHI-mitigation effects. These were investigated by Météo France and CSTB (2012) and Wei and He (2013). Météo France and CSTB (2012) define their UHI-mitigation index as the comparison of average air temperature measured 2 m and 30 m a.g.l. between 3 and 6 am (local daylight savings time: UTC+2) from August 8th to 13th, 2003 with and without watering. Wei and He (2013) use an indicator called heat island potential (HIP) which reflects the average temperature difference between urban surfaces and the atmosphere. Therefore, a positive HIP indicates that urban surface temperatures are warmer on average than that of the ambient air. Wei and He (2013) compare HIP with and without watering. Reported results are presented in Table 3.4.

Table 3.4 – UHI-mitigation effects.

Author	Parameter	Height	Max
Météo France and CSTB (2012)	UHI-mitigation	2 m	-0.5°C
Météo France and CSTB (2012)	UHI-mitigation	30 m	NA
Wei and He (2013)	HIP	NR	-25°C

In addition to the differences in watering strategies, these two indicators are too different for findings from these articles to be compared. It should be noted that pavement-watering following Météo France and CSTB (2012)'s scenario reduces UHII by -0.5°C 2 m a.g.l. while no effect is detectable 30 m a.g.l.. In short, the vertical permeation of pavement-watering cooling is limited.

Thermal Comfort Indicators Several of the considered studies take thermal comfort effects into account as well. Among them, Wet-Bulb Globe Temperature (WBGT) is the most represented thermal comfort index, and is calculated on the basis of dry- (T_a) and wet-bulb ($T_{wet-bulb}$ air temperatures as well as black globe temperature as defined by Azer and Hsu (1977) for outdoor (equation 3.4) and indoor conditions or in the absence of solar radiation (equation 3.4):

$$WBGT = 0.7T_{wet-bulb} + 0.2T_g + 0.1T_a \quad (3.3)$$
$$WBGT = 0.7T_{wet-bulb} + 0.3T_g \quad (3.4)$$

Kinouchi and Kanda (1997, 1998) use three different comfort indexes: the Discomfort Index, Thermal Load and Thermal Sensation. Few details are given on these indexes and their supporting papers are in Japanese preventing us from us from obtaining further details. The only information available is that the Discomfort Index is calculated from air temperature and RH, while the Thermal Load estimates the energy budget of a human being on the basis of the heat gains from received radiation and metabolic rate and the heat losses from LW radiation emission and convective and latent heat fluxes.

The reported thermal comfort effects of pavement-watering are summarized in Table 3.5.

Table 3.5 – Reported thermal comfort effects.

Author	Parameter	Height	Max
Kinouchi and Kanda (1997)	Discomfort Index	1 m	-
Kinouchi and Kanda (1997)	Thermal Load	NR	-10 W/m^2
Kinouchi and Kanda (1998)	Thermal Sensation	NR	-3°C
Yamagata et al. (2008)	WBGT	0.5 m	-2°C
Maillard et al. (2014)	WBGT	1.5 m	-0.5°C

All findings indicate that pavement-watering positively affects pedestrian thermal comfort. Due to differences in indexes and measuring heights, it is not possible to compare findings in further detail.

A recent indicator used more and more frequently in articles investigating outdoor thermal comfort is the UTCI (Musy et al., 2014; Fröhlich and Matzarakis, 2014). UTCI was developed by international experts from Commission 6 of the International Society of Biometeorology and European COST Action 730 from the year 2000 to 2009. Its purpose is to offer a universal thermal comfort index that can be used for both cold and warm conditions for a wide variety of applications and that takes advantage of the most recent developments in biometeorology (Blazejczyk et al., 2010).

Air temperature, humidity, wind speed and MRT are used in conjunction with certain assumptions on the metabolic activity and clothing of pedestrians to calculate an equivalent air temperature for reference conditions which would create an identical physiological response to the real case (Blazejczyk et al., 2010). The equivalent temperature scale is divided into bands corresponding to thermal stress levels.

The source code for UTCI is freely available as well as a fast-calculation script written by Peter Bröde in 2009 (Bröde, 2009).

Other outdoor indexes such as Perceived Temperature (PT) or Physiological Equivalent Temperature (PET) and also function on the basis of an equivalent temperature in reference conditions on the basis of an energy budget model of the human body (Mayer and Höppe, 1987; Staiger et al., 2012; Fröhlich and Matzarakis, 2014).

Thermal Indicators

The thermal effects of pavement-watering have been a recurrent focus point of the reviewed studies. These include pavement temperatures and heat fluxes at different depths. Data is generally gathered from infrared (IR) camera or thermocouple and flowmeter measurements.

Surface Temperature Surface temperature reductions are often reported and have been found to range from 8°C to 30°C (Kinouchi and Kanda, 1997, 1998; Yamagata et al., 2008). Table 3.6 summarizes the effects reported in the selected literature.

Table 3.6 – Reported pavement surface temperature effects.

Author	Instrument	Height	Max
Kinouchi and Kanda (1997)	IR thermometer	1 m	-10° to -30°C
Kinouchi and Kanda (1998)	Net radiometer	65 cm	-14° to -18°C
Kubo et al. (2006)	Thermocouple	0 cm	-16.4°C
Yamagata et al. (2008)	IR camera	NA	-3° to -8°C
Nakayama and Fujita (2010)	NA	0 cm	-5° to -20°C
Bouvier et al. (2013)	IR camera	NA	-6°C
Maillard et al. (2014)	NA	-1 cm	-5°C
Wei and He (2013)	numeric	NR	-5°C

Kinouchi and Kanda (1997) report the highest maximum temperature reductions, however four measurement points were used. Results from these points range from -10° to -30°C. This broad range reflects their watering method. Indeed, the snow-melting pipes are laid in the center of the road and deliver water at a constant 15°C. Surface temperature reductions are therefore highest at the center of the road where surface temperatures reached 17°C, while the lowest reductions are observed near the sidewalk with surface temperatures of 35°C. Nakayama and Fujita (2010) report results ranging from -5° to -20°C depending on the reference material (grass, concrete, ...). No comparison of the same material in dry and wet conditions is made.

Taking this into account, we conclude that the selected studies agree on a surface temperature reduction of approximately 10°C under insolation. Nighttime reductions are reported by a few authors and range from -3°C to -6°C (Yamagata et al., 2008; Bouvier et al., 2013; Wei and He, 2013).

Pavement Temperature No papers focusing solely on the watering of impervious street surfaces were found that report pavement temperature observations. Kinouchi and Kanda (1998) report temperature effects 5 cm below the pavement surface and Li et al. (2013) investigate effects 1.3 cm, 3.8 cm, 6.4 cm and 25.4 cm deep for two different permeable pavements compared to a standard impervious pavement. Reported findings are summarized in Table 3.7.

Table 3.7 – Reported pavement temperature effects.

Author	Instrument	Depth	Max
Kinouchi and Kanda (1998)	Thermocouple	5 cm	-7°C
Li et al. (2013)	Type-T thermocouple	1.3 cm	-7°C
Li et al. (2013)	Type-T thermocouple	3.8 cm	-12°C
Li et al. (2013)	Type-T thermocouple	6.4 cm	-14°C
Li et al. (2013)	Type-T thermocouple	25.4 cm	-15°C

Maximum effects described by Li et al. (2013) are higher than those reported by Kinouchi and Kanda (1998) and are greater the deeper they are measured. This may be caused by differences in measurement frequency and initial water temperature. Indeed, average effects reported by Li et al. (2013) are much lower than those which are apparent from Kinouchi and Kanda (1998)'s data. Unfortunately, insufficient information is provided in either study to investigate this further.

Latent Heat Flux Four studies estimate or measure the latent heat flux created by pavement-watering (Kinouchi and Kanda, 1997; Yamagata et al., 2008; Nakayama et al., 2012; Météo France and CSTB, 2012). Their findings are summarized in Table 3.8. It should be noted that the latent flux is estimated both experimentally and numerically by Nakayama et al. (2012). The method used for the former estimation is not provided.

Table 3.8 – Reported latent heat flows.

Author	Instrument	Max
Kinouchi and Kanda (1997)	Energy balance	1,300 W/m^2
Kinouchi and Kanda (1997)	Gradient method	400 W/m^2
Kinouchi and Kanda (1998)	estimated	600 W/m^2
Yamagata et al. (2008)	Evaporation gauge	1,850 $kJ/m^2.d$
Nakayama et al. (2012)	NA	337 W/m^2
Nakayama et al. (2012)	numeric	345 W/m^2
Météo France and CSTB (2012)	numeric	180 W/m^2

Kinouchi and Kanda (1997) use two methods to determine the latent flux on the basis of their measurements: from the energy balance and from the gradient method. The former uses measurements of the heat flow into the pavement at its surface. As they encountered difficulties with this measurement, their second estimation is deemed more reliable and agrees better with other authors. On average during watering, the latent heat flux determined by the gradient method is in the order of 200-300 W/m^2, with a localized peak of 400 W/m^2.

Kinouchi and Kanda (1997), Nakayama et al. (2012) and Météo France and CSTB (2012) report similar results. Because Yamagata et al. (2008) presents daily latent energy transfers, it is difficult to compare their findings with those of the other authors.

Pavement Heat Flux Kinouchi and Kanda (1997, 1998) are alone in reporting the pavement heat flux effects of pavement-watering. Kinouchi and Kanda (1997) attempt to measure the downwards heat flux at the surface with a heatflowmeter but encounter difficulties, while Kinouchi and Kanda (1998) place their heatflowmeter 5 cm below the surface of a pervious pavement slab. Their findings are summarized in Table 3.9.

Table 3.9 – Reported pavement heat flux effects.

Author	Instrument	Depth	Max
Kinouchi and Kanda (1997)	Heatflowmeter	0 cm	-1,300 W/m^2
Kinouchi and Kanda (1998)	Heatflowmeter	-5 cm	-50 W/m^2

As watering begins, Kinouchi and Kanda (1997) report a "nose-dive" in pavement heat flux in the order of 1,300 W/m^2 followed by smaller effects thereafter, even negative at times. Judging by their graph, Kinouchi and Kanda (1998) observe a halving of pavement heat flux 5 cm below the pavement surface, i.e. a reduction in the order of 50 W/m^2.

In addition, Kinouchi and Kanda (1998) analyze a linear relation found between pavement heat flux 5 cm deep and net radiation.

3.3 Conclusion

As can be seen, twelve articles investigating the effects of pavement-watering have been found. Among them, a wide variety of cooling indicators are used, including micro-climatic and thermal indicators. Several watering methods were described in varying detail, however few efforts to optimize them and their water consumption were reported. Finally, only Bouvier et al. (2013) focus on the method's effectiveness during heat-waves.

Overall, surface temperature reductions under insolation showed good agreement and comparability between studies, with reported reductions of approxi-

mately -10°C. In addition, RH 1-2 m a.g.l. is reported to increase by a few percentage points.

Unfortunately, the other reported micro-climatic effects are not comparable due to significant differences in measurement heights, instruments and analysis methods. This issue was previously identified by Johansson et al. (2014) and may hide other ones potentially caused by site- or climate-specificities. Also, the limited number of studies investigating these effects makes more evidence necessary to confirm them.

Furthermore, the reliability of the analysis method used to determine micro-climatic effects in the field is unclear. Indeed, the analyses are based on the direct comparison of micro-climatic measurements made at case and control areas. This method tacitly assumes that inter-area differences are equal to zero in the absence of watering. Given the complexity of urban environments, this hypothesis may not be valid in cities where pavement-watering is most likely to be implemented and raises questions as to the reliability of findings from field experiments. Because other UHI-countermeasures have only rarely been studied in the field, no other method in the literature is known to us.

Another limitation is the applicability of reported micro-climatic effects to dense cities and in European climates. Indeed, studies have chiefly been conducted in low density cities in Japan, under its humid and hot summers. Nagaoka City, which has a population density of approximately 300 persons/km^2 (`www.city.nagaoka.niigata.jp`), is much less dense than Paris' 21,000 persons/km^2 (`www.insee.fr`) meaning that results may not be valid for dense cities. This also the case of thermal effects which have mainly been studied in unmasked conditions, as can be derived from solar irradiance data in the considered articles (Kinouchi and Kanda, 1997, 1998; Kubo et al., 2006; Nakayama and Fujita, 2010; Li et al., 2013).

Finally, existing efforts to optimize the applied watering methods are insufficient. Indeed, an optimization method should be formally described with the definition of clear targets and goals.

Table 3.10 summarizes the type, i.e. experimental (exp.) or numeric (num.), and the micro-climatic and thermal indicators used by the different articles reviewed.

Having conducted our review of the existing literature and identified remaining knowledge gaps, we now propose corresponding research questions.

Table 3.10 – Literature review summary.

		Micro-climatic Indicators					Thermal Indicators			
Author	Type	T_a	RH	MRT/T_g	UHI	Thermal Comfort	T_{surf}	$T_{pavement}$	lE	V
Kinouchi and Kanda (1997)	exp.	×	×	×		×		×	×	×
Kinouchi and Kanda (1998)	exp.						×	×	×	×
Yamagata et al. (2008)	exp.	×				×	×		×	
Takahashi et al. (2010)	exp.	×								
Nakayama and Fujita (2010)	exp.						×			
Li et al. (2013)	exp.							×		
Bouvier et al. (2013)	exp.	×	×				×			
Maillard et al. (2014)	exp.					×	×			
Kubo et al. (2006)	num.	×								
Nakayama et al. (2012)	num.	×							×	
Météo France and CSTB (2012)	num.	×	×		×				×	
Wei and He (2013)	num.			×	×		×			

CHAPTER 4

Knowledge Gaps and Remaining Research Questions

Several aspects related to the study of cool pavements used to improve thermal comfort or to counter UHI have been covered in Chapter 2. While thermal effects, generally pertaining to surface temperature, pavement temperature or pavement heat flux effects, have been vastly analyzed both in the lab and in the field, micro-climatic effects have seldom been studied experimentally.

In this last regard, pavement-watering stands out among UHI countermeasures. Indeed, its micro-climatic effects have been studied in the field on a number of occasions (Kinouchi and Kanda, 1997; Yamagata et al., 2008; Takahashi et al., 2010; Bouvier et al., 2013; Maillard et al., 2014), in addition to work on its thermal effects (Kinouchi and Kanda, 1997, 1998; Kubo et al., 2006; Nakayama and Fujita, 2010; Li et al., 2013; Bouvier et al., 2013; Maillard et al., 2014). However, several limitations of varying gravity have been identified. These are related to how representative their experimental conditions are of dense urban areas, to their relatively small number and difficult comparability. This leaves much uncertainty as to the validity of reported pavement-watering effects and its water footprint.

To address this, we propose to pursue the following research questions for dense urban environments in heat-wave conditions, using Paris as a case study:

- Can the direct comparison method be reliably used to evaluate the real-world effects of anti-UHI techniques?
- What micro-climatic effects can be expected of pavement-watering?
- What are the UHI-mitigation effects of pavement-watering?
- What can be said of the thermal effects of pavement-watering?

- Finally, how much water is required for pavement-watering and how can its watering efficiency be improved?

The answers to these questions will help complete the identified knowledge gaps and reinforce previous findings.

Our results will inform decision-makers on the costs and benefits of pavement-watering when it is applied to dense urban areas during heat-waves. This information is crucial for cities interested in including the method in their UHI-mitigation and/or climate change adaptation strategy.

To answer these questions, measurements obtained by a pavement-watering experiment conducted at two sites in Paris, France over the summers of 2013 and 2014 will be analyzed. Part 1 will focus on the microclimatic effects of pavement-watering. Part 2 will study the thermal effects of pavement-watering. Finally, Part 3 will analyze how sprinkled water contributes to observed cooling and propose ways to improve the watering efficiency of pavement-watering.

The chapters included in Parts 1, 2 and 3 are based on the peer-reviewed work published in *Applied Thermal Engineering*, *Urban Climate* and the *Journal of Sustainable Development of Energy, Water and Environment Systems* in 2014 and 2015 (Hendel et al., 2014, 2015a,b), and work currently being reviewed by *Urban Climate* (Hendel et al., 2015).

Part 1

MICRO-CLIMATIC EFFECTS OF PAVEMENT-WATERING

CHAPTER 5

Introduction to Part 1

Countermeasures to the UHI effect are of growing interest to decision makers. Certain measures have been encouraged or made mandatory for new buildings through local legislation or regulation, such as California's Title 24 in the case of cool roofs (California Energy Commission, 2010). Such policies are supported by the growing scientific literature on the topic of UHI countermeasures previously discussed, yet proper evaluation tools are required in order to analyze their effectiveness in the field. Indeed, actual measurements of the atmospheric effects of UHI countermeasures are of great importance to the scientific community, to help validate simulation models for instance, but also for decision-makers who wish to evaluate the effectiveness of anti-UHI policies.

To date, cool materials, which can be reflective, permeable or covered with low vegetation such as grass, have been thoroughly studied in the lab or on small-scale prototypes (Li et al., 2013; Karlessi et al., 2011; Kubo et al., 2006; Levinson et al., 2007; Takebayashi and Moriyama, 2007, 2009). Results indicate that surface temperatures are significantly reduced compared to standard materials. This in turn is expected to result in lower contributions to urban heating as sensible heat flows are reduced following lower urban surface temperatures. Equivalent work on green spaces has mostly focused on existing parks (Jauregui, 1990; Ca et al., 1998), though smaller scale testing has also been conducted (Spronken-Smith and Oke, 1999). Parks have been found to be up to a few degrees cooler than their surroundings through the combined effects of evapotranspiration and shading. However, field evaluations and monitoring of large-scale applications of cool materials or new urban green spaces are scarce (Santamouris, 2013; Bowler et al., 2010). Indeed, large-scale micro-climatic effects have been almost exclusively studied with the help of computer simulations (Akbari et al., 2001; Nakayama et al., 2012; Météo France and CSTB, 2012; Wei and He, 2013).

Pavement-watering stands out as an exception and has been studied in the field via several independent studies (Kinouchi and Kanda, 1997, 1998; Yamagata et al.,

2008; Takahashi et al., 2010; Bouvier et al., 2013; Maillard et al., 2014). This technique, consisting of spraying water onto an impervious or a permeable pavement surface, is viewed as an efficient means of reducing UHI intensity. Known locally as "Uchimizu", Japan has traditionally practiced pavement-watering for centuries up to this day (Japan Water Forum, 2015). Scientific work began in the 1990's with the use of preexisting pavement-watering installations in Nagaoka City (Kinouchi and Kanda, 1997, 1998) or block-scale demonstrators in Tokyo (Yamagata et al., 2008). More recently, the city services of Paris or Lyon have conducted their own field studies with the use of cleaning trucks or watering infrastructure prototypes (Bouvier et al., 2013; Maillard et al., 2014). In France and especially Paris, the predicted increases in heat wave intensity and frequency due to climate change (Lemonsu et al., 2013), combined with the high sensitivity of dense cities to such episodes (Robine et al., 2008; Li and Bou-Zeid, 2013), have focused efforts on the development of appropriate adaptation tools.

In all of these cases, the methodology applied is a direct comparison between case and control measurements. The observed interstation difference is thus interpreted as the effect of pavement-watering. This analysis method implies that interstation differences in the absence of watering are equal to zero for the studied micro-climatic parameters. However, given the complexity of urban environments this hypothesis may not be applicable in cities where UHI countermeasures will be implemented.

This Part uses a pavement-watering experiment conducted in Paris, France during the summers of 2013 and 2014 to determine the suitability of the direct comparison method to measure the field effects of UHI countermeasures in cities. In the process, further light will be shed on the effects of pavement-watering on micro-climatic parameters and pedestrian thermal comfort in the field. Through this case study, we will demonstrate that the frequently-seen direct case-control comparison is not suited to dense urban environments and we will propose an alternative interpretation method. Focus will be set on the methodological difficulties encountered during the analysis of collected data and the alternatives that we developed to overcome them. The resulting methodology can be generalized to all UHI countermeasures if sufficient time is available to study the micro-climatic conditions present before the countermeasure is put into place. The work presented in this Part is based on the work submitted to *Urban Climate* currently being peer-reviewed (Hendel et al., 2015).

The initial methodology will first be described in Chapter 6. Chapter 7 will then present the results of the analysis and reveal the shortcomings of the direct comparison method. An alternative analysis method will be proposed and tested in Chapter 8.

CHAPTER 6

Methodology

The following chapter will describe the method adopted for the analysis conducted in this Part. Certain aspects of the field experiment useful for Parts 2 and 3 will also be presented.

As noted previously in the literature review (see Chapter 3), most previous work has studied the effects of watering only pavement surfaces, leaving the sidewalks untreated (Kinouchi and Kanda, 1997, 1998; Yamagata et al., 2008; Takahashi et al., 2010; Maillard et al., 2014). Yet, pedestrians mostly use sidewalks and should therefore benefit significantly from sidewalk watering in addition to pavement watering. We therefore set out to test both methods at the two different sites.

6.1 Location

Local micro-climatic data was recorded during the summers of 2013 and 2014 on the rue du Louvre, located near Les Halles at the edge of the 1st and 2nd Arrondissements, and on two streets, rue Lesage and rue Ramponeau, near Belleville in the 20th Arrondissement. Both sites will be respectively referred to as the Louvre and Belleville sites hereafter. Site positions within Paris are illustrated in Figure 6.1.

These test sites were selected within Paris' municipal borders in order to maximize UHI intensity. Other factors were also taken into account in order to filter out other influences and facilitate the detection of the pavement-watering effect. Each pair was therefore selected following strict criteria, including a minimum distance between case (watered) and control (dry) stations (10 times street width at least), minimal immediate presence of vegetation, identical street orientations, canyon aspect ratios and street widths. Pairs were also chosen so that the urban materials around them, e.g. roads or building façades, were as similar as

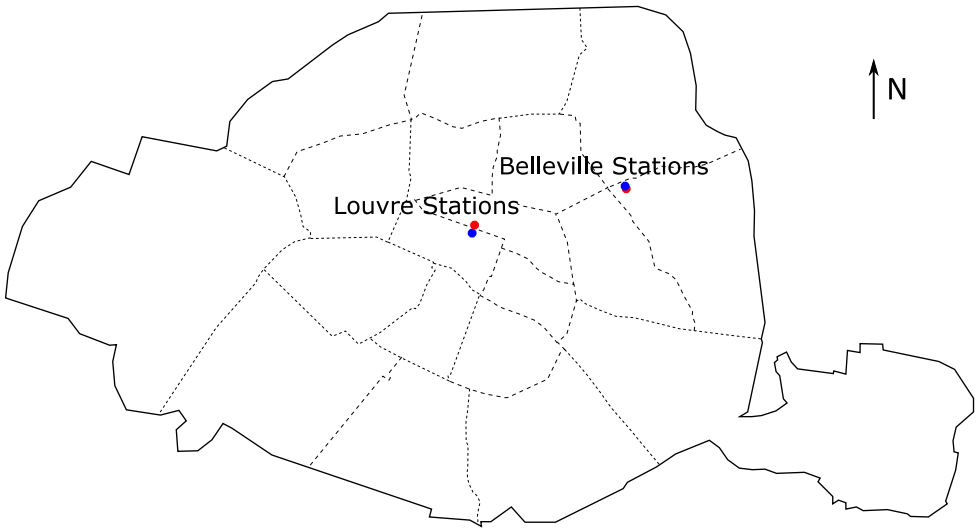

Figure 6.1 – Position of Experimental Sites in Paris

possible. Road traffic, surrounding parks and vegetation, station shading and topography were also controlled for. These criteria narrowed down the areas where the experiment could take place.

Following the Blue Paper's recommendations (Paris City Council, 2012a), a selection criterion was included for watering to be conducted autonomously and directly from the existing non-potable water network with minimal modification, e.g. a temporary watering pipe installed a few days prior to watering. This condition excluded candidate sites where network water pressure was low. Furthermore, the temporary watering pipe required a site with limited pedestrian and road traffic to avoid disturbance or damage and proximity with a facility where it could be stored between watering campaigns. Field investigations revealed that these criteria were met at the Belleville site, located near the Engineering School of the City of Paris (EIVP). Because watering at Belleville would be continuous and largely unsupervised, only the pavement was watered to avoid watering pedestrians as well as flooding and damage to adjacent buildings.

Since the sidewalk at the Belleville site was not watered, the Louvre site was selected where pavement and sidewalk were watered with a cleaning truck and manual operator (see Section 6.2).

Watered and control weather station positions are illustrated in Figure 6.2. Two twin weather stations were positioned for each site, each pair measuring identical parameters. Thermal effects were only observed at the rue du Louvre site.

Louvre stations were positioned approximately 200 meters apart in the same street, while the Belleville stations were positioned in two parallel streets, rue Lesage and rue Ramponeau. In terms of road materials, impervious asphalt concrete approximately 16 cm deep is laid on a 16 cm cement-treated base at the

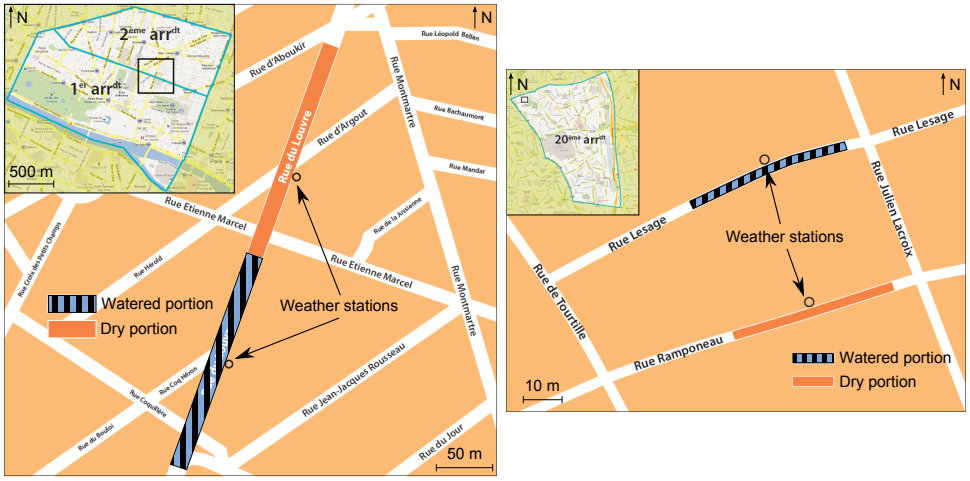

Figure 6.2 – Station Positions at the Louvre (left) and Belleville (right) Sites

Louvre stations. At the Belleville stations, different cobblestones are used at the watered and control sites, with sandstone pavers at the case and granite pavers at the control. While the Louvre site is representative of Paris' more recent large avenues and streets, the Belleville site is an example of Paris' older narrow streets.

Rue du Louvre, rue Lesage and rue Ramponeau have an aspect ratio approximately equal to one (H/W=1). Rue du Louvre has a N-NE−S-SW orientation, while at Belleville both streets have an E-NE−W-SW orientation.

In order to evaluate the quality of the resulting match between stations, Figure 6.3 compares solar irradiance measurements 4 m a.g.l. at the case and control stations for Louvre and Belleville on a cloudless day, July 14th, 2013.

While solar irradiance measurements at the Louvre stations are highly consistent with each other, significant differences are visible between the Belleville stations, occurring from 9 am to 2 pm and from 5 pm to 6 pm. Imperfectly matched building heights and slight differences in street orientation between paired stations are thought to explain them. In addition, another contributor to differences at Belleville not visible with solar irradiance measurements is a street sign directly South of the control station which shaded the globe thermometer a few hours a day at midday over the summer period. This sign should have been removed after station installation by the city services but in reality never was.

Overall, the match between stations is much better for Louvre than for Belleville.

6.2 Watering Method

The adopted pavement-watering method was designed on the basis of previous work by Kinouchi and Kanda (1997, 1998); Yamagata et al. (2008); Takahashi et al. (2010); and Bouvier et al. (2013).

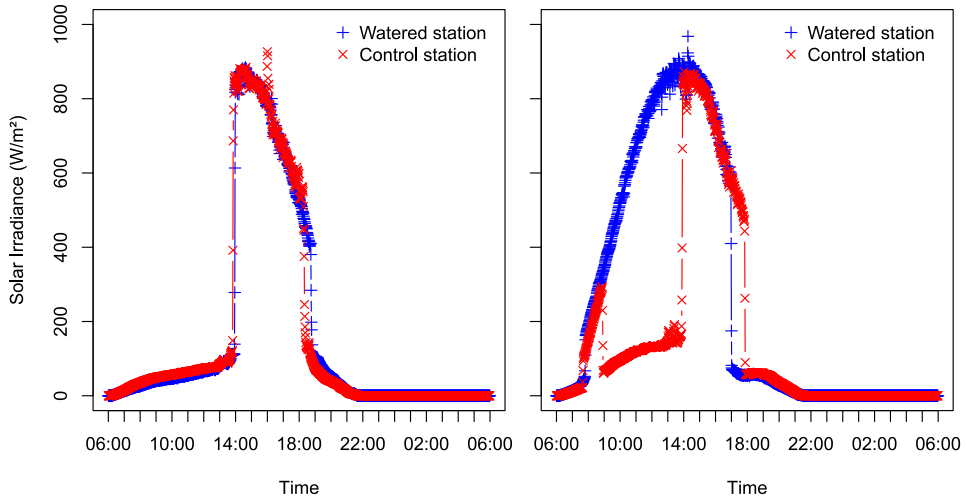

Figure 6.3 – Solar irradiance at Louvre (left) and Belleville (right) on July 14th 2013

Weather conditions

Ideally, since the goal is to study the effects of pavement-watering in heat wave conditions, watering trials should be undertaken during a heat wave. However, only two heat-wave warning days occur during the average Parisian summer (Lemonsu et al., 2013). Requiring strict heat-wave warning days would therefore mean running the risk of severely reducing the number of watered days. The weather conditions used to begin pavement-watering were thus loosened, including air temperature, wind speed and sky conditions. They are presented in Table 6.1 and are calculated on the basis of Météo-France's three-day forecast. The conditions for heat-wave warnings in Paris are also presented. BMI_{Max} and BMI_{Min} refer to the 3-day mean of daily maximum T_x and minimum T_n air temperatures.

Table 6.1 – Weather conditions required for pavement-watering and heat-wave warnings (Hendel et al., 2015a)

Parameter	Pavement-watering	Heat-wave warning level
T_n	$BMI_{Min} \geq$ 16°C	$\geq$ 21°C
T_x	$BMI_{Max} \geq$ 25°C	$\geq$ 31°C
v	$\leq$ 10 km/h	-
Sky conditions	Sunny (less than 3 oktas cloud cover)	-

Water Sprinkling Technique

Figure 6.4 indicates the watering method applied at both sites. Watering frequency, period and rate are provided as well as the targeted surface areas and the ratio of watered-to-total width between parentheses.

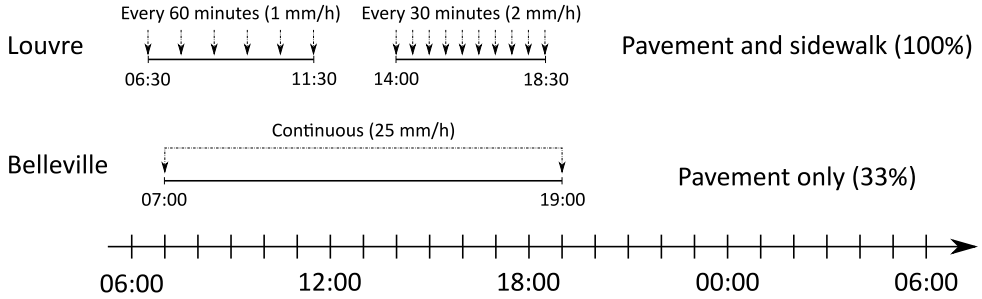

Figure 6.4 – Diagram describing the applied watering method at both sites.

On rue du Louvre, cleaning trucks were used to sprinkle approximately 1 mm (equivalent to 1 L/m^2) every hour from 6:30 am to 11:30 am and every 30 minutes from 2 pm until 6:30 pm on the sidewalk and pavement. Both watered and dry portions of the street are approximately 180 m long and 20 m wide. Watering cycle times were recorded by drivers on a timetable and were compared with time-lapse visible images taken from a rooftop above the watered station.

At Belleville, a removable 40 m watering pipe was laid along the gutter to water the cobblestone pavement on rue Lesage continuously from 7 am to 7 pm across its 4 meter width. Water use at the Belleville site was approximately 25 mm/h (i.e. 25 L/m^2.h). In terms of the watered-to-total area ratio, rue du Louvre was 100% watered, while rue Lesage was approximately 33% watered. The watering process is illustrated for both sites in Figure 6.5.

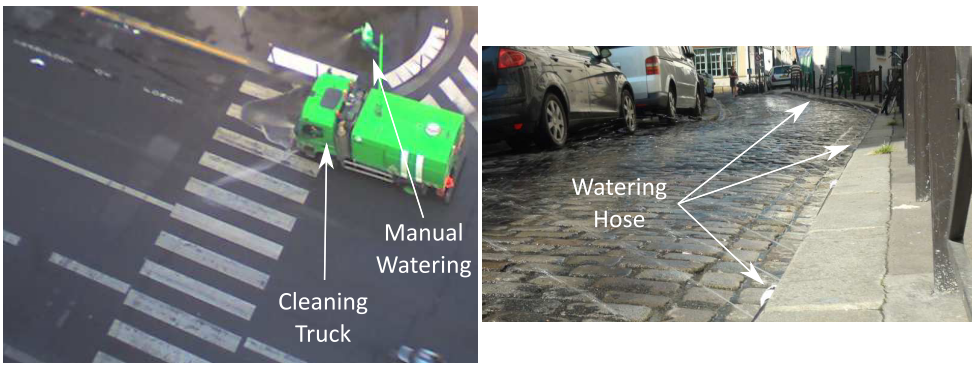

Figure 6.5 – Watering on rue du Louvre (left, from Hendel et al. (2014)) and rue Lesage (right)

Water used for this experiment was supplied by the city's 1,600 km non-potable water network, principally sourced from the Ourcq Canal. Water temperature was

not measured in 2013, but its typical summertime range is 20°-25°C. This range was confirmed in 2014 with a spot Pt-100 thermometer measuring water at the outlets of the watering devices.

6.3 Instruments

Weather stations were designed to record weather data relevant to pedestrian thermal comfort such as air temperature, RH, MRT and wind speed.

Only air temperature, relative humidity and mean radiant temperature should be affected by pavement-watering. In addition, pavement heat flux and temperature 5 cm below the pavement surface as well as surface temperature were recorded at rue du Louvre to determine the thermal effects of pavement-watering. Station design is presented in Figure 6.6 for rue du Louvre.

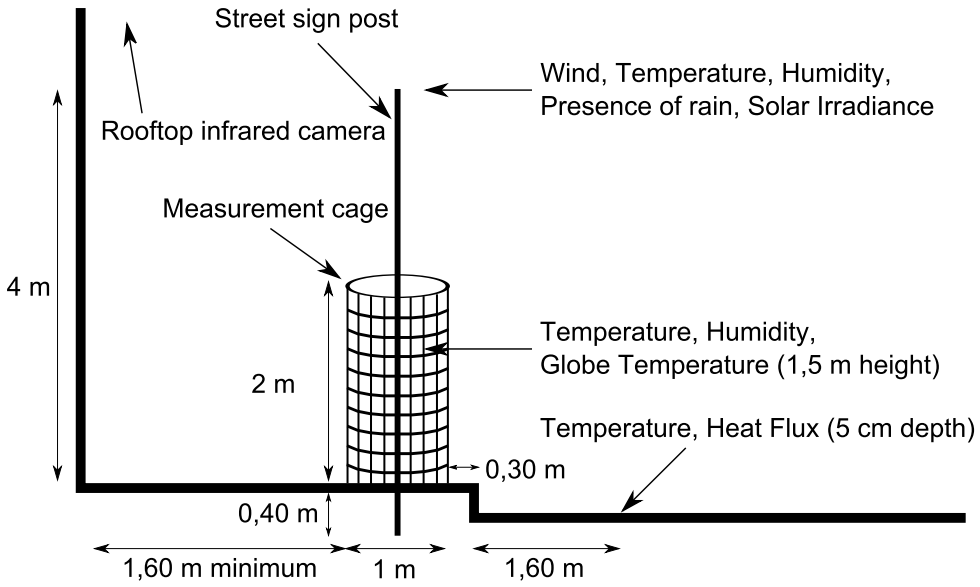

Figure 6.6 – Weather station design and instrumentation (rue du Louvre).

Instruments within pedestrian reach were protected behind a cylindrical white-painted steel cage. Air temperature and relative humidity were measured with a sheltered DMA 672.1 sensor supplied by LSI LASTEM combining a Pt100 and a capacitive hygrometer. Black globe temperature was measured with LSI LASTEM's EST 131 globe thermometer. Finally wind speed and direction were measured with a 2-axis Wind Sonic ultrasonic anemometer supplied by Gill Instruments. Table 6.2 summarizes the properties of the meteorological instruments installed at the fixed weather stations, including measurement height and instrument uncertainty.

Black globe temperature (T_g), air temperature (T_a) and wind speed (v) measurements from the weather station were used to estimate MRT following

Table 6.2 – Type, height and uncertainty of meteorological instruments. Adapted from Hendel et al. (2015).

Parameter	Instrument	Height	Symbol	Uncertainty
Air temperature	Sheltered Pt100	1.5 m 4 m	T_a	0.1°C
Relative humidity	Sheltered capacitive hygrometer	1.5 m 4 m	RH	1.5%RH
Globe temperature	Black globe thermometer	1.5 m	T_g	0.15°C
Wind speed	2D ultrasonic anemometer	4 m	v	2%

ASHRAE (2001).

Louvre and Belleville stations are identical except for the height of the instrument cage and the presence of a pavement sensor. Indeed, the instrument cage is 2 m high at Louvre vs. 3 m at Belleville. This results from differing safety precautions requested by the city services to authorize station installation. No pavement sensor was installed at Belleville.

A photograph of each station is provided in Figure 6.7.

Figure 6.7 – Photographs of watered and control weather stations *in situ*. From left to right: watered and control Louvre stations, watered and control Belleville stations (Hendel et al., 2015).

6.4 UHI Mitigation Potential

The principal aim of UHI countermeasures is to reduce their intensity.

To evaluate this impact, we adopt a similar criterion to that used by Météo France and CSTB (2012). They used 2 m air temperatures averaged between 3 am and 6 am local time, when UHI intensity is greatest.

For our purposes, we use 1.5 m and 4 m air temperature averaged over the same period.

6.5 Thermal Comfort Evaluation

UTCI was calculated from these measurements for each station to estimate pedestrian thermal comfort (Blazejczyk et al., 2010).

As seen in the literature review, UTCI is more and more popular and should therefore ensure good comparability with existing or future studies. Air temperature, humidity, wind speed and MRT are used as well as assumptions on the metabolic activity and clothing of pedestrians to calculate an equivalent air temperature for reference conditions.

For the purpose of our analyses, UTCI equivalent temperature was fast-calculated with the FORTRAN code written by Peter Bröde in 2009 which we adapted for use with the R software environment. The source code is freely available (Bröde, 2009).

Inaccuracies are introduced into both MRT and UTCI by the use of 4 m wind speed rather than 1.5 m and 10 m wind speeds, respectively, as well as by globe temperature measured inside the cylindrical cage. The latter causes shading of the instrument leading to the underestimation of daytime MRT.

6.6 Heat Transfer Analysis

Figure 6.8, adapted from Hendel et al. (2015a), shows a diagram of the surface heat exchanges at the pavement surface.

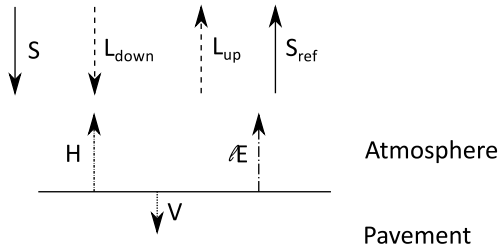

Figure 6.8 – Diagram of pavement heat budget at surface (Hendel et al., 2015).

Pavement heat flux density at the surface is noted V. Solar irradiance received by the pavement is referred to as S. S_{ref} is the reflected SW radiation, while

L_{up} and L_{down} represent LW upwards and downwards radiation, respectively. H represents the sensible heat transfer from the pavement towards the atmosphere, while lE is the latent heat flux density. In addition to the latent heat flux, the sprinkled water film absorbs sensible heat from the pavement, though this heat transfer mechanism is not shown in Figure 6.8.

The pavement heat balance will be analyzed in more detail in Part 2, however it will help us understand the physical phenomena behind possible micro-climatic effects.

The cooling flux created by pavement-watering is expected to affect micro-climatic conditions, including air and mean radiant temperature reductions and relative humidity increases. Firstly, lower pavement surface temperatures will result in lower convective heat flux, which in turn should cause air temperature reductions. Secondly, relative humidity is expected to increase as a result of water evaporation. Finally, increased SW absorptivity as a result of surface wetting (Lekner and Dorf, 1988) and lower surface temperatures are expected to reduce upward SW and LW radiation from the pavement, resulting in a reduction of mean radiant temperature. These effects will be commensurate to the size of the watered zone.

In terms of thermal comfort, the increase in relative humidity has the opposite effect of the reductions in air and mean radiant temperature. Therefore watering may in fact result in greater thermal discomfort for pedestrians if the humidity increase is too great in comparison to the other expected cooling effects. It is therefore uncertain whether the combination of these effects will improve or degrade pedestrian thermal comfort.

6.7 Data Series

All measurements were recorded continuously by the station dataloggers every minute and are presented in local daylight savings time (UTC +2).

As previously stated, pavement-watering has the advantage over other UHI countermeasures of being fully reversible, i.e. watering can be conveniently turned on or off without modifying the preexisting conditions. Indeed, most UHI countermeasures are meant to be permanent and it is very difficult if not impossible to revert back to the preexisting state. Days with watering, referred to as watered days, can therefore easily be compared with days without watering, referred to as reference days.

For better comparability between reference and watered days, temperature data is presented over 24 hour periods extending from 6 am until 5:59 am on the next day, i.e. July 20th refers to data from 6 am on July 20th until 5:59 am on July 21st. This helps better outline the effect of pavement-watering, which begins between 6:30 and 7 am and ends between 6:30 and 7 pm. In addition, only days of Pasquill stability class A or A-B will be considered in the upcoming analyses (Pasquill, 1961). This condition implies nearly clear skies (less than 3 oktas cloud

cover) and low wind speeds (< 3 m/s). All watered days are of Pasquill stability class A or A-B.

Over the summer of 2013, 10 days met the weather conditions required for pavement-watering and 23 additional ones could be used as reference days. Of the 10 watered days, July 8th-10th and 16th were the coolest ($T_x \approx 30$°C, *31%* $\leq RH \leq$ *81%*), with July 22nd, 23rd and August 1st and 2nd being the warmest ($T_x \geq 35$°C, $T_n \geq 20$°C, 22% $\leq RH \leq$ 73%). August 23rd and September 5th were also watered and had intermediate temperatures (35°C$\geq T_x \geq 30$°C, 25% $\leq RH \leq$ 64%). Over this period, the control station on rue du Louvre was vandalized and thus nonoperational from July 19th to August 19th and from September 4th until the end of the summer. Over the same period, the Belleville control station was unpowered from 4 pm on July 22nd until 5 pm on July 25th.

Although 2014 is France's warmest year since the 1900's as of this writing (Météo France, 2015), only two days met the required weather conditions for pavement-watering over the summer of 2014 and five could be used as reference days. July 17th and 18th are the two watered days. August 2014 was particularly cool with a monthly temperature approximately 1.5°C colder than average (Météo France, 2014). Although no events caused any of the stations to fail during the summer of 2014, road work occurred at the Louvre watered station from July 29th until the end of the summer.

6.8 Interpretation of Micro-climatic Effects

For the upcoming analyses, the one-minute data series are smoothed with a ten-minute moving average.

As described earlier, the standard method used in previous work on pavement-watering is to interpret its effect on each considered micro-climatic parameter as the difference between measurements from two stations or areas: one experimental (watered) and one control (unwatered) (Kinouchi and Kanda, 1997, 1998; Yamagata et al., 2008; Takahashi et al., 2010; Bouvier et al., 2013; Maillard et al., 2014). In doing so, the hypothesis is implicitly made that under normal conditions without pavement-watering, the difference between station measurements should be constant and equal to zero.

We adopt the same approach for our own micro-climatic measurements, in addition to the condition that considered days be of Pasquill atmospheric stability class A or A-B (Pasquill, 1961).

Unless specified otherwise, the following analyses focus on the difference between case and control stations, calculated in the following fashion:

$$y_{diff} = y_{case} - y_{control}$$

Negative values therefore indicate that the watered station parameter is lower than that of the control station, and vice versa. The difference between case and control measurements will be referred to as the interstation difference.

CHAPTER 7

Direct Case-Control Comparison

This chapter presents the interstation difference profiles for measured parameters at Louvre and Belleville from July 2nd to July 19th 2013, period during which all stations were operational without interruption.

7.1 Results

Figure 7.1 presents the interstation difference between the case and control stations for T_a and RH at 1.5 m and 4 m, and MRT and UTCI, for rue du Louvre between July 2nd and July 19th. Figure 7.2 shows the same curves for Belleville. Reference days are in red, watered days in blue, while days that were not of Pasquill stability class A or A-B are in grey.

Judging solely by the reference days (red), it is immediately apparent that the assumption that measurements at twin stations are constant or equal is unfounded. The differences in insolation at the Belleville site revealed that those stations were imperfectly matched. It is therefore not surprising for significant differences to exist between the Belleville stations. However, insolation at the Louvre stations was close to identical and thus differences of the amplitude seen in Figure 7.1 are unexpected.

Even after smoothing the data, filtering meteorological conditions and selecting station positions as similar as possible, measurements at paired stations cannot be considered to be equal, even up to a constant, no matter which parameter is considered at 1.5 or 4 m a.g.l. Moreover, the data exhibits variation from one reference day to the next, complicating the interpretation of the watering effect further. Only RH at the Louvre site shows clear changes on watered days compared to reference ones, but they are difficult to quantify.

Although this possibility is not considered in the reviewed pavement-watering literature, it should be noted that Kinouchi and Kanda (1997) do point out that micro-climatic conditions were either equal on average or were warmer and dryer at

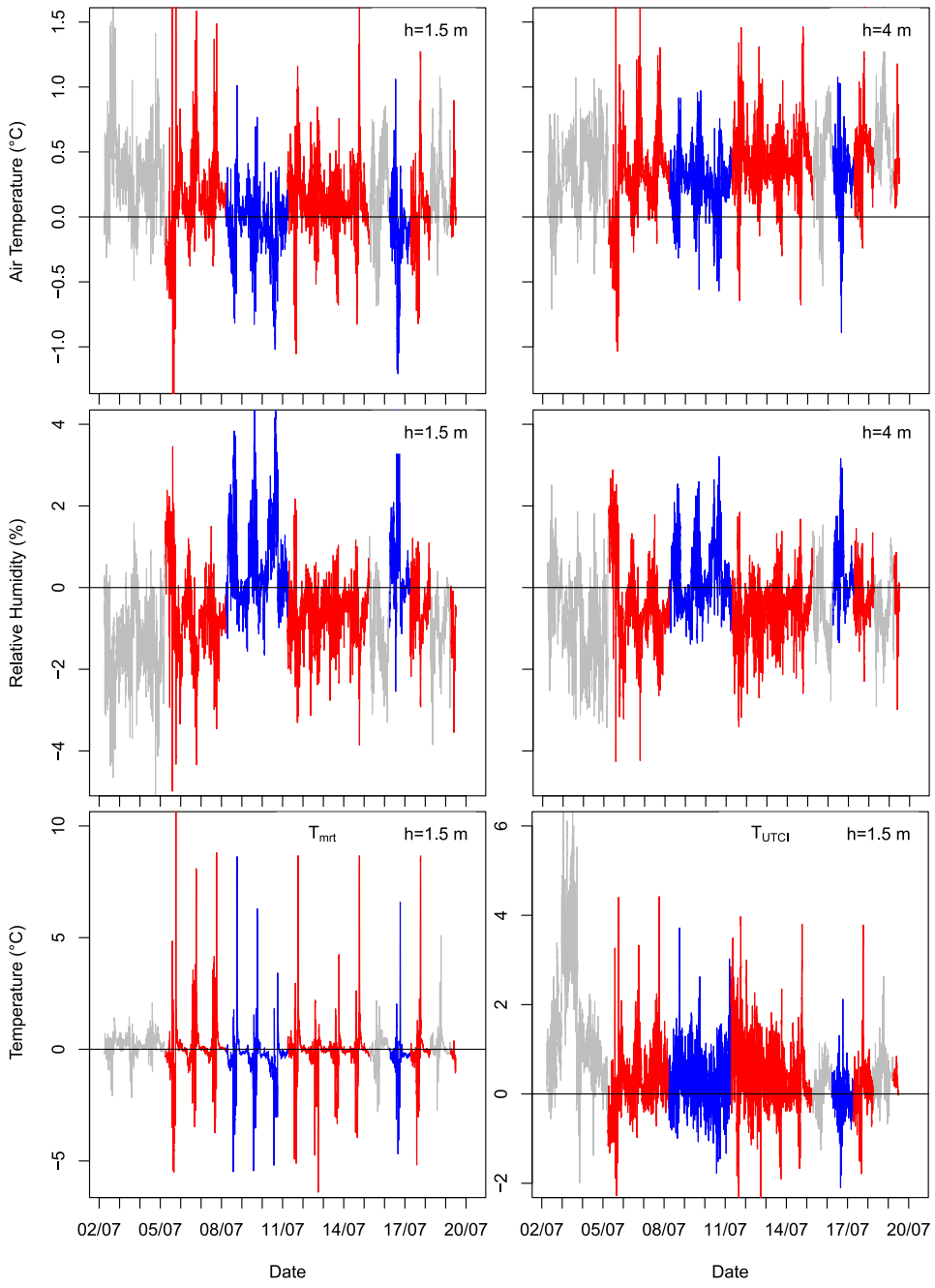

Figure 7.1 – Differences between Louvre case and control stations from July 2nd to 19th, 2013 (top to bottom) for T_a and RH at 1.5 m (left) and 4 m (right) height and MRT (bottom left) and UTCI (bottom right). Watered days are in blue, reference days are in red. Days with uncomparable weather conditions are in grey (Hendel et al., 2015).

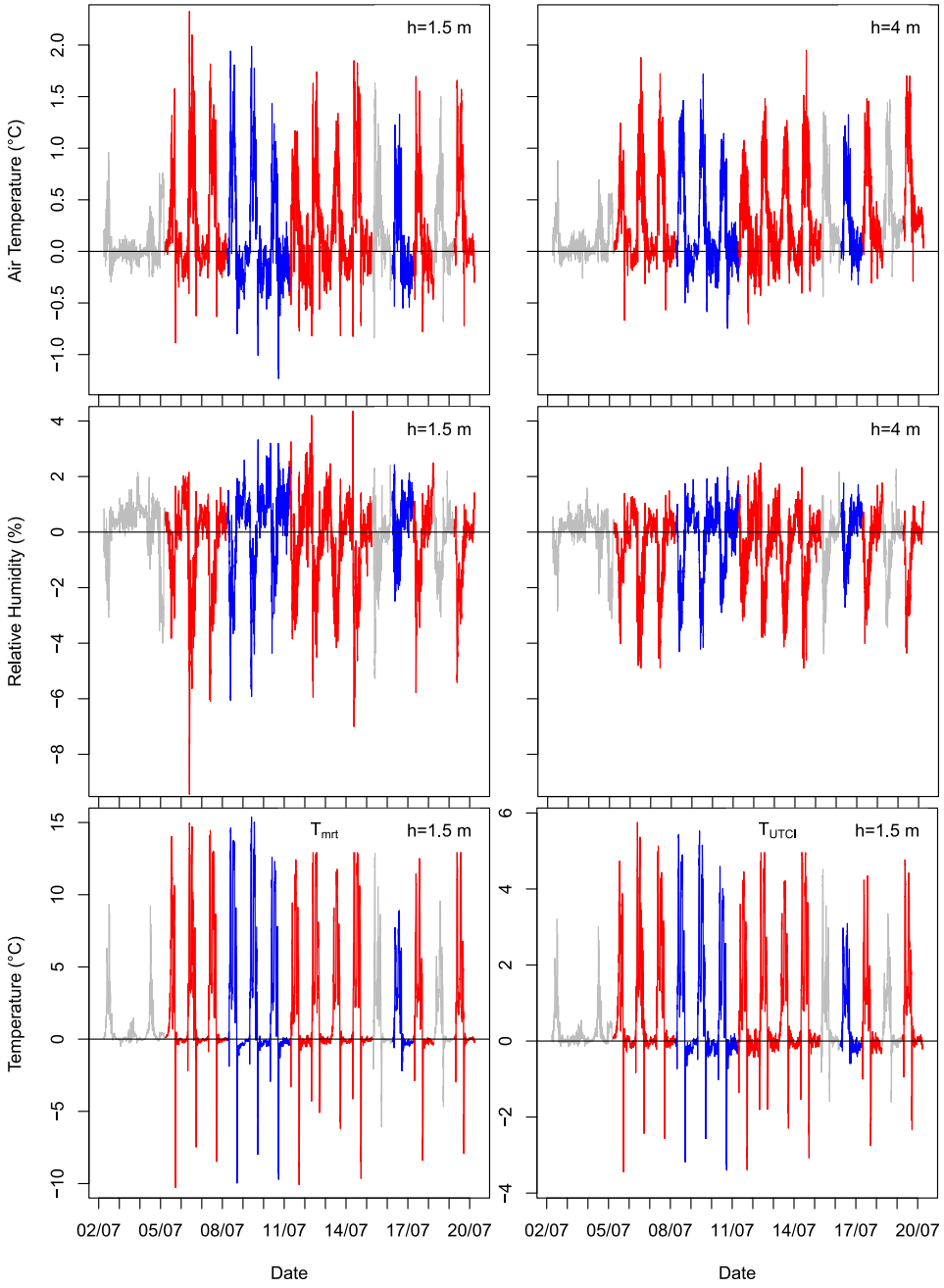

Figure 7.2 – Differences between Belleville case and control stations from July 2nd to 19th, 2013 (top to bottom) for T_a and RH at 1.5 m (left) and 4 m (right) height and MRT (bottom left) and UTCI (bottom right). Watered days are in blue, reference days are in red. Days with uncomparable weather conditions are in grey.

the watered site a few hours before and after pavement-watering. This assessment was not investigated further in their analysis of pavement-watering effects.

7.2 Interstation Profile on Reference Days

Studying these curves does however provide insight into the relative behavior of the paired stations. Table 7.1 summarizes the mean differences observed on reference days for each parameter, height and site over the summers of 2013 and 2014, when data is available.

Table 7.1 – Average case-control difference on reference days over the summers of 2013 and 2014 (Hendel et al., 2015).

Parameter	Height	Louvre	Belleville
T_a	1.5 m	+0.26°C	+0.21°C
	4 m	+0.40°C	+0.31°C
RH	1.5 m	-0.99%	-0.40%
	4 m	-0.81%	-0.56%
MRT	1.5 m	-0.13°C	+1.35°C
UTCI	1.5 m	+0.52°C	+0.72°C

On reference days air temperatures at 1.5 m and 4 m for both Louvre and Belleville are generally higher at the case station than at the control station, while RH is generally lower. The average air temperature differences, in the order of a few tenths of a degree Celsius, are increased at both sites at 4 m relatively to 1.5 m.

MRT difference curves exhibit high amplitudes during periods of direct insolation (see Figure 6.3 for details), reaching up to 15°C at Belleville and 10°C at Louvre. This is due to the high influence of insolation on MRT. Even short-lasting differences in insolation between stations due to a passing cloud for example can cause high amplitude differences in MRT. Finally, UTCI is warmer at the case station for both sites.

On average, the case station is therefore warmer and drier than the control station at both sites and paired station measurements are not equal on reference days. The low average difference in MRT between the Louvre stations vouches for the good match in shading conditions between them. This is not the case for the Belleville site where insolation is much stronger at the case station than at the control, as seen in Figure 6.3.

As can be seen by comparing the MRT and UTCI curves for Belleville, the difference in MRT is the main driver for the UTCI difference during insolation. This is consistent with the sensitivity analyses conducted by Bröde et al. (2012),

i.e. that for air temperatures higher than 20°C, UTCI equivalent temperature increases by about 3°C for every 10°C increase in MRT.

7.3 24-hour Average Differences

As a first approach, we compare the daily interstation differences on watered and reference days.

If pavement-watering effects do exist, a variation in the average interstation difference should occur on watered days compared to reference days. The daily-averaged interstation differences on watered days and their variation compared to reference days are reported in Table 7.2.

Table 7.2 – Daily interstation difference on watered days and variation from reference days over the summers of 2013 and 2014. Adapted from Hendel et al. (2015).

Parameter	Height	Watered days		Variation	
		Louvre	Belleville	Louvre	Belleville
T_a	1.5 m	0.01°C	+0.15°C	-0.25°C	-0.06°C
	4 m	+0.26°C	+0.31°C	-0.14°C	+0.00°C
RH	1.5 m	+0.47%	-0.10%	+1.46%	+0.29%
	4 m	+0.11%	-0.47%	+0.93%	+0.09%
MRT	1.5 m	-0.27°C	+1.67°C	-0.40°C	+0.32°C
UTCI	1.5 m	+0.22°C	+0.68°C	-0.29°C	-0.04°C
UHI-mitigation	1.5 m	-		-0.14°C	-0.08°C
	4 m			-0.09°C	-0.09°C

Results show that the average case-control differences are lower for each parameter on watered days compared to reference days at Louvre, except for RH which is increased. T_a and UTCI are reduced in the order of 0.1°C, MRT is reduced by a few tenths of a degree Celsius, while RH is increased by about one percentage point at Louvre. Similar changes occur at Belleville except that 4 m air temperature is unchanged and MRT is increased by 0.32°C. Furthermore, UHI-mitigation effects are also detected, in the order of one tenth of a degree Celsius.

The changes in case-control differences are indicative of pavement-watering effects. It does seem at first glance that pavement-watering reduces air and UTCI temperatures and increases RH over 24 hours, while MRT effects at Louvre and Belleville are contradictory. However, it is unclear how stat. sign. they may be.

In order to account for data variability, a statistical analysis of the data is necessary and will be applied in Chapter 8.

7.4 Conclusion

The measurements recorded in July 2013 at the Louvre and Belleville sites clearly demonstrate that the assumption that meteorological parameters are equal up to a constant between case and control stations on reference days is incorrect. Interstation difference profiles on reference days exhibit high hourly and daily variability. In the absence of these reference day measurements, the inadequacy of the methodology may not have been detected and the effects of pavement-watering may well have been overlooked or found to worsen pedestrian thermal stress.

Although direct comparisons between case and control weather stations may be valid in certain situations, and could be sufficient for RH at the Louvre site, it is unlikely that this is the general case, especially in dense urban environments which are quite complex. We therefore argue that direct case-control comparison is not a valid method to determine the field effects of UHI countermeasures in cities.

As a first attempt to compensate for this, the daily interstation differences on watered and reference days were also compared. Unfortunately, though certain effects may be apparent, it is unclear how stat. sign. they are.

These conclusions are not specific to pavement-watering and can be generalized to other UHI countermeasures. This leads to our first recommendation for field assessments of UHI countermeasures: test sites should be characterized before the studied countermeasure is implemented. By detecting preexisting interstation behavior, normal differences between sites will not be misinterpreted as UHI mitigation effects or the absence thereof. While none of the field experiments of pavement-watering we found in the literature proceed in this fashion, it is noteworthy that numerical simulation studies naturally use this method. Indeed, they typically compare the same site in identical conditions, apart from the implementation of the UHI countermeasure. This recommendation is also made by Bowler et al. (2010) as they conclude their meta-analysis of the cooling effects of urban greening.

The original approach must therefore be modified. An alternative, statistical approach is proposed and tested in Chapter 8.

CHAPTER 8

Interstation Behavior on Reference and Watered Days

In the previous Chapter, we demonstrated that the micro-climatic effects of UHI countermeasures such as pavement-watering cannot be detected by direct comparisons between case and control stations in cities. We now propose a method based on comparisons of the average interstation difference profile on days with and without watering.

8.1 Statistical Analysis Method

The two-sample t-test is used to compare watered and reference day interstation profiles for each considered parameter.

First, the average interstation profile is established for reference and watered days. Respectively, all reference and watered day observations are grouped by time of day for each minute. For example, all observations made at 2:07 pm on reference days over the summers of 2013 and 2014 are grouped together, thus forming the "2:07 pm reference day observations" sample. 1,440 one-minute samples are obtained for both reference and watered days, i.e. a total of 2,880 samples. From each of these, a sample mean $\left(\mu_i^{wet/dry}\right)$ and sample variance can be calculated. A time series is obtained by ordering the respective sample means in chronological order, representing the average interstation difference profile for reference or watered days:

$$\forall i \in [\![1; 1440]\!],\ \overline{y_{diff}^{wet/dry}}(t_i) = \mu_i^{wet/dry}$$

Having obtained the sample mean interstation difference profiles, the values obtained on watered and reference days are compared minute-by-minute, i.e. sample pair by sample pair.

A two-sample t-test is conducted for each minute-by-minute difference, i.e. the difference between μ_i^{wet} and μ_i^{dry} for $i \in [\![1; 1440]\!]$. The null hypothesis (H_0^i) chosen states that μ_i is greater on watered days than on reference days. The alternative hypothesis (H_a^i) states that μ_i is strictly lower on watered days than on reference days. These hypotheses constitute a one-tailed test. For this analysis, the opposite of RH and RH_{4m} will be used in order to avoid reformulating the hypotheses for these two parameters. Both hypotheses can be summarized as follows:

$$\forall i \in [\![1; 1440]\!], \quad \begin{array}{ll} H_0^i: & \mu_i^{wet} - \mu_i^{dry} \geq 0 \\ H_a^i: & \mu_i^{wet} - \mu_i^{dry} < 0 \end{array}$$

Using the field data, a two-sample t-test of the null hypothesis is conducted with a significance level of 0.05. If the obtained p-value is lower than the significance level, the null hypothesis is rejected.

8.2 Results

Figure 8.1 and Figure 8.2 plot the average change detected on watered days compared to reference days (solid blue line) for the Louvre and Belleville sites, respectively.

Values above the x-axis represent increases while values below the x-axis represent decreases on watered days compared to reference days. In other words:

$$y = \overline{y_{diff}^{wet}} - \overline{y_{diff}^{dry}}$$

The confidence interval is illustrated by the two red dashed curves. If the solid curve is in between the dashed curves, then the average effect at that time of day is not stat. sign..

Watered days exhibit mostly negative changes in T_a, T_{a4m}, MRT and UTCI and mostly positive ones for RH and RH_{4m}. In other words, the environment around the case stations is cooler and more humid, yet overall more comfortable, on watered days than on reference days. In short, watering is more effective at Louvre than at Belleville.

Taking a closer look, it appears that the greatest effects occur in the afternoon between 2 pm and 7 pm for all parameters, i.e. during pavement insolation. Of all considered parameters, RH is the one that best reflects watering events. Indeed, changes in RH at Louvre are simultaneous to watering which occurs from 6:30 am and 6:30 pm with an interruption between 11:30 am and 2 pm. This is not as clear at Belleville which had continuous watering from 7 am to 7 pm.

Although effects are greater at Louvre than at Belleville, maximum effects are comparable and occur in the afternoon for all parameters. While differences in street orientation may play a role, the higher average effects at Louvre are attributed to the difference in watering strategies between sites. In other words,

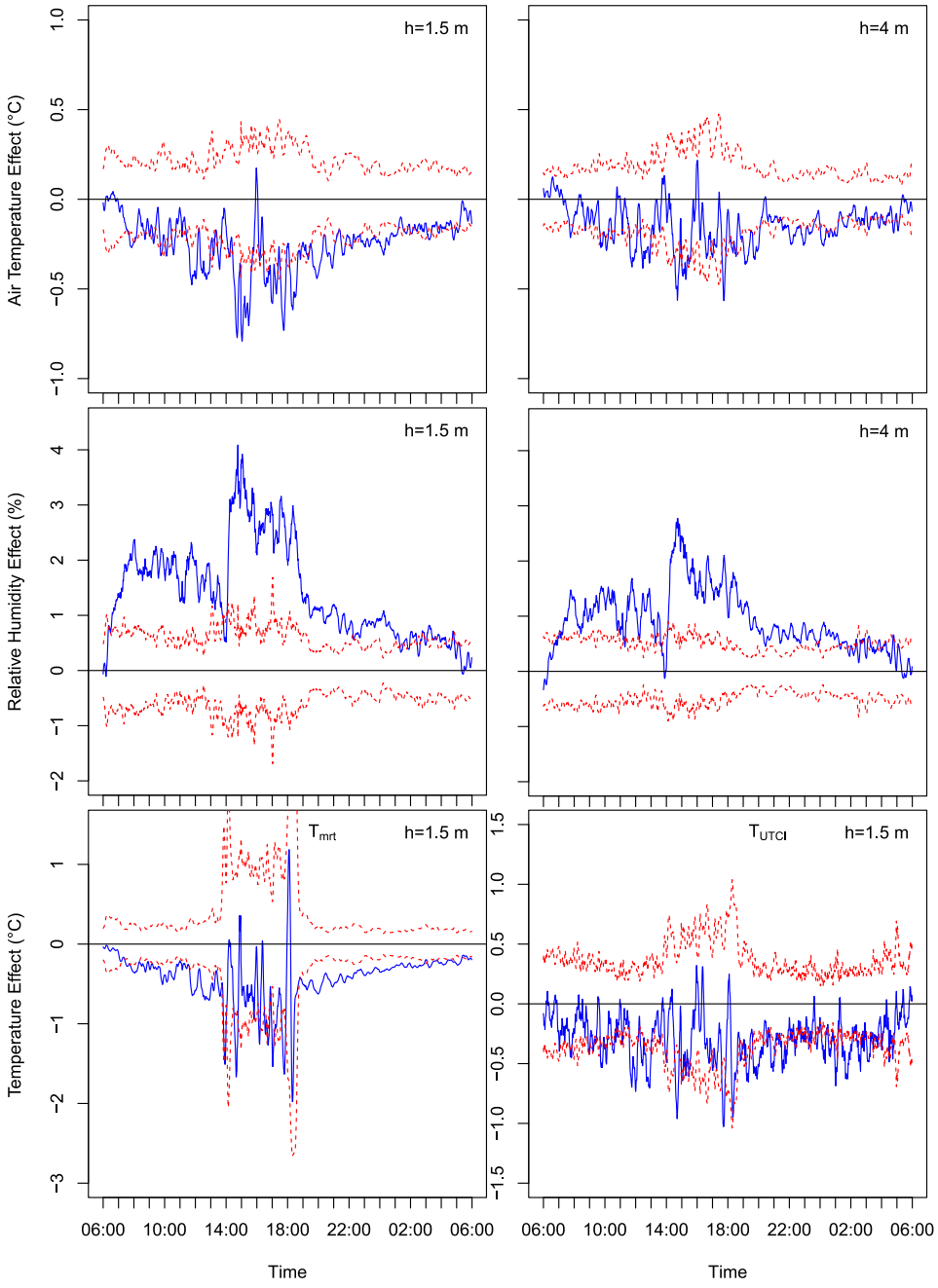

Figure 8.1 – Average watering effect at Louvre over the summers of 2013 and 2014 (top to bottom) for T_a and RH at 1.5 m (left) and 4 m (right) a.g.l. and MRT (bottom left) and UTCI (bottom right). Average effects are solid blue, confidence intervals are dashed red (Hendel et al., 2015).

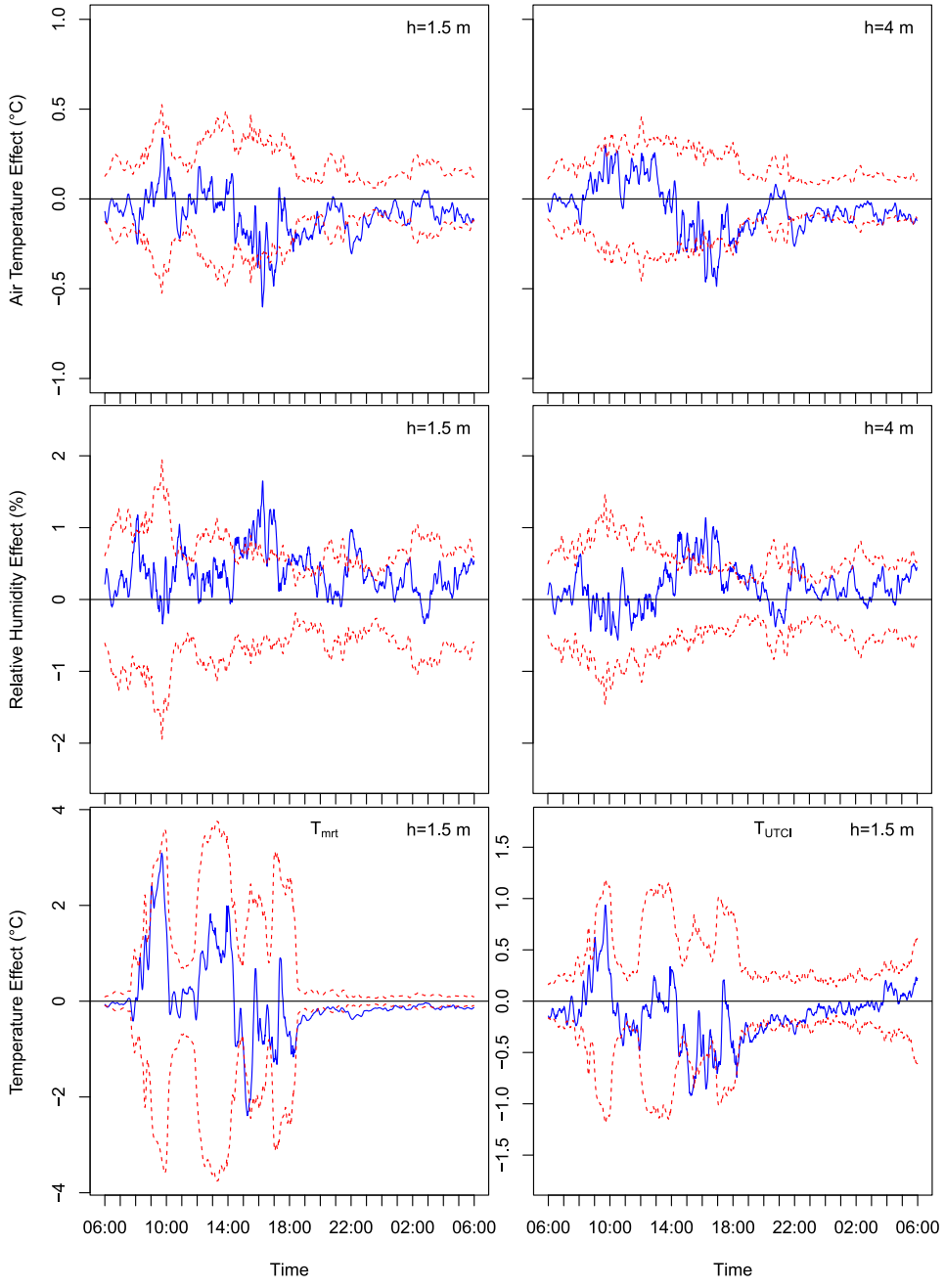

Figure 8.2 – Average watering effect at Belleville over the summers of 2013 and 2014 (top to bottom) for T_a and RH at 1.5 m (left) and 4 m (right) a.g.l. and MRT (bottom left) and UTCI (bottom right). Average effects are solid blue, confidence intervals are dashed red (Hendel et al., 2015).

we confirm that watering 100% of the street surface is more effective than watering 33% of its surface.

While average effects positively affect weather conditions, they are not always stat. sign.. Table 8.1 and Table 8.2 summarize the duration of stat. sign. effects as well as the mean and maximum values reached during that time for T_a, RH, MRT and UTCI for both sites.

Overall, watering effects are more often stat. sign. at Louvre, in addition to greater average effects. Looking at the temporal distribution of stat. sign. effects, it appears that for both Louvre and Belleville they occur most often at night (after 6 pm) for T_a, T_{a4m}, MRT and UTCI and most often during the day for RH and RH_{4m}.

Table 8.1 – Duration, mean and maximum values of stat. sign. effects for Louvre over the summers of 2013 and 2014 (Hendel et al., 2015).

Parameter	Height	Duration (hours/day)	Mean effect	Maximum effect
T_a	1.5 m	16.7	-0.31°C	-0.79°C
	4 m	12.2	-0.22°C	-0.57°C
RH	1.5 m	22.0	+1.5%RH	+4.1%RH
	4 m	20.3	+1.1%RH	+2.8%RH
T_{mrt}	1.5 m	19.5	-0.43°C	-1.67°C
UTCI	1.5 m	12.2	-0.42°C	-1.03°C

Table 8.2 – Duration, mean and maximum values of stat. sign. effects for Belleville over the summers of 2013 and 2014 (Hendel et al., 2015).

Parameter	Height	Duration (hours/day)	Mean effect	Maximum effect
T_a	1.5 m	7.0	-0.21°C	-0.60°C
	4 m	7.0	-0.19°C	-0.49°C
RH	1.5 m	7.6	+0.7%RH	+1.6%RH
	4 m	5.2	+0.6%RH	+1.1%RH
T_{mrt}	1.5 m	10.5	-0.29°C	-2.39°C
UTCI	1.5 m	6.3	-0.39°C	-0.92°C

At Louvre, T_a effects start to become stat. sign. after 8 am and mostly remain so until 2 am the following day. For RH, stat. sign. effects occur practically as soon as watering starts at 6:30 am and remain so until 4 am on the next day with a few minor interruptions, particularly during the watering interruption at midday. MRT effects are stat. sign. as early as 7:30 am until 2 pm and from 6:30 pm until 6 am the next morning. Statistically significant effects do occur in the afternoon

but are more sporadic than in the morning or at night. UTCI stat. sign. effects are more sporadic and mainly occur between 9:30 am and 3 am the next day.

Effects at Belleville are stat. sign. much less frequently than at Louvre. For T_a and RH, they mainly occur between 3 pm and 5 pm and between 2 am and 3 am. For MRT they can be mostly found between 5:30 pm and 2 am. Finally, UTCI stat. sign. effects are sporadically spread out between 11 am and 9 pm.

Pavement-watering therefore has stat. sign. cooling effects up to several hours after watering has ended, although maximum effects occur in the afternoon when conditions are warmest and driest. Watering was also found to have stat. sign. up to 4 m a.g.l. on air temperature and humidity. Furthermore, the comparison between Louvre and Belleville shows that pavement-watering should target the largest possible portion of street width in order to best improve pedestrian thermal comfort.

8.3 Discussion

Our findings support that pavement-watering is an effective method for limiting maximum daily heat stress, while having stat. sign., although limited, UHI-reducing potential.

Maximum effects include reductions of up to 0.79°C and 0.57°C for 1.5 and 4 m a.g.l. air temperature, increases of up to 4.1%RH and 2.8%RH for 1.5 and 4 m RH, and decreases of up to 2.39°C and 1.0°C for MRT and UTCI, respectively. Apart for RH, effects are chiefly stat. sign. at night, although maximum effects occur in the afternoon. Furthermore, effects at Louvre are greater than those observed at Belleville.

Numerical studies automatically account for natural background trends by comparing the same site in identical conditions apart from the implementation of the UHI countermeasure. Our findings compare well with those from such studies. Overall, good agreement with the findings reported in numerical studies is found. This is namely the case with Météo France and CSTB (2012) if the difference in scale is taken into account, i.e. city-wide watering vs. watering a single street portion. Indeed, they report maximum 2 m cooling of up to 2°C T_a and UHI mitigation of between 0.25°C and 0.5°C averaged from 3 am to 6 am local time. Other simulation work at the district-scale conducted by Wei and He (2013) also agrees well with our findings with maximum reductions in MRT reaching 2.7°C in similar situations to our own (see their passage i-j). Air temperature, RH or thermal comfort effects were not investigated in their analysis. Kubo et al. (2006) also conduct a district-scale simulation and find maximum reductions of 0.73°C for 1.5 m air temperature, very similar to our own, and 2.13°C at a height of 0.5 m.

Despite the difference in interpretation method, we now present the findings of previous field trials of pavement-watering. In Paris in 2012, Bouvier et al. (2013) report up to 0.4°C cooling of 2 m air temperature and 4% increase in RH for

a single nighttime watering event. In Lyon, Maillard et al. (2014) find a 0.5°C reduction in 1.5 m WBGT in the afternoon. In Nagaoka, Japan, Kinouchi and Kanda (1997) report reductions of up to 1°C in T_a and 4°C in T_g as well as a 4% increase in RH at 1 m a.g.l.. Average effects are in the order of 0.5°C for T_a, 2°C for T_g and 3% for RH. Also in Nagaoka, Takahashi et al. (2010) discuss cooling of up to 2°C in the morning and 4°C in the afternoon for 0.9 m air temperature. Finally in Tokyo, Yamagata et al. (2008) find up to 3°C and 2°C reductions in 0.5 m air temperature and WBGT, respectively.

Given the methodological shortcomings of these analyses underlined in Chapter 7, it is difficult to compare them with our own. Among these papers, Takahashi et al. (2010)'s findings exhibit the greatest difference with our own. Part of the difference is attributable to their lower measurement height, as proximity to the watered surface is expected to increase the detected effect. However, the difference in findings is substantial nevertheless. It may be the case that their watered area is naturally cooler than their control area even without watering. As no information on this possibility is provided, it cannot be investigated further. This goes for the other field works as well where natural background differences between chosen case and control sites may cause over- or underestimation of reported cooling effects. Most of the differences in reported cooling effects are attributable to differing measurement heights, generally lower than our own. Generally-speaking, differences in meteorological conditions may play a significant role, such as summertime temperatures or RH.

The developed method can also be applied to the 24-hour differences initially reported in Table 7.1 and Table 7.2. Using the daily-averaged field data, two-sample t-tests of the null hypothesis are conducted with a significance level of 0.05. The p-values and average effects are summarized in Tables 8.3 for Louvre and Belleville, over the summers of 2013 and 2014. No value is given for average effects which are not stat. sign..

Table 8.3 – p-value and average stat. sign. (CI: 0.95) effect at Louvre and Belleville over the summers of 2013 and 2014 (Hendel et al., 2015).

Parameter	Height	Louvre		Belleville	
		p-value	Average effect	p-value	Average effect
T_a	1.5 m	0.000324	-0.25°C	0.134383	not stat. sign.
	4 m	0.00131	-0.14°C	0.482932	not stat. sign.
RH	1.5 m	6.18E-11	+1.46%	0.037265	+0.29%RH
	4 m	9.26E-09	+0.93%RH	0.298622	not stat. sign.
T_{mrt}	1.5 m	0.000127	-0.40°C	0.779618	not stat. sign.
UTCI	1.5 m	0.000346	-0.29°C	0.368533	not stat. sign.
UHI-mitigation	1.5 m	0.034415	-0.14°C	0.131961	not stat. sign.
	4 m	0.015935	-0.09°C	0.050258	not stat. sign.

At the Louvre site, the p-value is much lower than 0.05 and even 0.01 for all parameters, i.e. the daily effects observed are highly stat. sign.. On the other hand, this is not the case at the Belleville site. With a significance level of 0.05, only 1.5-m RH shows a stat. sign. daily effect of +0.29%RH. When UHI-mitigation effects are considered, they are found to be stat. sign. for Louvre only, with -0.14°C and -0.09°C at 1.5 and 4 m a.g.l., respectively. 4 m UHI-mitigation effects at Belleville are nearly significant with an average value of -0.09°C.

This confirms that pavement-watering at Louvre is far more effective than at Belleville where daily effects cannot be clearly separated from preexisting background noise.

More generally-speaking, the observed results agree well with expectations based on the physical phenomena behind pavement-watering and the observations of thermal effects made later on. Details of this agreement can be found in Part 2. In short, micro-climatic effects are highest during insolation, as are pavement surface temperature and heat flux reductions. This is especially true for RH, providing very good correspondence with watering cycles and the estimated evaporation rates. This good agreement significantly strengthens our microclimatic findings which can thus be backed by thermal observations and predicted physical phenomena.

The difference between Louvre and Belleville effects is likely best explained by the difference in watering strategies between both sites. Indeed, the greater the watered surface, the more total sensible heat flow and total upwards radiation are reduced. Since 100 % of the street surface is watered at Louvre compared to 33% watering at Belleville, the difference between sites is unsurprising. In addition, watering at Belleville only targeted the pavement, but not the sidewalk where the weather stations were placed and where pedestrians are likely to be. Belleville stations are therefore further away from the watered area than they are at Louvre. Finally, the differences in street orientation also play a role, since pavement cooling was found to be greatest during insolation. Differences in insolation patterns and durations will therefore alter the effects of pavement-watering. The combination of these effects is expected to amplify the differences between sites. We therefore conclude that watering one third of the street is much less effective than watering all of it, and should at the very least target the area to which pedestrians are most exposed, i.e. the sidewalk.

One limitation of the analysis of Louvre effects is the absence of the warmest days observed over both summers, i.e. August 1st and 2nd, 2013. In addition, the influence of the watered area on the control area cannot be excluded due to their proximity. These limitations can be overcome by evaluating Louvre effects against the Belleville control station. Table 8.4 provides the p-value and average daily effects determined in this manner. Figure 8.3 and Table 8.5 summarize the effects found with the 10-minute smoothed data.

Detected maximum effects are increased for all parameters, but only marginally for 1.5 m T_a and RH. This supports the hypothesis that the watered area influences dry area measurements. However, the significance of the detected effects

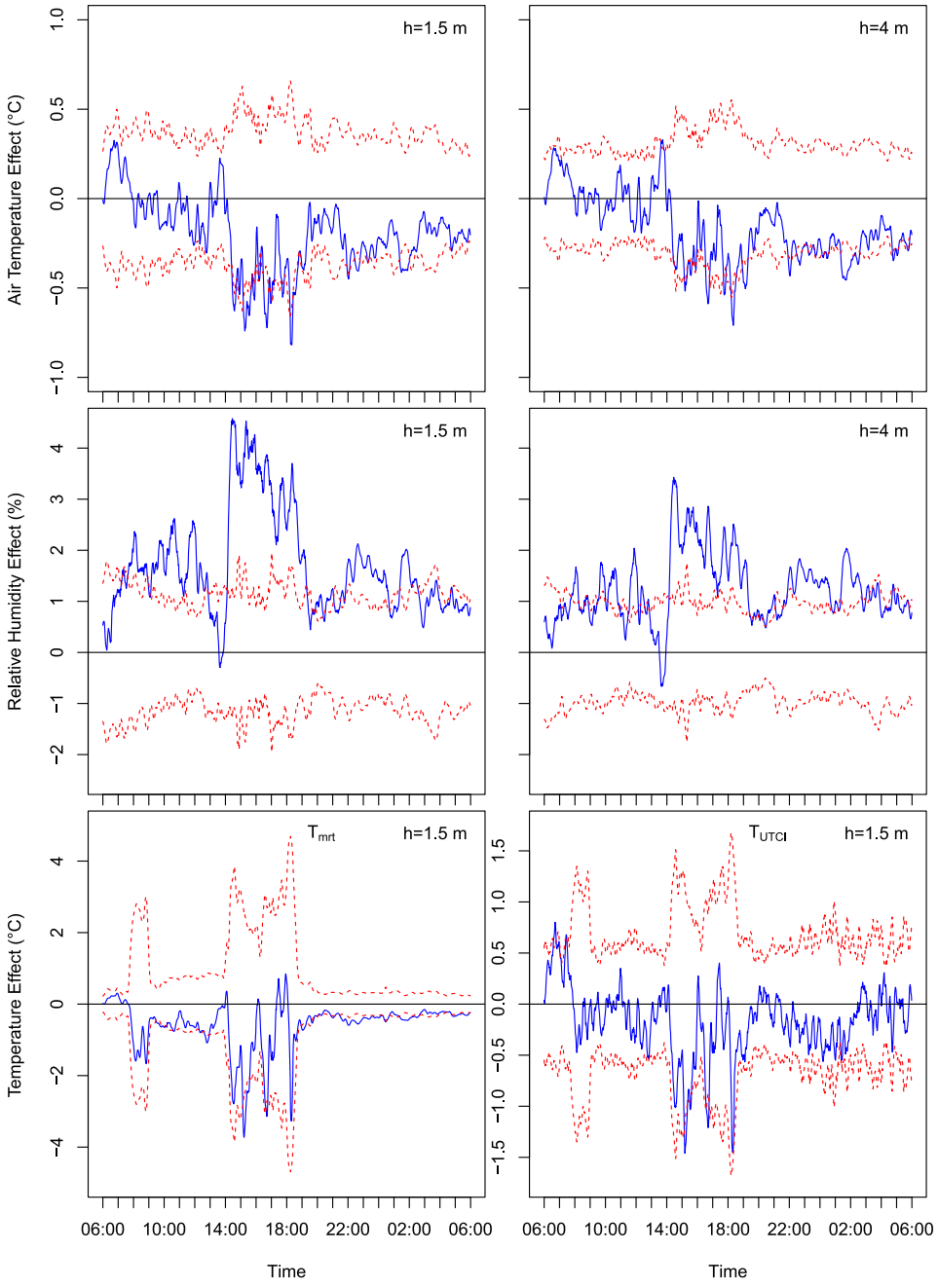

Figure 8.3 – Average watering effect at Louvre detected using the Belleville control stations over the summers of 2013 and 2014 (top to bottom) for T_a and RH at 1.5 m (left) and 4 m (right) height and MRT (bottom left) and UTCI (bottom right). Average effects are solid blue, confidence intervals are dashed red (Hendel et al., 2015).

Table 8.4 – p-value and average stat. sign. (CI: 0.95) effect at Louvre using the Belleville control station over the summers of 2013 and 2014 (Hendel et al., 2015).

Parameter	Height	Louvre with Belleville control	
		p-value	Average effect
T_a	1.5 m	0.001035	-0.24°C
	4 m	0.020352	-0.17°C
RH	1.5 m	6.92E-07	+1.87%RH
	4 m	1.45E-07	+1.33%RH
T_{mrt}	1.5 m	0.000813	-0.70°C
UTCI	1.5 m	0.150749	not stat. sign.
UHI-mitigation	1.5 m	0.104996	not stat. sign.
	4 m	0.042564	-0.22°C

Table 8.5 – Duration, mean and maximum values of stat. sign. effects for Louvre, using the Belleville control station (Hendel et al., 2015).

Parameter	Height	Duration (hours/day)	Mean effect	Maximum effect
T_a	1.5 m	6.2	-0.45°C	-0.82°C
	4 m	7.9	-0.35°C	-0.71°C
RH	1.5 m	18.0	+2.0%RH	+4.6%RH
	4 m	18.2	+1.5%RH	+3.4%RH
T_{mrt}	1.5 m	11.1	-0.60°C	-3.73°C
UTCI	1.5 m	1.3	-0.95°C	-1.46°C

deteriorates, particularly for air temperature and UTCI. This can be attributed to increased differences in insolation patterns within the new site pair as compared to the initial pairs. In terms of UHI-mitigation, only effects 4 m a.g.l. are stat. sign. and reach -0.22°C.

The range of obtained UHI mitigation effects, i.e. -0.09°C to -0.22°C, is consistent with those reported by Météo France and CSTB (2012).

This example provides interesting feedback on the potential and the limits of the proposed method. While strictly paired stations benefit from reduced data variance and therefore have higher accuracy, strict site selection criteria filter out large numbers of candidate sites for experimentation. This example demonstrates that the analysis can be successfully conducted in much less favorable conditions if need be. Indeed, despite significantly different street orientations, several kilometers between paired stations and different environments, the method successfully provides comparable values of daily and maximum watering effects. The tradeoff

for this added flexibility however is the widened confidence intervals, resulting from increased signal noise, which reduces the statistical significance of the detected effects. In our example, UTCI and UHI-mitigation 1.5 m a.g.l. effects are not stat. sign. for this reason.

Confidence intervals are greatest during periods of instrument insolation. Using aspirated instrument shields should help address this issue for air temperature and humidity measurements by eliminating the influence of insolation differences between stations on these parameters. Unfortunately, no equivalent solution exists for the globe thermometer.

Additional limits more specific to our experimental setup can be identified. Among these, the influence of the cage used to protect the datalogger and instruments installed 1.5 m a.g.l. should be noted, though instruments installed outside of the cage are not expected to be affected.

The cage is designed to limit its influence on the meteorological parameters measured within it as much as possible. Indeed, the cage mesh is 4 cm by 4 cm, resulting in a highly permeable design. In addition, it is entirely painted white to reduce atmospheric heating which may result from its exposure to direct insolation. Therefore, the influence of the cage on air temperature and humidity is expected to be negligible.

Nonetheless, the cage inevitably causes partial shading of the globe thermometer during insolation and shields the instrument from environmental radiation. MRT is therefore likely underestimated in the day. At night, competing effects are at work. On the one hand, the cage partially obstructs the low temperature sky radiation, which will tend to cause an overestimation of MRT. On the other hand, the higher temperature ground and wall radiation is also inhibited by the cage, which will tend to cause an underestimation of MRT. It is uncertain which of these tendencies is dominant at night.

While a dedicated study of the influence of the cage on the measured parameters is necessary to confirm this preliminary analysis, cage effects are expected to mainly affect the estimation of MRT from globe temperature.

8.4 Conclusion

As a result of the analysis conducted in Chapter 7, a statistical analysis method was developed to determine the micro-climatic effects of pavement-watering.

The alternative method consists of a two-sample t-test of the difference between mean interstation differences on watered and reference days. Pre-existing differences between experimental and control stations are thus taken into account, previously ignored by the dominant method of directly comparing measurements between them.

The method was successfully tested with data collected at well-paired stations, but also with stations paired between sites, despite their large differences. Results show that pavement-watering is an effective means of reducing maximum heat

stress, while also having UHI-mitigation effects. Indeed, we found that conditions at the case stations on watered days were cooler and more humid than reference days in varying intensity over the course of the day. However, these effects weren't always statistically significant.

Results demonstrate that pavement-watering is an effective means of reducing maximum heat stress, with up to 1°C cooling in UTCI equivalent temperature in the late afternoon when conditions were warmest. In addition, stat. sign. effects were also detected at night between 3 am and 6 am, thus demonstrating UHI-reducing potential. Indeed, the analysis demonstrated that watered days were cooler and more humid than reference days in varying intensity over the course of the day and that these effects weren't always stat. sign.. RH, followed by MRT, air temperature and UTCI, were most often affected in a stat. sign. manner by pavement-watering. Furthermore, significant effects occurred most often at night for air, mean radiant and UTCI-equivalent temperatures, while they occurred most often during the watering for RH. However, maximum significant effects occurred during the day, when conditions are hottest and driest. Maximum reductions of 0.79°C and 0.57°C occurred for 1.5 and 4 m air temperatures, 1.67°C for MRT and 1.03°C for UTCI-equivalent temperature. Maximum increases of 4.1%RH and 2.8%RH were found for 1.5 and 4 m RH.

Best results were obtained in the case of 100% watering at Louvre, with effects being much less stat. sign. at Belleville where only 33% of the street portion was watered, as demonstrated by daily-averaged effects. Indeed, no daily stat. sign. effects were found at Belleville, while all effects at Louvre were. These effects reached -0.25°C and -0.14°C for 1.5 and 4 m air temperature, +1.5%RH and +0.9%RH for 1.5 and 4 m relative humidity, -0.40°C for MRT and -0.29°C for UTCI equivalent temperature. Finally, UHI-migitation effects of between -0.09° and -0.22°C were detected.

CHAPTER 9

Conclusion of Part 1

In this Part, we investigated the micro-climatic effects of pavement-watering, used as a case study of UHI countermeasures.

Field measurements were obtained from an experiment conducted over the summers of 2013 and 2014 at two sites in Paris, France. Both sites have an aspect ratio H/W=1, the Louvre site having an approximate N–S street orientation and Belleville an approximate E–W orientation. The full width of the Louvre site was watered from 6:30 am to 11:30 am and from 2 pm to 6:30 pm, while only a third of the Belleville site was watered from 7 am to 7 pm without interruption.

First and foremost, we revealed in Chapter 7 that the dominant method of directly comparing measurements between experimental and control stations is flawed and cannot reliably detect the real-world micro-climatic effects of UHI countermeasures in cities. The assumption behind this method is that the inter-station case-control difference is zero under preexisting conditions. Based on this hypothesis, the interstation difference is directly interpreted as the effect of the implemented UHI countermeasure.

However, our continuous measurements showed that interstation differences are neither constant nor equal to zero. Furthermore, they exhibit high natural variability from one day to the next, even among days of Pasquill Stability Class A or A-B. Interstation differences observed after implementation can therefore not be attributed to the studied countermeasure, at least in dense urban environments.

In response to this difficulty, we proposed and tested an alternative methodology in Chapter 8. It consists of a two-sample t-test of the difference between mean interstation differences on watered and reference days. The method was successfully tested with data collected at well-paired stations, but also with stations paired between sites distant by several kilometers and with different urban environments and street orientations.

Relative humidity, followed by MRT, air temperature and UTCI, was most often affected in a stat. sign. manner by pavement-watering. Furthermore,

significant effects occurred most often at night for air, mean radiant and UTCI-equivalent temperatures, while they occurred most often during the day for RH. However, maximum significant effects occurred during the day for all parameters, when conditions are hottest and driest. Maximum reductions reported reached 0.79°C and 0.57°C for air temperature 1.5- and 4-m a.g.l., 1.67°C for MRT and 1.03°C for UTCI-equivalent temperature. Maximum increases in relative humidity reached 4.1%RH 1.5 m a.g.l. and 2.8%RH 4-m a.g.l..

Daily-averaged data was also considered and revealed that daily watering effects were stat. sign. in the case of 100% watering at Louvre, but not so with one-third watering at Belleville. Average effects at Louvre reached -0.25°C and -0.14°C for 1.5- and 4-m air temperature, +1.5%RH and +0.9%RH for 1.5- and 4-m relative humidity, -0.40°C for MRT and -0.29°C for UTCI-equivalent temperature. UHI-mitigation effects were investigated using air temperatures 1.5 and 4 m a.g.l. averaged between 3 am and 6 am. These effects ranged respectively reached -0.09°C to -0.22°C.

These results show that pavement-watering is an effective means of reducing heat stress, with maximum effects occurring when weather conditions are hottest during the day. In addition, stat. sign. average cooling effects were detected between 3 am and 6 pm, therefore demonstrating UHI reducing effects. Best results were obtained at the Louvre site, which was 100% watered at regular intervals, while poor results were obtained at Belleville, where only 33% of its surface was continuously watered.

The developed methodology was applied to the case of pavement-watering. This countermeasure has the advantage over other more permanent ones of being immediately reversible. Indeed, when watering is not taking place, the study sites revert to their preexisting (dry) state. Firstly, this greatly facilitated the assessment that interstation differences are not equal to zero in the absence of watering. Had measurements begun only after a permanent UHI countermeasure had been put in place, this may have been overlooked entirely. Secondly, it allowed us to record data that could be used to build an average interstation difference profile for both watered and reference days which could then be compared with the two-sample t-test.

In the case of long-lasting countermeasures, it is not possible to record reference data once the measure has been implemented. It is therefore necessary to start monitoring the test site sufficiently ahead of countermeasure implementation to allow for enough reference data to be recorded. This data is crucial to our method and must provide a representative image of the preexisting interstation differences. Since weather conditions are highly variable, there is no telling how long this reference period must last and it will depend on the weather conditions of interest. We estimate that it may range from several weeks up to a few years. In our case, heat wave conditions were the focus point. While we were fortunate that the summer of 2013 exhibited such a large number of relevant days and was sufficient for our analysis, the summer of 2014, with only two watered and five reference days, would not have provided sufficient data to conduct a reliable

analysis.

The length of the investigation period is one of the limits of the method. Requiring data series spanning over several months or years implies that the only change expected is the implementation of the UHI countermeasure. However, urban environments are ever changing and preexisting conditions determined over a certain period may become rapidly obsolete in certain areas. This adds additional burden to the site selection criteria which must not be significantly modified over the full investigation period apart for the studied countermeasure.

Fortunately, it was found that these criteria can be made more flexible by using station pairs whose urban configurations are not as identical as the ones selected here. This added flexibility is obtained at the cost of reduced precision, i.e. larger confidence intervals. In order to put the odds in the favor of the investigator, the distance between stations and the differences in their insolation patterns should be as limited as possible.

The strength of our findings on the effects of pavement-watering will increase as data collection continues. Paths for improvement include the use of high precision instruments calibrated against each other on a regular basis in a laboratory-controlled chamber and the use of aspirated solar shelters to eliminate the influence of insolation on air temperature and humidity measurements. Furthermore, the influence of the instrument cage on weather instruments must be better quantified.

In addition, the application of our methodology to other sites with different UHI countermeasures will provide additional feedback as to its relevance and applicability in the field. Unfortunately, since the investigation period must be long, so will the time before significant feedback has been gathered.

Finally, other approaches and tools may also prove useful or even better suited to the task at hand. These include the use of a network of control stations spread across a given area to compensate for poorly matched stations, the use of financial analysis tools for data deseasonalization or data mining and machine learning (e.g. neural networks) techniques.

Having determined the micro-climatic effects of pavement-watering, we now turn our attention to its thermal effects in Part 2.

Part 2

THERMAL EFFECTS OF PAVEMENT-WATERING

CHAPTER 10

Introduction to Part 2

Part 1 focused on determining the micro-climatic effects of pavement-watering. Maximum effects reached up to 1°C UTCI equivalent temperature at 1.5 m a.g.l. and UHI mitigation effects of up to -0.22°C were found 4 m a.g.l..

These results compare well with previous work and provide additional evidence to support the claim that pavement-watering has beneficial effects on pedestrian thermal comfort and on the urban micro-climate. However, the thermal effects of pavement-watering have still not been determined.

The thermal effects of pavement-watering have been a recurrent focus point of previous studies. Surface temperature reductions are often reported and have been found to range from 8°C to 30°C (Kinouchi and Kanda, 1997, 1998; Yamagata et al., 2008). The effects on pavement heat flux and temperature 5 cm below the surface have been studied by Kinouchi and Kanda (1998), though precise results were not reported. In addition, judging by the authors' own accounts or by their solar irradiance measurements, many of these studies took place in nearly unmasked conditions (Asaeda et al., 1996; Kinouchi and Kanda, 1997, 1998). It is therefore difficult to determine how representative the findings reported actually are of dense urban areas, though they do provide a basis for comparison.

Understanding the effects of pavement-watering on the pavement heat budget is important as they are the direct consequence of watering. The modified pavement heat budget causes changes in the exchanges towards the atmosphere and environment. Indeed, lowered upward sensible and radiative heat flows and an increased latent flow are the primary suspects for the micro-climatic effects described in Part 1. Changes in surface temperature, radiative budget and heat storage are expected to be the main contributors to the observed cooling effects. The thermal effects therefore provide fundamental knowledge on pavement-watering which can may be used to improve its micro-climatic effects. In addition, this information can be used to validate numeric or experimental studies at different scales.

This Part will determine the thermal effects of pavement-watering. As discussed, a field experiment of pavement-watering was conducted over the summers of 2013 and 2014 in Paris, France following a computer simulation and prototype field study (Météo France and CSTB, 2012; Bouvier et al., 2013). Pavement temperature and heat flux observations made at the Louvre site over the summer of 2013 will be analyzed with this goal.

While the general methodology (site description, watering method, weather station design, ...) has been described in Chapter 6, methodological aspects specific to the study of the thermal effects of pavement-watering will be presented in Chapter 11. Chapter 12 will focus on the effects of pavement-watering on pavement heat flux 5 cm below the pavement surface, Chapter 13 on surface temperature effects and Chapter 14 will look into pavement temperature effects 5 cm deep.

This Part is based on the peer-reviewed work published in *Applied Thermal Engineering*, *Urban Climate* and the *Journal of Sustainable Development of Energy, Water and Environment Systems* (Hendel et al., 2015a, 2014, 2015b; Hendel and Royon, 2015).

CHAPTER 11

Methodology

The following Chapter will describe the methodology specific to this Part. More general methodological information is provided in Chapter 6.

11.1 Instruments

In addition to meteorological instruments, the Louvre site was equipped with a pavement sensor measuring temperature and heat flux density 5 cm below the surface. Solar irradiance was measured by the weather station 4 m a.g.l. and surface temperature was monitored by an IR camera. Table 11.1 summarizes the characteristics of the instruments used in this chapter. The pavement sensor was taylor-made by a the French manufacturer Captec while the pyranometer was supplied by LSI Lastem.

Table 11.1 – Type, height and uncertainty of thermal instruments. Adapted from Hendel et al. (2014, 2015a,b).

Parameter	Instrument	Height/Depth	Symbol	Uncertainty
Pavement heat flux	Taylor-made flowmeter	-5 cm	G	5%
Pavement temperature	Type T Thermocouple	-5 cm	T_{5cm}	1°C
Surface temperature	FLIR B400 infrared camera (7.5 – 13 µm)	0 cm	T_S	2°C
Solar irradiance	Second Class Pyranometer - ISO 9060	4 m	S'	10% daily

Figure 11.1 provides a top view of the pavement sensor installed on rue du Louvre. A picture of the site taken from above is also shown in Figure 11.3.

Measured data was recorded by the weather station positioned at the Eastern end of the cable.

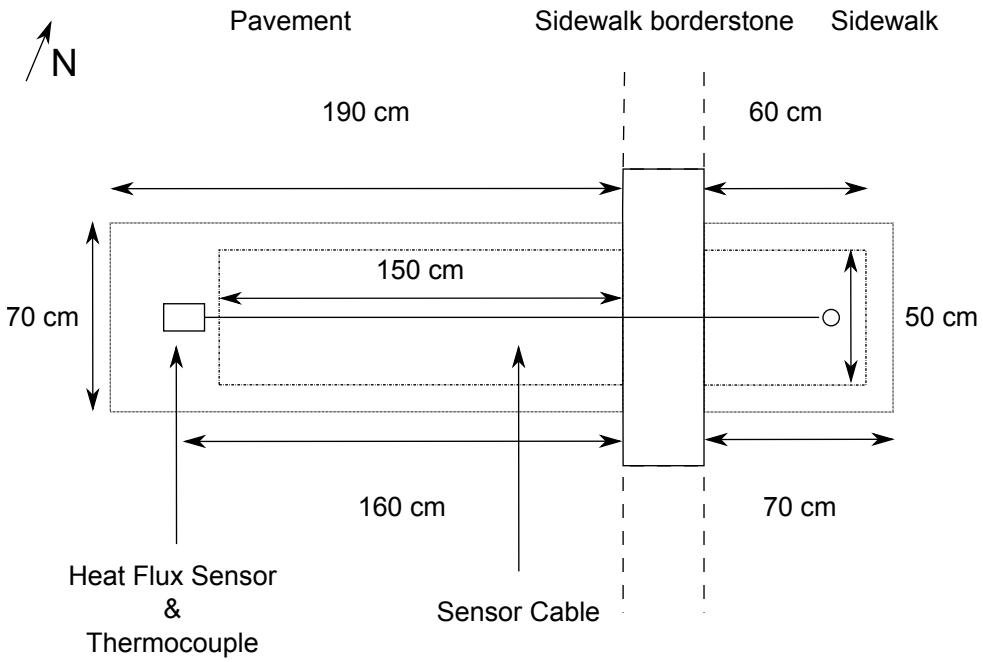

Figure 11.1 – Top view of pavement sensor (Hendel et al., 2015a).

The sensor was placed in the middle of the North-bound bus lane, causing no traffic disturbances once installed. Unauthorized parking and a 100 m distant traffic light ensured that only very limited shading or localized heat exhaust was caused by vehicles. Figure 11.2 shows a detailed cross-section of how the pavement sensor was set in place before filling.

As indicated in Table 11.1, pavement surface temperature was monitored with a FLIR B400 IR camera with a spectral range of 7.5-13 µm. The camera was placed on the roof terrace of the building located directly in front of the watered station, located at 46 rue du Louvre, approximately 20 meters a.g.l.. The camera recorded false-color IR thermal and visible images simultaneously every hour on non-watered days and every 10 or 15 minutes on watered days. These images were used to estimate pavement surface temperature.

Apparent (measured) surface temperatures, also known as brightness temperatures, were corrected with the parameters indicated in Table 11.2, as measured by the weather station below, in order to obtain directional radiometric temperatures. The emissivity of the studied surfaces was obtained by the reference black body method, using an adhesive with a known emissivity of 0.95. MRT, calculated from the weather station measurements, was used as the reflected temperature for IR camera measurement corrections. Although this causes an underestimation of directional infrared temperatures since MRT is greater than the actual sky ir-

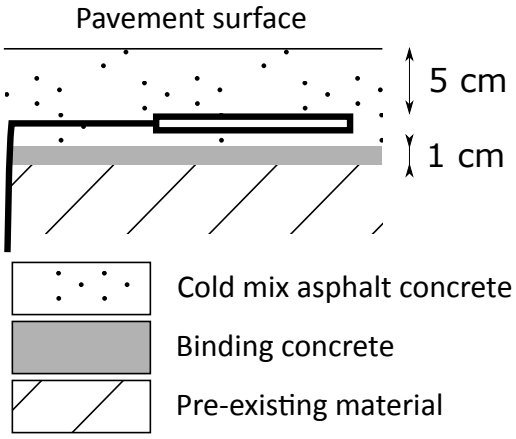

Figure 11.2 – Cross-section detail of pavement sensor filling materials (Hendel et al., 2015a).

radiance temperature, the error remains limited due to the high emissivity of the studied surfaces.

Table 11.2 – Parameters used to correct apparent surface temperature (Hendel et al., 2014)

Parameter	Correction value
Emissivity	0.97
Distance to target (height)	20 m
Reflected temperature	MRT measured by weather station
RH	As measured at 1.5 m by weather station
T_a	As measured at 1.5 m by weather station

The camera operated continuously from 8 am on July 8th until 8 am on September 6th. Interruptions occurred between 7:20 pm on July 8th until 6 pm on July 11th and from 6 pm on July 12th until 2:30 pm on July 15th. These are due to failures of the camera's time-lapse computer.

11.2 Pavement Zones

The surface temperatures of three street areas were surveyed as illustrated in Figure 11.3 (left): pavement zone 1, located above the pavement sensor, pavement zone 2, located further towards the street's center and a sidewalk zone.

All three had an emissivity of 0.97 despite different surface composition and texture. No change in emissivity was applied for the wet pavement. It is assumed that the wet pavement has the emissivity of a water film, i.e. 0.98.

The studied zones were selected according to the presence of thermal disturbance sources, detected via a nighttime IR photograph of the area provided in Figure 11.3 (right) taken at 3:20 am. The use of a nighttime thermal image taken several hours after sunset prevents interpretation errors due to differences in insolation or shading. Thermally disturbed areas are either significantly warmer or colder than their surroundings, once differences in emissivity have been accounted for.

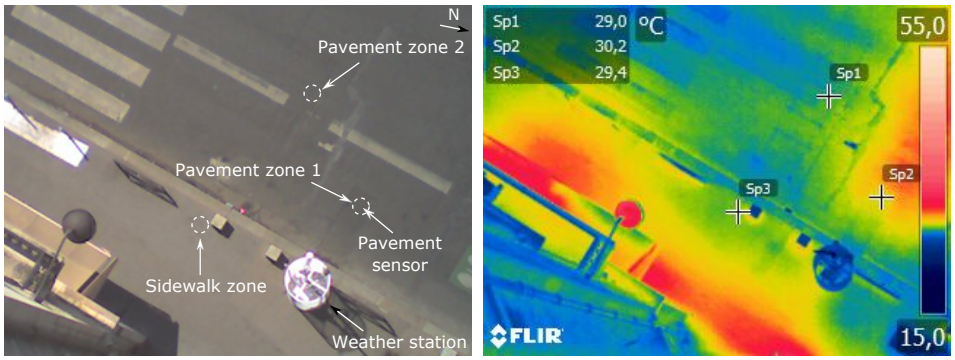

Figure 11.3 – Surface temperature measurement zones (left) and corresponding nighttime corrected infrared photograph on July 22nd at 3:20 am (right). Temperature scale is in degrees Celsius. Sp2: pavement zone 1; Sp1: pavement zone 2; Sp3: sidewalk zone (Hendel et al., 2014).

The principal disturbance is caused by a district heating main, which runs below the sidewalk along the edge of the building and crosses the street below the weather station. It is most easily recognized in its sidewalk portion in the form of a distinct red band running from left to right from the awning to the bottom edge of the false-color IR image. It then runs perpendicularly, from bottom to top, underneath the weather station where it is not as visible, and continues to the other side of the street, reappearing with rough contours just after pavement zone 1 (Sp2).

The presence of this main was confirmed by winter observations and the district heating operator. In the summertime, the heating network supplies minimal heat solely for domestic hot water production, as confirmed by heat flux observations which balance out over 24 hours (see Chapter 12). This heat source and the difference in overlying materials (see Table 11.3) are responsible for the temperatures of pavement zone 1 being up to 2°C warmer than the surrounding pavement at night. Pavement zone 2 was therefore added to complement the data collected in zone 1, above the pavement sensor.

Another identified heat source is an air conditioning exhaust vent emitting hot air underneath the awning of the nearby grocery shop on the left side of the image in front of the pedestrian crosswalk. This exhaust vent explains the red hot spot visible at the center of the awning itself and on the sidewalk directly below it.

This heat source does not significantly affect the weather station measurements due to its position and height, however the sidewalk zone was selected to avoid its area of influence as well as that of the district heating main and areas shaded by other obstacles.

Table 11.3 describes the underlying materials and their respective thicknesses for each zone. Only the composition of pavement zone 1 is known with certainty thanks to the construction work undertaken to place the pavement sensor 5 cm below the surface. The other pavement structures are described based on data provided by the Roads and Traffic Division of Paris City Hall. It should be noted that the sidewalk's asphalt surface course does not include medium or coarse aggregates such as those used in asphalt concrete and is therefore much smoother than the road pavement surfaces. Furthermore, the differing road composition below pavement zone 1 is most likely attributable to the presence of the district heating main.

Table 11.3 – Pavement structure in each zone (Hendel et al., 2014).

Zone	Course	Composition	Thickness
Pavement zone 1	Surface	Cold-mixed asphalt concrete	6 cm
	Base	Concrete	34 cm
	Subgrade	Compacted ground	-
Pavement zone 2	Surface and Binder	Hot-mixed asphalt concrete	16 cm
	Base	Cement-treated base material	20 cm
	Subgrade	Compacted ground	-
Sidewalk zone	Surface	Asphalt	2 cm
	Base	Concrete	10 cm
	Subgrade	Compacted ground	-

11.3 Pavement Heat Balance

Figure 11.4, based on Kinouchi and Kanda (1998), shows a diagram of the heat flux densities relevant to this experiment.

Pavement heat flux density at the surface is noted V and as G at a depth of 5 cm. The difference between V and G is noted ΔQ and represents the heat flux density absorbed by the top 5 cm layer of pavement. Solar irradiance measured by the pyranometer at a height of 4 m is referred to as S' and that received by the pavement as S. S_{ref} is the reflected SW radiation, while L_{up} and L_{down} represent LW upwards and downwards radiation, respectively. H represents the sensible heat transfer from the pavement towards the atmosphere, while lE is the latent heat flux density.

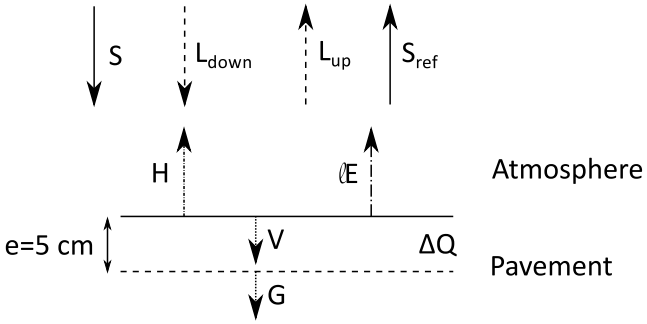

Figure 11.4 – Diagram of pavement heat budget at surface (Hendel et al., 2015a).

11.4 Data Analysis

The data analysis method for pavement heat flux and temperature measurements will now be described. Pavement heat flux density, surface and pavement temperatures will be considered in a similar manner, consisting of a direct comparison between reference and watered day observations.

Although sun trajectories can change very rapidly during certain periods of the year, these changes are relatively small during the month of July. The daylight period on July 20th is approximately 25 minutes shorter than on July 8th, while solar zenith is reduced by less than 2°. The magnitude of these changes can be seen in Figure 11.5 which illustrates solar irradiance as measured by the weather station on July 8th and 22nd for comparison. Daily shading conditions were checked with time-lapse visible images and were found to be unmodified for the studied surfaces between July 8th and July 21st. For the purpose of this discussion, we therefore consider the changes in sun trajectory to be negligible.

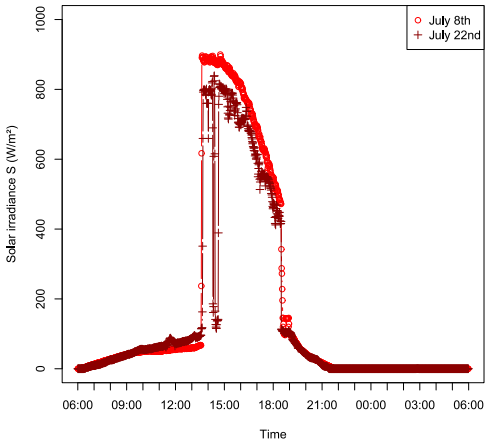

Figure 11.5 – Solar irradiance measured on July 8th and 22nd (Hendel et al., 2014).

Due to the different positions, pavement zone 1 and 2 and the sidewalk zone

are not insolated simultaneously. Pavement zone 2 becomes insolated first at approximately 1:15 pm, followed by pavement zone 1 at 1:35 pm and finally the sidewalk zone at 1:55 pm.

Pavement Heat Flux

For the analysis of pavement heat flux G, measurements from July 11th, 14th and 20th (reference days) will be compared with observations from July 8th, 22nd and 10th (watered days).

Surface Temperature

For surface temperature, IR camera measurements from July 8th, 22nd (watered), 20th and 21st (control) will be considered. Unfortunately, it is not possible to compare wet pavement surface temperatures from July 8th with dry pavement surface temperatures made a few days before or later in comparable weather conditions, the nearest days being July 7th or 11th, during which the IR camera was offline. July 20th is the closest control day with available data which meets these weather criteria (see Chapter 6), however atmospheric temperatures were warmer than on July 8th, with a respective BMI_{Min} and BMI_{Max} of 19° and 30.3°C on July 20th versus 18° and 29°C on July 8th.

Pavement Temperature

For pavement temperature, reference day measurements from July 7th, 11th and 20th will be compared to watered day measurements from July 8th, 10th and 22nd, respectively.

11.5 Deriving Pavement Solar Irradiance

Solar irradiance S', measured 4 m a.g.l. by a pyranometer, was continuously recorded by the weather station's datalogger starting on July 2nd, 2013. Because of the difference in positioning of the pyranometer and pavement sensor (below pavement zone 1), S' is not equal to S and can therefore not be used in its place for the upcoming heat transfer analyses in Chapter 18. S must therefore be derived from S'.

Apart from possible insolation interruptions due to road traffic not visible in S', the only difference is the insolation period. The visible images taken by an IR rooftop camera reveal a 20 minute time lag between the beginning of pavement sensor and pyranometer insolation during the month of July. The time lag is immediately identifiable when comparing the graphs of G and S' for July 11th in Figure 11.6.

The beginning and end of pavement and pyranometer insolation are illustrated by the two dashed and long-dashed vertical lines, respectively. These coincide with

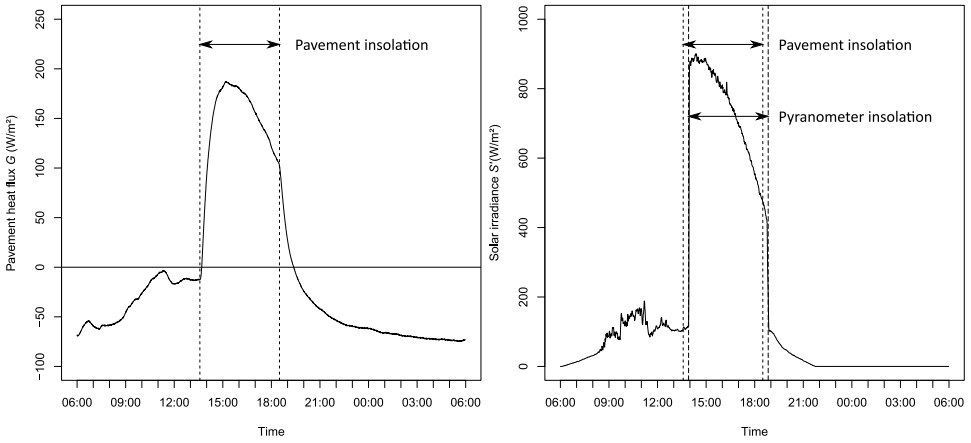

Figure 11.6 – G (left) and S' (right) measured on July 11$^{\text{th}}$ (Hendel et al., 2014)

.

the sudden increases and declines seen in each signal. The insolation period of the pavement is approximately 1:35 pm to 6:30 pm, while that of the pyranometer is 1:55 pm to 6:50 pm. No signal distortion other than the time lag is expected nor taken into account.

With these hypotheses, a modification of S' during the two 20-minute-long exclusive disjunctions of pyranometer and pavement insolation is undertaken to obtain S. The rest of the signal is unchanged, apart for distortions due to vehicles. Finally, to ensure signal continuity, the 5 minutes following and/or preceding these 20-minute periods are also modified.

CHAPTER 12

Pavement Heat Flux Effects

This chapter will focus on the analysis of the effects of pavement-watering on pavement heat flux G, measured 5 cm deep below the pavement surface. To accomplish this, reference day observations from July 11th, 14th and 20th will be compared with watered day observations from July 8th, 22nd and 10th, as was described in Chapter 11.

12.1 Results

Reference days

G and S on July 11th, 14th, and 20th are presented in Figure 12.1. S ranges from 0 W/m^2 to 200 W/m^2 during shading and from 200 W/m^2 to 900 W/m^2 during direct insolation. G ranges from -75 W/m^2 to 215 W/m^2.

In terms of heat flux, each day can be divided into three periods: two of net heat release ($G < 0$) in the morning and evening and one of net heat storage ($G > 0$) during the day. The net release of heat by the pavement lasts about 18 hours, while heat is stored during the remaining 6 hours, approximately between 1:30 pm and 7 pm.

When the pavement becomes directly insolated, G enters a transient period during which the top 5 cm layer of pavement begins to store heat, i.e. during which $\Delta Q \neq 0$. The transient period unfolds between the first dotted vertical line and the daily peak in heat flux, as seen in Figure 12.1. After the transient period, G and S follow a similar trend. The last dashed vertical line indicates the instant when the pavement is shaded, at 6:30 pm.

It should be noted that an illegally-parked vehicle covered the pavement sensor for 30 minutes on July 20th. S was corrected in order to take this into account.

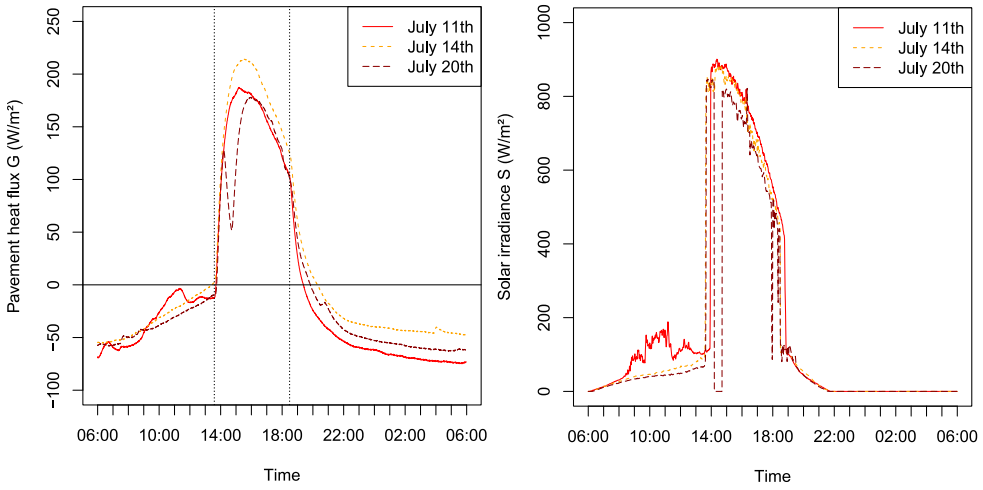

Figure 12.1 – Pavement heat flux G (left) and SW radiation S (right) on control days (Hendel et al., 2014).

Over 24 hours, pavement heat flux more or less balances out to zero, indicating that the heat supplied by the district heating main is minimal (Hendel et al., 2015b).

Watered days

Watered days will now be considered in the following order: July 8th, 22nd and 10th. Figure 12.2 illustrates G and S on those dates. S is in the same range as found on control days, while G ranges from -75 W/m^2 to 130 W/m^2.

The watering methods applied in the afternoon on watered days and the daily maximum value of G are summarized in Table 12.1. Watering cycles occurred at the specified frequencies except for a 50 minute interruption on July 22nd at approximately 3 pm.

Table 12.1 – Actual watering method on considered watered days (Hendel et al., 2015a).

Watering method parameter	July 8th	July 22nd	July 10th
Watering rate (mm/h)	1.33	2	2
Watering cycle period (min)	45	30	30
Delay of watering vs. insolation start (min)	35	65	<5
Daily maximum value of G (W/m^2)	115	130	70

The maximum value of G is about half that reached on control days, ranging from 70 W/m^2 to 130 W/m^2, approximately half that observed on control days. Between 3 pm and 6:30 pm, the average reduction in pavement heat flux compared

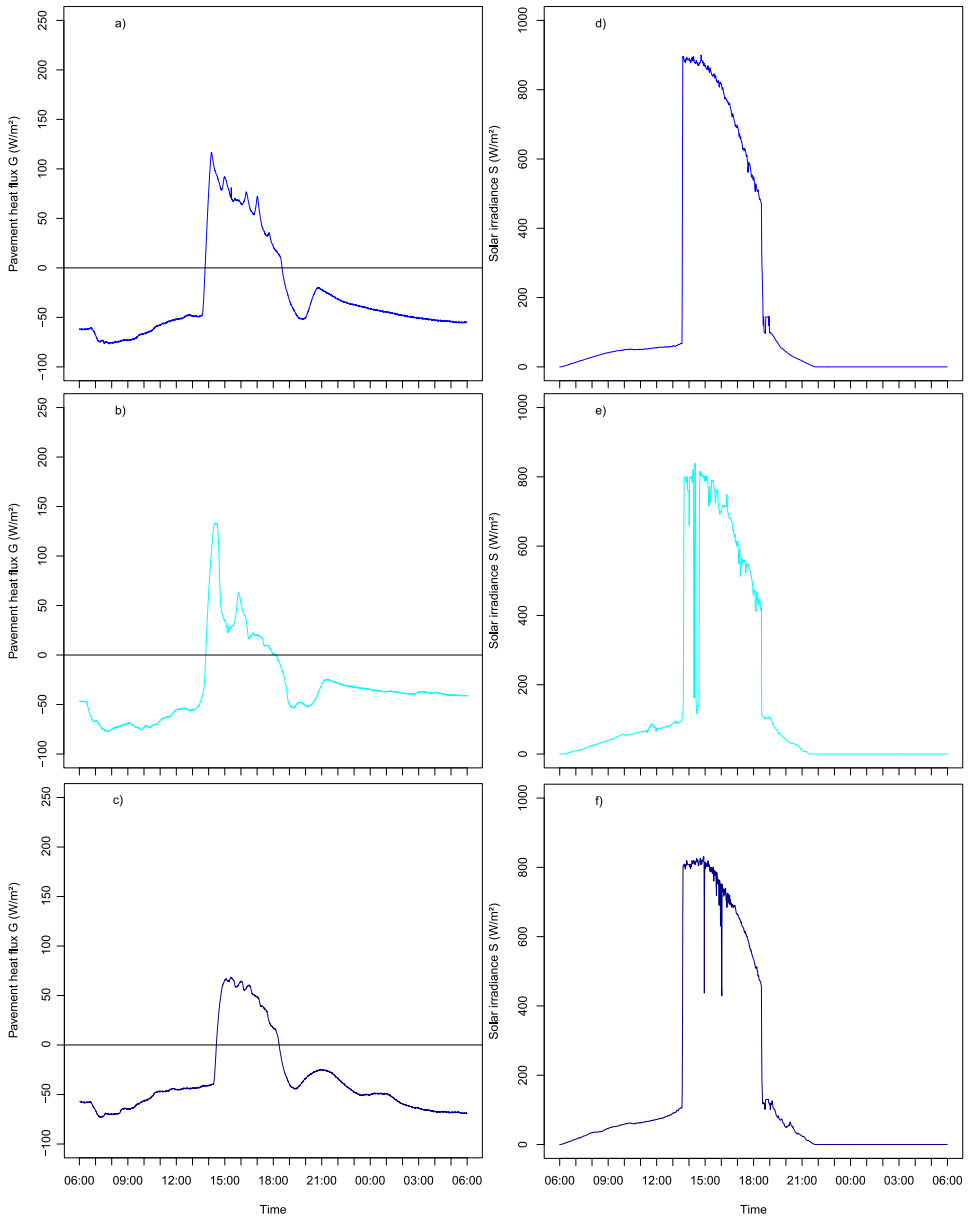

Figure 12.2 – Pavement heat flux G and SW radiation S on watered days: a) and d) July 8th; b) and e) July 22nd; c) and f) July 10th (Hendel et al., 2015a).

to different reference days is found to be between 100 and 150 W/m^2. Table 12.2 summarizes these reductions. In the morning, G is reduced by approximately 15 W/m^2 after the first watering cycle and by up to 50 W/m^2 around 11 am. Morning heat flux is stabilized by watering compared to reference days, which explains why effects increase as the morning goes by.

Table 12.2 – Average heat flux density reduction in W/m^2 on watered days (Hendel et al., 2015a).

Date	July 8th		July 22nd		July 10th	
Reference	July 11th	July 14th	July 14th	July 20th	July 11th	July 14th
Average change	-100	-120	-130	-150	-110	-130

In addition, several spikes in heat flux are apparent, the first and largest occurring as insolation begins. The first one seems proportional to the delay between watering and pavement insolation, while the ones thereafter are inversely proportional to the watering frequency as reported in Table 12.1. A last, significantly smoother spike also occurs 2 to 2.5 hours after the end of pavement insolation.

Indeed, they are most numerous on July 8th and nearly nonexistent on July 10th. Only two large spikes are visible on July 22nd and are linked to a passing cloud, as is visible with Figure 12.2 e). The amplitude of these spikes is in the order of 50 W/m^2 on July 8th. On July 22nd and 10th, their amplitude is significantly reduced, while insolation conditions are comparable. In the morning, no heat flux spikes are clearly visible.

These aspects will be analyzed in more detail in Part 3.

12.2 Discussion

The comparison of G on watered days with control days therefore reveals strong effects due to pavement-watering. On the one hand, heat flux density reductions were found to be highest in the afternoon during pavement insolation with G being more than halved. The average reduction is between 100 and 150 W/m^2 during this period. Morning heat flux density, when the pavement is shaded, was also reduced by pavement-watering in the order of 15 W/m^2 just after the first watering cycle and by up to 50 W/m^2 around 11 am. On the other hand, spikes in G were observed.

These effects demonstrate that pavement-watering effectively reduces heat storage on behalf of the pavement. As heat storage is one of the mechanisms involved in the formation of UHIs, pavement-watering can be expected to reduce their intensity. Indeed, lower heat storage during the day should mean lower heat release at night. This trend is clearly visible when comparing G at night on

watered and reference days after pavement drying (see Figures 12.1 and 12.2). Indeed, G's amplitude is about half that observed on reference days.

Overall, these observations are consistent with previous work. On control days, the trend in heat flux is comparable to measurements made without pavement-watering by Kinouchi and Kanda (1998), also 5 cm deep, although inside a porous pavement. The heat flux values are about twice as large as what Asaeda et al. (1996) observed 20 cm below the asphalt pavement surface. Given the difference in depth, this discrepancy is not considered surprising. On watered days, observations are similar to those of Kinouchi and Kanda (1997, 1998) as well: the first watering cycle on all watered days coincides with a small "nose-dive" in G in the order of 15 W/m^2. Moreover, the net storage period observed in this experiment is shorter than in reports from Kinouchi and Kanda (1998) or Asaeda et al. (1996), but they were working in nearly unmasked conditions.

Finally, no heat flux spikes were observed in previous work. This is interpreted as a consequence of the watering method, continuous in the case of Kinouchi and Kanda (1998) and discrete in our own. Cross-examination of pavement heat flux spikes and visible images of pavement zone 1 (above the pavement sensor) reveal that these spikes coincide with surface drying. These spikes will be analyzed further in Part 3.

12.3 Conclusion

The effects of pavement-watering on pavement heat flux density 5 cm deep (G) were determined in this Chapter.

G was found to be more than halved by pavement-watering during insolation, with morning and afternoon reductions reaching up to 50 and 150 W/m^2, respectively. Subsequent heat release by the pavement is also reduced in the evening following watering. In addition, heat flux spikes were detected and coincide with pavement drying.

We now turn to the effects of pavement-watering on surface temperatures.

CHAPTER 13

Surface Temperature Effects

The effects of pavement-watering on pavement heat flux density (G) were studied in Chapter 12. The daily peak was found to be more than halved by pavement-watering during insolation, with morning and afternoon reductions reaching up to 50 and 150 W/m^2, respectively. Subsequent heat release by the pavement is also reduced in the evening following watering.

This chapter will focus on the analysis of the effects of pavement-watering on pavement surface for three street zones. Once again, reference (July 20th and 21st) and watered day (July 8th and 22nd) observations will be compared. As stated previously, due to IR camera malfunctions, no reference day measurements a few days before or after July 8th could be used.

13.1 Results

Figure 13.1 presents directional radiometric temperature for the three defined areas of the street: the (o) series represents pavement zone 1; the (+) series represents pavement zone 2; the (x) series represents the sidewalk. Some data points are missing due to passing or parked vehicles over the measurement areas. Vertical dot-dashed lines indicate watering cycles for July 8th and 22nd. As previously noted in Table 12.1, afternoon watering on July 8th occurred about every 45 minutes, while it was every 30 minutes on July 22nd.

On July 20th and 21st, surface temperatures reach a low of 24°C between 6 am and 7 am and a high of 50-54°C at 4 pm. All three surfaces follow a very similar approximately bell-shaped curve. Morning temperatures increase slowly until they spike when the pavement becomes insolated around 1:30 pm. Pavement shading causes an exponential decrease in temperatures starting between 6 pm and 7 pm. Pavement zone 1 is generally the warmest, followed by pavement zone 2 and the sidewalk, with nocturnal temperatures being the most similar between zones, with differences smaller than 2°C. Temperature differences are more pronounced during

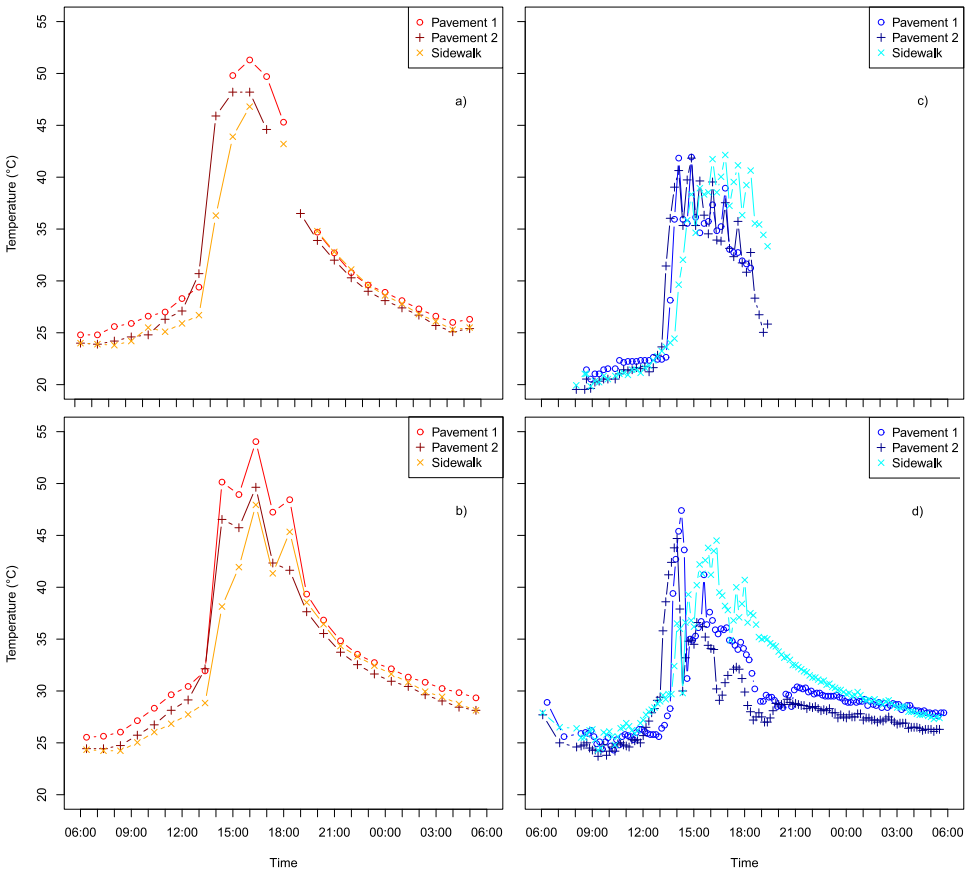

Figure 13.1 – Pavement directional radiometric temperature on reference days: a) July 20th and b) July 21st; and on watered days: c) July 8th and d) July 22nd (Hendel et al., 2014).

the day, particularly during insolation. It should be noted that the temperature fluctuations which occur on July 21st are due to the passing of isolated clouds.

On July 22nd, the daily low was about 25°C, but this temperature was maintained from 7:30 am until 12 pm and was approximately 3°C lower than the single temperature measurement prior to watering. A maximum temperature of about 47°C was reached just before afternoon pavement-watering began. The bell shape of the temperature curves is greatly affected by watering. Morning increases are slower, insolated surface temperatures are several degrees lower and nighttime temperatures follow a more linear decrease, except for the sidewalk zone. After watering begins, the temperature of all surfaces remains below 45°C. Furthermore, unlike on control days, the sidewalk becomes the warmest area after afternoon watering begins and remains so until late in the night. Similar temperatures and trends are observed in available data from July 8th.

A dip in the temperature of pavement zone 2 and that of the sidewalk should

be noted around 5-6 pm on July 22nd. It occurs due to shade caused by the buildings across the street. This shade event did not occur before this date and did not concern pavement zone 1.

In addition to these changes, several temperature spikes are present in the afternoon on both July 8th and 22nd. For pavement zones 1 and 2, these are mainly found on July 8th, with nearly all occurring during afternoon watering. On July 8th, the detected spikes are up to two 15-minute measurements wide. On July 22nd, when watering occurs more frequently, only two spikes are visible, excluding the temperature dip due to building shading. For the sidewalk zone, spikes are visible on both days. The amplitude of these local maxima is in the order of 5°C on July 8th for all three zones. On July 22nd, the amplitude of the sidewalk maxima is reduced to about 2-3°C while temperatures are comparable. In the morning of July 22nd, small temperature spikes may occur for the sidewalk zone, but these are of low amplitude and are hard to distinguish. Also, as was seen with pavement heat flux, a last, smoother spike is visible on July 22nd about 2 hours after the end of insolation for pavement zones 1 and 2.

Table 13.1 summarizes the average changes in surface temperatures between 6:30 am and 1 pm and between 3 pm and 6:30 pm on July 22nd (watered) compared to the average observations from July 20th and 21st (control).

Average temperature reductions on July 22nd are most important in the afternoon and most pronounced for pavement zone 1 followed by pavement zone 2. The sidewalk has the lowest average cooling of the three zones. In fact, the sidewalk is actually found to be 1.1°C warmer on the morning of July 22nd than on July 20th or 21st, despite pavement-watering. This is attributed to temperatures being about 5°C warmer in the hours preceding 6 am on July 22nd compared to July 20th and 21st (see Figure 13.1). While radiometric temperatures were about 25°C at 6 am on July 20th and between 3 am and 6 am on July 21st, reduced nighttime cooling, due to warmer meteorological conditions, on July 21st caused these temperatures to increase to roughly 30°C. Therefore, the calculation of the morning cooling effect on July 22nd should take this aspect into account. When this is the case, pavement-watering is found to reduce morning temperatures by about 4°C for the pavement surfaces and 2°C for the sidewalk.

Table 13.1 – Average temperature reductions observed on July 22nd (watered) compared to average control day temperatures (July 20th and 21st) (Hendel et al., 2014).

Time span	Pavement 1 (o)	Pavement 2 (+)	Sidewalk (x)
6:30 am – 1 pm	1.6°C	0.73°C	-1.1°C
3 pm – 6:30 pm	13°C	11°C	6.2°C

13.2 Discussion

Pavement-watering was found to reduce morning surface temperatures between 2° and 4°C and afternoon surface temperatures by between 6° and 13°C, depending on the surveyed area. In addition, the daily minimum temperature on watered days was the same as on control days despite warmer temperatures the night before. Also, pavement-watering maintained this minimum temperature for several hours instead of it being reached only briefly on control days. The maximum temperature reached was also reduced by several degrees. Finally, temperature spikes were observed on watered days, both before and during afternoon pavement-watering, which were not present on control days. No clear unquestionable spikes were observed in the morning.

As was seen with pavement heat flux, these effects demonstrate that pavement-watering limits the conditions favorable to the formation of UHIs. Indeed, reduced surface temperatures entail lower sensible atmospheric heating by convection. In contrast to high albedo pavements, this is accomplished without compromising pedestrian comfort as the radiant heat fluxes are not increased by watering. Indeed, while high albedo pavements also have lower surface temperatures and therefore reduce sensible heat flows to the atmosphere, they have been shown to increase daytime pedestrian radiant loads via increased SW reflection (Erell et al., 2013). In the case of pavement-watering, surface wetting tends to decrease pavement albedo, thus lowering reflected SW radiation (for further details on albedo change due to surface wetting, see Lekner and Dorf (1988)). However, the expected increase in air humidity caused by watering may negatively affect pedestrian comfort and should be accounted for.

Differences in surface temperatures in zones 1 and 2 may be explained by differences in pavement materials (hot- versus cold-mixed asphalt concrete), pavement geometry (different surface slopes) and the presence of the district heating main.

These pavement temperature observations are consistent with those made by Kinouchi and Kanda (1997, 1998) and Yamagata et al. (2008) who also conducted pavement-watering experiments in urban environments in Japan with regular or pervious asphalt pavements in similar conditions.

Furthermore, the temperature spikes observed are consistent with the heat flux spikes reported in Chapter 12 and coincide with pavement drying.

13.3 Conclusion

Pavement surface temperatures were found to be reduced by several degrees by pavement-watering, both during watering and several hours afterwards. Morning temperatures were reduced up to 4°C, while they were reduced on average by 13°C in the afternoon. Effects were greater for the pavement than the sidewalk.

Furthermore, temperature spikes similar to heat flux spikes described in Chapter 12 were also detected and are indicative of pavement drying.

CHAPTER 14

Pavement Temperature Effects

Having studied pavement-watering effects on pavement heat flux and surface temperature, we will now consider the temperature inside the pavement, 5 cm below its surface. Temperature data from July 7th, 8th, 10th, 11th, 20th and 22nd will be considered.

14.1 Results

Figure 14.1 illustrates pavement temperature measurements 5 cm below the surface on July 7th, 8th, 10th, 11th, 20th and 22nd, corresponding to paired reference and watered days.

On reference days, pavement temperatures range from a low of 23°-29°C to a high of 38°-43°C, with an average temperature amplitude of approximately 14.6°C. Temperatures decrease on average by 0.5°C from 6 am until approximately 8 am when they reach their daily low value. They then slowly increase until pavement insolation begins at 1:35 pm. At that time, temperatures rise sharply and level off at their daily maximum about one hour before insolation ends at 6:30 pm. Pavement temperatures then decrease until the next day when the cycle starts over.

On watered days, this range is reduced to between 23°-30°C and 31°-37°C, and the daily temperature amplitude is nearly halved, averaging approximately 7.7°C. Compared to reference days, morning pavement-watering significantly increases and prolongs the temperature decrease phase from 8 am to 1:35 pm. The morning temperature drop is increased to 2.8°C on average. As a result, daily minimum temperatures are practically unchanged compared to control days despite higher temperatures at 6 am, before morning watering. In the afternoon, the temperature increase is significantly shortened, leveling off much sooner as watering resumes. The time at which the daily high temperature is reached is unchanged by watering. As pavement insolation ends, temperatures decrease until the end of the day. In all

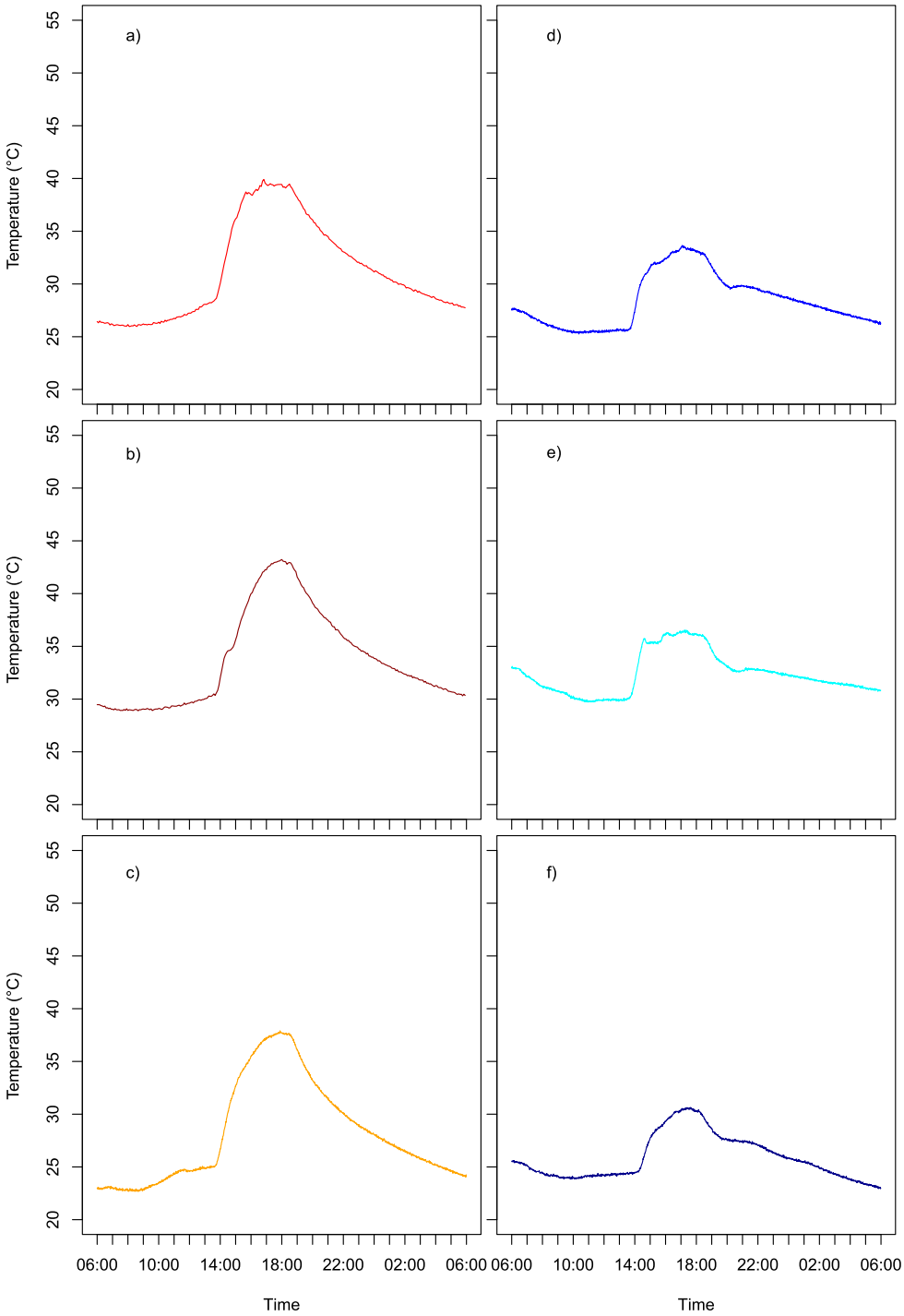

Figure 14.1 – Pavement temperature on reference days: a) July 7th, b) July 20th and c) July 11th; and on watered days : d) July 8th, e) July 22nd and f) July 10th (Hendel and Royon, 2015).

the watered days considered here, an interruption in this decrease occurs about 2.5h after sunset, as the remaining water film completely evaporates from the pavement surface.

Unlike in the case of pavement heat flux or surface temperatures, no spikes are detected for 5 cm temperatures.

Average temperatures between 3 pm and 6:30 pm are reduced by 6°C on July 8th compared to July 7th, by 5°C on July 22nd compared to July 20th, and by 6.5°C on July 10th compared to July 11th.

Table 14.1 summarizes daily low and high pavement temperatures as well as the daily temperature amplitude. Reference and watered days are paired to improve comparability and presented by intensifying watering strategy (see Chapter 12).

Table 14.1 – Daily low, high, and temperature amplitude on July 7th, 8th, 10th, 11th, 20th and 22nd, 2013 (Hendel and Royon, 2015).

Date	Low (°C)	High (°C)	Amplitude (°C)
July 7th	26.0	39.9	14.0
July 8th	25.3	33.7	8.4
July 20th	28.8	43.3	14.5
July 22nd	29.7	36.6	6.8
July 11th	22.7	37.9	15.2
July 10th	22.9	30.7	7.7

14.2 Discussion

The effect of pavement-watering on 5 cm pavement temperatures is clear: compared to control days, temperatures drop by an average 5.9°C in the afternoon and the morning temperature decrease is increased by 2.3°C and is prolonged until the beginning of pavement insolation. Furthermore, the daily temperature amplitude is nearly halved. Sensible heat storage by the pavement 5 cm below its surface is therefore offset by about five hours.

These effects indicate reduced heat storage on behalf of the pavement and therefore agree well with pavement heat flux observations made earlier (see Chapter 12). This adds evidence to the claim that pavement-watering limits the formation of UHIs.

These findings compare well with previous work by Asaeda et al. (1996), Kinouchi and Kanda (1998) and Li et al. (2013). Indeed, Asaeda et al. (1996) studied a 30 cm thick slab of asphalt concrete in Japan in nearly unmasked conditions instrumented with thermocouples at different depths including 5 cm. In their paper, the authors report 5 cm temperatures ranging from 26° to 48°C, thus an amplitude of 22°C, for air temperatures ranging from approximately 23°

to 35°C. No watering of the pavement slabs was conducted. Also in Japan, Kinouchi and Kanda (1998) studied a watered permeable pavement, also in nearly unmasked conditions, equipped with a pavement sensor at a depth of 5 cm. Air temperatures on the reported days ranged from 20°-23°C to 30°-35°C. The authors found daily low and high pavement temperatures in the order of 25°C and 40°-45°C, similar to Asaeda et al. (1996), in dry conditions, respectively. On watered days, these temperature extremes were reduced to 23°C and 35-38°C. Finally, Li et al. (2013) also study standard and pervious asphalt pavements in Davis, California. Impervious and pervious pavement temperatures 6.5 cm deep are nearly identical in dry conditions and range from roughly 25°C to 51°C for air temperatures between 16°C and 37°C. Watering the pervious pavements causes a 5°-7°C drop in temperatures compared to the dry impervious asphalt concrete.

The temperatures described in these papers are higher than our own, though they are comparable. This is likely due to the absence of insolation masks and to generally warmer summertime weather conditions in Japan and California compared to Paris. In addition, the temperature trends reported by Kinouchi and Kanda (1998) after watering are very similar to ours, including the reduction in low and high daily temperatures as well as that of their amplitude from 15°-20°C to 12°-15°C on watered days compared to control days. While watering reported by Li et al. (2013) causes similar temperature drops to our own during insolation, no significant change in pavement temperature amplitude is visible. These lower changes in daily temperature amplitude may be caused by reduced evaporation due to sprinkled water seeping deep into the pavement, where temperatures are too low for significant evaporation to occur. Overall, our results are comparable with those of these authors.

14.3 Conclusion

Pavement temperature 5 cm deep was shown to be reduced by 5.9°C by watering in the afternoon. Morning low temperatures, reached at 8 am on reference days, were maintained until the beginning of pavement insolation at 1:35 pm on watered days and were decreased by 2.3°C considering temperatures recorded at 6 am. In addition, the daily low-high temperature amplitude was nearly halved.

Finally, unlike the case of pavement heat flux and surface temperatures, no spikes in pavement temperature 5 cm deep were detected.

CHAPTER 15

Conclusion of Part 2

The field study conducted on rue du Louvre in Paris over the summer of 2013 has allowed us to assess the thermal effects of pavement-watering on a pavement area located 1.6 m away from the eastern sidewalk in a street with an aspect ratio H/W=1 and of approximate N–S orientation.

First, pavement heat flux density 5 cm deep (G) was found to be more than halved by pavement-watering during insolation, with morning and afternoon reductions reaching up to 50 and 150 W/m^2, respectively. Subsequent heat release by the pavement is also reduced in the evening following watering.

Second, pavement surface temperatures were found to be reduced by several degrees, both during watering and several hours after it had ended. Morning temperatures were reduced up to 4°C, while they were reduced by 13°C on average in the afternoon. Effects on the pavement were greater than for the sidewalk.

Third, pavement temperature 5 cm deep in the afternoon was shown to be reduced by 5.9°C by watering. Morning low temperatures, reached at 8 am on reference days, were maintained until the beginning of pavement insolation on watered days and were decreased by 2.3°C considering temperatures recorded at 6 am. Also, the daily low-high temperature amplitude was nearly halved.

Both heat flux and surface temperature spikes were observed on watered days and are indicative of pavement drying. None were found for 5 cm pavement temperature.

These trends are in good agreement with each other and the existing literature. Our results confirm that several of the fundamental mechanisms responsible for UHI formation and pedestrian thermal stress are affected by pavement-watering. Indeed, pavement heat absorption and storage are significantly reduced as evapotranspiration is artificially reintroduced into the urban environment. This was shown with pavement heat flux and temperature measurements. This results in a reduction of heat release at night, long after watering has ended, as was confirmed

by our observations. In addition, reduced heat absorption causes reduced surface temperatures both day and night, which have two positive consequences.

The first is the reduction of atmospheric sensible heating. Since the convective heat transfer is directly dependent on surface temperatures, atmospheric heating by the pavement is reduced or even reversed in watered areas. Consequently, the greater watered areas are, the greater atmospheric cooling will be. Wider-area watering should therefore result in greater cooling, as is confirmed when comparing Louvre and Belleville micro-climatic measurements.

The second consequence of lowered surface temperatures is reduced LW emission from the pavement, thus alleviating the radiative burden of pedestrians. Unlike in the case of reflective materials, this effect is not compensated for by increased SW reflection during periods of insolation due to increased reflection (Erell et al., 2013). On the contrary, the effects of the reduced LW radiation are reinforced by the effect of surface wetting as it reduces surface reflectivity (Lekner and Dorf, 1988). Combined with reduced emission, pavement-watering therefore reduces pavement radiosity as a whole. The pedestrian radiative load is thus improved both during insolation and during shading. This is confirmed with our observations of the effects of pavement-watering on MRT in Part 1.

On the other hand, increases in humidity will tend to adversely affect pedestrian comfort if they are high enough, but given that watering should occur when conditions are already quite dry (less than 50% RH), the humidity increase may be negligible from a thermal comfort standpoint. This is confirmed by the analysis conducted in Part 1 which found that relative humidity increases did not compensate for the other cooling effects of pavement-watering in the field conditions encountered.

We now have a better understanding of the fundamental mechanisms behind pavement-watering that help explain the micro-climatic effects determined in Part 1. The data and trends gathered here may be useful for the validation of numeric or experimental studies at different scales (see Chapter 22 and Appendices A, B and C). In an effort to propose improvements to the watering method, we now attempt to evaluate the costs of pavement-watering. Ways of reducing them while maximizing positive effects will be pursued.

With this goal in mind, pavement heat flux and temperature spikes will be analyzed and used to improve the watering frequency and period in Part 3. Moreover, the water intensity of the method will be determined and proposals to significantly reduce it while only marginally affecting pavement cooling will be made.

Part 3

IMPROVING THE WATER USE OF PAVEMENT-WATERING

CHAPTER 16

Introduction to Part 3

The micro-climatic effects of pavement-watering have been discussed in Part 1. Air temperature, mean radiant and UTCI-equivalent temperature reductions respectively reaching up to 0.8°C, 1.7°C and 1°C were found, while relative humidity was increased by less than 4.1%RH. These effects find their cause in the direct and indirect consequences of pavement-watering on the fundamental mechanisms which determine the urban micro-climate. These consequences include a 13°C reduction in surface temperature, a 5.9°C reduction in 5 cm pavement temperature and the halving of the daily pavement heat flux peak value during pavement insolation, as was determined in Part 2. Useful information on the benefits of pavement-watering in micro-climatic and physical terms has been obtained for dense urban environments.

However, we have not yet discussed the negative impacts of pavement-watering. Specifically, as climate change is expected to change the region's seasonal precipitation distribution (Burton et al., 2010; Jouzel et al., 2014), water use optimization of the technique will be crucial.

Pavement-watering implies the choice of a watering method and a corresponding urban infrastructure. For any given target-area, every watering method can be characterized by three parameters: the watering period, the watering rate and the watering frequency. The first outlines the period(s) of each day during which pavement-watering is active, the second is the average amount of water delivered per unit area and per unit time (expressed in mm/h, equivalent to L/m^2.h) and the last is the frequency of the watering cycles in the case of discontinuous watering. Of these parameters, the watering rate and period are the ones that define the method's water consumption. Their knowledge is therefore highly important for decision-makers who face growing public pressure to reduce urban water use and yet are considering pavement-watering as a UHI-countermeasure.

Several watering methods have been proposed or studied in the existing literature. For methods including vertical surface watering, a closed-loop watering

system is usually designed. He and Hoyano (2008) describe such a system with a water supply of 12 L/m^2.h for watered building walls. Wei and He (2013) conduct a similar simulation but include watering of the surrounding pavements which are water-retaining. The simulated permeable pavement is saturated at midnight, but no detail is given as to the amount of water required. In 2008, the City of Paris funded a numerical study aimed at testing different climate change adaptation strategies for heat wave events (Météo France and CSTB, 2012). This work analyzed a daytime pavement-watering method based on a hypothetical infrastructure using the city's non-potable water network. Pavements and sidewalks were watered at a rate of 0.2 mm/h for a duration of 3 minutes and a frequency of every hour. In parallel, a nighttime watering experiment was conducted over the summer of 2012 (Bouvier et al., 2013). A single watering event of the pavement and sidewalk was conducted by a cleaning truck around 10 pm, sprinkling 1 L/m^2 which is estimated by city officials as the maximum retention capacity of standard Parisian pavements.

Field studies conducted in Nagoaka City, Japan used an existing snow-melting infrastructure which consists of a ground-water network used to water the road surface. Kinouchi and Kanda (1997) ran this system continuously at a rate of 11 mm/h, while Takahashi et al. (2010) ran it intermittently to deliver an average 2 mm/h with 3-minute sprinkles activated as soon as the pavement dried, every 30 minutes on average. Yamagata et al. (2008) used reclaimed waste water sprinkled onto a water-retentive pavement by temporary pipes placed on a central road planter. The watering method parameters used are not specified in this study nor are they in any of the other cited studies previously mentioned.

Of these, only Takahashi et al. (2010) and Météo France and CSTB (2012) describe attempts to optimize the watering method with atmospheric cooling parameters. Takahashi et al. (2010) optimize both watering rate and frequency based on surface and 90 cm air temperature observations over a period of one hour after watering. Météo France and CSTB (2012) base their own optimization on findings from Takahashi et al. (2010) with the hypothesis of a pavement water-holding capacity of 1 mm. They optimize the watering rate based on 2 m a.g.l. air temperature simulations with a one-hour time step. Watering rates are deemed optimal as soon as marginal cooling gains are minimal. However, these analyses are only briefly described, with no mention of explicit targets or goals in either study.

This Part looks into the optimization of an adapted version of the pavement-watering method used by Bouvier et al. (2013). The pavement's thermal behavior, analyzed in Part 2 will be used to accomplish this.

We will demonstrate how pavement heat flux and surface temperatures measurements can be used to fine-tune the watering frequency, and how a surface heat transfer analysis combined with a linear relation found between heat flux and solar irradiance during pavement insolation can provide information on the watering rate. On this basis, we will propose significant reduction of the watering rate without significantly affecting obtained cooling.

First, Chapter 17 will present the methodology specific to this Part. Chapter 18 will then estimate the cooling flux created by pavement-watering in the afternoon on the basis of a linear relation between pavement heat flux and solar irradiance. Therefrom the evaporation rate will be determined. Chapter 19 will focus on improving the watering period and frequency on the basis of the thermal effects reported in Part 2. Finally, Chapter 20 will attempt to optimize the watering rate.

This Part is based on the peer-reviewed work published in *Applied Thermal Engineering* and in *Urban Climate* (Hendel et al., 2015a, 2014).

CHAPTER 17

Methodology

The methodology specific to this Part will now be presented.

17.1 Heat Transfer Analysis

Figure 17.1, already provided in Chapter 11, shows a diagram of the heat fluxes relevant to this experiment.

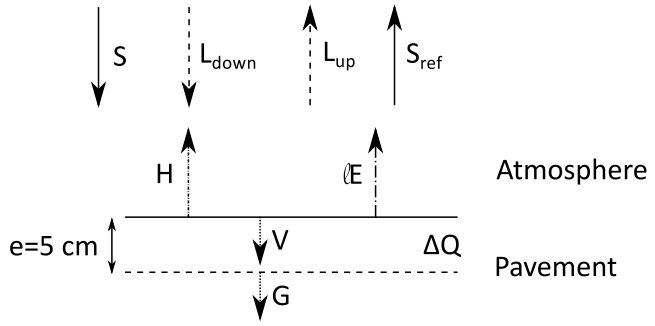

Figure 17.1 – Diagram of pavement heat budget at surface (Hendel et al., 2015a).

Heat absorption by the water film is not illustrated in Figure 17.1 but is taken into account in the last item of the heat budget in equation 17.3, defined in equation 17.6. Indeed, in the case of excessive watering, significant runoff towards the sewer system may occur, thus transfering heat by advection into the sewers.

Asaeda et al. (1996) and Kinouchi and Kanda (1998) characterize the energy balance of the pavement surface with the following equations:

$$R_n = S + L_{down} - L_{up} - S_{ref} \tag{17.1}$$

$$R_n^{dry} = H^{dry} + V^{dry} \tag{17.2}$$

$$R_n^{wet} = H^{wet} + V^{wet} + \Phi \tag{17.3}$$

$$V = G + \Delta Q \tag{17.4}$$

$$\Phi = \Phi_{lat} + \Phi_{adv} \tag{17.5}$$

$$\Phi = lE + \rho c_p \frac{V_S}{t_0} \left(T_S^{wet} - T_W \right) \tag{17.6}$$

R_n is the net downward radiation received by the pavement surface and is the sum of solar irradiance (downward SW radiation) S, downward LW radiation L_{down}, reflected SW radiation S_{ref} and upward LW radiation L_{up}; H is the upward atmospheric sensible heat flux, due to convection; V is the downward pavement heat flux at the surface; l is the latent heat of vaporization of water (2,260 kJ/kg); E is the evaporation rate; c_p is the specific heat of water (4.18 kJ/kg.K); ρ is the density of water (1,000 kg/m^3); V_S is the water volume dispersed per unit surface area (1 L/m^2); t_0 is the water cycle period in seconds; T_W is the water temperature; ΔQ is the heat flux absorbed by the first 5 cm layer of pavement. Φ designates the pavement-watering cooling flux.

The pavement-watering cooling flux Φ has two components, a latent flux component Φ_{lat} and an advective flux component Φ_{adv}. Both components are positive and are dependent on the watering rate (V_S/t_0).

By subtracting equation 17.3 by equation 17.2, we obtain:

$$\Phi = H^{dry} - H^{wet} + V^{dry} - V^{wet} + L_{up}^{dry} - L_{up}^{wet} + S_{ref}^{dry} - S_{ref}^{wet} \tag{17.7}$$

According to Jürges (1924), convective heat flux can be written as:

$$H = h \left(T_S - T_a \right) \tag{17.8}$$

T_S is the surface temperature of the pavement and T_a is that of the air above it. h is the convective heat transfer coefficient.

Furthermore, following the Stefan-Boltzmann law and infrared reflection, L_{up} can be expressed as:

$$L_{up} = \epsilon \sigma T_S^4 + (1 - \epsilon) L_{down} \tag{17.9}$$

ϵ is the emissivity of the emitting surface, while σ is the Stefan-Boltzmann constant.

By definition, S_{ref} can be expressed as:

$$S_{ref} = \alpha S \tag{17.10}$$

Where α is the surface albedo, i.e. its SW reflectance.

Hence:

$$L_{up}^{dry} - L_{up}^{wet} = \sigma \left(\epsilon_{dry} T_S^{dry^4} - \epsilon_{wet} T_S^{wet^4} \right) + (\epsilon_{wet} - \epsilon_{dry}) L_{down} \tag{17.11}$$

And :

$$S_{ref}^{dry} - S_{ref}^{wet} = (\alpha_{dry} - \alpha_{wet}) S \tag{17.12}$$

From these equations, the following can be derived:

$$\begin{aligned}\Phi &= h\left(T_S^{dry} - T_S^{wet} + T_a^{wet} - T_a^{dry}\right) + V_{dry} - V_{wet} + (\alpha_{dry} - \alpha_{wet})\, S \\ &\quad + \sigma\left(\epsilon_{dry} T_S^{dry^4} - \epsilon_{wet} T_S^{wet^4}\right) + (\epsilon_{wet} - \epsilon_{dry})\, L_{down}\end{aligned} \tag{17.13}$$

The resulting heat budget is analogous to that used by He and Hoyano (2008) and Wei and He (2013) for a vertical surface with a water film.

Therefore, knowledge of G, ΔQ, L_{down}, S, h, air, water and pavement surface temperatures as well as pavement emissivity and albedo under dry and wet conditions allows an estimation of the latent heat flux and thus the evaporation rate.

Unfortunately, L_{down} was not measured. In dry conditions, the asphalt surface's emissivity (ϵ_{dry}) was measured to be 0.97, while in wet conditions the surface's emissivity (ϵ_{wet}) is that of water, equal to 0.98. Because the difference in emissivity between the wet and dry pavements is minor, it is neglected in the second term of equation 17.11. Thus:

$$L_{up}^{dry} - L_{up}^{wet} = \sigma\left(\epsilon_{dry} T_S^{dry^4} - \epsilon_{wet} T_S^{wet^4}\right) \tag{17.14}$$

Furthermore, pavement albedo was not measured either. According to Santamouris et al. (2001), the typical albedo range for asphalt is 0.05 to 0.20, the former value referring to new asphalt pavements, the latter to older ones. Because of the road work necessary to lay the pavement sensor, the pavement above it was practically new. We therefore assume an albedo of 0.05 in dry conditions. According to Lekner and Dorf (1988), since $\alpha_d << 1$, both dry and wet asphalt have approximately equal albedos: $\alpha_w \approx \alpha_d$. Therefore: $S_{ref}^{dry} - S_{ref}^{wet} \approx 0$. This holds true for the rest of the pavement surface as well if an albedo of 0.10 is assumed.

Finally, several empirical formulæ exist to calculate h based on wind speed (v). These include equation 17.15 used by Kusaka et al. (2001) and equation 17.16 by Duffie and Beckman (1991).

$$h = 6.15 + 4.18v \tag{17.15}$$

$$h = 5.7 + 3.8v \tag{17.16}$$

Under the field conditions described (hourly wind speed approximately equal to 1 m/s), h is approximately equal to 10 W/m².K.

With these approximations, the following expression of Φ is obtained:

$$\Phi = h\left(T_S^{dry} - T_S^{wet} + T_a^{wet} - T_a^{dry}\right) + \sigma\left(\epsilon_{dry} T_S^{dry^4} - \epsilon_{wet} T_S^{wet^4}\right) + V^{dry} - V^{wet} \tag{17.17}$$

Thus, knowledge of G, ΔQ, air, water and pavement surface temperatures under dry and wet conditions is sufficient to estimate the latent heat flux.

The analysis of the mass convection transport problem can also be used to estimate the evaporation rate, although it is inadequate at optimizing the watering frequency. This method assumes that evaporation is uninterrupted, i.e. that the watered surface does not dry out. Pagliarini and Rainieri (2011) use such a method to determine the evaporation rate on a continuously-watered glass roof. Adapted to our problem by assuming that the water film and the road surface have the same temperature, their equation becomes:

$$lE = 0.622 \frac{lh}{c_{p_{air}} p_0} T_S^{wet} \left(\frac{p_s}{T_S^{wet}} - \frac{p_v}{T_a^{wet}} \right) \tag{17.18}$$

p_0, p_s and p_v represent total air pressure, saturation vapor pressure at the water film temperature $T_{S,wet}$ and partial air vapor pressure at $T_{a,wet}$ in Pa, respectively. c_{pair} is air specific heat (1.005 J/g.K).

The meteorological data used to solve this equation later on was recorded by Météo-France's Montsouris weather station and consists of hourly measurements. This approach will be used to confront the results obtained from the heat transfer analysis in Chapter 18.

17.2 Optimization Goals

Optimizing the watering parameters (watering period, rate and frequency) requires that we define a set of optimization goals. The goal of pavement-watering is to improve micro-climatic conditions as much as possible while creating minimal negative impacts.

As was previously discussed, micro-climatic effects are the result of pavement cooling caused by watering. Therefore, the goal of maximizing improvements to micro-climatic conditions will be replaced by the goal of maximizing pavement cooling Φ.

The first negative impact which comes to mind when considering pavement-watering is water consumption. Daily water consumption is determined by the combination of the watering rate and the watering period. Pavement-watering effects only last as long as the pavement remains wet. Since reducing the watering period will directly affect the duration of the sought-after effects, we will focus on minimizing the watering rate. As a last resort after other optimization efforts have been made, the watering period can be reduced if daily water consumption remains too high for feasibility.

In addition to using water, pavement-watering as it was conducted in our experiment implies the use of cleaning trucks. These create disturbances for traffic and pedestrians, noise- and air-pollution as well as energy consumption and green house gas emissions. Considering each cleaning truck pass as a negative impact that must be minimized, we include minimizing the pavement-watering frequency in our optimization goals, in addition to maximizing pavement cooling and minimizing the watering rate and period.

Our optimization goals are thus the following, by order of importance:

1. Minimize the watering frequency, i.e. maximize t_0
2. Maximize obtained pavement cooling, Φ
3. Minimize the watering rate, V_S/t_0
4. Minimize the watering period

Goals # 2 and # 3 can be recombined as :
Minimize the watering rate to pavement cooling ratio, $\left(\frac{V_S}{t_0}\right)/\Phi$.

These goals are tailored to our watering method, i.e. short sprinkling events occurring at regular intervals over a given period of the day. However, they can easily be adapted to the case of a watering infrastructure that runs continuously or causes no negative impacts. In that case, goal # 1 can be dropped, while goals # 2, # 3 and # 4 remain valid.

CHAPTER 18

Cooling Flux Φ: Determining the Evaporation Rate

We now proceed to determine the surface cooling flux Φ attributable to pavement-watering in order to determine the evaporation rate.

Kinouchi and Kanda (1998) put into perspective a correlation between R_n and G. They proceeded by plotting G as a function of R_n. Camuffo and Bernardi (1982) explore the hysteris cycles found between surface heat fluxes and net radiation for soil, including V as a function of R_n. Other authors such as Asaeda et al. (1996), studying the effect of pavement heat storage on the lower atmosphere, also look into this hysteris cycle for asphalt and concrete pavements.

Because net radiation was not measured, we shall proceed in an analogous fashion with S instead. This will permit the estimation of the surface cooling effect of pavement-watering based on a relation between S and G during pavement insolation. From this an estimate of the evaporation rate is obtained.

18.1 Results

Figure 18.1 shows G as a function of S on reference days: a) July 11th, b) July 14th, c) July 20th ; and on watered days: d) July 8th, e) July 22nd and f) July 10th. The chronological order of the data points is counterclockwise. The least square regression line of G according to S between 3 pm and 6:30 pm, when the pavement has been both insolated and watered for at least 30 minutes, is plotted for each date.

The parameters from the linear regression can be formalized as:

$$G = \beta S + G_0 \tag{18.1}$$

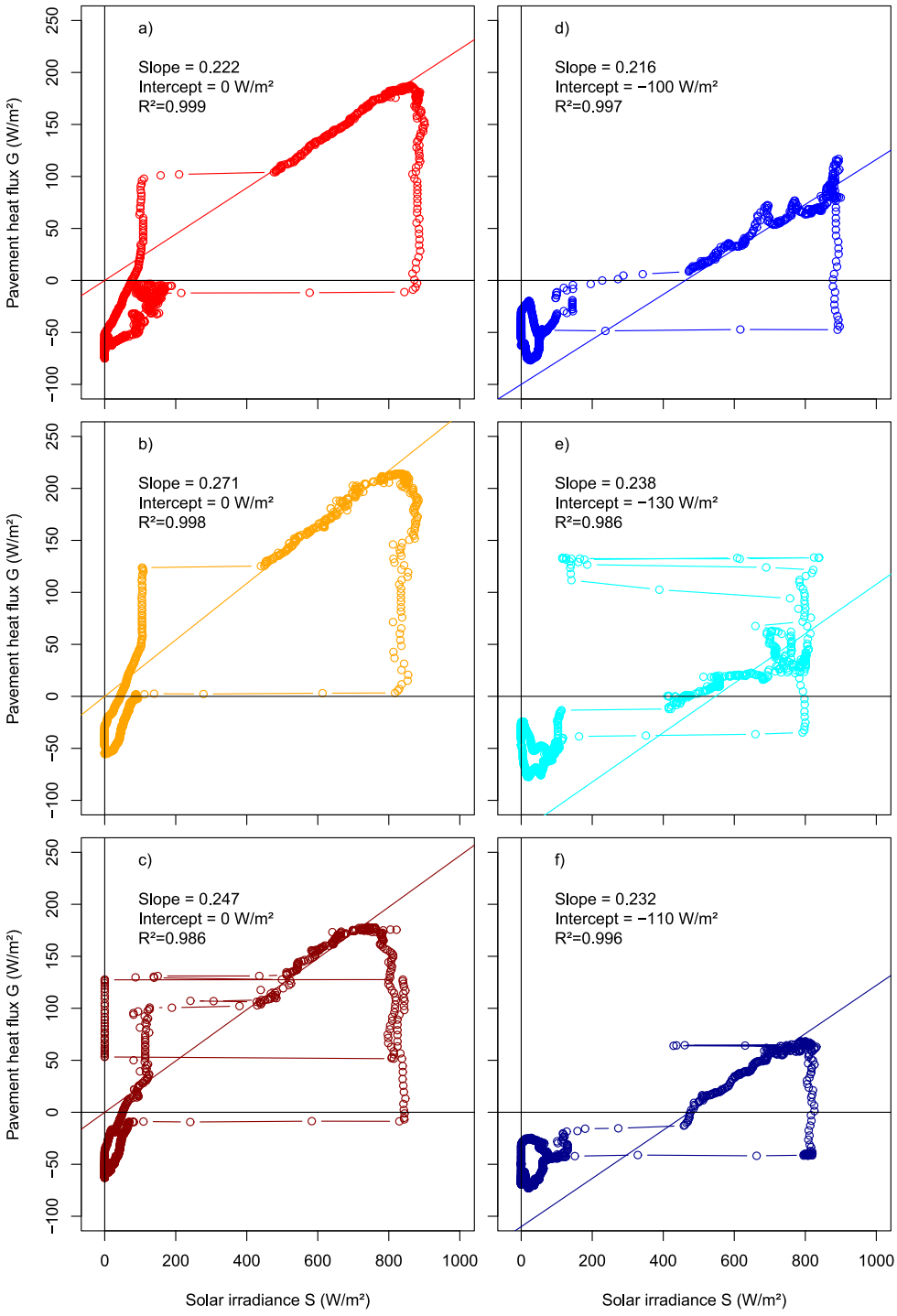

Figure 18.1 – G as a function of S on control and watered days. a) July 11th, b) July 14th, c) July 20th, d) July 8th, e) July 22nd, f) July 10th, 2013 (Hendel et al., 2015a).

β is the conversion coefficient of solar irradiance to pavement heat flux 5 cm below the pavement surface, while G_0 is the intercept heat flux under these conditions.

The regressions were conducted for reference and watered days. On reference days, an intercept of 0 W/m² was used. Table 18.1 summarizes the regression parameters for reference days.

Table 18.1 – β and R^2 on reference days (Hendel et al., 2015a).

	July 11th	July 14th	July 20th
β	0.222	0.271	0.247
R^2	0.999	0.998	0.986

Each fit is stat. sign., with coefficients of determination in excess of 0.98. Overall, the conversion coefficients derived on reference days range from 22% to 27%.

On watered days, different intercepts, corresponding to the average reduction of G found in Table 12.2, were tested. Using these intercepts, similar slopes to those found on control days were obtained. Table 18.2 summarizes the regression parameters using the different intercepts for watered days.

Table 18.2 – β, R^2 and G_0 (W/m²) on watered days. The value of G_0 was input by the user (Hendel et al., 2015a).

	July 8th		July 22nd		July 10th	
Control	July 11th	July 14th	July 14th	July 20th	July 11th	July 14th
G_0	-100	-120	-130	-150	-110	-130
β	0.216	0.244	0.237	0.269	0.232	0.262
R^2	0.997	0.995	0.986	0.985	0.996	0.996

Regardless of the intercept value used, the conversion coefficients deviate only slightly from those derived on reference days, remaining in the same 22-27% range. Considering the statistical significance of these regression parameters, it is concluded that pavement-watering does not significantly affect the conversion coefficient, but adds a constant heat flux, G_0.

Solar energy is thus transmitted in the same manner 5 cm below the pavement surface when wet or dry up to a constant. It can therefore be assumed that ΔQ is unchanged by watering during insolation, i.e. $\Delta Q_{wet} = \Delta Q_{dry}$. In other words, V is also unchanged up to the same constant as G when dry or watered in insolated conditions. This hypothesis is in agreement with experimental data presented by Kinouchi and Kanda (1998), which illustrate that ΔQ is unaffected by pavement-watering.

This information allows the estimation of the cooling created by the sprinkled water. The contribution from water advection is found to be between 23 and 35 W/m², while that of evaporation is 269-341 W/m².

This is derived by using the regression parameters from equation 18.1 in equation 17.13, resulting in the following equation:

$$\Phi = h(T_S^{dry} - T_S^{wet} + T_a^{wet} - T_a^{dry}) + \sigma(\epsilon_d T_S^{dry^4} - \epsilon_w T_S^{wet^4}) - G_0 \qquad (18.2)$$

As stated in Chapter 6, previous studies of pavement-watering report air temperature reductions of up to 4°C (Kinouchi and Kanda, 1997, 1998; Takahashi et al., 2010; Yamagata et al., 2008; He and Hoyano, 2008; Wei and He, 2013; Météo France and CSTB, 2012; Bouvier et al., 2013; Maillard et al., 2014). It is assumed that $-2°C \leq T_a^{wet} - T_a^{dry} \leq 0$ for the purpose of this analysis. Uncertainty propagation due to estimated parameters such as this one is integrated following Kline and McClintock (1953).

In addition, collected surface temperature data (see Chapter 13) reveal an average reduction during insolation of 13°C, from 50°C (323 K) to 37°C (310 K). These findings agree well with observations made by (Kinouchi and Kanda, 1997) and (Wei and He, 2013). Having found that $h = 10\ W/m^2.K$, and considering that $110\ W/m^2 \leq -G_0 \leq 150\ W/m^2$ on days with 30-minute watering:

$$304\ W/m^2 \leq \Phi \leq 364\ W/m^2$$

As stated in Chapter 6, past non-potable water analyses conducted by the city services have shown that its temperature is in the 20-25°C range on hot summer days. Assuming that the runoff temperature increases to 35°C by contact with the pavement, we obtain:

$$\begin{cases} 23\ W/m^2 \leq \Phi_{adv} \leq 35\ W/m^2 \\ 269\ W/m^2 \leq lE \leq 341\ W/m^2 \end{cases}$$

These assumptions on non-potable water temperature were confirmed by field measurements conducted during the summer of 2014 using a spot Pt-100 temperature sensor. Water temperature was measured at the cleaning truck hose and at the sewer inlet after watering.

Considering a latent heat of vaporization of 2,260 kJ/kg, it can be asserted that the evaporation rate is between 0.119 and 0.151 g/m².s, i.e. between 0.43 and 0.54 mm/h. This means that for each 30-minute watering cycle, 0.21 to 0.27 mm evaporate. Since the preliminary pavement heat flux analysis has shown that the pavement dries off after 30 minutes, it can be asserted that the rest of the water runs off into the sewer system.

18.2 Confrontation with Mass Convection Transport Problem

This solution will now be compared to the solutions obtained with the mass convection transport problem. Table 18.3 provides the relevant meteorological parameters and the solutions obtained by solving equation 17.18 for days with 30-minute watering, i.e. July 22nd and 10th, 2013. The values indicated are the averages of each parameter recorded by Météo-France at their Montsouris station between 3 pm and 6:30 pm.

Table 18.3 – Average value of meteorological parameters on July 22nd, and 10th, 2013 between 3 pm and 6:30 pm and corresponding solutions to equation 17.18 (Hendel et al., 2015a).

	July 22nd	July 10th
p_0 (Pa)	100,500	100,900
T_{Swet} (K)	310	310
T_a (K)	306	299
RH	33%	45%
p_s (Pa)	6,295	6,295
p_v (Pa)	1,665	1,516
lE (W/m^2)	641	655
E (g/m^{2}s)	0.284	0.290

As can be seen from Table 18.3, the evaporation rates thus obtained are about three times higher than those obtained by solving the heat transfer problem. Since both methods were taken from the existing literature and are rigorous, they should agree if the shared parameters and assumptions are correct.

One implicitly shared assumption is that evaporation at the pavement surface is continuous between 3 pm and 6:30 pm. Since the pavement remained wet in between watering cycles (e.g. absence of heat flux spikes), this assumption is correct and is therefore not the cause of the observed discrepancy.

The only remaining shared parameter that must have been incorrectly estimated is the convective heat transfer coefficient h. Good agreement between both methods is found if h is assumed equal to 3.5 W/m^2.K.

Previous overestimation of h is attributed to the use of 4 m wind speed measurements. These may not be representative of wind conditions closer to the pavement responsible for the convective transfers taking place. Although 3.5 W/m^2.K may seem rather low based on equations 17.15 and 17.16 used in Chapter 17, it should be noted that the weather conditions under which pavement-watering was conducted are chosen to be representative of heat waves, with high temperatures, strong insolation and low wind speeds. They are therefore not representative of typical weather conditions for Paris. This also explains the low

RH observed on these two days.

Table 18.4 presents the results from the mass convection transport problem with the corrected convective transfer coefficient.

Table 18.4 – Solutions to equation 17.18 obtained with $h = 3.5\ W/m^2.K$ (Hendel et al., 2015a).

	July 22nd	July 10th
lE (W/m²)	224	229
E (g/m².s)	0.099	0.101

With $h = 3.5\ W/m^2.K$, total pavement cooling found using equation 18.2 amounts to between 232 and 279 W/m², divided between water advection and evaporation as follows:

$$\begin{cases} 23\ W/m^2 \leq \Phi_{adv} \leq 35\ W/m^2 \\ 198\ W/m^2 \leq lE \leq 256\ W/m^2 \end{cases}$$

This corresponds to an evaporation rate of between 0.087 and 0.113 g/m².s, i.e. between 0.31 and 0.41 mm/h. This means that for each 30-minute watering cycle 0.16 to 0.20 mm of water evaporate.

18.3 Discussion

The analysis of G as a function of S during insolation after the initial transient period has allowed us to estimate Φ to between 232 to 279 W/m² of pavement surface cooling attributable to pavement-watering.

This cooling flux corroborates our previous claims that pavement-watering may reduce UHI intensity as it creates a cooling flux, mainly based on latent heat exchange by water evaporation. Pavement-watering can be considered as a form of evapotranspiration on behalf of the pavement, helping it better regulate its temperature and thus reduce atmospheric heating.

Our estimations of latent heat flux are consistent with those reported by Météo France and CSTB (2012) who find that latent heat flux can reach up to 180 W/m². They also agree well with findings by He and Hoyano (2008) who report an advective heat flux of 23-47 W/m² and a latent heat flux of 250-320 W/m² for a westward-facing building wall cooled by a circulating water film.

Another consequence of these results is information on the water-holding capacity of the pavement. Since the pavement dries 30 minutes after watering during insolation (see Chapter 13 for further details), the water-holding capacity of the pavement is therefore equal to the amount of water evaporated in between watering cycles, i.e. between 0.16 and 0.20 mm. This is significantly less than that assumed by Météo France and CSTB (2012), but is only valid for the portion of

pavement surveyed by the heat flux sensor. This portion has a specific geometric configuration and surface composition (cold- versus hot-mix asphalt concrete).

Sources of uncertainty in these estimations lie in the use of S rather than R_n, assumptions regarding water temperature changes and those regarding ΔQ. Concerning the latter, observations over several days by Kinouchi and Kanda (1998) substantiate our assumption as does the presented analysis of G which is unchanged up to a constant in dry and wet conditions over the considered time span.

18.4 Conclusion

A linear relation was found between pavement heat flux G and solar irradiance S during insolation (equation 18.1), unchanged up to a constant on watered days compared to reference days. Inputting this information into the heat transfer analysis described in Chapter 17 then allowed us to estimate the pavement-watering cooling flux Φ to 232-279 W/m^2 and thus the evaporation rate to between 0.31 and 0.41 mm/h. In the process, the water-holding capacity of pavement zone 1 was estimated to between 0.16 and 0.20 mm. The estimation of the evaporation rate was confirmed by an independent evaluation obtained by solving the mass convection problem.

In the study conditions, evaporation was found to represent at least 85% of total cooling, while representing a mere 20% at most of water use. This will be analyzed further in Chapter 20 to optimize the watering method. First, we now attempt to optimize the watering frequency in Chapter 19.

CHAPTER 19

Watering Frequency Optimization

Following the goals set in Chapter 17, we now attempt to minimize the watering frequency while maximizing pavement watering cooling. We proceed by comparing the spikes detected in the series analyzed in Part 2 with the occurrence of watering cycles. Watering cycle times were reported by the cleaning truck drivers and crosschecked with visible images from the rooftop IR camera (see Chapter 6).

19.1 Results

The measurement data for G, pavement surface and 5 cm temperatures will now be analyzed with this goal.

Pavement Heat Flux

Figure 19.1 illustrates G (solid line) on watered days and watering cycles (dot-dashed vertical lines).

As can be seen, spikes in G coincide nearly perfectly with watering cycles, allowing for the imprecision of watering time reporting. As is confirmed by visible images taken by the rooftop IR camera, these spikes are indicative of pavement drying.

The daily peak of pavement heat flux is thus found to coincide with the beginning of afternoon watering on all considered days except on July 10th when afternoon watering began at the same time as pavement insolation. Furthermore, spikes in the afternoon coincide with watering cycles that are 45 minutes apart or more, apart for the secondary spike on July 22nd which is linked to a 50 minute interruption in watering. Finally, the last peak, much smoother than the others, occurs 2-2.5 hours after the end of insolation.

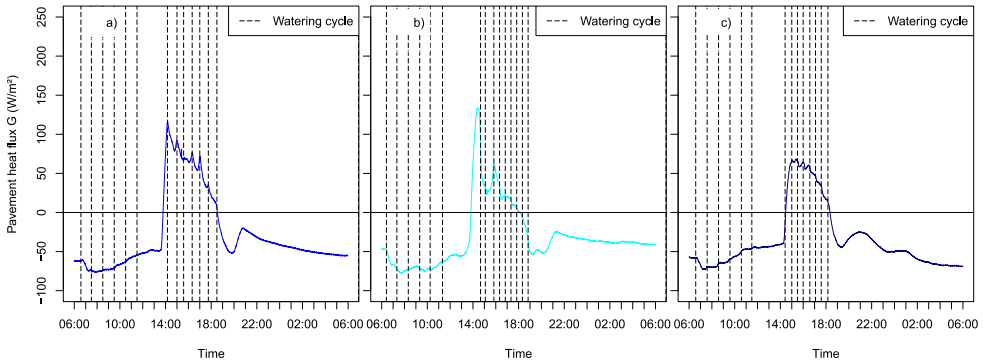

Figure 19.1 – Watering cycles and pavement heat flux on a) July 8th, b) July 10th and c) July 22nd, 2013.

This provides insight on two aspects of the watering method: its watering period and its frequency. First, the value of the daily maximum of G depends on the start of afternoon watering relatively to pavement insolation. Second, if the pavement watering frequency is too low, the pavement surface has enough time to dry and G rises towards its normal reference value until the next watering cycle.

As was noted in Chapter 12, the observed reduction is inversely proportional to the delay between the start of afternoon watering and the start of pavement insolation. In order to minimize the daily heat flux peak, watering should therefore begin just a few minutes prior to pavement insolation. This will ensure that the pavement is wet when the sun begins to shine on it, limiting its heat absorption and the daily heat flux peak.

Furthermore, the watering frequency must be adjusted to prevent the pavement surface from drying between cycles. Our observations suggest that a period of 45 minutes is too long, while 30 minutes is nearly optimal during insolation. In the morning in shaded conditions, the data suggests that watering every hour is sufficient, but a lower frequency may be achievable without causing surface drying. Evidence to support this is found in the last peak which occurs 2-2.5 hours after the end of insolation, which indicates that the time required for the pavement to dry in the shade is in the order of two hours. It may therefore be possible to halve the morning watering frequency, especially considering that air temperatures are cooler than in the evening.

Surface Temperatures

Surface temperature spikes both before and during pavement-watering were detected on watered days, as seen in Chapter 13. Figure 19.2 illustrates surface temperature measurements alongside watering cycles, marked by vertical dot-dashed lines.

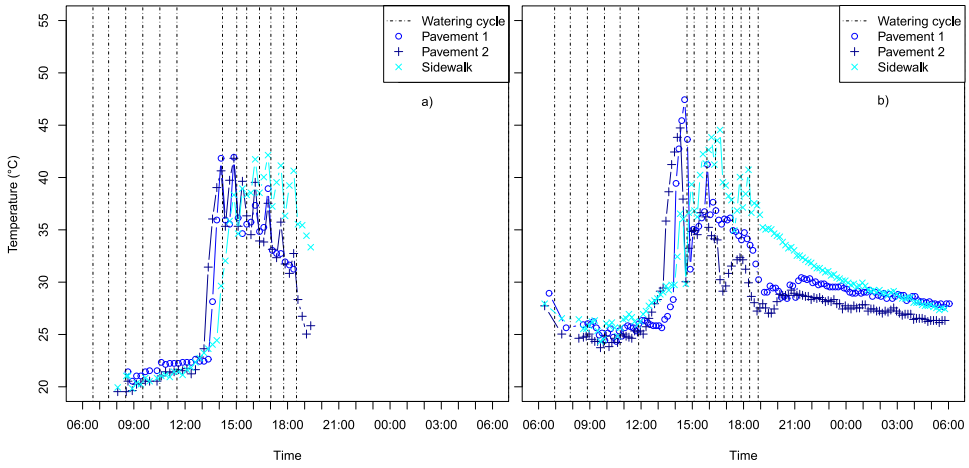

Figure 19.2 – Surface temperature and watering cycles on watered days: a) July 8th and b) July 22nd.

As was seen with pavement heat flux G, surface temperature spikes coincide very well with watering cycles. Spikes just before afternoon watering begins occur for the pavement zones only. This is because the studied areas are not insolated simultaneously and pavement-watering began before the sidewalk was insolated, but not before the pavement zones were.

Similarly to pavement heat flux, the daily surface temperature peaks are found to coincide with the first afternoon watering cycle for both pavement zones, apart for the sidewalk zone which is insolated only after watering resumes. Also, their intensity is proportional to the delay in afternoon watering vs. surface insolation.

Spikes ensue in the afternoon if watering is applied every 45 minutes, except for the sidewalk for which 30-minute watering does not prevent their appearance. Indeed, for pavement zones 1 and 2 the second spike on July 22nd occurs after a 50-minute long interruption in watering. Although sidewalk spikes occur on both days, they are smaller on July 22nd.

These local temperature spikes allow us to make recommendations to improve the effect of pavement-watering: as was seen with pavement heat flux spikes, afternoon watering should begin just before surface insolation to limit the initial temperature increase, while a watering cycle period of 30 minutes for the pavement seems sufficient to erase spikes which occur during afternoon pavement-watering. However, 30-minute watering remains too long for the sidewalk which requires a higher frequency. One-hour watering is sufficient for morning shaded conditions for all surfaces, but a lower frequency may be achievable without deteriorating the obtained results. As was found for heat flux, a last peak occurs 2-2.5 hours after the end of insolation. This also indicates that it may be possible to halve the morning watering frequency without affecting cooling.

The trends seen here are similar to those found for pavement heat flux. The

first spikes in surface temperatures are reached because the first afternoon watering cycle occurs too late compared to the last morning watering cycle. The spikes observed once afternoon watering is underway indicate an insufficient watering frequency. Watering earlier should reduce the daily temperature maximum by slowing the temperature increase, while increasing the watering frequency should erase these temperature spikes. The former recommendation was applied on July 10th, but the IR camera was nonoperational on that date. However, similar changes to those seen for G are expected. The second recommendation is confirmed by comparing temperatures from July 8th with 22nd, when the watering cycles occurred every 45 and 30 minutes, respectively.

Since spikes are still visible for the sidewalk zone even with 30-minute watering, a higher watering frequency is necessary to reach maximum cooling for that surface. This is due to the sidewalk's asphalt surface course whose texture is significantly smoother than that of the pavement zones. It therefore retains less water than the pavement, resulting in shorter-lasting cooling and increased runoff. The difference in watering method, with the manual hose rather than the vehicle's sprinkler, may also explain part of this difference as it was more difficult to uniformly water the sidewalk due to the presence of pedestrians and other obstacles.

Judging by the behavior of sidewalk temperatures between watering cycles, the optimal watering frequency seems to be between every 10 and 20 minutes.

5 cm Pavement Temperatures

In comparison to the 5 cm pavement heat flux and surface temperature observations, no significant 5 cm temperature spikes are visible before or during afternoon watering.

No conclusions can therefore be drawn from these observations to improve the watering method.

19.2 Discussion

Heat flux and surface temperature spikes coincide well with watering cycles and as such are indicative of pavement drying, as was confirmed with visible images. They were thus used to adjust the watering period and frequency to keep the pavement surface wet as long as possible, particularly during pavement insolation. Watering just before the beginning of insolation and every 30 minutes thereafter for pavement zones 1 and 2 were recommended as a result, but was found to be insufficient for the sidewalk zone. One-hour watering in the morning was found to be acceptable for all surfaces but it is likely that this frequency can be halved without affecting obtained cooling. No spikes were detected for pavement temperature 5 cm deep, which could therefore not be used for this analysis.

Our recommended watering frequency is the same as that used by Takahashi et al. (2010) who also use a watering rate of 2 mm/h. However, it is twice as fast as

that found by Météo France and CSTB (2012), despite cooler weather conditions. Reasons for this discrepancy are likely linked to their hypothesis on the pavement water-holding capacity, assumed to be 1 mm. Indeed, we found in Chapter 18 that the pavement water-retaining capacity of our studied area was between 0.16 and 0.20 mm, i.e. at least five times lower than their assumption. However, if the water-retaining capacity of our pavement was 1 mm, given our evaporation rate of 0.31-0.41 mm/h, watering every 2.5-3 hours would have been sufficient. Differences in pavement water-holding capacities are therefore unable to explain the observed discrepancy. Other factors may include dissemblance between the average Parisian urban canyon computed by Météo France and CSTB (2012) and the rue du Louvre canyon, the decrease in insolation intensity between the months of July and August or the one-hour time step of their simulation. It is difficult to favor one of these over the others.

We now turn to the potential limits of our analysis for each parameter, the explanations thereof and potential solutions.

Pavement Heat Flux

As pavement heat flux measurements are conducted continuously every minute, no heat flux spike omissions are expected. Still, the heat flux signal 5 cm below the pavement surface is necessarily dampened by the overlying materials. This reduces the sensitivity of G as an indicator of pavement drying, possibly leaving spikes occurring in the last minutes before watering or seemingly insignificant ones undetected. For example, the small variations in G on July 10th may indicate surface drying but were disregarded in light of their limited amplitude.

Fortunately, watering recommendations made on the basis of heat flux spikes and surface temperature spikes are in good agreement. Since surface temperatures are not dampened by any overlying materials, the good agreement found indicates that G is only marginally affected by the inertia of surface course materials. However, surface temperature measurements were only made every 10 minutes at best, leaving room for undetectable spikes to appear.

From the point of view of optimizing the watering frequency, heat flux measurements have the advantage of being nearly continuous. Since signal spikes can be detected immediately with little or no risk of omitting any, the optimal watering frequency can be determined from watering the target area a single time and measuring the time it takes for it to dry. Indeed, the best watering frequency is the lowest one which prevents the target area from drying between cycles, i.e. the time it takes for the surface to dry. Two to three such measurements on the hot days are likely sufficient to determine the best pavement-watering in our case: one in the morning and one at the beginning of pavement insolation. If need be, another such measurement can be conducted a couple of hours before the end of insolation, representative of the lower insolation intensity. The optimal frequency for the morning and the afternoon would therefore be known. In the case of periods of extreme heat, a correction factor may need to be applied.

On the other hand, pavement heat flux measurements require very costly and invasive road work to install relevant sensors. Furthermore, they are unable to survey several areas at a time. This is not the case of surface temperature measurements conducted with IR instruments.

Surface Temperatures

Because the surface temperature measurement frequency is 10 minutes at best, surface temperature spikes may have been omitted in the last minutes prior to watering cycles, in between two consecutive IR camera measurements. Closer analysis of the temporal distribution of the data shows that measurements occur as little as four minutes before watering cycles on July 22nd without the detection of spikes. However, this does not exclude the possibility of undectected spikes during these last four minutes.

To remedy this, measurements can either be more frequent or they can be synchronized with watering cycles so as to occur a few seconds before watering. In the case of a manual watering method such as ours, it is not possible to reliably synchronize measurements with watering cycles. Watering cycles are not distributed as regularly as planned due to operator error or to traffic or to the presence of pedestrians. In this situation, the sampling frequency should be increased. In order to be sure that the error window is limited and no worse than what is described here, a 5-minute frequency is recommended at least.

In the case of an automated pavement-watering system, synchronization should be more feasible and the sampling rate could even be reduced to the watering frequency: as long as the measurement is made right before watering, no spikes should be missed. Nonetheless, if the watering frequency is deemed insufficient following the data analysis, this sampling rate provides no indication on what the correct frequency might be, thus requiring multiple follow-up field trials. A frequency at least two or three times as high as the watering frequency will help narrow down the optimal watering frequency band significantly, saving time and effort.

As mentioned earlier, the recommendations formulated on the basis of surface temperature and pavement heat flux data show good agreement. This is due to good correspondence between heat flux and surface temperature spike observations. It should be noted however that temperature spikes have a relatively greater amplitude than heat flux spikes. This is unsurprising as heat flux 5 cm below the surface is naturally less sensitive to surface conditions than surface temperatures are.

However, this greater sensitivity means that minor heat flux spikes which may have been disregarded, such as those apparent in the afternoon of July 10th, may correspond to significant surface temperature spikes. The absence of surface temperature data on that date prevents us from exploring this possibility further, but these considerations emphasize the need for measurements within the last few minutes preceding watering cycles.

As a result, it is tempting to increase the measurement frequency further. One-minute measurements would be ideal and would ensure that no significant spikes are missed. The amount of time required to empirically determine the optimal watering frequency would be significantly reduced as well since only one trial would be needed if no field-of-view obstructions occur, similarly to what was discussed earlier for pavement heat flux measurements.

Such a high frequency creates large numbers of data files. Apart from requiring a higher storage capacity, the treatment load will also increase significantly if corrections cannot be integrated automatically and must be applied manually. For this reason, automatic corrections are necessary for one-minute measurements to be simple to analyze and interpret.

Given that the information sought after is the detection of temperature spikes, the corrections may be unnecessary in certain situations. Indeed, if the IR imaging device is only a few meters away from its target and the surface material has high emissivity, i.e. both atmospheric and reflected temperature influence are low, uncorrected brightness temperature should suffice to detect surface drying in the form of temperature spikes. In this case, it is recommended to proceed with one-minute measurements if storage capacity is sufficient.

To summarize, if the instrument data is readily usable for analysis, either because brightness temperature is sufficient or corrections are automatically applied, one-minute measurements are recommended. Otherwise, if it is found that manual data correction and analysis are too resource-intensive, five-minute measurements should be enough, especially if these can be synchronized with the watering cycles.

5 cm Pavement Temperatures

Pavement heat flux and surface temperature spikes were shown to be reliable indicators of surface drying, relevant to the improvement or optimization of the pavement-watering method. In the absence of such spikes, a similar analysis of 5 cm pavement temperatures could not be conducted.

The absence of spikes is caused by strong dampening of the temperature signal by the thermal inertia of the pavement's surface course. We therefore conclude that pavement temperature measurements below high-inertia surface courses cannot be used to improve the watering frequency. However, they may still be useful in the case of surface courses with low thermal inertia, although they are expected to remain less accurate than pavement heat flux or surface temperature measurements.

19.3 Conclusion

Spikes observed in pavement heat flux and surface temperature measurements were used to optimize the watering frequency. As none were detected for 5 cm temperatures, this parameter was unhelpful for this purpose. Spikes occurring before pavement-watering resumes in the afternoon indicate that watering should

begin before surface insolation, while those found in between watering cycles indicate that the watering frequency should be increased. These adjustments ensure that the pavement is wet when insolation begins and between watering cycles.

For asphalt concrete pavement surfaces in a N-S street in Paris in the month of July, watering every 30 minutes during insolation is optimal and every two hours during shading is probably sufficient. This does not hold true for asphalt sidewalks, for which 30 minutes was found to be too long during insolation. The best frequency for the sidewalk was estimated to be between every 10 and 20 minutes. The conclusions reached independently with pavement heat flux and surface temperatures agree well with each other for pavement zone 1.

The pavement-watering frequency and period can therefore be successfully optimized on the basis of the detection of surface drying, manifested in the form of rapid heat flux or surface temperature changes. The pavement sensor used and time-lapse IR camera temperature surveys are able to meet this requirement if they are frequent enough to detect the temperature spikes which may occur in the last moments preceding watering cycles. Pavement heat flux measurements were conducted every minute and were deemed sufficient. For surface temperatures, a measurement rate of 5 minutes or less ensures that minimal temperature spikes are omitted, while 1-minute measurements are ideal where possible.

In retrospect, the watering period could be extended further to be 24 hours long, thus fulfilling goal # 2. However, judging by the micro-climatic and thermal effects determined in Parts 1 and 2 and their temporal distribution, pavement-watering effects are greatest during pavement insolation.

On this basis, the watering period could also be shortened to only include the insolation period, eliminating morning watering altogether apart for one watering cycle a few minutes before pavement insolation. This would help fulfill goal # 4. However, while initial morning effects may be limited, they gradually increase as hours pass. Indeed, while initial effects are about 2°C and 15 W/m^2, maximum morning effects reach up to 4°C and 50 W/m^2 at the last morning watering cycle. We therefore recommend that morning watering be maintained although it may be delayed by a few hours, until 9:30 am for example. A similar analysis of watering effects in the evening reveals that watering just after the end of insolation seems worthwhile for the same reasons.

Having proposed optimal watering frequencies for the Louvre site, we now focus on optimizing the watering rate in Chapter 20.

CHAPTER 20

Watering Rate Optimization

Optimal watering frequencies were proposed in Chapter 19. This chapter will now focus on optimizing the watering rate, crucial to limiting the total water consumption of pavement-watering.

20.1 Pavement Cooling Flux Φ

The analysis of G as a function of S conducted in Chapter 18 allowed us to demonstrate that pavement-watering is responsible for 232 to 279 W/m^2 of surface cooling. Pavement cooling has an evaporative and an advective component, which were found to be:

$$\begin{cases} 23\ W/m^2 \leq \Phi_{adv} \leq 35\ W/m^2 \\ 198\ W/m^2 \leq lE \leq 256\ W/m^2 \end{cases}$$

The latent flux is equivalent to an evaporation rate E of between 0.087 and 0.113 g/m^2.s, i.e. between 0.31 and 0.41 mm/h. This means that for each 30-minute watering cycle 0.16 to 0.20 mm of water evaporate.

Judging by these results, at least 85% of total cooling attributable to pavement-watering is produced by evaporation and 15% at most by water advection.

The relative contributions of advection and evaporation contrast strongly with the amount of water used by each of these phenomena which is respectively 2 mm/h and 0.31 to 0.41 mm/h. Pavement cooling by water advection is therefore much less water efficient than that from evaporation: 12 to 18 W/m^2 of cooling per 1 mm/h of sprinkled water, compared to 628 W/m^2 per 1 mm/h of evaporated water. However, evaporation cannot increase past a certain value, dependent on the local meteorological conditions.

Figure 20.1 illustrates pavement cooling Φ (left) and the watering rate to cooling ratio (right) as a function of the watering rate, assuming a constant water

and pavement surface temperature differential and a maximum evaporation rate of 0.41 mm/h. The 0.41 mm/h mark is emphasized by the long-dashed vertical lines in Figure 20.1. It is clear that once evaporation has been maximized, pavement cooling is only marginally increased by additional watering as the advective contribution increases.

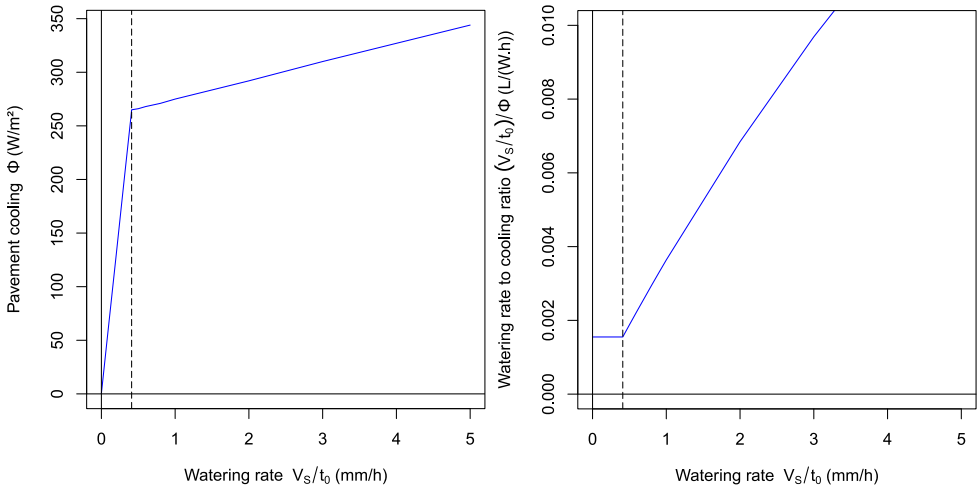

Figure 20.1 – Pavement cooling Φ (left) and watering rate to pavement cooling ratio $\frac{V_S}{\Phi t_0}$ (right) according to the applied watering rate (Hendel et al., 2015a).

In regards to the optimization goals, the watering rate to pavement cooling ratio is minimized for a watering rate anywhere below the maximum evaporation rate. Therefore, any of the values below that rate are optimal. However, in order to maximize pavement-watering's cooling effect, the best watering rate is that of the maximum evaporation rate.

We therefore recommend adjusting the watering rate to match the maximum evaporation rate exactly. In the described experimental conditions, this would lower advective cooling to between 4 and 7 W/m², bringing total pavement cooling down to between 201 and 263 W/m², i.e. a 6-13% reduction for a 80-84% water saving.

Météo France and CSTB (2012) found an optimal watering rate of 0.2 mm/h for all of Paris' road surfaces. This value was obtained by testing different watering rates with a frequency of every hour and a water-holding capacity of 1 mm. However, it is a daily and city average for watering every hour between 5 am and 7 pm and is not more accurately defined for individual street configurations. Furthermore, the authors were limited in the choice of the watering frequency since the model's time step was one hour and was found sufficient considering a water-holding capacity of 1 mm. The findings reported here are therefore deemed to be consistent with theirs.

Sources of uncertainty in these estimations lie in the use of S rather than

R_n and assumptions regarding ΔQ. Concerning the latter, observations over several days by Kinouchi and Kanda (1998) substantiate our assumption as does the presented analysis of G which is unchanged up to a constant in dry and wet conditions over the considered time span.

Net radiation measurements would help address the sources of uncertainty in this analysis. In addition, these measurements would help verify the conjecture on optimal watering during pavement shading in the morning via a similar approach to that used for the afternoon. The 2014 campaign hoped to address this issue, but as previously mentioned, the nonoperational pavement sensor prevented us from doing so. If all goes well, the 2015 campaign will provide data suitable to optimize the watering method in the morning.

In the mean time, if it is assumed that the watering frequency used in the morning is optimal, morning evaporation can be estimated to between 0.16 and 0.20 mm/h.

20.2 Pavement Surface Temperatures

Based on the previous findings and on the analysis conducted on pavement temperatures, only the water-retaining capacities of the studied surfaces are needed to optimize the method's water consumption on the sole basis of surface temperature measurements. Temperature 5 cm below the pavement surface cannot be used to optimize the watering method.

Indeed, the optimal watering rate was determined from the pavement cooling flux Φ as consisting of sprinkling the exact water-holding capacity of the targeted area, at the frequency required for that volume to evaporate. Therefore, once the water-holding capacity of the pavement is known, only the frequency needs to be determined, which can be done on the basis of pavement surface temperature observations.

20.3 Conclusion

Only pavement heat flux measurements could be used to adjust the watering rate, except if the pavement water-holding capacity is determined independently in which case surface temperatures are also suitable.

In order to improve the watering method to meet our optimization goals, it is advised to match the watering rate with the evaporation rate. In the case of the asphalt concrete in pavement zone 1, this amounts to 0.31-0.41 mm/h during insolation. Given the water-holding capacity of pavement zone 1, this translates to watering cycles of 0.16-0.20 mm every 30 minutes. In the morning, the evaporation rate could not be determined, though 60-minute watering cycles and a watering rate of 0.16 to 0.20 mm/h are acceptable. There may however still be significant room for improvement.

In the experimental conditions described here, the proposed watering rate would use at least 80% less water while still providing at least 87% of observed pavement cooling. The watering method has therefore been significantly improved without significantly modifying the watering period.

CHAPTER 21

Conclusion of Part 3

The thermal effects of pavement-watering determined in Part 2 were used to improve the watering method and its water consumption for a N-S oriented street in Paris, France during the month of July.

Watering of the asphalt concrete pavement should deliver 0.16-0.20 mm/cycle at the lowest frequency which prevents surface drying. In the afternoon, watering every 30 minutes is recommended until the end of pavement insolation, but is inadequate for the asphalt sidewalk which requires watering every 10-20 minutes. In the morning, 60-minute watering at a rate of 0.16-0.20 mm/cycle is sufficient, but can likely be improved by 50% as indicated by spikes detected in heat flux and surface temperature 2-2.5 hours after watering in the evening. Finally, the watering period should be extended to include the minutes preceding the beginning of insolation, but the start of morning watering can presumably be delayed until approximately 9:30 am.

Generally speaking, the most efficient method of pavement-watering is to match the watering rate with the evaporation rate at the watered surface. Having defined the watering rate, the water-holding capacity of the targeted area determines the suitable watering frequency. Of course, the evaporation rate will depend on the surface temperature reached by the target area when wet and therefore depends on the sprinkled material's properties.

Field trials were conducted over the summer of 2014 in order to confirm these recommendations, although the watering rate applied by the cleaning trucks could only be halved at best, i.e. 0.5 mm per watering cycle. Unfortunately, pavement sensor measurements were significantly different compared to the summer of 2013 in similar conditions. The instrument was therefore considered faulty. The cause of this change is suspected to be pavement material creeping. Besides, only two watered days occurred over that summer, during which the IR camera experienced power supply failures. It was therefore not possible to determine whether or not the reduced watering rate applied at Louvre was successful in reducing

water use without significantly affecting pavement cooling. Another campaign will take place during the summer of 2015, but unfortunately it will occur after this manuscript is completed.

In order to reduce the watering frequency further and thus cause less disturbance associated with watering cycles and to simplify the watering method, the pavement water-holding capacity would need to be increased. Indeed, were the water-holding capacity equal to 1 mm, afternoon watering of 1 mm/cycle would only need to occur every 2.5-3 hours during insolation.

As Parisian streets are currently designed to evacuate surface water as fast as possible, a change in street design is necessary to meet this objective. One alternative that can be considered is to use water-retaining pavement materials. The new street material would have to store water at or near its surface in order not to hinder evaporation, relying on capillarity for example (Akagawa and Komiya, 2005). This option would also prevent puddling and thus avoid related traffic safety hazards and pedestrian discomfort.

Such a material would permit the delivery of larger amounts of water per watering cycle without runoff thanks to higher water storage and thus reduce the watering frequency. Moreover, the new road structure may be able to store rainfall from summer storms or water already being used today for street cleaning long enough for evaporation on hot days. This would lead to additional water savings all while having positive impacts on rainwater runoff management. Reducing runoff discharge to the Seine and other local rivers is already pursued by Paris' city services to reach local Water Framework Directive goals (EU2, 2000).

Regardless of the outcome of the 2015 trials, this analysis gives a first estimate of the water intensity of pavement-watering for Paris in the month of July. Conducted continuously from 9:30 am until 6:30 pm, i.e. no more than 0.20 mm per cycle every two hours in the morning until 1:30 pm and every 30 minutes thereafter until 6:30 pm, this strategy would result in the daily use of less than 2.2 mm/d.

Generalized to all of Paris' 2,550 ha of street surfaces (Météo France and CSTB, 2012), this would amount to approximately 56,100 m^3/d or 25 L per day per capita, i.e. equivalent to less than half a shower. This volume amounts to less than 30% of current non-potable water production in Paris and is well within installed capacity (in the order of 500,000 m^3/d). This can be compared with potential evapotranspiration in Paris during summer, i.e. the approximate water consumption of green spaces. Typical values in July reach 7-8 mm/d and up to 9 mm/d during heat-waves, i.e. more than three times more than for pavement-watering. Given the relevance credited to urban greening as a UHI-countermeasure, the water footprint of pavement-watering is deemed reasonable enough for consideration as a viable UHI-mitigation technique for Paris. This is reinforced by the opportunities offered by the use of the city's non-potable water network and the sustainable sourcing potential of its water supply, but will also depend on how resource availability evolves over the coming decades in the region.

Since streets within the same city often have different configurations or use

different materials, the conclusions drawn from our two sites cannot be generalized to the entire city. Indeed, among other things the evaporation rate of the watered surface will depend on the surface's properties. It is therefore recommended to study several characteristic streets before a city-wide pavement-watering strategy can be developed. However, installing a heat flux sensor in combination with solar instruments over long periods of time is an expensive and invasive procedure and requires close cooperation with the relevant city services. It is therefore difficult to install large numbers of these sensors in a dense urban environment for this purpose. Fortunately, we demonstrated that surface temperature measurements with IR cameras are a viable alternative. Combined with an independent measurement of the water-holding capacity of the pavement, the method's total water consumption and watering frequency can be optimized simultaneously.

Pyrometers, which measure spot surface temperatures and are significantly cheaper, could also be used, but unlike IR cameras they do not allow the simultaneous survey of different areas. Given their lower cost, it may still be more feasible to install several of these in order to compensate for this weakness. Installation of either instrument in the street is simple and non-invasive compared to pavement sensors, making them well suited to dense urban environments. Street lamps make suitable candidates for power supply requirements, but many Parisian streets have lamps mounted directly onto building facades where adding additional weight may not be permitted. Furthermore, since vehicles, pedestrians and other objects may enter the line-of-site of radiometric instruments, it is recommended to include a synchronized webcam. As was seen in the case of our site, many thermal disturbance sources exist in urban environments and need to be clearly identified before instrument targets are selected in order to avoid misinterpretation. Thermal images can be of valuable assistance in this task.

In addition to that of street configurations, the role of materials should not be overlooked. Indeed, dark pavements are not expected to react the same way as light-colored ones to pavement-watering, nor are materials of differing surface texture, which may affect their water-retaining capacity. Paris currently employs a wide variety of standard materials used to pave public spaces, including granite pavers, granite or sandstone cobblestones, asphalt concrete paving, or asphalt sidewalks. The diversity of urban street materials makes devising a city-wide pavement-watering strategy difficult and costly if it must be based on field investigations.

One solution to this problem consists of studying the thermal behavior of pavement materials in the lab. The required setup must be able to expose different road material samples to identical weather/insolation cycles, allowing the user to compare their behavior more accurately than in the field. Furthermore, lab conditions make it possible to easily include several instruments at different depths within the road samples, providing a wider variety of information than is feasible in the urban environment.

Such an experiment was constructed and five different kinds of materials used in Parisian public spaces were compared in dry conditions. These samples include

standard asphalt concrete pavement, asphalt and granite-paved sidewalk samples seen in streets, as well as stabilized sand and lawn samples found in Parisian parks. While further testing is required, some preliminary results have been presented at three conferences. The corresponding conference articles (two of them in French) can be found in Appendices A, B and C.

CHAPTER 22

Conclusion

We have now completed the analysis of the data collected from the field experiment conducted in Paris, France over the summers of 2013 and 2014. This experiment considered two sites, Louvre and Belleville, where watering was applied discontinuously and continuously on all and on one third of the street width, respectively. We now look back at the research questions we defined in Chapter 4 for dense cities under heat-wave conditions. As a reminder, these were:

- Can the direct comparison method be reliably used to evaluate the real-world effects of anti-UHI techniques?
- What micro-climatic effects can be expected of pavement-watering?
- What are the UHI-mitigation effects of pavement-watering?
- What can be said of the thermal effects of pavement-watering?
- Finally, how much water is required for pavement-watering and how can its watering efficiency be improved?

22.1 Results

The research discussed here has provided answers to each of these questions. The direct comparison method was shown to be ill-suited to our experiment, the micro-climatic effects of pavement-watering were quantified as well as its UHI-mitigation potential. The thermal effects of pavement-watering were also analyzed for a dense urban environment, and finally the method's water consumption was determined and optimized.

Analysis Method The direct comparison method, which interprets the difference measured between case and control sites as the effect of pavement-watering, was called into question. This followed the identification of a risk of mistaking preexisting differences for the effects of pavement-watering.

In Chapter 7, we found that the direct comparison method was unreliable to detect the real-world effects of anti-UHI techniques in dense cities such as Paris. Our data showed that in general the effects of pavement-watering could not be reliably differentiated from pre-existing differences between case and control sites. This assessment is not specific to pavement-watering and holds true for other UHI countermeasures.

In Chapter 8, an alternative analysis method was developed and applied to our case study. The method was tested both with strictly paired sites and with sites distant by several kilometers. Both approaches were successful, the latter being much more flexible in the field than the former. Its statistical significance was lower due to higher background noise , caused by the poorer match between sites due to differences in insolation resulting from the distance between them as well as their differing street configurations.

Micro-climatic Effects The micro-climatic effects of pavement-watering were successfully determined. No stat. sign. daily effects were found at the Belleville site, where only the road surface was watered (approx. 33% of total width), except for relative humidity 1.5 m a.g.l.. At Louvre, which was entirely watered, stat. sign. daily effects were detected for all parameters, i.e. air temperature, relative humidity, mean radiant temperature and UTCI.

Maximum effects were found to be stat. sign. for both sites and were in the same order of magnitude. These occurred around 6 pm, when meteorological conditions were warmest. Maximum effects reached -0.79°C for air temperature, +4.1% for relative humidity, -2.39°C for mean radiant temperature and -1.03°C for UTCI-equivalent temperature.

UHI-Mitigation Potential UHI-mitigation effects were also investigated. As was the case for daily effects, no stat. sign. mitigation effects were detected at the Belleville site. At the Louvre site, UHI reduction reached up to -0.22°C.

Thermal Effects The thermal effects of pavement-watering were analyzed in Part 2 for the Louvre site. Effects on pavement heat flux 5 cm deep as well as both surface and 5 cm deep temperatures were investigated. Sidewalk surface temperatures were also analyzed.

In Chapter 12, the pavement heat flux was found to be more than halved by watering during insolation, with morning and afternoon reductions reaching up to 50 and 150 W/m^2, respectively. In addition, heat release by the pavement was reduced in the evening following watering.

Surface temperatures were studied in Chapter 13. Reductions of up to 4°C in the morning and 13°C on average in the afternoon were found, and were greater for the pavement than for the sidewalk.

Finally in Chapter 14, watering was found to reduce temperatures 5 cm deep by 5.9°C in the afternoon, and by 2.3°C in the morning.

Signal spikes were found for heat flux and surface temperature, but not for temperatures 5 cm deep.

Watering Method and Water Consumption Using the results obtained in Part 2, the water consumption of the method and ways of improving it were determined and discussed in Part 3.

In Chapter 18, the surface cooling flux created by watering was determined on the basis of a linear relation found between pavement heat flux and solar irradiance in the afternoon. This cooling flux was partitioned into its latent and advective components. It was found that evaporation accounted for at least 85% of total cooling, while representing less than 20% of total water consumption (0.31-0.41 mm/h in the afternoon). The water-holding capacity of the pavement was also estimated to 0.16-0.20 mm.

The optimal watering frequency was assessed in Chapter 19, using the signal spikes detected in Part 2. It was found that for the Louvre pavement, the optimal watering frequency is every 30 minutes. Due to its smoother texture and different design, this frequency is increased to every 10-20 minutes for the sidewalk. The optimal frequency in the morning was estimated to be every hour, but may be reduced to every 2.5 hours.

Finally, it was found that the optimal watering rate should match the evaporation rate, i.e. 0.31-0.41 mm/h in the afternoon. It was estimated to be 0.16-0.20 mm/h in the morning, but may also be reduced by 50%.

Ways of simplifying the watering optimization process with the use of automated surface temperature sensors were also discussed in Chapter 21.

Although pavement-watering's cooling effects are lower than cooling expected from green spaces, its water consumption is also estimated to be much lower. Furthermore, pavement-watering could used to cool highly built and mineral areas where greening may not be possible. Thanks to Paris' high population density and the presence of its dual water network, pavement-watering is well suited and merits further consideration as a potential adaptation and anti-UHI tool.

The research questions listed in Chapter 4 have therefore been successfully answered. However, other areas where more light needs to be shed were also identified.

22.2 Future Research

The development of our statistical analysis method in Part 1 comes with a variety of questions regarding its limits and reliability. Other questions also arose in

regards to the experimental method used to determine micro-climatic effects. The new questions are as follows:

- What is the benefit of using aspirated solar shields on air temperature and humidity signal noise, particularly for use with distant case and control sites?
- What is the influence of the measurement cage?
- How feasible is the use of the statistical analysis method developed here to other, longer-lasting UHI countermeasures?
- What improvements can tools such as time series analysis bring to our method?

The expected benefit of using aspirated solar shields for the thermohygrometer is the reduction of signal noise during periods of direct insolation. Indeed, differences in solar irradiance between sites may have an impact on air temperature and humidity measurements which will blur the cooling signal from pavement-watering. The potential for improvement with the use of aspirated instruments should therefore be investigated.

As described in Part 1, a measurement cage was used to protect instruments positioned 1.5 m a.g.l., i.e. within pedestrian reach. For weather stations implemented for several weeks or months at a time, such a device is essential for urban areas. While the cages were designed in order to minimize their impact on the measurements, some level of shading is unavoidable. The significance of this impact and possible ways of accounting for it should be explored if measurement cages are to be used in future long-term studies. This should consider wind speed measurements inside the cage as well as opposed to above it as conducted during our trials.

In Chapter 9, we emphasized the complexity of the proposed analysis method when applied to other longer-lasting UHI countermeasures. Because a reference period must be studied long enough to be reliably compared with a case period (after countermeasure implementation), field campaigns using our analysis method may last up to several years. The feasibility of the method must therefore be determined, especially considering that urban environments are ever-changing. Future studies relying on the method should provide relevant feedback, but will be slow to gather relevant information.

In the meantime, other methods should be considered as well. Given the periodicity of meteorological observations, time series analysis may be relevant, namely to decompose the studied series into their trend, seasonal and residual components. The study of these components may shed further light on studied cooling effects. Other tools from the field of data mining or machine learning may also prove useful.

Also, although the micro-climatic effects of pavement-watering have been better quantified for two particular configurations in Paris, several other questions need to be answered before a city-wide pavement-watering strategy can be devised:

- What cumulative effects can be expected when larger areas are watered?
- How does street orientation affect pavement-watering effects?
- What about canyon-aspect ratio?
- How does the method perform on other street materials?
- What material properties are responsible for differences in watering effects?

The first question reflects the fact that the effects determined here were obtained by watering a single site surrounded by vast areas left untreated. It is reasonable to expect that watering larger areas would lead to cumulative effects resulting in greater cooling. None of the work we are aware of has quantified the cumulative effects that may be expected.

The following two questions address a gap in our research in regards to the influence of urban morphology. While sites with different orientations were tested, the watering methods applied differed too greatly for the influence of street orientation to be determined. This is true of the influence of canyon aspect ratio as well. Given the diversity of street orientations and shapes within cities, the influence of these parameters on pavement-watering efficiency should be determined. Given the importance of insolation on pavement-watering thermal effects, the influence of these morphological parameters may be limited to their impact on insolation conditions at the pavement-level.

Similarly, our experiment did not permit us to quantify the influence of the materials being watered, despite the significant difference between the Louvre and Belleville sites. Among material properties, the water-holding capacity of the watered material was identified as having an important influence on the watering frequency and was discussed in Part 3. Considering the wide variety of materials used in Paris and other cities, this aspect is of particular importance. Understanding this influence and which material properties are responsible for it would help better target watering strategies and help design street structures more efficient from a climatic standpoint. This latter point has synergies with the rainwater runoff management goals of the City if the water-holding capacity is increased (Paris City Council, 2012a).

As mentioned in Chapter 21, we began developing a laboratory experiment to investigate the role of materials. To date, initial testing has been completed and results are deemed satisfactory compared to our field observations previously described. Preliminary results provide a first impression of the relative thermo-climatic performance of five Parisian street structures and are described in three conference papers (two of them French) included in Appendices A, B and C. Further testing with watering cycles should allow us to determine the performance of pavement-watering on these different materials and propose new improvements and urban structures better suited to urban climate improvement goals. Such materials may also help reach substantial water savings by storing rainfall or water

already used for street cleaning which currently run off into the sewers. This work is conducted in partnership with the Roads and Traffic Division of Paris City Hall.

Finally, on a more general note, our research has omitted the impacts of pavement-watering other than its cooling effects and water footprint.

Among these, air quality improvement was mentioned in the Introduction. In Paris, particulate matter (PM) pollution is usually the main concern for air quality deterioration. Street cleaning is suspected to reduce PM resuspension and has begun to be investigated by other authors (Amato et al., 2010). Pavement-watering may reduce PM resuspension as well and thus improve PM air pollution. Ozone pollution has been increasing in the Paris region as well as in other cities and may also be reduced by pavement-watering. Indeed, ozone formation is highly temperature sensitive and may therefore be hindered by pavement-watering's cooling effects. These potential pavement-watering benefits have yet to be explored.

Furthermore, the financial and environmental costs of pavement-watering should also be estimated before cities can consider pavement-watering as part of their adaptation and UHI reduction strategies. These estimations should take both positive and negative impacts into account, such as benefits from possible cooling energy savings vs. energy spent for watering and associated costs. The study of these parameters however implies that a city-wide watering method and infrastructure have already been proposed or selected. Given the work remaining, it is too early to begin studying these impacts at present.

Bibliography

(2000). Directive 2000/60/EC of the European Parliament and of the Council of 23 October 2000 establishing a framework for Community action in the field of water policy.

Akagawa, H. and H. Komiya (2005). Development of wet-style pavements and lightweight rooftop garden using a unique textile. In *2005 World Sustainable Building Conference*, Volume 2005, Tokyo, Japan, pp. 27–29.

Akbari, H. (2014). Cool Roofs In Cold Climates : Savings Or Penalties ? In *Third International Conference on Countermeasures to Urban Heat Island*, 13-15 October, Venice, Italy, pp. 986–997.

Akbari, H. and H. D. Matthews (2012, December). Global cooling updates: Reflective roofs and pavements. *Energy and Buildings 55*, 2–6.

Akbari, H., M. Pomerantz, and H. Taha (2001, January). Cool surfaces and shade trees to reduce energy use and improve air quality in urban areas. *Solar Energy 70*(3), 295–310.

Akbari, H. and H. Taha (1992, February). The impact of trees and white surfaces on residential heating and cooling energy use in four Canadian cities. *Energy 17*(2), 141–149.

Amato, F., X. Querol, C. Johansson, C. Nagl, and a. Alastuey (2010, July). A review on the effectiveness of street sweeping, washing and dust suppressants as urban PM control methods. *The Science of the total environment 408*(16), 3070–84.

Arnfield, A. (1990). Street design and urban canyon solar access. *Energy and Buildings 14*(2), 117–131.

Asaeda, T., V. T. Ca, and A. Wake (1996, February). Heat storage of pavement and its effect on the lower atmosphere. *Atmospheric Environment 30*(3), 413–427.

ASHRAE (2001). *ASHRAE Fundamentals Handbook 2001* (SI Edition ed.). American Society of Heating, Refrigerating, and Air-Conditioning Engineers.

Azer, N. and S. Hsu (1977). OSHA Heat Stress Standards and the WBGT Index. In *ASHRAE Transactions*, Volume 83, Part 2, Halifax, NS.

Blazejczyk, K., P. Bröde, D. Fiala, G. Havenith, I. Holmér, G. Jendritzky, B. Kampmann, and A. Kunert (2010). Principles of the new Universal Thermal Climate Index (UTCI) and its Application to Bioclimatic Research in European Scale. *Miscellanea Geographica 14*, 91–102.

Bouvier, M., A. Brunner, and F. Aimé (2013). Nighttime watering streets and induced effects on the surrounding refreshment in case of hot weather. The city of Paris experimentations. *Techniques Sciences Méthodes* (12), 43–55 (in French).

Bowler, D. E., L. Buyung-Ali, T. M. Knight, and A. S. Pullin (2010, September). Urban greening to cool towns and cities: A systematic review of the empirical evidence. *Landscape and Urban Planning 97*(3), 147–155.

Bretz, S. E. and H. Akbari (1997, January). Long-term performance of high-albedo roof coatings. *Energy and Buildings 25*(2), 159–167.

Bröde, P. (2009). UTCI Fast Calculation Script.

Bröde, P., D. Fiala, K. Błażejczyk, I. Holmér, G. Jendritzky, B. Kampmann, B. Tinz, and G. Havenith (2012, May). Deriving the operational procedure for the Universal Thermal Climate Index (UTCI). *International Journal of Biometeorology 56*(3), 481–94.

Burton, A., H. Fowler, S. Blenkinsop, and C. Kilsby (2010, February). Downscaling transient climate change using a Neyman–Scott Rectangular Pulses stochastic rainfall model. *Journal of Hydrology 381*(1-2), 18–32.

Ca, V. T., T. Asaeda, and E. M. Abu (1998, December). Reductions in air conditioning energy caused by a nearby park. *Energy and Buildings 29*(1), 83–92.

California Energy Commission (2010). Efficiency Standards for Residential and Nonresidential Buildings.

Camuffo, D. and A. Bernardi (1982, July). An observational study of heat fluxes and their relationships with net radiation. *Boundary-Layer Meteorology 23*(3), 359–368.

Cantat, O. (2004). L'îlot de chaleur urbain parisien selon les types de temps. *Norois 191*, 75–102.

Colombert, M., Y. Diab, J.-L. Salagnac, and D. Morand (2011, October). Sensitivity study of the energy balance to urban characteristics. *Sustainable Cities and Society 1*(3), 125–134.

Dandou, A., M. Tombrou, E. Akylas, N. Soulakellis, and E. Bossioli (2005). Development and evaluation of an urban parameterization scheme in the Penn State/NCAR Mesoscale Model (MM5). *Journal of Geophysical Research D: Atmospheres 110*(10), 1–14.

de Dear, R. (1987). Ping-pong globe thermometers for mean radiant temperatures. *Heating and Ventilating Engineer 60*(81), 10–11.

De Munck, C., A. Lemonsu, R. Bouzouidja, V. Masson, and R. Claverie (2013). The GREENROOF module (v7. 3) for modelling green roof hydrological and energetic performances within TEB. *Geoscientific Model Development Discussions 6*(1), 1127–1172.

Djedjig, R., E. Bozonnet, and R. Belarbi (2013). Experimental study of the urban microclimate mitigation potential of green roofs and green walls in street canyons. *International Journal of Low-Carbon Technologies* (April 2013), 1–11.

Duffie, J. A. and W. A. Beckman (1991). *Solar Engineering of Thermal Processes* (2nd Editio ed.). New York.

Erell, E., D. Pearlmutter, D. Boneh, and P. B. Kutiel (2013, October). Effect of high-albedo materials on pedestrian heat stress in urban street canyons. *Urban Climate*.

Fontana, L. (2010). Experimental study on the globe thermometer behaviour in conditions of asymmetry of the radiant temperature. *Applied Thermal Engineering 30*(6-7), 732–740.

Fröhlich, D. and A. Matzarakis (2014). Human-biometeorological estimation of adaptation- and mitigation potential of urban green in Southwest Germany. In *Third International Conference on Countermeasures to Urban Heat Island*, 13-15 October, Venice, Italy, pp. 351–362.

Girard, L. (1923). Lutte contre la poussière. In *Le nettoiement de Paris*, Chapter 13, pp. 109–120. Paris, France: Léon Eyrolles.

Grimmond, C. S. B., M. Blackett, M. J. Best, J. J. Baik, S. E. Belcher, J. Beringer, S. I. Bohnenstengel, I. Calmet, F. Chen, A. Coutts, A. Dandou, K. Fortuniak, M. L. Gouvea, R. Hamdi, M. Hendry, M. Kanda, T. Kawai, Y. Kawamoto, H. Kondo, E. S. Krayenhoff, S. H. Lee, T. Loridan, A. Martilli, V. Masson, S. Miao, K. Oleson, R. Ooka, G. Pigeon, A. Porson, Y. H. Ryu, F. Salamanca, G. J. Steeneveld, M. Tombrou, J. a. Voogt, D. T. Young, and N. Zhang (2011). Initial results from Phase 2 of the international urban energy balance model comparison. *International Journal of Climatology 31*(2), 244–272.

Grimmond, S. (2007). Urbanization and global local effects of environmental change : urban. *The Geographical Journal 173*(1), 83–88.

Haselbach, L., M. Boyer, J. T. Kevern, and V. R. Schaefer (2011, December). Cyclic Heat Island Impacts on Traditional Versus Pervious Concrete Pavement Systems. *Transportation Research Record: Journal of the Transportation Research Board* (2240), 107–115.

Hassid, S., M. Santamouris, N. Papanikolaou, A. Linardi, N. Klitsikas, C. Georgakis, and D. N. Assimakopoulos (2000). Effect of the Athens heat island on air conditioning load. *Energy and Buildings 32*(2), 131–141.

He, J. and A. Hoyano (2008, January). A numerical simulation method for analyzing the thermal improvement effect of super-hydrophilic photocatalyst-coated building surfaces with water film on the urban/built environment. *Energy and Buildings 40*(6), 968–978.

Hendel, M., M. Colombert, Y. Diab, and L. Royon (2014, December). Improving a pavement-watering method on the basis of pavement surface temperature measurements. *Urban Climate 10*(December), 189–200.

Hendel, M., M. Colombert, Y. Diab, and L. Royon (2015a, March). An analysis of pavement heat flux to optimize the water efficiency of a pavement-watering method. *Applied Thermal Engineering 78*, 658–669.

Hendel, M., M. Colombert, Y. Diab, and L. Royon (2015b, March). Measurement of the Cooling Efficiency of Pavement-Watering as an Urban Heat Island Mitigation Technique. *Journal of Sustainable Development of Energy, Water and Environment Systems 3*(1), 1–11.

Hendel, M., P. Gutierrez, M. Colombert, Y. Diab, and L. Royon (2015). Measuring the Effects of UHI Mitigation in the Field: Application to the Case of Pavement-Watering in Paris. *Urban Climate* ((under review)).

Hendel, M. and L. Royon (2015). The effect of pavement-watering on subsurface pavement temperatures. *Urban Climate* ((submitted)).

Jaffal, I., S.-E. Ouldboukhitine, and R. Belarbi (2012). A comprehensive study of the impact of green roofs on building energy performance. *Renewable Energy 43*, 157–164.

Japan Water Forum (2015). Let's Uchimizu.

Jauregui, E. (1990, January). Influence of a large urban park on temperature and convective precipitation in a tropical city. *Energy and Buildings 15*(3-4), 457–463.

Johansson, E., S. Thorsson, R. Emmanuel, and E. Krüger (2014, January). Instruments and methods in outdoor thermal comfort studies – The need for standardization. *Urban Climate*.

Jouzel, J., G. Ouzeau, M. Déqué, M. Jouini, S. Planton, and R. Vautard (2014). Scénarios régionalisés : édition 2014 pour la métropole et les régions d'outre-mer. Technical report, Ministère de l'Ecologie, du Développement durable et de l'Energie.

Jürges, W. (1924). Die Wärmeübergang an einer ebenen Wand. *Beihefte zum Gesundheits-Ingenieur 19*(1), 1227–1249 (in German).

Karlessi, T., M. Santamouris, A. Synnefa, D. Assimakopoulos, P. Didaskalopoulos, and K. Apostolakis (2011, March). Development and testing of PCM doped cool colored coatings to mitigate urban heat island and cool buildings. *Building and Environment 46*(3), 570–576.

Kinouchi, T. and M. Kanda (1997). An Observation on the Climatic Effect of Watering on Paved Roads. *Journal of Hydroscience and Hydraulic Engineering 15*(1), 55–64.

Kinouchi, T. and M. Kanda (1998). Cooling Effect of Watering on Paved Road and Retention in Porous Pavement. In *Second Symposium on Urban Environment*, Albuquerque, NM, pp. 255–258.

Kline, S. J. and F. A. McClintock (1953). Describing Uncertainties in Single-Sample Experiments. *Mechanical Engineering 75*, 3–8.

Kubo, K., H. Kido, and M. Ito (2006). Study on pavement technologies to mitigate the heat island effect and their effectiveness. In *10th International Conference on Asphalt Pavements*, Quebec City, Canada, pp. 223–232.

Kusaka, H., H. Kondo, and Y. Kikegawa (2001). A simple single-layer urban canopy model for atmospheric models: comparison with multi-layer and slab models. *Boundary-Layer Meteorology 101*(3), 329–358.

Lekner, J. and M. C. Dorf (1988, April). Why some things are darker when wet. *Applied optics 27*(7), 1278–80.

Lemonsu, A., R. Kounkou-Arnaud, J. Desplat, J. L. Salagnac, and V. Masson (2013, July). Evolution of the Parisian urban climate under a global changing climate. *Climatic Change 116*(3-4), 679–692.

Lemonsu, A., V. Masson, L. Shashua-Bar, E. Erell, and D. Pearlmutter (2012, November). Inclusion of vegetation in the Town Energy Balance model for modelling urban green areas. *Geoscientific Model Development 5*(6), 1377–1393.

Levinson, R., H. Akbari, and J. C. Reilly (2007, July). Cooler tile-roofed buildings with near-infrared-reflective non-white coatings. *Building and Environment 42*(7), 2591–2605.

Li, D. and E. Bou-Zeid (2013, September). Synergistic Interactions between Urban Heat Islands and Heat Waves: The Impact in Cities Is Larger than the Sum of Its Parts. *Journal of Applied Meteorology and Climatology 52*(9), 2051–2064.

Li, H., J. Harvey, and D. Jones (2013, December). Cooling Effect of Permeable Asphalt Pavement Under Dry and Wet Conditions. *Transportation Research Record: Journal of the Transportation Research Board 2372*(-1), 97–107.

Maillard, P., F. David, M. Dechesne, J.-B. Bailly, and E. Lesueur (2014). Characterization of the Urban Heat Island and evaluation of a road humidification mitigation solution in the district of La Part-Dieu, Lyon (France). *Techniques Sciences Méthodes* (6), 23–35 (in French).

Masson, V. (2000). A physically-based scheme for the urban energy budget in atmospheric models. *Boundary-Layer Meteorology 94*(3), 357–397.

Masson, V., C. Marchadier, L. Adolphe, R. Aguejdad, P. Avner, M. Bonhomme, G. Bretagne, X. Briottet, B. Bueno, C. de Munck, O. Doukari, S. Hallegatte, J. Hidalgo, T. Houet, J. Le Bras, A. Lemonsu, N. Long, M.-P. Moine, T. Morel, L. Nolorgues, G. Pigeon, J.-L. Salagnac, V. Viguié, and K. Zibouche (2014, April). Adapting cities to climate change: A systemic modelling approach. *Urban Climate*, 1–23.

Mayer, H. and P. Höppe (1987). Thermal comfort of man in different urban environments. *Theoretical and Applied Climatology 38*(1), 43–49.

Météo France (2014). 2014 en France : dans le top 3 des années les plus chaudes depuis 1900 ?

Météo France (2015). 2014 : année record pour les températures en France et en Europe.

Météo France and CSTB (2012). EPICEA - Rapport de synthèse. Technical report.

Morille, B., M. Musy, and L. Malys (2014). Preliminary study of the impact of urban vegetated devices on energy consumption of building at a district scale. In *Third International Conference on Countermeasures to Urban Heat Island*, 13-15 October, Venice, Italy, pp. 1397–1409.

Musy, M., L. Malys, B. Morille, A. Szucs, C. Inard, E. Bozonnet, R. Djedjig, R. Belarbi, A. Lemonsu, C. de Munck, and K. Chancibault (2014). Impact of vegetation on urban climate , thermal comfort and building energy consumption – Overview of VegDUD project results. In *Third International Conference on Countermeasures to Urban Heat Island*, 13-15 October, Venice, Italy, pp. 719–730.

Nakayama, T. and T. Fujita (2010, May). Cooling effect of water-holding pavements made of new materials on water and heat budgets in urban areas. *Landscape and Urban Planning 96*(2), 57–67.

Nakayama, T., S. Hashimoto, and H. Hamano (2012, July). Multiscaled analysis of hydrothermal dynamics in Japanese megalopolis by using integrated approach. *Hydrological Processes 26*(16), 2431–2444.

Newman, P. W. G. and J. R. Kenworthy (1989). Gasoline Consumption and Cities. *Journal of the American Planning Association 55*(1), 24–37.

Ng, E., L. Chen, Y. Wang, and C. Yuan (2012, January). A study on the cooling effects of greening in a high-density city: An experience from Hong Kong. *Building and Environment 47*, 256–271.

Oke, T. (1973). City size and the urban heat island.

Oke, T. (1982). The energetic basis of the urban heat island. *Quarterly Journal of the Royal Meteorological Society 108*(455), 1–24.

Oke, T. (1988). Street design and urban canopy layer climate.

Oke, T. R. (1981). Canyon geometry and the nocturnal urban heat island: Comparison of scale model and field observations. *Journal of Climatology 1*(3), 237–254.

Pagliarini, G. and S. Rainieri (2011, February). Dynamic thermal simulation of a glass-covered semi-outdoor space with roof evaporative cooling. *Energy and Buildings 43*(2-3), 592–598.

Paris City Council (2007). Paris Climate Protection Plan. Technical report, Paris City Council, Paris, France.

Paris City Council (2012a). Blue Paper. Technical report, Paris City Council, Paris, France (In French).

Paris City Council (2012b). Paris Climate and Energy Action Plan. Technical report, Paris City Council, Paris, France.

Pasquill, F. (1961). The estimation of the dispersion of windborne material. *The Meteorological Magazine 90*(1063), 33–49.

Pigeon, G., D. Legain, P. Durand, and V. Masson (2007). Anthropogenic heat release in an old European agglomeration (Toulouse, France). *International Journal of Climatology 27*(14), 1969–1981.

Redon, E., A. Lemonsu, M. Musy, V. Masson, C. De Munck, and K. Chancibault (2014). Modelling of Urban Vegetation as a Thermal Regulator and Management of Associated Water Resources for Neighbourhood to City-scale Applications Methoda , Validation And Perspectives. In *Third International Conference on Countermeasures to Urban Heat Island*, 13-15 October, Venice, Italy, pp. 850–852.

Robine, J.-M., S. L. K. Cheung, S. Le Roy, H. Van Oyen, C. Griffiths, J.-P. Michel, and F. R. Herrmann (2008, February). Death toll exceeded 70,000 in Europe during the summer of 2003. *Comptes rendus biologies 331*(2), 171–178.

Rosado, P., H. Gilbert, M. Pomerantz, B. Mandel, and R. Levinson (2014). Cool Pavement Demonstration and Study. In *Third International Conference on Countermeasures to Urban Heat Island*, Venice, Italy 13th-15th October, 2014, pp. 815–826.

Rosenfeld, A. H., H. Akbari, J. J. R. Tv, and M. Pomerantz (1998). Cool communities: strategies for heat island mitigation and smog reduction '. *Energy and Buildings 28*, 51–62.

Santamouris, M. (2013, October). Using cool pavements as a mitigation strategy to fight urban heat island—A review of the actual developments. *Renewable and Sustainable Energy Reviews 26*, 224–240.

Santamouris, M., N. Papanikolaou, I. Livada, I. Koronakis, C. Georgakis, A. Argiriou, and D. Assimakopoulos (2001, January). On the impact of urban climate on the energy consumption of buildings. *Solar Energy 70*(3), 201–216.

Santamouris, M., A. Synnefa, and T. Karlessi (2011). Using advanced cool materials in the urban built environment to mitigate heat islands and improve thermal comfort conditions. *Solar Energy 85*(12), 3085–3102.

Sleiman, M., T. Kirchstetter, P. Berdahl, H. Gilbert, S. Chen, R. Levinson, H. Destaillats, and H. Akbari (2014). Aging of Cool Roof Materials : New Accelerated Laboratory Test Method for Mimicking the Change in Solar Reflectance. In *Third International Conference on Countermeasures to Urban Heat Island*, 13-15 October, Venice, Italy, pp. 1571–1582.

Spronken-Smith, R. and T. Oke (1999). Scale modelling of nocturnal cooling in urban parks. *Boundary-Layer Meteorology* (93), 287–312.

Staiger, H., G. Laschewski, and A. Grätz (2012). The perceived temperature - a versatile index for the assessment of the human thermal environment. Part A: Scientific basics. *International Journal of Biometeorology 56*(1), 165–176.

Taha, H. (1997, January). Urban climates and heat islands: albedo, evapotranspiration, and anthropogenic heat. *Energy and Buildings 25*(2), 99–103.

Takahashi, R., A. Asakura, K. Koike, S. Himeno, and S. Fujita (2010). Using Snow Melting Pipes to Verify the Water Sprinkling's Effect over a Wide Area. In *NOVATECH 2010*, pp. 10.

Takebayashi, H., K. Miki, K. Sakai, Y. Murata, T. Matsumoto, S. Wada, and T. Aoyama (2014). Examination on Aging Experiment and Accelerated Aging Test Method of Solar Reflectance of the High Reflectance Paint in Japan. In *Third International Conference on Countermeasures to Urban Heat Island*, 13-15 October, Venice, Italy, pp. 630–641.

Takebayashi, H. and M. Moriyama (2007, August). Surface heat budget on green roof and high reflection roof for mitigation of urban heat island. *Building and Environment 42*(8), 2971–2979.

Takebayashi, H. and M. Moriyama (2009, August). Study on the urban heat island mitigation effect achieved by converting to grass-covered parking. *Solar Energy 83*(8), 1211–1223.

Thorsson, S., F. Lindberg, I. Eliasson, and B. Holmer (2007, November). Different methods for estimating the mean radiant temperature in an outdoor urban setting. *International Journal of Climatology 27*(14), 1983–1993.

Wang, S. and Y. Li (2015). Suitability of acrylic and copper globe thermometers for diurnal outdoor settings. *Building and Environment 89*, 279–294.

Wei, J. and J. He (2013, March). Numerical simulation for analyzing the thermal improving effect of evaporative cooling urban surfaces on the urban built environment. *Applied Thermal Engineering 51*(1-2), 144–154.

Wong, N. H., A. Y. K. Tan, P. Y. Tan, and N. C. Wong (2009, December). Energy simulation of vertical greenery systems. *Energy and Buildings 41*(12), 1401–1408.

Yamagata, H., M. Nasu, M. Yoshizawa, A. Miyamoto, and M. Minamiyama (2008, January). Heat island mitigation using water retentive pavement sprinkled with reclaimed wastewater. *Water science and technology: a journal of the International Association on Water Pollution Research 57*(5), 763–771.

Yoshino, M. (1990). Development of urban climatology and problems today. *Energy and Buildings 15*(1-2), 1–10.

APPENDIX A

Congrès Français de Thermique 2015 : Thermique de l'Habitat et de la Ville

Quel est le meilleur revêtement pour limiter la formation des îlots de chaleur urbains ?

What is the best surfacing material for urban heat island mitigation?

Quel est le meilleur revêtement pour limiter la formation des îlots de chaleur urbains ?

Martin HENDEL[1,2,3*], Arnaud GRADOS[3], Morgane COLOMBERT[2], Youssef DIAB[2], Laurent ROYON[3]

[1]Mairie de Paris, Service Technique de l'Eau et de l'Assainissement, F-75014, Paris, France
[2]Université Paris-Est, Lab'Urba, EA 3482, EIVP, F-75019, Paris, France
[3]Univ Paris Diderot, Paris Sorbonne Cité, MSC, UMR 7057, CNRS, F-75013, Paris, France
[*](auteur correspondant : martin.hendel@paris.fr)

Résumé - Les matériaux utilisés en milieu urbain ont un fort impact sur le climat urbain et par conséquent sur le confort thermique du piéton. Selon leurs propriétés thermiques, ils peuvent contribuer au développement d'îlots de chaleur urbains. Pour diminuer leur effet, différentes stratégies sont étudiées, comme la végétalisation ou l'arrosage de l'espace urbain.

Notre étude s'inscrit dans ce cadre et propose d'analyser le comportement thermo-climatique de revêtements urbains dans des conditions similaires à une canicule. La sollicitation climatique est découpée en une période diurne de 8h, avec une température de l'air de 35°C, 35% d'humidité et un ensoleillement artificiel, et une période nocturne de 16h à 25°C, 70% d'humidité et sans ensoleillement.

Les échantillons se présentent sous la forme d'éprouvettes cylindriques de 16 cm de diamètre pour 32 cm de hauteur, entourées d'une couche isolante de 5 cm (Figure 1). La température de surface de chaque échantillon est suivie par un thermocouple de type K. Un indicateur de l'échauffement atmosphérique par les échantillons est proposé pour les caractériser.

Des essais menés sur trois cycles consécutifs de 24h ont permis de classer les structures par leur contribution à l'échauffement atmosphérique. Les structures noires sont les plus chaudes, suivies des structures claires et du gazon, largement plus frais que les autres revêtements. Enfin, la succession des cycles expérimentaux sur trois jours ont permis d'identifier le gazon et les trottoirs comme les structures qui manifestent le plus d'effets cumulatifs. Le trottoir asphalte devient ainsi la structure la plus chaude au troisième jour.

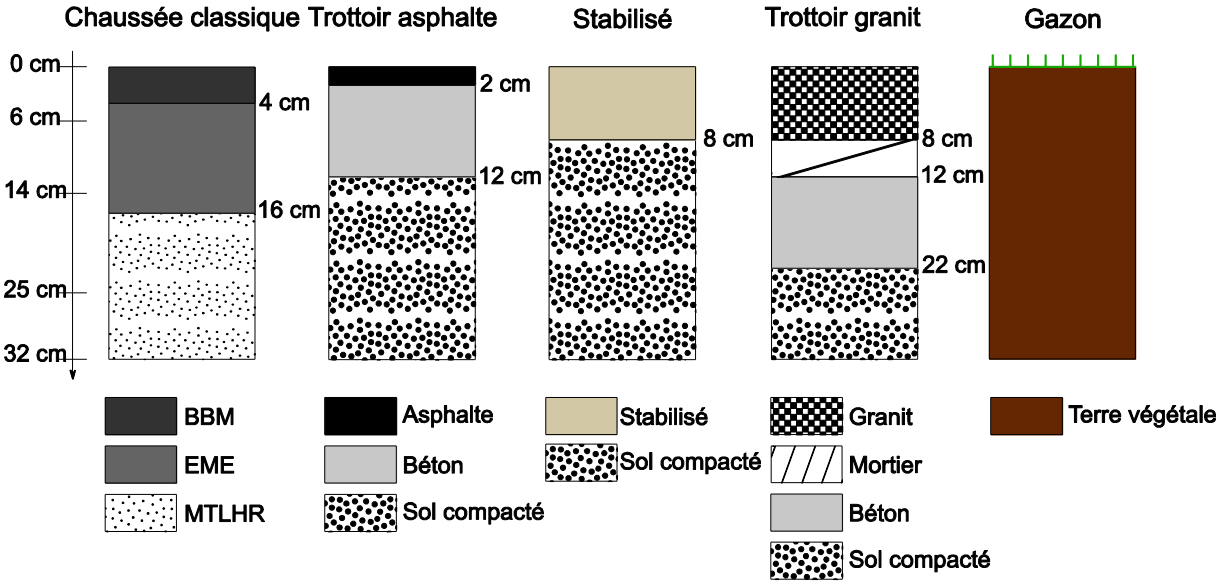

Figure 1 : *Structure des échantillons étudiés*

Nomenclature

BBM	béton bitumineux mince	*GLO*	grande longueur d'onde (3-100 µm)
CLO	courte longueur d'onde (0,3-3 µm)	*GLO*	grande longueur d'onde (3-100 µm)
EME	enrobé à module élevé	*MTLHR*	matériaux traités au liant hydraulique

1. Introduction

Les matériaux utilisés en milieu urbain ont un fort impact sur le climat urbain et par conséquent sur le confort thermique du piéton [1]. Selon leurs propriétés thermiques, ils peuvent contribuer plus ou moins fortement au développement d'îlots de chaleur urbains [2]. Pour diminuer leur effet, différentes stratégies sont étudiées, comme l'arrosage ou la végétalisation de l'espace urbain [3], [4]. Ces moyens d'adaptation sont particulièrement importants pour limiter l'impact sanitaire des canicules en ville [5].

Pour autant, les travaux existants sur le comportement des revêtements se focalisent sur les couches de surface, sans tenir compte de la superposition de plusieurs couches de matériaux différents [6]–[8]. Afin d'éclairer leurs choix de revêtements, les décideurs ont donc besoin de s'appuyer sur l'analyse du comportement des structures réellement mises en œuvre.

Notre étude s'inscrit dans ce cadre et propose de caractériser le comportement thermo-climatique de revêtements urbains dans des conditions similaires à une canicule. Pour cela, cinq structures de la voirie parisienne sont soumises à une même sollicitation climatique.

2. Matériels et méthodes

2.1. Structures étudiées

Cinq structures ont été retenues pour l'analyse, à savoir une chaussée classique, un trottoir asphalte, un sable stabilisé, un trottoir granit et un gazon. Ces structures sont couramment employées à Paris dans les rues, parcs et jardins de la capitale. La chaussée classique et le trottoir asphalte sont des revêtements minéraux noirs, le stabilisé et le trottoir granit sont des revêtements minéraux clairs tandis que le gazon est le seul revêtement végétal.

Le Tableau 1 présente les valeurs d'albédo et d'émissivité de chacune de ces structures. Seules les valeurs d'émissivité ont été mesurées, celles d'albédo étant tirées de la littérature.

	Chaussée classique	Trottoir asphalte	Stabilisé	Trottoir granit	Gazon
Albédo	0,05-0,12	0,05-0,12	0,3-0,5	0,3-0,4	0,25
Emissivité	0,98	0,98	0,92	0,99	0,98

Tableau 1 : *Propriétés radiatives des échantillons*

Les échantillons se présentent sous la forme d'éprouvettes cylindriques de 16 cm de diamètre pour 32 cm de hauteur, entourées d'une couche isolante de 5 cm composée de mousse polyuréthane expansée. La température de surface de chacun des échantillons est suivie à l'aide d'un thermocouple de type K. Leur composition est illustrée à la Figure 1.

2.2. Protocole expérimental

Placé dans une enceinte climatique sous température et humidité contrôlées, l'échantillon est soumis à une sollicitation climatique cyclique d'une période de 24h pendant 72h. La sollicitation est découpée en une période diurne de 8h, avec une température de l'air de 35°C, 35% d'humidité, et une période nocturne de 16h à 25°C, 70% d'humidité.

Entre les essais, chaque échantillon est entreposé à une température de 20°C. Afin de s'assurer de son équilibre avant le lancement de l'essai, celui-ci est installé au moins 24h avant dans l'enceinte réglée en mode nuit. Le gazon est prélevé dans un parc dans les 10 jours précédents l'essai et est abondamment arrosé en attendant son installation dans l'enceinte climatique.

L'ensoleillement artificiel est assuré par 7 ampoules halogènes dichroïques de température de couleur 5 600 K. Bien que ne reproduisant pas parfaitement le spectre solaire, ce dispositif est adapté pour des matériaux à réponse radiative uniforme entre 0,3 et 3 µm. En revanche, ce dispositif ne permettrait pas de reproduire fiablement le comportement de revêtements réfléchissants dans le proche infrarouge comme il en existe pour les toitures [9].

Le Tableau 2 résume les caractéristiques du cycle climatique et la Figure 2 illustre la fiabilité réelle de l'enceinte mesurée par un thermo-hygromètre placé dans l'enceinte.

	Jour	Nuit
Durée	8h	16h
Température de l'air	35°C	25°C
Humidité relative	35%	70%
Rayonnement CLO (0,3-3 µm)	1 320 W/m²	0
Rayonnement GLO (3-100 µm)	230 W/m²	430 W/m²

Tableau 2 : *Découpage et paramètres de la sollicitation climatique*

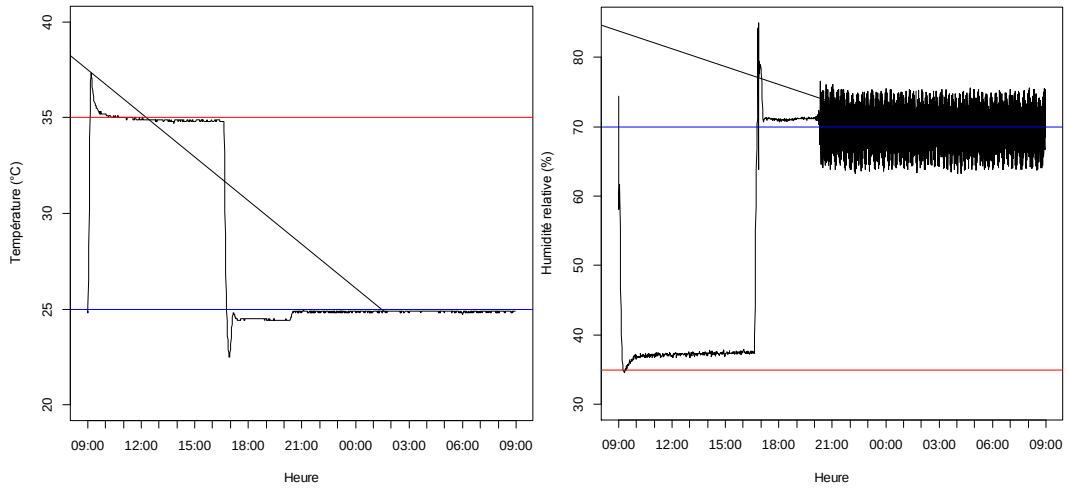

Figure 2 : *Profil de la température (gauche) et de l'humidité relative (droite) dans l'enceinte climatique. Les droites rouge et bleue indiquent les consignes jour et nuit, respectivement.*

2.3. Indicateur de l'échauffement atmosphérique provoqué par les structures étudiées

Les revêtements urbains sont susceptibles d'aggraver les effets des canicules lorsque ceux-ci contribuent à augmenter la température atmosphérique, c'est-à-dire lorsqu'ils sont plus chauds que l'air ambiant. Pour comparer les contributions diurnes et nocturnes des structures, on suppose un coefficient de convection identique pour tous les échantillons et on s'intéresse à l'aire entre la courbe de température de surface et la température de consigne pendant chaque phase. Par analogie avec le domaine du bâtiment et l'unité « degré-jour », utilisée pour quantifier un besoin de chauffage ou de rafraîchissement, on utilisera l'unité « degré-heure » pour quantifier la contribution atmosphérique des structures étudiées. Ainsi construit, 1°C.h correspond à une heure pendant laquelle la surface est un degré plus chaude que l'air.

Ayant supposé que le coefficient de convection est le même pour toute les structures, cet indicateur est homogène à une énergie transférée à l'air par unité de surface de revêtement.

3. Résultats et discussion

Dans l'analyse des données observées, on se focalisera dans un premier temps sur les données obtenues à J, puis dans un second temps aux observations de J à J+2.

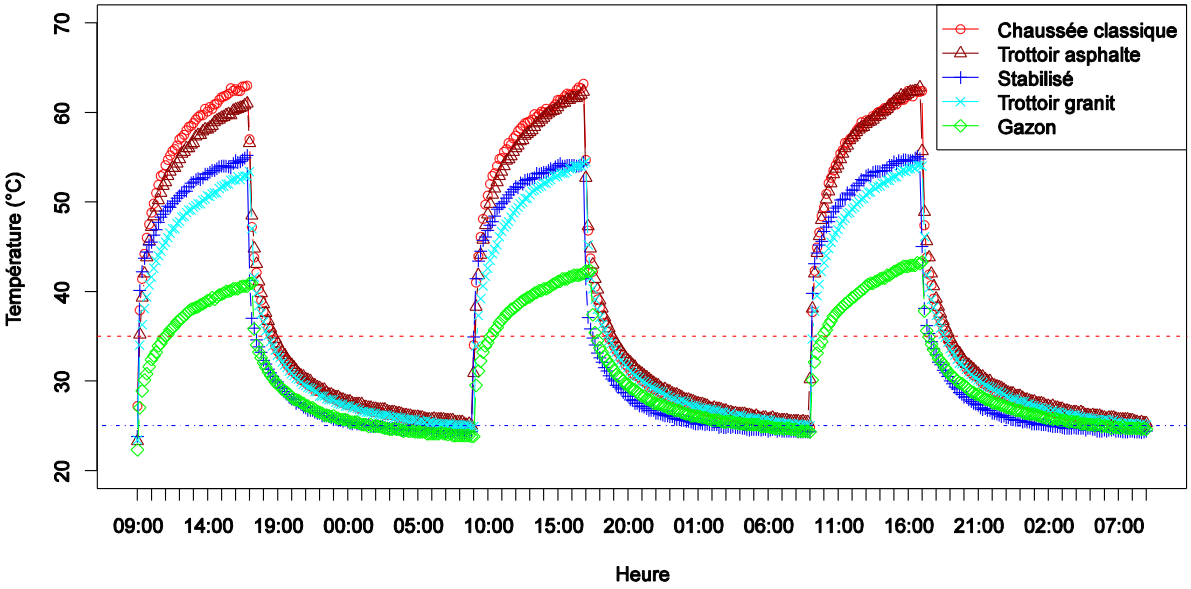

Figure 3 : *Evolution des températures de surface sur 72h*

La Figure 3 représente l'évolution des températures de surface de tous les échantillons étudiés pendant trois journées consécutives. Les lignes horizontales bleue (pointillés-tiretés) et rouge (tirets) indiquent les températures de consigne nocturne et diurne, respectivement.

3.1. Observations au bout du premier jour de sollicitation (J)

On remarque tout d'abord qu'en début d'expérimentation les températures de surfaces sont en dessous de la consigne nocturne, c'est-à-dire que les échantillons sont plus froids que l'air ambiant. Cela se répète pour certains échantillons en fin de cycle également. Ceci est expliqué par le faible rayonnement ambiant présent au sein de l'enceinte climatique, dû à ses parois métalliques lisses à basse émissivité. La température de surface stabilisée pendant la période nocturne est de 23,5°C environ pour tous les échantillons.

Quelle que soit la structure envisagée, les températures croissent très fortement dès que l'ensoleillement est enclenché et dépassent la consigne de 35°C dès les premières minutes d'ensoleillement, sauf pour le gazon qui met deux heures à franchir ce seuil.

Après une première phase de croissance exponentielle qui dure entre deux et trois heures selon la structure, la température croît de manière quasi-linéaire jusqu'à l'arrêt de l'ensoleillement.

Pendant la phase diurne, deux catégories de structures se distinguent selon l'évolution de leur température de surface : les matériaux « chauds », dont la température dépasse 60°C, et les matériaux « frais » qui restent en deçà de ce seuil. Les structures « noires », c'est-à-dire la chaussée et le trottoir asphalte appartiennent à la première catégorie, tandis que le stabilisé, le

trottoir granit et le gazon appartiennent à la deuxième. Le gazon, plus de 10°C plus frais que les deux autres structures, pourrait constituer sa propre catégorie de matériaux « très frais ».

Intervenant au bout de 8h d'ensoleillement, l'arrêt de la lampe provoque une chute exponentielle des températures qui tendent ensuite vers la température initiale. On remarque qu'aucune des structures ne retrouve l'état d'équilibre initial, le différentiel le plus élevé étant de 2,5°C environ pour le trottoir asphalte. Ainsi, toutes les structures terminent le cycle avec un surplus d'énergie par rapport à la situation de départ.

Dès la première heure après extinction de la lampe, les structures se regroupent en deux groupes, avec d'une part le stabilisé et le gazon qui sont les plus fraiches, et d'autre part les structures restantes, significativement plus chaudes. Le granit, pourtant classé en tant que matériau frais en journée, rejoint le niveau de température des structures noires pendant la nuit.

Par ailleurs, on remarque que la chaussée, qui était pourtant la structure la plus chaude en journée, est plus fraîche que le trottoir asphalte au bout de quelques minutes suivant l'arrêt de l'ensoleillement.

La Figure 4 exprime la contribution à l'échauffement atmosphérique pendant le premier jour de chacune des structures étudiées en « degré-heure ». Les contributions diurnes sont indiquées en rouge tandis que les contributions nocturnes sont en bleu.

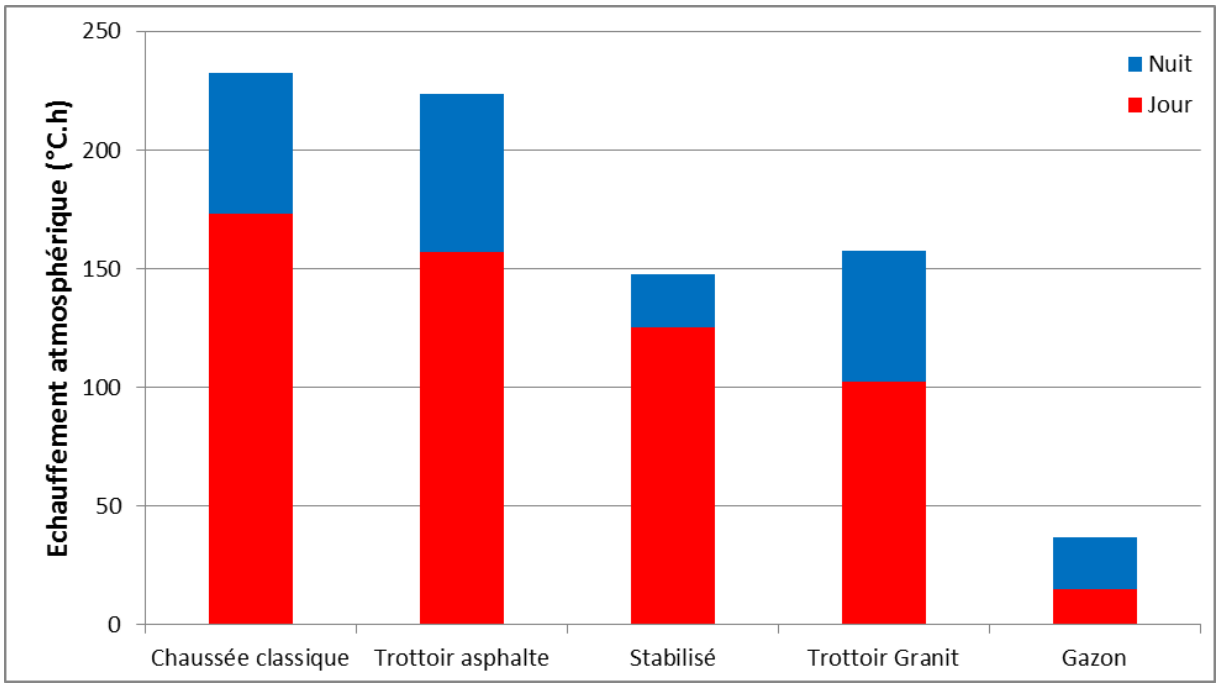

Figure 4 : *Contribution à l'échauffement atmosphérique à J*

Pour tous les échantillons, l'échauffement diurne est le plus important, sauf pour le gazon. Pour autant, les contributions nocturnes ne sont pas négligeables et sont déterminantes pour classer les échantillons par leur contribution atmosphérique. Les regroupements effectués à partir des températures de surface se retrouvent, avec les structures noires étant les plus chaudes, le gazon étant la structure la plus fraîche et les structures claires se situant à un niveau intermédiaire. C'est donc le gazon qui contribue le moins à échauffer l'air ambiant, alors que les matériaux noirs ont la contribution la plus importante, suivis par les matériaux clairs.

3.2. Effets cumulatifs de J à J+2

Au bout de trois journées consécutives, les structures manifestent des signes d'accumulation de chaleur. Si le comportement de la chaussée classique et du stabilisé n'est que très peu modifié à J+1 et J+2 par rapport à J, ce n'est pas le cas du trottoir asphalte, du trottoir granit ou du gazon. Ces trois structures voient effectivement leur température de surface augmenter avec l'enchainement des cycles climatiques, comme le montre l'évolution des températures maximales résumée au Tableau 3.

Structure	Tmax à J	Tmax à J+1	Tmax à J+2
	°C	°C	°C
Chaussée classique	63,3	63,2	62,7
Stabilisé	55,2	54,6	55,1
Trottoir asphalte	61,2	62,3	62,9
Trottoir granit	53,6	54,6	54,3
Gazon	40,9	42,3	43,4

Tableau 3 : *Température de surface maximale atteinte à J, J+1 et J+2.*

Les observations nocturnes réalisées à J ne sont pas significativement modifiées à J+2. La température du gazon est celle qui augmente le plus, se distinguant nettement de la température du stabilisé par rapport à ce qui était observé à J.

La Figure 5 résume la contribution atmosphérique diurne et nocturne des structures à J+2. Toutes les contributions observées à J+2 sont augmentées par rapport à J. Conformément à ce qui avait été indiqué à partir des courbes de température de surface, la chaussée classique et le stabilisé sont les structures les moins affectées avec moins de 5% d'augmentation, tandis que la contribution du gazon est presque doublée, même si elle reste faible. Les contributions des trottoirs asphalte et granit augmentent de 10% environ. Ceci vaut au trottoir asphalte de détrôner la chaussée classique comme revêtement échauffant le plus l'atmosphère.

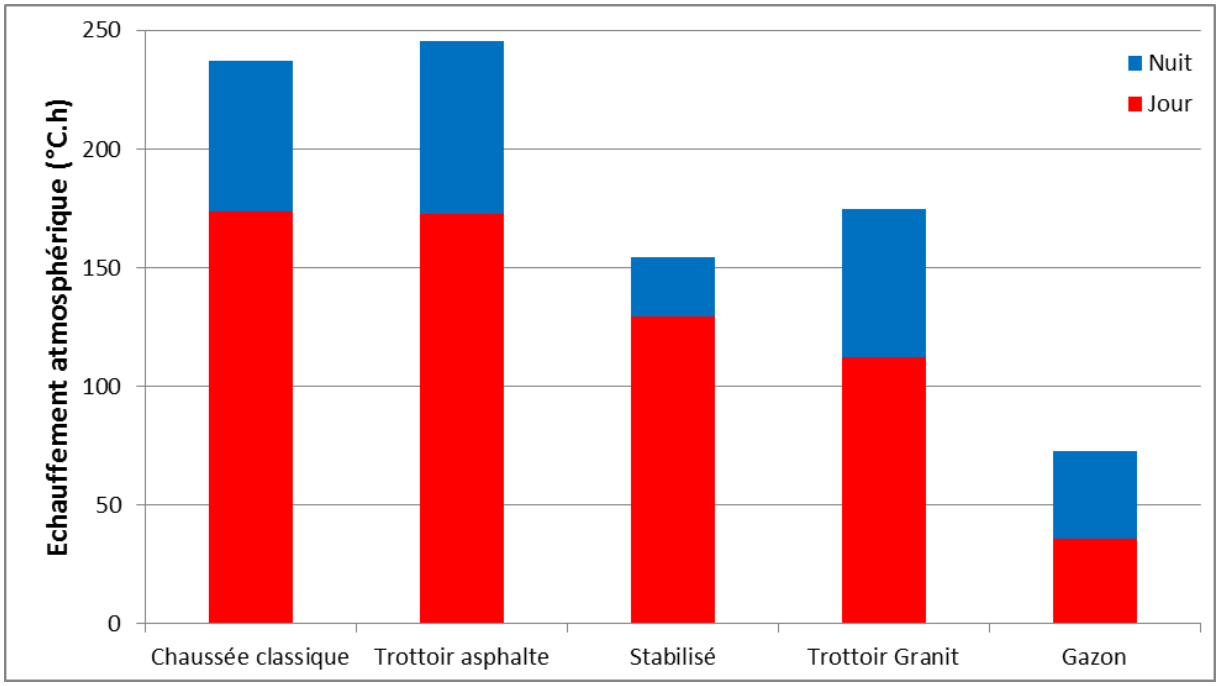

Figure 5 : *Contribution à l'échauffement atmosphérique à J+2*

Le gazon est donc le plus concerné par les effets cumulatifs provoqués par l'enchainement de plusieurs « journées caniculaires », suivi du trottoir granit et du trottoir asphalte.

3.3. Discussion

Le classement des revêtements sur la base des températures obtenues à J correspond bien à ce qui est attendu à partir de leur albédo. En effet, les matériaux noirs, à faible albédo, sont les plus chauds, tandis que les matériaux plus clairs sont plus frais.

Pour autant, l'albédo ne suffit pas pour expliquer toutes les observations. En effet, le gazon, pourtant plus sombre que les matériaux clairs, est de loin le plus frais des revêtements. Cela est attribuable au rafraîchissement fourni par l'évapotranspiration de l'eau qu'il contient. Le rôle rafraîchissant des végétaux est signalé dans de nombreux travaux, mais ils soulignent souvent la condition de l'approvisionnement en eau [10]. Lors de nos essais, le gazon est resté largement alimenté en eau, lui permettant de rester très frais tout au long de l'expérience.

Par ailleurs, l'albédo ne permet pas d'expliquer l'évolution des températures d'un cycle climatique à un autre. En effet, alors que pour un état initial donné, le trottoir asphalte est plus frais que la chaussée, il devient la structure la plus chaude le 3^{e} jour. Ceci est dû aux matériaux sous-jacents, notamment à ses 10 cm de béton qui accumulent de la chaleur au fil des jours, avec un impact observable sur sa température de surface. Le même phénomène est à l'œuvre pour le trottoir granit. Le gazon voit sa température augmenter de 2°C entre le premier et le dernier jour. Cela est attribué à l'inertie de la terre mouillée.

Enfin, les températures de surface maximales atteintes à J sont cohérentes avec celles observées à l'occasion des travaux similaires [6], [7]. En effet, des températures maximales comprises entre 40°C pour le gazon et 65°C pour l'enrobé bitumineux y sont observées. Ces températures sont atteintes en extérieur sur des sites sans masque pour des conditions météorologiques semblables à celles de l'enceinte climatique. Les températures observées par Ueno et Tamaoki [8], bien plus faibles que les nôtres, ne sont pas comparables étant donné que leurs sollicitations climatiques ont une durée de quelques minutes seulement. On en déduit que le protocole expérimental utilisé ici permet de reproduire les températures maximales atteintes en extérieur pour un site sans obstruction en journée chaude d'été.

4. Conclusion

Cinq échantillons de structures couramment employés sur l'espace public parisien ont été soumis à des conditions caniculaires pendant trois journées consécutives. Nos observations ont permis de classer ces structures les unes par rapport aux autres en fonction de leur contribution à l'échauffement atmosphérique. Ainsi, les structures noires, à savoir la chaussée classique et le trottoir asphalte, y contribuent le plus, suivies des structures claires, à savoir le trottoir granit et le stabilisé, tandis que la structure gazon a la contribution la plus faible.

Si l'albédo des matériaux de surface joue un rôle déterminant dans les comportements observés, on a pu constater l'importance des couches sous-jacentes, notamment pour les effets cumulatifs. En effet, les matériaux sous-jacents stockent également une grande partie de l'énergie solaire accumulée et influence la température de surface des jours suivants. Les phénomènes cumulatifs affectent principalement les structures contenant une couche de béton ou de granit, faiblement poreuses. Le gazon montre également des phénomènes d'accumulation importants relativement à son faible échauffement de l'atmosphère. On retiendra également le rôle primordial de l'eau pour assurer les bonnes performances des surfaces végétalisées comme le gazon.

L'étude des températures et des flux de chaleur à différentes profondeurs permettra d'étudier plus précisément le rôle des différentes couches constitutives des structures étudiées ainsi que d'identifier le rôle de certaines de leurs propriétés thermiques.

Références

[1] E. Erell, D. Pearlmutter, D. Boneh, and P. B. Kutiel, "Effect of high-albedo materials on pedestrian heat stress in urban street canyons," *Urban Clim.*, Oct. 2013.

[2] M. Santamouris, "Appropriate materials for the urban environment," in *Energy and Climate in the Urban Built Environment*, M. Santamouris, Ed. 2001.

[3] A. H. Rosenfeld, H. Akbari, J. J. R. Tv, and M. Pomerantz, "Cool communities: strategies for heat island mitigation and smog reduction '," *Energy Build.*, vol. 28, pp. 51–62, 1998.

[4] M. Hendel, M. Colombert, Y. Diab, and L. Royon, "Effets thermiques de l'arrosage de l'espace public comme moyen d'adaptation au changement climatique," in *Congrès Français de Thermique 2014 : Approches Multi-échelles*, 2014.

[5] J.-M. Robine, S. L. K. Cheung, S. Le Roy, H. Van Oyen, C. Griffiths, J.-P. Michel, and F. R. Herrmann, "Death toll exceeded 70,000 in Europe during the summer of 2003.," *C. R. Biol.*, vol. 331, no. 2, pp. 171–178, Feb. 2008.

[6] T. Asaeda, V. T. Ca, and A. Wake, "Heat storage of pavement and its effect on the lower atmosphere," *Atmos. Environ.*, vol. 30, no. 3, pp. 413–427, Feb. 1996.

[7] H. Takebayashi and M. Moriyama, "Study on Surface Heat Budget of Various Pavements for Urban Heat Island Mitigation," *Adv. Mater. Sci. Eng.*, vol. 2012, pp. 1–11, 2012.

[8] T. Ueno and K. Tamaoki, "Thermal Characteristics of Urban Land Cover by Indoor Lamp-Irradiation Experiment," in *The Seventh International Conference on Urban Climate*, 2009, no. July, pp. 1–4.

[9] R. Levinson, H. Akbari, and J. C. Reilly, "Cooler tile-roofed buildings with near-infrared-reflective non-white coatings," *Build. Environ.*, vol. 42, no. 7, pp. 2591–2605, Jul. 2007.

[10] Météo-France and CSTB, "EPICEA - Rapport de synthèse," 2012.

Remerciements

Le matériel utilisé pour cette étude a été entièrement financée par l'Atelier Parisien d'Urbanisme (APUR). Les auteurs souhaitent exprimer leur gratitude au Laboratoire d'Essai des Matériaux de la Ville de Paris (LEM VP) pour la mise à disposition de son matériel et de son expertise en termes de revêtements parisiens.

APPENDIX B

XII^{ème} Colloque Interuniversitaire Franco-Québécois sur la Thermique des Systèmes

Comparaison des matériaux de l'espace public parisien : caractérisation de la contribution aux îlots de chaleur urbains

Comparison of Parisian urban materials: characterizing their contribution to urban heat islands

XII[ème] Colloque Interuniversitaire Franco-Québécois
sur la Thermique des Systèmes
8-10 juin 2015, Sherbrooke
Québec (Canada)

CIFQ2015 / ART-08-04

COMPARAISON DES MATERIAUX DE L'ESPACE PUBLIC PARISIEN : CARACTERISATION DE LA CONTRIBUTION AUX ILOTS DE CHALEUR URBAINS

Martin **HENDEL**[a,b,c*], Arnaud **GRADOS**[b], Morgane **COLOMBERT**[c], Youssef **DIAB**[c], Laurent **ROYON**[b]

[a] *Mairie de Paris, Service Technique de l'Eau et de l'Assainissement, F-75014, Paris, France*
[b] *Université Paris-Est, Lab'Urba, EA 3482, EIVP, F-75019, Paris, France*
[c] *Univ Paris Diderot, Paris Sorbonne Cité, MSC, UMR 7057, CNRS, F-75013, Paris*

RÉSUMÉ

Un protocole expérimental a été mis au point pour étudier le comportement thermo-climatique de revêtements urbains en période caniculaire. Le protocole permet de reproduire de manière satisfaisante le comportement observé sur le terrain à Paris. Par ailleurs, l'albédo de la couche de surface et la conductivité thermique apparente des différentes couches des revêtements ont pu être déterminés. Un indicateur qualifiant la propension d'une structure à absorber et transmettre un rayonnement incident en profondeur a également été élaboré, calculé à partir des propriétés thermiques précédemment déterminées. Ce protocole peut donc être utilisé pour caractériser d'autres revêtements ou déterminer l'effet de l'arrosage urbain si un dispositif d'arrosage lui est intégré.

Mots Clés : *Revêtements urbains, adaptation au changement climatique, ilots de chaleur urbain, canicule, matériaux*

NOMENCLATURE

Symboles :	
a	absorptivité solaire
BBM	béton bitumineux mince
CLO	courte longueur d'onde (0,3-3 µm)
e	épaisseur de couche, m
EME	enrobé à module élevé
GLO	grande longueur d'onde (3-100 µm)
H	densité de flux convectif, W/m²
k	coefficient d'absorption-transmission, -
L	rayonnement GLO, W/m²
MTLHR	matériaux traités au liant hydraulique
R_n	rayonnement net, W/m²
S	rayonnement CLO, W/m²
T	température, °C
V	densité de flux conductif, W/m²
z	profondeur, m
Lettres grecques :	
α	albédo (réflectivité CLO), -
ε	émissivité, -
λ	conductivité thermique, W/m.K
Φ	densité de flux mesurée, W/m².K
Indices / Exposants :	
0	référence
éq.c.n.	équivalent à un corps noir à la même température
down	rayonnement incident
n	indice de couche (entier strictement positif)
up	rayonnement émis et/ou réfléchi
g	global

1. INTRODUCTION

Les matériaux utilisés en milieu urbain ont un fort impact sur le climat urbain et par conséquent sur le confort thermique du piéton [1]. Selon leurs propriétés thermiques, ils peuvent contribuer plus ou moins fortement au développement d'îlots de chaleur urbains [2]. Pour diminuer leur effet, différentes stratégies sont étudiées, comme l'arrosage ou la végétalisation de l'espace urbain [3], [4]. Ces moyens d'adaptation sont particulièrement importants pour limiter l'impact sanitaire des canicules en ville [5].

Pour autant, les travaux existants sur le comportement des revêtements se focalisent sur les températures à différentes profondeurs des couches de surface, sans tenir compte de la superposition de couches de matériaux différents ou des flux thermiques

* auteur correspondant
Adresse électronique : martin.hendel@paris.fr

en leur sein [6]–[8]. Afin d'éclairer leurs choix de revêtements, les décideurs ont donc besoin de s'appuyer sur l'analyse du comportement des structures réellement mises en œuvre.

Notre étude s'inscrit dans ce cadre et propose de caractériser le comportement thermo-climatique de revêtements urbains dans des conditions caniculaires. Pour cela, cinq structures de la voirie parisienne sont soumises à une même sollicitation climatique.

2. MATERIELS ET METHODES

2.1. Structures étudiées

Cinq structures ont été retenues pour l'analyse, à savoir une chaussée classique, un trottoir asphalte, un sable stabilisé et un trottoir granit. Ces structures sont couramment employées à Paris dans les rues, parcs et jardins de la capitale. La chaussée classique et le trottoir asphalte sont des revêtements minéraux noirs, tandis que le stabilisé et le trottoir granit sont clairs.

Le Tableau 1 présente les valeurs d'albédo et d'émissivité de chacune de ces structures. Seule l'émissivité a été mesurée expérimentalement, les valeurs d'albédo sont tirées de la littérature [9].

Tableau 1 : Propriétés radiatives des échantillons

	Chaussée classique	*Trottoir asphalte*	*Stabilisé*	*Trottoir granit*
α	0,05-0,12	0,05-0,12	0,3-0,5	0,3-0,4
ε	0,99	0,93	0,91	0,99

Les échantillons sont des éprouvettes cylindriques de 16 cm de diamètre et 32 cm de hauteur, isolées par une couche de 5 cm de mousse polyuréthane expansée. Leur composition est illustrée à la Figure 1.

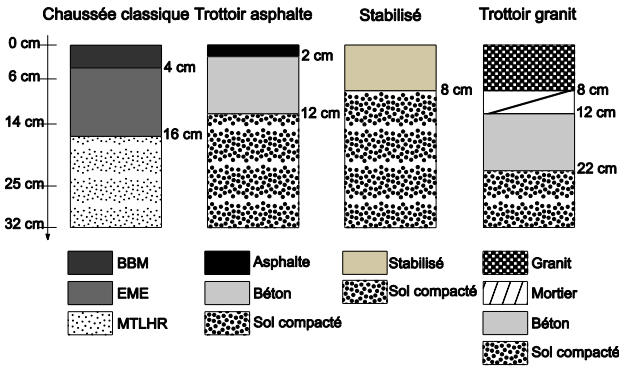

Figure 1 : Structure des échantillons étudiés

2.2. Protocole expérimental

Chaque structure est placée dans une enceinte climatique et soumise à une sollicitation cyclique d'une période de 24 heures sur trois journées consécutives. Chaque journée est découpée en une phase diurne d'une durée de 8 heures (9h-17h), et d'une phase nocturne d'une durée de 16 heures (17h-9h).

Pendant la phase jour, l'échantillon est ensoleillé par 7 ampoules halogènes dichroïques de température de couleur de 5 600 K, dans une atmosphère réglée à 35°C et 35% d'humidité relative. Pendant la nuit, la lampe est éteinte et l'air est à 25°C et 70% d'humidité relative.

Le Tableau 2 résume les caractéristiques de la sollicitation climatique que subissent les échantillons.

Tableau 2 : Caractéristiques du cycle climatique

	Jour	*Nuit*
Durée	8h	16h
Température de l'air	35°C	25°C
Humidité relative	35%	70%
Rayonnement CLO	1 320 W/m²	0
Rayonnement GLO	230 W/m²	430 W/m²

2.3. Bilan de surface

La Figure 2 est une modélisation des échanges thermiques à la surface des échantillons, adaptée de Kinouchi et Kanda [10].

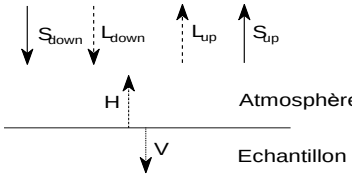

Figure 2 : Modélisation des échanges thermiques

S_{down} et L_{down} représentent respectivement les rayonnements CLO et GLO incidents, tandis que S_{up} et L_{up} sont les rayonnements CLO et GLO réfléchis et/ou émis. H représente la densité de flux convectif vers l'atmosphère, V la densité de flux conductif descendant. On notera R_n le rayonnement net.

Par définition de l'albédo et de l'émissivité, on a :

$$S_{up} = \alpha \cdot S_{down} \quad (1)$$

$$L_{up} = (1-\varepsilon)L_{down} + \varepsilon\sigma T_{surf}^4 \quad (2)$$

En conséquence, ainsi qu'en vertu de la conservation de l'énergie, on a :

$$R_n = H + V = (1-\alpha)S_{down} + \varepsilon L_{down} - \varepsilon\sigma T_{surf}^4 \quad (3)$$

2.4. Instrumentation

La surface des échantillons est équipée de deux capteurs de flux, l'un de flux global, peint en noir, et l'autre de flux radiatif. Le capteur de flux radiatif mesure le rayonnement net équivalent à celui d'un corps noir à la même température de surface que l'échantillon réel, ci-après désigné « équivalent corps noir ». Pour sa part, le capteur de flux global mesure la convection et le rayonnement net équivalent corps noir. Cela est résumé par les deux équations suivantes :

$$\Phi_g = R_n^{éq.c.n.} - H = V_{éq.c.n.} \quad (4)$$

$$\Phi_{rad} = R_n^{éq.c.n.} = S_{down} + L_{down} - \sigma T_{surf}^4 \quad (5)$$

Aux différentes profondeurs indiquées à gauche dans la Figure 1, les échantillons sont équipés de thermo-fluxmètres, sauf pour les couches de matériaux meubles (sol compacté ou MTLHR) qui sont équipées uniquement d'un thermocouple de type T. Les thermo-fluxmètres intègrent un thermocouple de type T.

En supposant que l'isolation latérale empêche toute déperdition de chaleur, en régime permanent, le flux traversant la couche n-1 et la couche n sont égaux :

$$V_n = \frac{\lambda_n}{e_n}\left(T_{n-1} - T_n\right) = V_{n-1} \quad (6)$$

Ainsi, la connaissance des températures aux interfaces n-1 et n permet d'estimer la conductivité apparente de la couche intercalaire à partir de la connaissance du flux à n-1 (amont) ou à n (aval).

3. RESULTATS

3.1. Flux conductif

La Figure 3 présente la densité de flux conductif mesuré à 6 cm de profondeur dans les 4 échantillons.

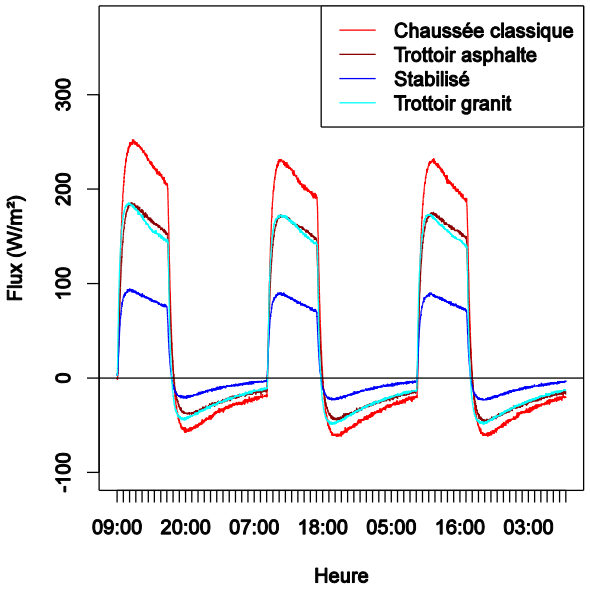

Figure 3 : Flux conductif mesuré à 6 cm de profondeur

La chaussée classique connaît la variation de flux la plus importante. Au maximum, celui-ci atteint 250 W/m² en début de phase diurne et -65 W/m² au minimum en début de phase nocturne. Pour leur part, les trottoirs asphalte et granit ont un comportement comparable, avec un flux conductif compris entre 185 W/m² et -50 W/m². Enfin, le stabilisé présente les variations de flux les plus faibles, entre 100 W/m² et -25 W/m².

C'est donc le stabilisé qui transmet le moins de chaleur à 6 cm de profondeur, alors que la chaussée classique en transmet le plus. Les structures de trottoir se situent à un niveau intermédiaire. La transmission de chaleur à cette profondeur dépend principalement des caractéristiques radiatives de la couche superficielle.

La Figure 4 présente le flux conductif mesuré à 14 cm de profondeur pour la chaussée et le trottoir granit, les seuls à être équipés d'un deuxième fluxmètre.

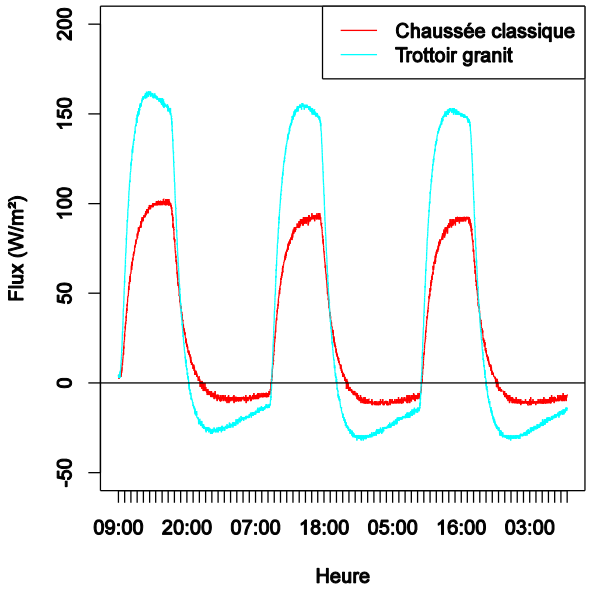

Figure 4 : Flux conductif à 14 cm de profondeur

Le flux à cette profondeur est moins intense, oscillant entre -30 et 160 W/m² pour le trottoir granit et -10 et 100 W/m² pour la chaussée classique. Le trottoir granit transmet le plus de chaleur à 14 cm de profondeur, avec une amplitude environ 50% plus importante que la chaussée classique.

Les mesures à 6 cm de profondeur peuvent être comparées à celles de Hendel et al. réalisées à Paris pendant l'été 2013 [11]. Pour une structure de chaussée similaire, située dans une rue Nord-Sud et pour un ensoleillement moins intense et d'une durée de 5h environ, un flux compris entre 215 W/m² et -75 W/m² est observé à 5 cm de profondeur.

L'expérimentation menée en laboratoire ne permet pas de faire varier la température de façon progressive. Il n'est donc pas étonnant que l'évolution du flux observé sur le terrain en période ombragée (matin puis soir) ne soit pas reproduite. Par ailleurs, en tenant compte de la différence de profondeur entre les essais in situ de Hendel et al. et celle décrite ici, il apparaît que les flux obtenus en laboratoire sont surestimés de quelques dizaines de W/m² par rapport aux observations de terrain. Pour autant, l'allure générale des observations de terrain est reproduite de façon satisfaisante par le protocole utilisé ici.

3.2. Estimation de l'albédo des échantillons

Une fois que la couche superficielle de 6 cm de profondeur a atteint le régime permanent, la différence entre le flux global mesuré en surface et le flux à 6 cm correspond à la part réfléchie du rayonnement incident.

En effet, en vertu de l'équation (4), on a :

$$\Phi_g - V_{6cm} = R_n^{éq.c.n.} - H - V_{6cm} \quad (7)$$

Or, (6) nous donne :

$$V_{6cm} = V_{0cm} = R_n - H \quad (8)$$

D'où :

$$\Phi_g - V_{6cm} = R_n^{éq.c.n.} - R_n \quad (9)$$

En remplaçant grâce aux équations (3) et (5) :

$$\Phi_g - V_{6cm} = \alpha S_{down} + (1-\varepsilon)(L_{down} - \sigma T_{surf}^4) \quad (10)$$

On obtient alors :

$$\alpha = \frac{\Phi_g - V_{6cm} + (1-\varepsilon)(\sigma T_{surf}^4 - L_{down})}{S_{down}} \quad (11)$$

L'équation (11) est appliquée aux données mesurées pendant les deux dernières heures de chacune des trois phases diurnes, qui correspondent au régime permanent de la couche superficielle. Les valeurs moyennes ainsi obtenues sont reportées au Tableau 3 et sont en bon accord avec celle du Tableau 1, tirées de la littérature. Cette méthode donne donc des résultats satisfaisants pour la détermination de l'albédo des échantillons.

Tableau 3 : Albédo des revêtements étudiés

Chaussée classique	*Trottoir asphalte*	*Stabilisé*	*Trottoir granit*
0,098	0,155	0,369	0,313

La chaussée et le trottoir asphalte absorbent donc le plus le rayonnement CLO, tandis que le trottoir granit et le stabilisé sont les plus réfléchissants. On considère que les matériaux des couches de surface sont des corps gris.

3.3. Détermination du rayonnement net

Ayant déterminé l'albédo des échantillons et connaissant leur émissivité ainsi que le flux incident, on peut déduire R_n et V_{0cm}. Ce dernier est présenté Figure 5.

Globalement, V_{0cm} est assez similaire d'un échantillon à un autre. Il est compris entre -382 W/m² et 511 W/m². Ces extrema de flux sont similaires à ceux rapportés par Kinouchi et Kanda lors d'un essai mené au Japon sur une chaussée imperméable [10].

Pour autant, les observations du flux conductif à 6 cm ne peuvent s'expliquer entièrement par les propriétés radiatives, comme en témoigne le faible écart observé Figure 5 entre le stabilisé et le trottoir granit. On s'intéresse donc à la conductivité des matériaux.

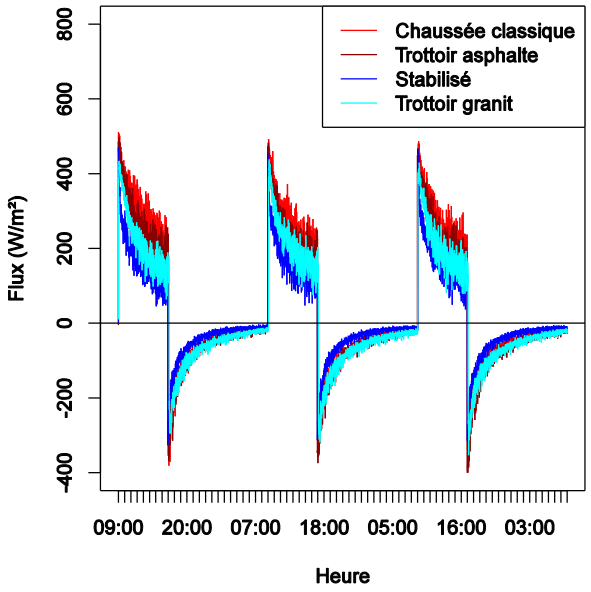

Figure 5 : Flux conductif V_0

3.4. Conductivité apparente des premières couches

On s'intéresse à présent aux conductivités obtenues en appliquant directement l'équation (6). Cette équation n'est valable qu'en régime permanent, c'est-à-dire en fin de période diurne ou de période nocturne. Graphiquement, cela correspond à un palier.

La Figure 6 illustre l'évolution de la conductivité calculée pour la première couche de 6 cm d'épaisseur.

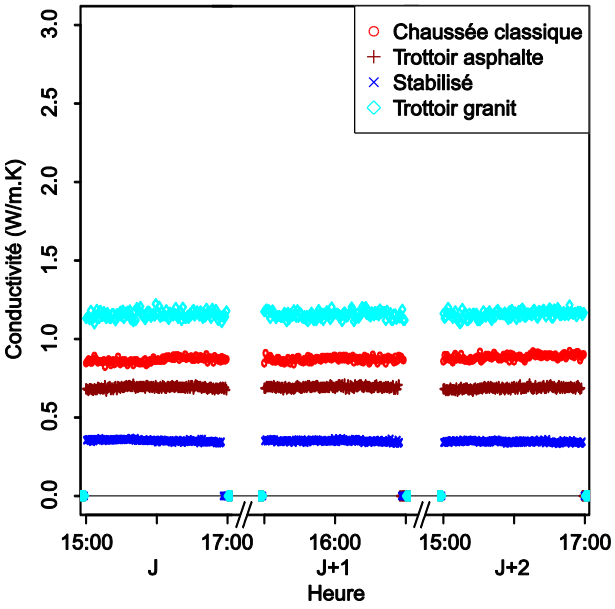

Figure 6 : Cond. app. entre 0 et 6 cm (aval)

Parce que la résolution des mesures de température est faible, les paliers obtenus en phase nocturne, lorsque

les écarts de température sont réduits, ne sont pas exploitables. On relève donc les valeurs moyennes des paliers atteints pendant la dernière heure de la phase diurne, résumées au Tableau 4. Les conductivités de la couche située entre 14 et 25 cm ne sont pas estimées car cette couche n'atteint pas le régime permanent.

Tableau 4 : Conductivités apparentes (en W/m.K)

Couche	*Chaussée classique*	*Trottoir asphalte*	*Stabilisé*	*Trottoir granit*
0-6 cm	0,89	0,69	0,35	1,16
6-14 cm	0,97-2,03	1,52	0,64	1,49-1,56

La Figure 7 et la Figure 8 présentent ces mêmes conductivités pour la couche suivante, située entre 6 et 14 cm, par la méthode aval et amont respectivement, calculées de la même façon. Faute de fluxmètre à 14 cm de profondeur pour le trottoir asphalte et le stabilisé, seule la méthode amont peut être appliquée.

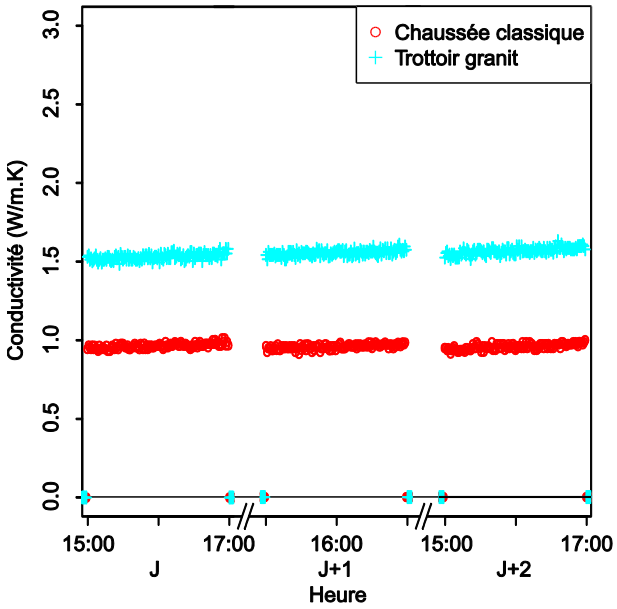

Figure 7 : Cond. app. entre 6 et 14 cm (aval)

On remarque tout d'abord que les paliers calculés par la méthode aval pour la couche 6-14cm ne sont pas parfaitement horizontaux. Toutefois, en croisant ces résultats avec les conductivités obtenues par la méthode amont, on peut se rendre comptes des écarts trop importants et rejeter les valeurs discordantes.

Les valeurs estimées pour la couche 6-14 cm par la méthode aval et amont sont en bon accord pour le trottoir granit, mais pas pour la chaussée. En effet, les valeurs obtenues vont du simple au double. On en déduit que l'hypothèse de régime permanent n'est pas vérifiée à cette profondeur pour cette structure.

Pour la couche superficielle, les valeurs sont en bon accord avec les valeurs trouvées dans la bibliographie [12]. La chaussée classique, composée de 6 cm d'enrobé, a bien une conductivité comparable à celle d'un enrobé bitumineux. Le trottoir asphalte, composé de 2 cm d'asphalte et 4 cm de béton, a une conductivité correspondant à un asphalte ou à un béton moyen. Le stabilisé, composé de 6 cm de stabilisé, a la conductivité la plus faible, similaire à un sable ou un ciment. Enfin, le trottoir granit, composé de 6 cm de granit, a la conductivité la plus élevée, mais celle-ci est faible vis-à-vis des 3,5 W/m.K attendus [12].

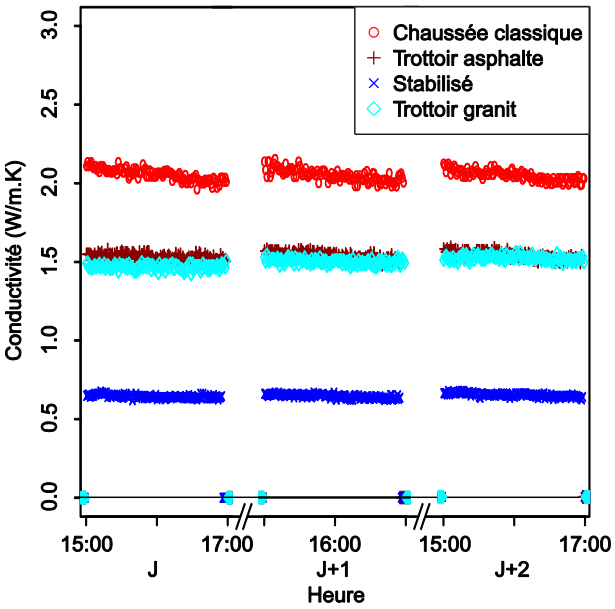

Figure 8 : Cond. app. entre 6 et 14 cm (amont)

Pour la couche située entre 6 et 14 cm de profondeur, les conductivités qui ont pu être obtenues sont en bon accord avec la bibliographie également. En effet, cette couche est principalement composée de béton pour le trottoir asphalte, d'une conductivité de l'ordre de 1,4-1,8 W/m.K [12]. Pour sa part, le stabilisé est principalement composé de sol compacté, d'une conductivité attendue de l'ordre de 0,5 W/m.K. Enfin, le trottoir granit est principalement composé de mortier, d'une conductivité attendue de 1,7 W/m.K.

Les conductivités obtenues expérimentalement sont donc cohérentes avec les valeurs issues de la littérature.

3.5. Coefficient d'absorption-transmission

On propose d'étudier la corrélation entre l'amplitude de la densité de flux conductif mesurée aux différentes profondeurs à un coefficient d'absorption-transmission du rayonnement incident, calculé à partir des propriétés thermo-radiatives des échantillons.

On définit ce coefficient d'absorption-transmission par l'équation (12), qui dépend de la profondeur z :

$$k(z) = a \cdot \frac{e_0 / \lambda_0}{\sum_k e_k(z) / \lambda_k} \qquad (12)$$

La conductance de référence e_0/λ_0 est égale à 1 W/m².K et permet d'homogénéiser l'équation. Pour z=0, *k* est égal à l'absorptivité du revêtement. Ce coefficient traduit à la fois l'absorption du rayonnement incident en surface et la propension des couches sous-jacentes à transmettre la chaleur ainsi absorbée.

La Figure 9 illustre le ratio entre l'amplitude du flux transmis (V_{max} - V_{min}) à 6 et 14 cm et le rayonnement incident pour chaque échantillon en fonction de *k*.

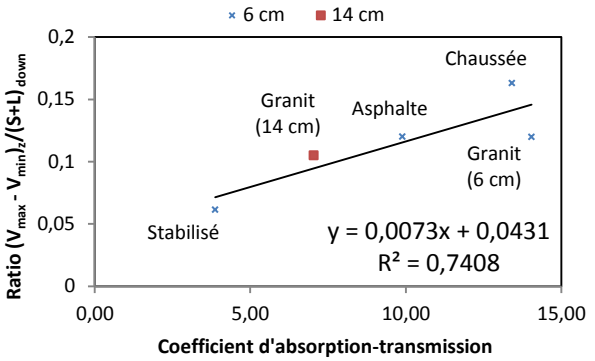

Figure 9 : Ratio entre l'amplitude du flux transmis sur le rayonnement total incident à la profondeur z en fonction du coefficient k

La droite d'interpolation linéaire des données est également illustrée, ainsi que son équation et son coefficient de détermination.

Les flux observés à 6 et 14 cm, rapportés au rayonnement incident, semblent donc proportionnels au coefficient *k* que nous avons défini à l'équation (12). Ainsi pour un même rayonnement incident, le flux transmis en profondeur sera d'autant plus important que les couches superficielles seront plus conductives et que la surface sera plus absorbante. C'est ainsi que le granit, plutôt réfléchissant mais très conducteur, transmet autant de chaleur à 6 cm que le trottoir asphalte ou plus de chaleur à 14 cm de profondeur que la chaussée.

Ce coefficient d'absorption-transmission peut servir de critère pour sélectionner des structures qui transmettent peu le rayonnement solaire en profondeur.

4. CONCLUSION

Un protocole expérimental permettant l'étude de revêtements de voirie a été mis au point. Celui-ci permet de reproduire le flux conductif et la température à différentes profondeurs de manière satisfaisante vis-à-vis d'observations réalisées sur le terrain.

D'une part, l'analyse des données permet de caractériser les matériaux constitutifs des revêtements étudiés. La conductivité et l'albédo ont notamment pu être déterminés de manière satisfaisante. Fort de ces conclusions, le protocole pourra être utilisé pour analyser l'effet de l'arrosage de ces revêtements [11].

D'autre part, un coefficient *k* d'absorption-transmission a été défini et est corrélé à l'amplitude du flux conductif observée au sein des revêtements à différentes profondeurs et rapporté au rayonnement incident. Ce coefficient pourrait servir de critère de sélection des matériaux constitutifs des revêtements de l'espace public afin de limiter leur stockage de chaleur et ainsi influer sur leur impact micro-climatique, notamment la formation des îlots de chaleur urbains.

D'autres essais permettront de déterminer l'importance de ce critère et de préciser les limites du protocole expérimental proposé.

REMERCIEMENTS

Cette étude a été financée par l'Atelier Parisien d'Urbanisme (APUR). Les auteurs souhaitent également remercier le Laboratoire d'Essai des Matériaux de la Ville de Paris (LEM VP) qui a gracieusement mis à disposition ses locaux, son expertise et son matériel.

RÉFÉRENCES

[1] E. Erell, D. Pearlmutter, D. Boneh, and P. B. Kutiel, "Effect of high-albedo materials on pedestrian heat stress in urban street canyons," Urban Clim., Oct. 2013.
[2] M. Santamouris, "Appropriate materials for the urban environment," in Energy and Climate in the Urban Built Environment, M. Santamouris, Ed. 2001.
[3] A. H. Rosenfeld, H. Akbari, J. J. R. Tv, and M. Pomerantz, "Cool communities: strategies for heat island mitigation and smog reduction '," Energy Build., vol. 28, pp. 51–62, 1998.
[4] M. Hendel, M. Colombert, Y. Diab, and L. Royon, "Improving a pavement-watering method on the basis of pavement surface temperature measurements," Urban Clim., vol. 10, no. December, pp. 189–200, Dec. 2014.
[5] J.-M. Robine, S. L. K. Cheung, S. Le Roy, H. Van Oyen, C. Griffiths, J.-P. Michel, and F. R. Herrmann, "Death toll exceeded 70,000 in Europe during the summer of 2003.," C. R. Biol., vol. 331, no. 2, pp. 171–178, Feb. 2008.
[6] T. Asaeda, V. T. Ca, and A. Wake, "Heat storage of pavement and its effect on the lower atmosphere," Atmos. Environ., vol. 30, no. 3, pp. 413–427, Feb. 1996.
[7] H. Takebayashi and M. Moriyama, "Study on Surface Heat Budget of Various Pavements for Urban Heat Island Mitigation," Adv. Mater. Sci. Eng., vol. 2012, pp. 1–11, 2012.
[8] T. Ueno and K. Tamaoki, "Thermal Characteristics of Urban Land Cover by Indoor Lamp-Irradiation Experiment," in The Seventh International Conference on Urban Climate, 2009, no. July, pp. 1–4.
[9] NASA, "Heat Island," 1999. [Online]. Available: http://www.ghcc.msfc.nasa.gov/urban/urban_heat_island.html. [Accessed: 06-Feb-2015].
[10] T. Kinouchi and M. Kanda, "Cooling Effect of Watering on Paved Road and Retention in Porous Pavement," in Second Symposium on Urban Environment, 1998, pp. 255–258.
[11] M. Hendel, M. Colombert, Y. Diab, and L. Royon, "An analysis of pavement heat flux to optimize the water efficiency of a pavement-watering method," Appl. Therm. Eng., vol. 78, pp. 658–669, 2015.
[12] M. Laurent and P. Vuillermoz, "Conductivité thermique des solides," Tech. l'Ingénieur, p. 32, 1993.

APPENDIX C

9th International Conference on Urban Climate jointly with 12th Symposium on the Urban Environment

Characterization of the thermal behavior of Parisian street materials

Charactérisation du comportement thermique de revêtements urbains parisiens

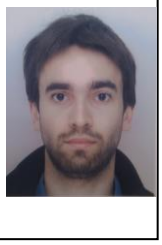

Characterization of the behavior of Parisian street materials

Martin HENDEL[1,2,3]*, Arnaud GRADOS[2], Morgane COLOMBERT[3],
Youssef DIAB[3], Laurent ROYON[2]
1 Paris City Hall, Water and Sanitation Department, F-75014, Paris, France
2 Univ Paris Diderot, Paris Sorbonne Cité, MSC, UMR 7057, CNRS, F-75013, Paris, France
3 Université Paris-Est, Lab'Urba, EA 3482, EIVP, F-75019, Paris, France
**(corresponding author: martin.hendel@paris.fr)*

1. Introduction

Materials used in urban environments have strong impacts on urban climates and consequently on pedestrian thermal comfort. Depending on their thermal properties, they contribute more or less to the urban heat island (UHI) effect (Asaeda, Ca, & Wake, 1996; Santamouris, 2013). Several UHI countermeasures involving cool materials, urban greening or urban watering have been studied (Akbari, Pomerantz, & Taha, 2001; Bowler, Buyung-Ali, Knight, & Pullin, 2010).

Previous work by the authors has focused on the field study of pavement-watering as a climate change adaptation measure for Paris against increasing and intensifying heat waves (Hendel, Colombert, Diab, & Royon, 2014, 2015a, 2015b). Testing over the summers of 2013 and 2014 has shown that the method reduces surface temperatures an average 13°C during pavement insolation in a N-S street paved with asphalt concrete. Air temperature reductions of up to 0.8°C as well as 2.4°C mean radiant and 1°C UTCI equivalent temperature reductions were found, while relative humidity was increased by 4%RH at most. Finally, the optimal watering rate was determined to be 0.16-0.21 mm/h during shading and 0.31-0.41 mm/h during pavement insolation.

These analyses also underlined the important role played by the materials being watered. Indeed, while a given watering frequency may be valid for asphalt road surfaces, they are unlikely to be valid for other materials with different water-holding capacities, albedo or other relevant properties. Given the wide variety of materials used in cities, it is important for decision-makers to be able to account for this when designing a city-wide pavement-watering strategy. Field trials however are expensive and impractical for this purpose.

This paper proposes a lab experiment that may be used to characterize the behavior of street materials with or without watering in heat-wave conditions. As a first step, this paper will focus on temperature observations made without watering for five pavement structures commonly used in Paris, France: asphalt concrete road surfaces, stabilized sand, asphalt and modular granite sidewalks and grass. Temperatures measured 6 cm, 14 cm, 25 cm and 32 cm deep will be discussed in particular. Previous work by the authors describes surface temperature and heat flux observations (Hendel, Grados, Colombert, Diab, & Royon, 2015a, 2015b).

2. Materials and methods

Five different street structures were compared, consisting of standard asphalt road and sidewalk structures as well as samples of cement-stabilized sand, granite-paver sidewalk and lawn structures. Each cylindrical sample is 32 cm tall and 16 cm in diameter. Fig. 1 describes the composition of the street structures constructed in the lab. Each sample was equipped with thermocouples and or flowmeters 0 cm, 6 cm, 14 cm and 25 cm deep. In addition, a thermocouple was positioned on the underside of the samples, 32 cm below the sample surface. The surface albedo was determined experimentally in previous work with the exception of the grass sample (Hendel, Grados, et al., 2015a). These albedo values are summarized in Table 1.

Once insulated with a polyurethane foam casing, each sample was submitted to identical a 24-hour climate cycle three days in a row. Air temperature and relative humidity were controlled by a climate chamber and insolation with a seven-bulb dichroic halogen lamp with a color temperature of 5,600 K. The characteristics of the climate cycles are described in Table 2, while Fig. 2 presents a diagram and photograph of the experimental setup.

Prior to the beginning of the three-day trials, each sample was stabilized for at least 24 hours in the climate chamber under nighttime conditions. In addition, the grass sample was sufficiently watered before the trials to ensure that evapotranspiration would not be interrupted over the course of the three day trial.

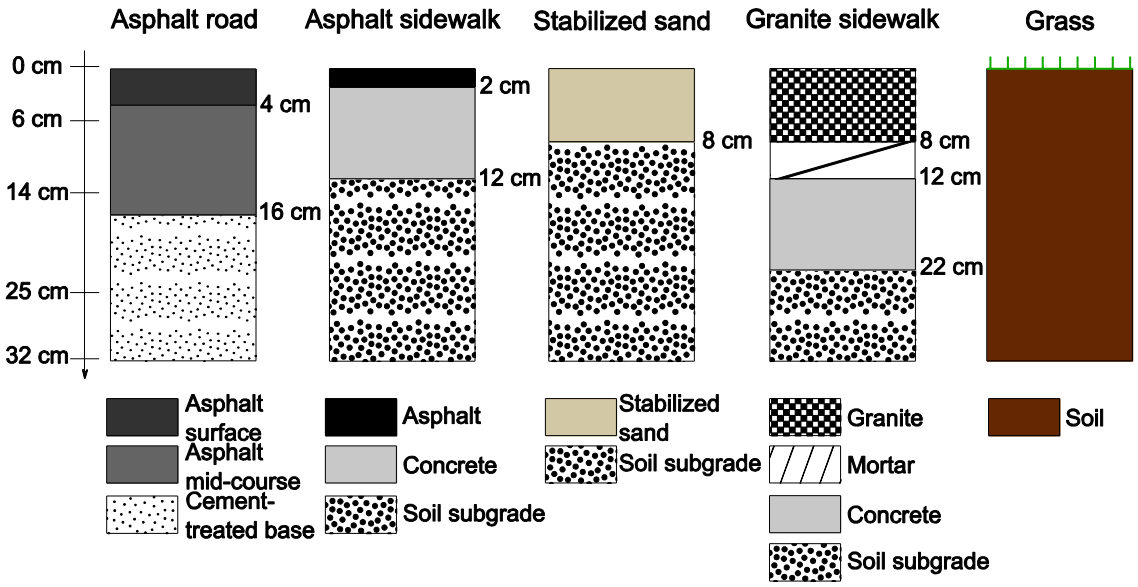

Fig. 1: Studied structure samples

Table 1: Albedo of the samples determined experimentally, except for the grass sample.

Asphalt road	*Asphalt sidewalk*	*Stabilized sand*	*Granite sidewalk*	*Grass*
0,098	0,155	0,369	0,313	0,25-0,30

Table 2: Daytime and nighttime conditions

	Day	*Night*
Duration	8h	16h
Air temperature	35°C	25°C
Relative Humidity	35%	70%
SW Radiation	1 320 W/m²	0
LW Radiation	230 W/m²	440 W/m²

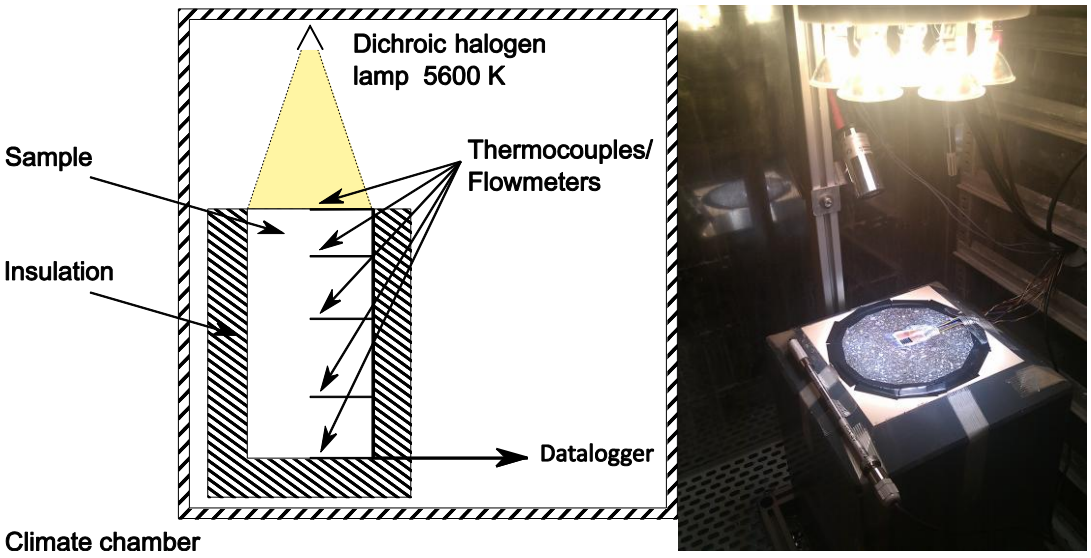

Fig. 2: Diagram (left) and photograph (right) of experimental setup.

3. Results and discussion

We begin by describing the temperature observations at the studied depths.

3.1. Results

Fig. 3 illustrates temperature measured 6 cm deep inside each sample. As can be seen, temperatures range from 23.3° to 50°C over the course of the three days, except for the grass sample whose initial temperature is 22.3°C. This is likely due to the additional latent cooling that the sample benefits from as a result of

evapotranspiration.

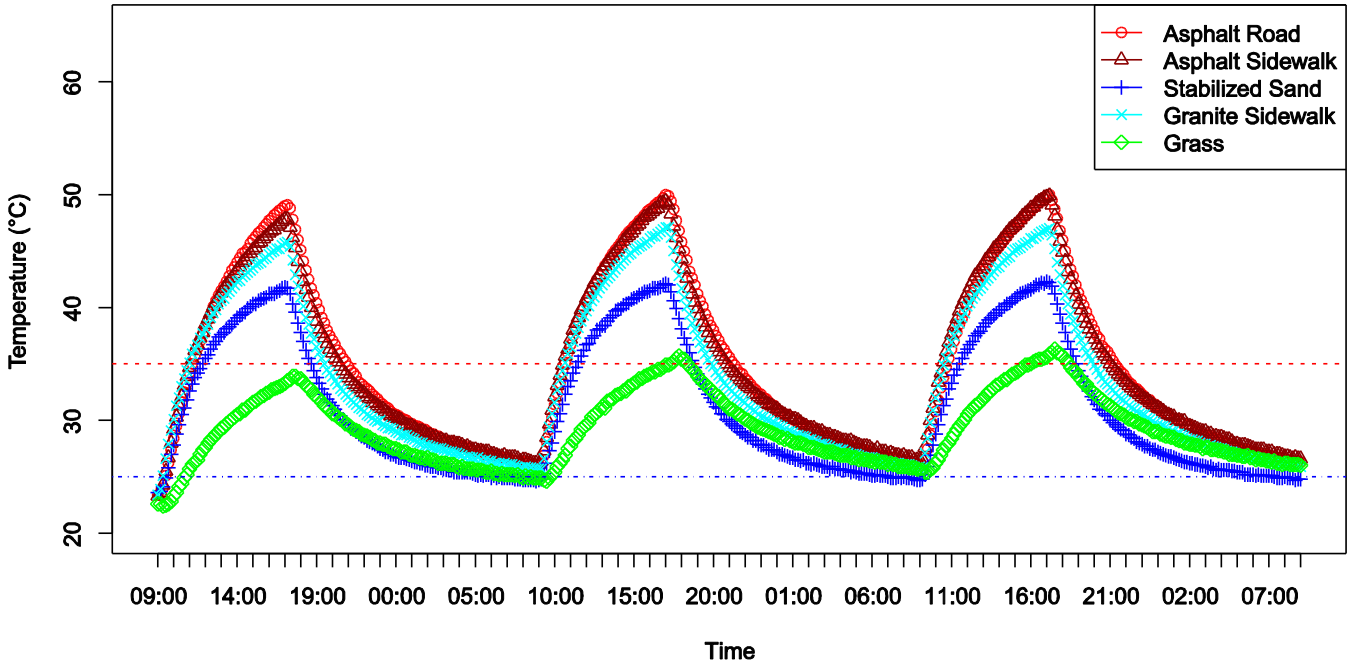

Fig. 3: Temperature measured 6 cm deep over 72 hours. The dotted red and blue lines respectively indicate the day and night setpoint temperatures inside the climate chamber.

The asphalt road and sidewalk structures are the warmest over the trial period, closely followed by the granite sidewalk structure, while the stabilized sand and grass samples are significantly cooler. The stabilized sand is warmer than the grass sample during the day, but at night it becomes cooler after the first two hours. After 24 hours, temperatures remain a few degrees warmer than the initial state.

Additionnally, inertial effects are manifested by the gradual increase in temperatures over the course of the three-day trial. While, the daily maximum temperature of the asphalt road and the stabilized sand samples increases by less than 1°C, it increases by 1.3°C for the granite sidewalk sample and by 2.2°C for the asphalt sidewalk and grass samples.

Fig. 4 illustrates temperatures measured 14 cm deep, which range from 23°C (22.3°C for the grass sample) to 42.9°C.

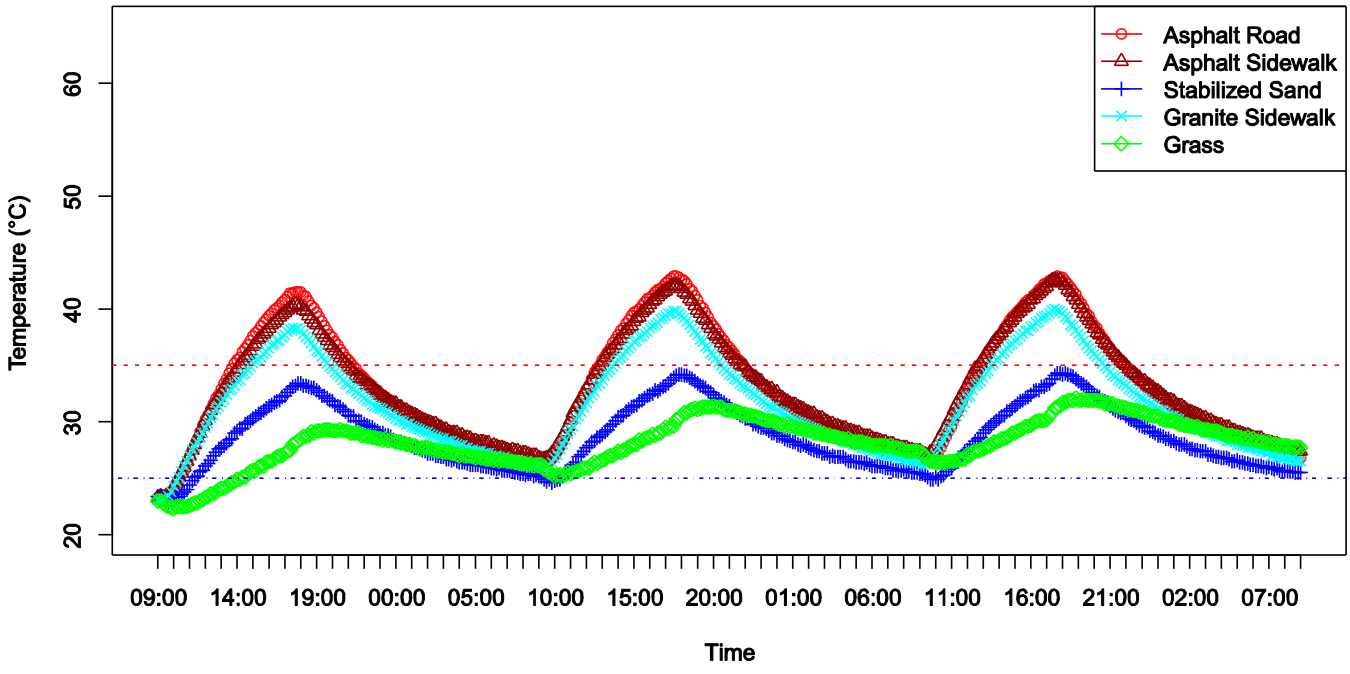

Fig. 4: Temperature measured 14 cm deep. The dotted red and blue lines respectively indicate the day and night setpoint temperatures inside the climate chamber

As was the case for temperatures measured 6 cm deep, the asphalt road and sidewalk samples are the

warmest, closely followed by the granite sidewalk structure, with the stabilized sand and grass samples being the coolest. Once more, the stabilized sand sample is warmer than the grass during the day, but becomes cooler six hours into the night phase. Compared to the temperature shifts observed 6 cm deep, those 14 cm deep occur approximately one hour later. The thermal inertia of the samples is visible at this depth as well, the grass sample exhibiting a nearly 3°C increase in daily maximum temperature over the course of the trial, followed by the asphalt and granite sidewalk structures with approximately 2°C.

Fig. 5 illustrates temperature measurements 25 cm deep.

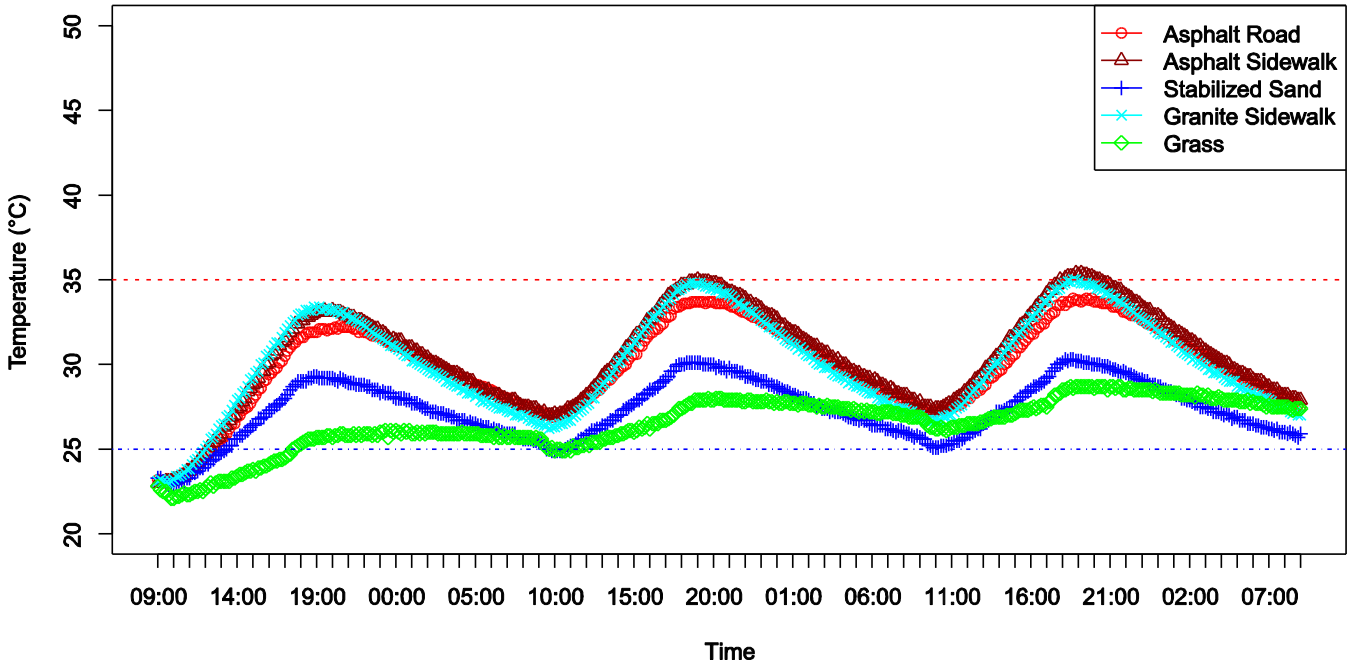

Fig. 5: Temperature measured 25 cm deep. The dotted red and blue lines respectively indicate the day and night setpoint temperatures inside the climate chamber.

Temperatures 25 cm deep range from 23° (22.1° for grass) to 35.4°C and no additional lag is visible compared to the 14 cm observations. For the first time, the granite sidewalk is warmer or nearly as warm as the asphalt road and sidewalk structures. All samples exhibit visible inertial effects, greatest for the asphalte sidewalk and grass structures (+2.2°C and +2.7°C daily maximum temperature increase resp.).

Fig. 6 illustrates temperatures measured 32 cm deep.

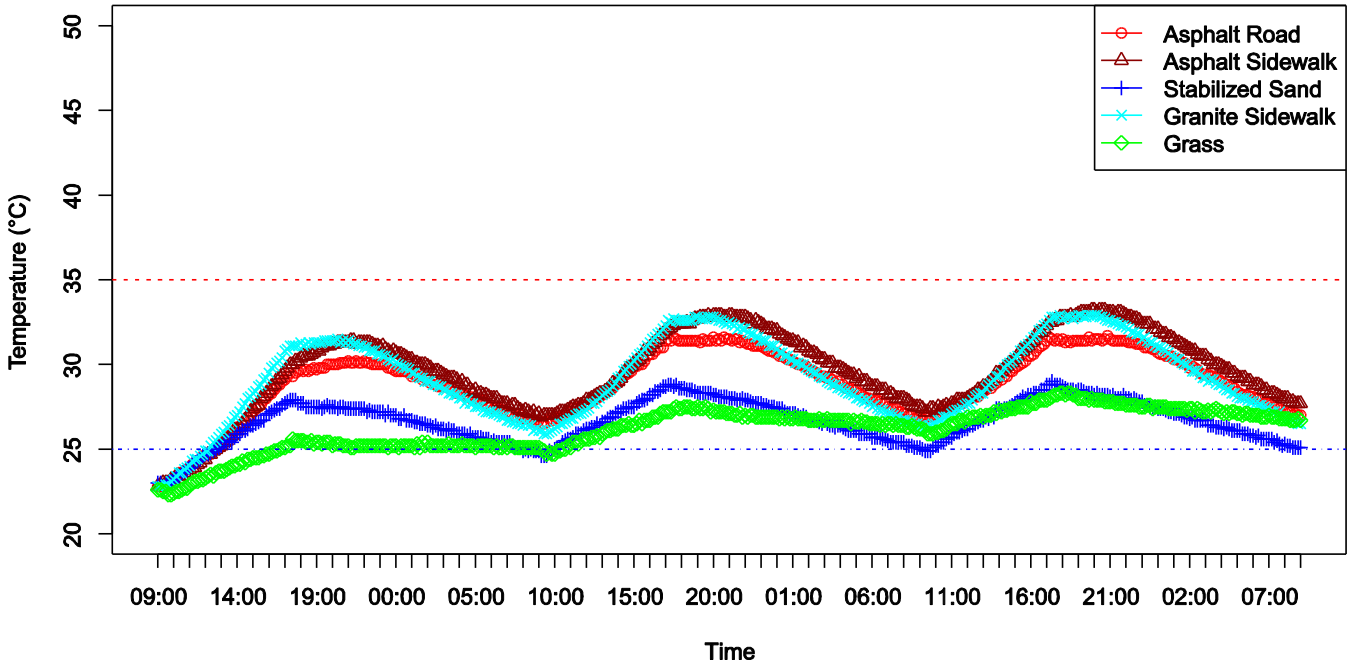

Fig. 6: Temperature measured 32 cm deep. The dotted red and blue lines respectively indicate the day and night setpoint temperatures inside the climate chamber.

Unlike at other depths, temperature spikes are visible. These coincide with the beginning of the night phase and are due to a faulty seal which allowed an air leak inside the insulating casing. This seal has since been corrected. At this depth, the grass sample is the coolest structure on the first day, but is warmer on average than the stabilized sand structure on the last day. Otherwise, temperature trends are similar to those 25 cm deep. Once again, intertial trends are clearly visible and greatest for the grass and asphalt sidewalk structures (+2;7°C and +3°C, resp.).

3.2. Discussion

While temperature observations 6 cm deep may not be identical, they agree well with field observations 5 cm deep made in a similar asphalt road in Paris, France over the summer of 2013 (Hendel & Royon, 2015). Differences between observations can be explained by the climate signal created in the la, which has longer and stronger insolation. Despite this, the overall trend obtained is deemed satisfactory.

Generally-speaking, these temperature observations agree well with the behavior expected of each sample given their surface albedo, with the notable exception of the granite sidewalk structure. Indeed, temperatures similar to those of the stabilized sand would be expected for this structure given its similar albedo. As previous work has revealed (Hendel, Grados, et al., 2015a), this is linked to the granite's high thermal conductivity. Heat is not only reflected away, it is also transmitted into the deeper layers of the structure, thus explaining the higher-than-expected temperatures 6 cm deep.

Overall, the data set provides a global view of how these structures react to a given climate signal. Indeed, the grass and stabilized sand structures are clearly the coolest, while the road and sidewalk structures have similar behavior at the considered depths.

In addition, inertial phenomena are clearly visible in varying intensity at the different depths considered. Table 3 summarizes the average increase in daily maximum temperature for each structure between the first and third day. By this metric, the grass and asphalt sidewalk structures have the highest inertia among the considered structures, while the stabilized sand has the lowest.

Table 3: Average daily maximum temperature increase from D to D+2.

Asphalt road	*Asphalt sidewalk*	*Stabilized sand*	*Granite sidewalk*	*Grass*
+1.3°C	+2.4°C	+0.88°C	+1.5°C	+2.6°C

While cooler material temperatures will have positive consequences such as lower atmospheric heating in cities, higher inertia will slow temperature increases when a heat spike arises. Ideally, urban materials should therefore combine both properties via high albedo for example. The urban materials used in Paris that have been considered here present either one property or the other, except for the grass structure.

4. Conclusion

A lab experiment was used to characterize the relative behavior of five Parisian street structures. 32 cm tall cylindrical samples were constructed and instrumented in the lab. Temperature measured 6 cm, 14 cm, 25 cm and 32 cm deep was used for this purpose. It was found that the stabilized sand and grass structures were the coolest, while the road and sidewalk structures were significantly warmer. Via these observations, it was found that the underlying layers of the asphalt sidewalk and grass structures have the highest inertia.

While low temperatures will result in lower atmospheric cooling in cities, high thermal inertia helps slow temperature rises in the case of heat spikes. Among the five structures considered, only the grass structure combines low temperatures with high thermal inertia. The second best option is either the stabilized sand structure which presents the second lowest temperatures, or the asphalt sidewalk which has the second highest temperature increase.

Further research efforts are needed to determine the full extent of the benefits of increasing the inertia of existing urban materials for pavements, but this may be achievable by including thicker layers of concrete or even phase change materials as has been studied previously for roofing materials (Santamouris, Synnefa, & Karlessi, 2011).

In the coming months, another set of tests will focus on the effects of pavement-watering of the considered samples in order to clarify the technique's effectiveness on other structures than asphalt roads.

Acknowledgments

The authors acknowledge the support of the Roads and Traffic and the Waste and Water Divisions of the City of Paris for their expertise and material support. Funding for this experiment was provided by APUR (Parisian urban planning agency).

References

Akbari, H., Pomerantz, M., & Taha, H. (2001). Cool surfaces and shade trees to reduce energy use and improve air quality in urban areas. *Solar Energy*, *70*(3), 295–310. doi:10.1016/S0038-092X(00)00089-X

Asaeda, T., Ca, V. T., & Wake, A. (1996). Heat storage of pavement and its effect on the lower atmosphere. *Atmospheric Environment*, *30*(3), 413–427. doi:10.1016/1352-2310(94)00140-5

Bowler, D. E., Buyung-Ali, L., Knight, T. M., & Pullin, A. S. (2010). Urban greening to cool towns and cities: A systematic review of the empirical evidence. *Landscape and Urban Planning*, *97*(3), 147–155. doi:10.1016/j.landurbplan.2010.05.006

Hendel, M., Colombert, M., Diab, Y., & Royon, L. (2014). Improving a pavement-watering method on the basis of pavement surface temperature measurements. *Urban Climate*, *10*(December), 189–200. doi:10.1016/j.uclim.2014.11.002

Hendel, M., Colombert, M., Diab, Y., & Royon, L. (2015a). An analysis of pavement heat flux to optimize the water efficiency of a pavement-watering method. *Applied Thermal Engineering*, *78*, 658–669. doi:10.1016/j.applthermaleng.2014.11.060

Hendel, M., Colombert, M., Diab, Y., & Royon, L. (2015b). Measurement of the Cooling Efficiency of Pavement-Watering as an Urban Heat Island Mitigation Technique. *Journal of Sustainable Development of Energy, Water and Environment Systems*, *3*(1), 1–11. doi:10.13044/j.sdewes.2015.03.0001

Hendel, M., Grados, A., Colombert, M., Diab, Y., & Royon, L. (2015a). Comparaison des matériaux de l'espace public parisien : caractérisation de la contribution aux îlots de chaleur urbains. In *CIFQ* (p. (Under Review, In French)). 8-10 Juin 2015, Sherbrooke, QC, Canada.

Hendel, M., Grados, A., Colombert, M., Diab, Y., & Royon, L. (2015b). Quel est le meilleur revêtement pour limiter la formation des îlots de chaleur urbains ? In *Congrès Français de Thermique 2015 : La Thermique de l'Habitat et de la Ville* (p. (under review) (in French)). 26-29 mai 2015, La Rochelle, France.

Hendel, M., & Royon, L. (2015). The effect of pavement-watering on subsurface pavement temperatures. *Urban Climate*, (submitted).

Santamouris, M. (2013). Using cool pavements as a mitigation strategy to fight urban heat island—A review of the actual developments. *Renewable and Sustainable Energy Reviews*, *26*, 224–240. doi:10.1016/j.rser.2013.05.047

Santamouris, M., Synnefa, A., & Karlessi, T. (2011). Using advanced cool materials in the urban built environment to mitigate heat islands and improve thermal comfort conditions. *Solar Energy*, *85*(12), 3085–3102. doi:10.1016/j.solener.2010.12.023

Résumé détaillé en français

Introduction

Le désert du Thar au Rajasthan est une des régions les plus chaudes et arides du sous-continent indien sur laquelle ont longtemps régné les maharajahs. Pour autant, ils n'épargnaient aucun moyen pour le rafraîchissement au pic de l'été, en faisant couler de l'eau parfumée sur les murs de leur palais par exemple. Plusieurs autres régions du globe ont développé des méthodes similaires. Au Japon, l'arrosage du sol pour rafraîchir les étés chauds et humides est appelé "Uchimizu" et est une tradition vieille de plusieurs siècles qui se pratique encore de nos jours.

Le fort courant hygiéniste à Paris du XIX^{e} siècle a mené au développement d'un double réseau d'adduction d'eau. Initialement conçu pour fournir l'eau potable de la capitale, le réseau d'eau non potable est aujourd'hui principalement approvisionné par le canal de l'Ourcq, la Seine ne représentant que 20% des apports. Depuis, le nettoyage de l'espace public s'effectue à l'eau non potable. Jusqu'à la moitié du XX^{e} siècle, les rues pouvaient être arrosées jusqu'à cinq fois par jour pour limiter la formation de nuages de poussière. D'après les témoignages des ingénieurs de l'époque, de nombreux habitants croyaient que ces arrosages rafraîchissaient également la ville. Avec l'avènement du nettoyage mécanisé et la fin des nuages de poussière, ces pratiques furent progressivement abandonnées.

L'arrosage de l'espace public est perçu aujourd'hui comme un outil permettant d'améliorer le confort thermique dans les villes en cas de chaleur intense. Les recherches scientifiques ont débuté au Japon dans les années 1990 et s'appuient soit sur des infrastructures d'arrosage préexistantes, pour le déneigement des routes par exemple, ou bien sur des dispositifs d'arrosage expérimentaux, ou encore sur des simulations numériques. Plus récemment, les services municipaux de Paris et Lyon ont réalisé leurs propres essais d'arrosage à l'aide d'engins mécanisés ou de prototype d'infrastructure d'arrosage. En France, et particulièrement à Paris, l'augmentation prévue en intensité et en fréquence des canicules ainsi que la forte vulnérabilité des villes à ces épisodes ont mobilisé les parties prenantes pour trouver des solutions d'adaptation telles que la végétalisation, les matériaux réfléchissants ou l'arrosage urbain.

L'intérêt de la Ville de Paris pour l'arrosage urbain s'est concrétisé par le vote unanime de son Livre Bleu par le Conseil de Paris en 2012. Celui-ci définit les

priorités stratégiques pour le développement et l'amélioration du service de l'eau et d'assainissement de la ville. Notamment, après deux décennies de semi-abandon, le Livre Bleu reconnaît officiellement le potentiel offert par le réseau d'eau non potable pour un usage durable de l'eau en ville. Trois missions sont confiées aux services de la Ville pour permettre au réseau de répondre aux enjeux de demain. La première consiste à substituer l'eau non potable aux usages d'eau potable, pour l'arrosage des espaces verts par exemple. Afin de limiter l'impact des usages de l'eau non potable sur les milieux aquatiques, l'étude de la diversification de l'alimentation du réseau par d'autres sources est également demandée. Enfin, les services sont chargées d'étudier la place de l'eau non potable pour rafraîchir la ville par fortes chaleurs.

Le Service Technique de l'Eau et de l'Assainissement s'est ainsi penché sur l'étude des coûts et des bénéfices de la méthode, afin de quantifier la faisabilité d'une stratégie d'arrosage généralisée à toute la capitale.

Le présent manuscrit vise à apporter des éléments de réponse à cette question. Toutefois, les termes "coûts" et "bénéfices" sont plutôt vagues et peuvent porter sur plusieurs thèmes différents.

Afin de réduire le nombre de possibilités, nous analysons le lexique associé à l'arrosage urbain dans le Livre Bleu. Le Livre décrit plusieurs buts pour l'arrosage, à savoir : "favoriser la baisse des températures lors de fortes chaleurs", "lutter contre les îlots de chaleur", "[favoriser] la thermorégulation urbaine", "[utiliser] l'eau à des fins de rafraîchissement [...] pendant les épisodes de chaleur". Ainsi, il est clairement fait référence aux effets rafraîchissants de l'arrosage, avec un intérêt particulier pour ses effets sur la température de l'air et sur les îlots de chaleur urbains (ICU), notamment lors d'épisodes caniculaires. L'importance accordée aux pics de chaleur fait écho à l'impact de la canicule de 2003 sur la sensibilité du public à ce risque naturel en France. Cet aspect est donc à prendre en compte.

Le seul coût identifié par le Livre Bleu est "l'impact sur la Seine et le canal de l'Ourcq" de l'arrosage urbain. Ainsi, la consommation d'eau de la méthode devra être étudiée.

Aucun autre bénéfice ou coût ne sont identifiés dans le Livre Bleu, cependant cette liste est loin d'être exhaustive. D'autres impacts positifs concernent par exemple l'amélioration de la qualité de l'air et de la propreté des rues, un meilleur écoulement des égouts, ou encore les impacts psychologiques et sociaux de l'arrosage sur les passants. Les coûts économiques et environnementaux de l'arrosage n'ont pas non plus été abordés par le Livre Bleu, comme par exemple le coût financier de l'infrastructure d'arrosage ou encore les émissions de gaz à effet de serre ou la consommation d'énergie associées à l'arrosage urbain. Bien que ces aspects soient importants, nous nous limitons ici à l'étude des coûts et bénéfices identifiés par le Livre Bleu.

Notre problématique de recherche peut donc être résumée par la question suivante : quels sont les effets rafraîchissants, notamment sur la température de l'air et la lutte contre les îlots de chaleur urbains, qui peuvent être attendus de l'arrosage urbain par temps caniculaire en milieu urbain dense et en échange de

quelle consommation d'eau ?

Avant de chercher à répondre à cette question, nous effectuerons un état de l'art de l'arrosage urbain afin d'y trouver d'éventuels éléments de réponse qui existeraient déjà. Cet état de l'art est précédé d'un bref descriptif scientifique du climat urbain et de la lutte contre les ICU.

Climat urbain et lutte contre les îlots de chaleur

L'ICU se manifeste par un réchauffement local de l'air en ville par rapport à sa campagne environnante. Cet échauffement est de l'ordre de quelques degrés en moyenne et peut atteindre jusque 10°C par temps anti-cyclonique. Les ICU sont le résultat du piégeage radiatif, de la faible évapotranspiration, de l'obstruction du vent et des fortes concentrations d'activités humaines trouvés en milieu urbain. Ces phénomènes sont liés à la morphologie urbaine, aux propriétés des matériaux urbains, au déficit de sols perméables et d'espaces verts et à l'inefficacité énergétique des systèmes urbains.

Pour réduire son intensité, les mesures anti-ICU peuvent s'attaquer à un ou plusieurs de ces phénomènes. De nombreux travaux existent à ce jour sur la conception de matériaux urbains frais qui parviennent à limiter l'élévation de leur température de surface grâce à un albédo important. Pour sa part, la végétalisation urbaine vise à compenser la faible évapotranspiration des villes en créant de nouveaux espaces verts ou en ajoutant des végétaux à la surface des rues et bâtiments. Ces solutions ont de longues durées de vie et peuvent être considérées comme permanentes.

Sur le principe, l'arrosage urbain vise aussi à réduire les températures de surface en créant des flux latent et sensible non atmosphérique. Ces flux sont créés par l'évaporation d'un film d'eau et par son absorption de chaleur sensible. Si l'arrosage est suffisant pour créer du ruissellement, le flux sensible est un échange advectif de chaleur. Par ailleurs, le mouillage des matériaux réduit leur réflectivité courte longueur d'onde (CLO). Tandis que la surface du sol est rafraîchie, ses échanges convectifs, sa puissance rayonnée émise et son rayonnement réfléchi diminuent, résultant en une atmosphère rafraîchie et une radiosité réduite.

Nous nous tournons à présent vers l'état de l'art sur l'arrosage urbain afin de trouver des éléments de réponse à notre problématique déjà présents dans la littérature. Nous nous focaliserons sur les effets rafraîchissants de la méthode, en particulier sur la température de l'air et contre les ICU, par temps caniculaire et sur la consommation d'eau des méthodes d'arrosage utilisées.

Etat de l'art

Douze articles traitant des effets de l'arrosage urbain ont été identifiés. Ceux-ci décrivent des expérimentations ou des simulations numériques d'arrosage de surfaces de l'espace public à l'échelle du laboratoire, de la rue ou du quartier. Certains travaux sur les revêtements perméables ont été inclus lorsque des com-

paraisons de performance à l'état sec et humide ont été effectuées, y compris en l'absence d'arrosage contrôlé. Les analyses d'arrosage de façade d'immeuble ne sont pas incluses dans cet état de l'art.

La Table 1 résume le type d'étude menée (expérimentale ou numérique) et les indicateurs pris en compte par les différents auteurs. On y relève un grand nombre d'indicateurs de rafraîchissement, y compris climatique et thermique. Plusieurs techniques d'arrosage ont été mises en oeuvre, mais peu d'efforts pour les optimiser ne sont décrits. Enfin, seul (Bouvier et al., 2013) ne s'intéresse à l'arrosage par temps caniculaire. Les paramètres des techniques d'arrosage (horaires, durée, débit, ...) sont résumées à la Figure 1.

Globalement, les effets sur la température de surface pendant l'ensoleillement direct sont comparables et s'accordent bien d'une étude à une autre sur une réduction de l'ordre de -10°C. C'est également le cas de l'humidité relative à 1-2 m de hauteur qui est augmentée de quelques points de pourcentage.

Malheureusement, les autres effets microclimatiques décrits ne sont pas comparables en raison de différences importantes de hauteur de mesure, d'instruments et de méthode d'analyse. Cette limite avait déjà été identifiée par (Johansson et al., 2014) et pourrait en cacher d'autres liées aux spécificités de site ou de climat. Par ailleurs, le nombre réduit d'études quantifiant ces effets affaibli leur robustesse. D'autres travaux seraient nécessaires pour la renforcer davantage.

Ensuite, la méthode d'analyse utilisée pour estimer les effets microclimatiques ne paraît pas entièrement fiable. En effet, les analyses reposent sur la comparaison deux-à-deux des mesures d'une zone arrosée et d'une zone témoin. La méthode suppose donc tacitement que la différence inter-zone serait égale à zéro sans arrosage. Etant donnée la complexité des zones urbaines, cette hypothèse a peu de chance d'être valable dans les milieux urbains denses où l'arrosage est le plus susceptible d'être mis œuvre. Cela remet ainsi en cause la validité des résultats obtenus par cette méthode. Etant donné le faible nombre d'études de mesures anti-ICU, aucune autre méthode d'analyse ne nous est connue.

Une autre limite importante à la portée des effets rapportés concernent leur validité pour les villes denses européennes. En effet, la plupart des travaux ont été réalisés dans des villes peu denses au Japon, dans des régions aux étés chauds et humides. Nagaoka City par exemple a une densité de 300 personnes/km^2, soit nettement moins que les 21 000 personnes/km^2 de Paris. Par ailleurs, si l'on s'intéresse à l'ensoleillement lorsqu'il est mesuré Kinouchi and Kanda (1997, 1998); Kubo et al. (2006); Nakayama and Fujita (2010); Li et al. (2013), on se rend compte que cela vaut aussi pour les effets thermiques, principalement étudiés dans des zones très faiblement masquées.

Enfin, les efforts d'optimisation des méthodes d'arrosage mises en œuvre sont insuffisants. Une démarche d'optimisation doit être décrite formellement avec une définition claire de ses objectifs, ce qui n'est pas le cas dans les rares études qui s'intéressent à ce problème.

Table 1 – Résumé de l'état de l'art.

		Indicateurs microclimatiques					Indicateurs thermiques			
Auteur	Type	T_a	HR	T_{mrt}/T_g	ICU	Confort thermique	T_{surf}	$T_{pavement}$	lE	V
Kinouchi and Kanda (1997)	exp.	×	×	×		×		×	×	×
Kinouchi and Kanda (1998)	exp.						×	×	×	×
Yamagata et al. (2008)	exp.	×				×	×		×	
Takahashi et al. (2010)	exp.	×								
Nakayama and Fujita (2010)	exp.						×			
Li et al. (2013)	exp.							×		
Bouvier et al. (2013)	exp.	×	×				×			
Maillard et al. (2014)	exp.					×	×			
Kubo et al. (2006)	num.	×								
Nakayama et al. (2012)	num.	×							×	
Météo France and CSTB (2012)	num.	×	×		×				×	
Wei and He (2013)	num.			×	×		×			

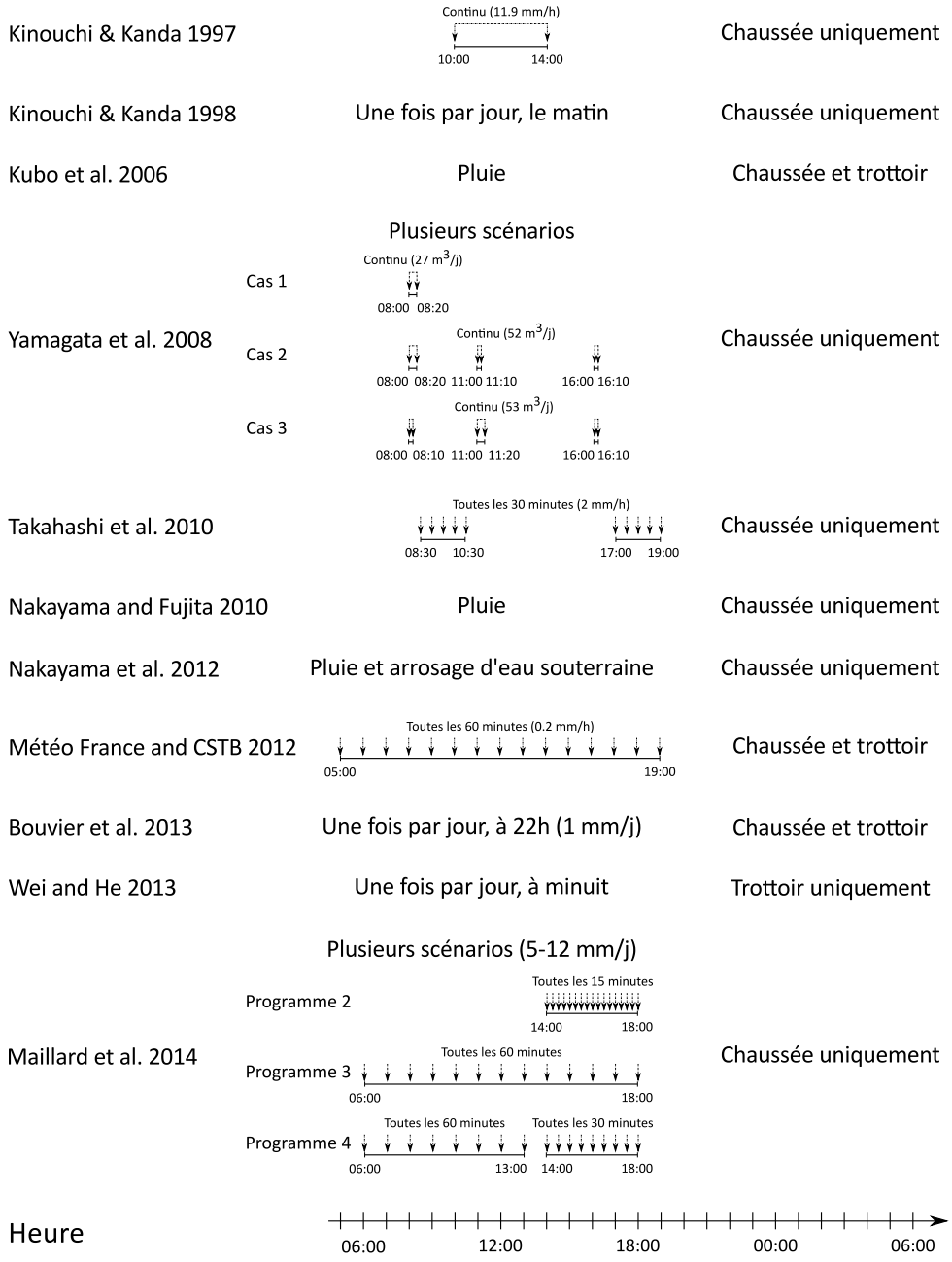

Figure 1 – Diagram of the watering methods used in the surveyed articles.

Connaissances manquantes et questions de recherche

Les connaissances manquantes identifiées au cours de notre état de l'art nous mènent à formuler les questions de recherche suivantes appliquées aux villes denses telles que Paris par temps caniculaire :

- La méthode de comparaison deux-à-deux peut-elle fiablement évaluer les effets des mesures anti-ICU sur le terrain ?
- Quels sont les effets microclimatiques de l'arosage urbain ?
- Quels sont ses effets dans la lutte contre les ICU ?
- Qu'en est-il des effets thermiques de l'arrosage ?
- Enfin, quelle est la consommation d'eau de l'arrosage urbain et comment peut-on l'améliorer ?

Nous chercherons par la suite à y répondre. Les résultats obtenus devraient permettre d'informer les décideurs sur les coûts et bénéfices de l'arrosage urbain pour les villes denses en période caniculaire. Ces informations sont essentielles pour les villes qui envisagent d'inclure l'arrosage urbain dans leur stratégie de réduction des ICU et/ou d'adaptation au changement climatique.

Méthode expérimentale

Une expérimentation de terrain a été effectuée à Paris pendant les étés 2013 et 2014 sur deux sites : Belleville et Louvre. Un plan de chaque site est fourni à la Figure 2. Les deux rue ont un ratio d'aspect $H/W = 1$, Louvre ayant une orientation approximativement N-S et Belleville une orientation E-W.

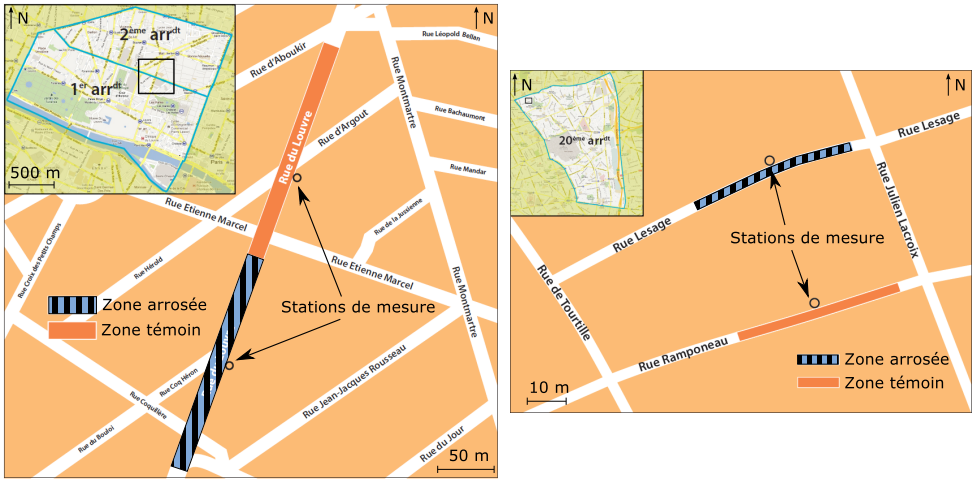

Figure 2 – Plan des stations des sites de Louvre (gauche) et de Belleville (droite).

Chaque site est équipé de deux stations, l'une arrosée et l'autre servant de témoin. La conception et l'instrumentation des stations utilisées sont identiques pour tous les sites. Seules les stations rue du Louvre sont équipées d'un capteur de chaussée mesurant température et flux de chaleur à 5 cm de profondeur et d'une

caméra thermique mesurant la température de surface, placée en toiture-terrasse au-dessus de la station arrosée.

Les instruments positionnés à hauteur d'homme sont protégés par une cage de mesure cylindrique d'un mètre de diamètre. Leur hauteur est de 2 m rue du Louvre et de 3 m à Belleville. La Figure 3 présente un schéma des stations utilisées rue du Louvre.

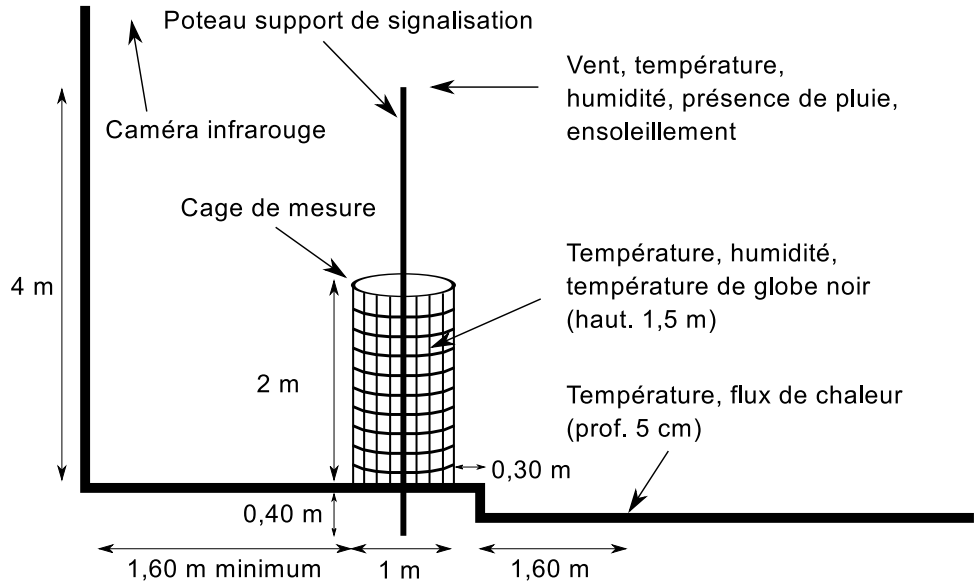

Figure 3 – Schéma et instrumentation des stations météorologiques (rue du Louvre).

Toute la largeur de la rue du Louvre a été arrosée de 6h30 à 11h30 puis de 14h à 18h30, tandis que seul un tiers du site arrosé à Belleville était arrosé en continu de 7h à 19h. La Figure 4 détaille graphiquement la méthode d'arrosage utilisée pour chaque site. L'arrosage est déclenché si certaines conditions météorologiques sont réunies, décrites dans la Table 2.

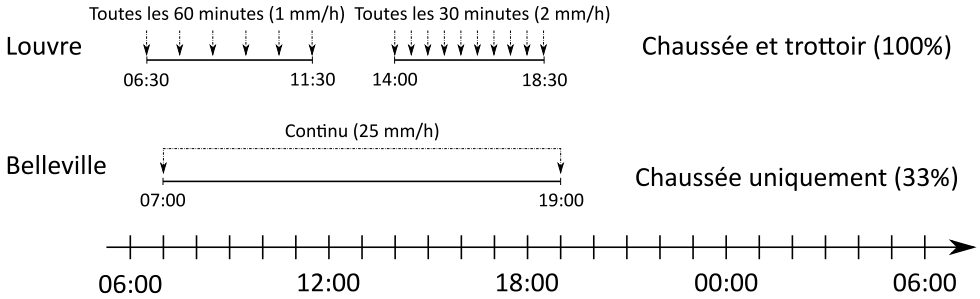

Figure 4 – Méthode d'arrosage pour Louvre et Belleville.

Table 2 – Conditions météorologiques nécessaires pour le déclenchement de l'arrosage urbain et conditions caniculaires pour Paris.

Paramètre	Déclenchement d'arrosage	Niveau d'alerte canicule
Température minimale	$BMI_{Min} \geq 16$°C	≥ 21°C
Température maximale	$BMI_{Max} \geq 25$°C	≥ 31°C
Vitesse du vent	≤ 10 km/h	-
Ciel	Clair (couverture inférieure à 3 octas)	-

Les mesures collectées par ces stations sont utilisées par la suite pour déterminer les effets microclimatiques et thermiques de l'arrosage. Ces derniers sont ensuite analysés pour améliorer la méthode d'arrosage employée.

Effets microclimatiques

Comme indiqué dans l'état de l'art, la littérature scientifique s'appuie sur des comparaisons directes entre stations expérimentales et témoins pour quantifier les effets de mesures anti-ICU en milieu urbain. Cette approche s'appuie sur l'hypothèse que les deux sites ont un comportement identique à l'état initial, les différences observées étant donc le fait de la mesure anti-ICU étudiée.

Pourtant, les mesures microclimatiques effectuées en continu montrent aussi bien pour Louvre que pour Belleville que cette hypothèse n'est pas valable. Non seulement la différence entre les sites n'est ni nulle ni constante, mais elle fait preuve d'une forte variabilité d'un jour à l'autre, même parmi des journées de Classe de Stabilité A ou A-B selon l'échelle de Pasquill (vent faible, ciel clair ou faiblement ennuagé), appelés jours de référence par la suite. Les différences observées entre stations observées après mise en œuvre ne peuvent donc pas être attribuées aux effets de la mesure anti-ICU étudiée, du moins dans les milieux urbains denses.

En réponse à cette difficulté, une méthode alternative a été développée et testée avec l'exemple de l'arrosage urbain. Elle consiste en un test de Student sur deux échantillons, à savoir les différences entre stations mesurées les jours arrosés et les jours de référence. Ce test permet de déterminer si la différence entre ces deux échantillons est signficative ou non d'un point de vue statistique. Cette méthode a été appliquée avec succès aux données issues des stations minutieusement appariées d'un même site, mais elle a également fonctionné en croisant les stations arrosées et témoins entre sites différents, pourtant distantes de plusieurs kilomètres et présentant des environnements urbains et orientations de rue différents.

L'humidité relative, suivie des températures moyenne de rayonnement, de l'air et équivalente-UTCI ont été les paramètres les plus affectés par l'arrosage de

manière statistiquement significative. Par ailleurs, les effets significatifs ont principalement eu lieu la nuit pour les températures moyenne de rayonnement, de l'air et équivalente-UTCI, mais principalement en journée pour l'humidité relative. Cependant, les effets maximaux de tous les paramètres ont été atteints en journée vers 18h lorsque les conditions sont les plus chaudes et les plus sèches. La température a ainsi été réduite jusqu'à 0,79°C et 0,57°C pour l'air à 1,5 et 4 m de hauteur respectivement, de 1,67°C pour la température moyenne de rayonnement et de 1,03°C pour la température équivalente-UTCI. L'augmentation maximale d'humidité relative s'est élevée à 4,1 % et 2,8 % à 1,5 et 4 m de hauteur.

Les effets moyennés sur 24 heures ont également été considérés et se sont montrés être statistiquement significatifs pour la rue du Louvre arrosée à 100 %, mais pas pour Belleville où seulement un tiers de la rue était arrosée. Les effets moyens à Louvre ont atteint -0,25°C et -0,14°C pour la température de l'air à 1,5 et 4 m de hauteur, $+1{,}5$ % et $+0{,}9$ % d'humidité relative à 1,5 et 4 m de hauteur, -0,40°C pour la température moyenne de rayonnement et -0,29°C pour la température équivalente-UTCI. Des effets anti-ICU ont également été observés avec une réduction moyenne des températures de l'air à 1,5 et 4 m de hauteur entre 3h et 6h du matin. Ces effets sont compris entre -0,09°C et -0,22°C.

Ces résultats montrent ainsi que l'arrosage urbain permet de réduire efficacement le stress thermique des piétons, avec des effets maximaux atteints au moment le plus chaud de la journée. Par ailleurs, des effets moyens significatifs ont été observés entre 3h et 6h du matin, témoignant d'effets anti-ICU. Les meilleurs résultats ont été atteints pour Louvre où 100 % de la largeur était arrosée à intervalles réguliers, tandis que les résultats étaient moins bons pour Belleville où 33 % de la rue étaient arrosés en continu.

La méthode d'analyse développée a été utilisée pour quantifier les effets de l'arrosage urbain. Cette mesure anti-ICU a l'avantage sur d'autres d'être immédiatement réversible. En effet, dès que l'arrosage s'arrête, les sites d'étude retournent à leur état initial (sec). D'une part, cela a grandement facilité le constat que la différence entre les stations appariées n'était pas nulle en l'absence d'arrosage. Si les mesures avaient démarrées qu'après la mise en place d'une mesure anti-ICU permanente, cette information aurait pu être entièrement négligée par notre analyse. D'autre part, cela nous a permis de construire une série de référence sans arrosage et une série expérimentale avec arrosage que nous avons comparées avec le test de Student à deux échantillons.

Dans le cas de mesures anti-ICU plus permanentes, il n'est plus possible d'enregistrer des données de référence après leur mise en œuvre. Il est donc nécessaire de caractériser les sites expérimentaux suffisamment en avance pour construire la série de référence. Ces données sont essentielles pour effectuer l'analyse avec la méthode développée et doivent fournir une image suffisamment représentative des conditions initiales des sites. Etant donnée la forte variabilité des conditions météorologiques, il est difficile d'estimer la durée de cette période de référence qui dépendra des conditions ciblées. Nous estimons que celle-ci peut durer de plusieurs semaines à quelques années. Dans notre cas, notre intérêt portait sur

les canicules. Alors que l'été 2013 suffisait pour effectuer notre analyse avec une certaine robustesse, ce n'était pas le cas de l'été 2014 avec ses deux journées arrosées et cinq journées de référence seulement.

La durée d'étude constitue une des limites de notre méthode d'analyse. L'exploitation de longues séries de données s'étalant sur plusieurs mois ou années implique que la seule modification pendant cette période est la mise en œuvre de la mesure anti-ICU étudiée. Pourtant, les zones urbaines sont en perpétuel changement et les conditions "initiales" déterminées à un moment donné peuvent rapidement devenir obsolètes. Cela rajoute une contrainte supplémentaire lors du choix du site qui ne doit pas être profondément modifié pendant la durée totale de l'étude.

Heureusement, notre analyse a montré que les critères de sélection de site pouvaient être assouplis pour inclure des paires de stations dont la configuration urbaine n'est pas aussi semblable que celles retenues ici. Cette flexibilité supplémentaire est obtenue au prix d'une perte en précision, c'est-à-dire d'intervalles de confiance plus importants. Pour limiter ce phénomène, il est conseillé de limiter le plus possible la distance ainsi que les différences d'ensoleillement entre les stations témoins et expérimentales.

La robustesse de nos résultats sur les effets de l'arrosage urbain s'accroîtra au fur et à mesure que de nouvelles données seront enregistrées. Des pistes d'amélioration possibles concernent l'usage d'instrument de haute précision calibrés les uns à par rapport aux autres régulièrement en chambre climatique de laboratoire ainsi que l'utilisation d'abri météorologique à convection forcée pour limiter l'influence de l'ensoleillement direct sur les mesures de température et d'humidité de l'air. Par ailleurs, l'impact sur la qualité des mesures de la cage de protection contre le vandalisme devrait être quantifier plus précisément.

L'application de notre méthode à d'autres sites et à d'autres mesures anti-ICU donneront également lieu à des retours d'expérience intéressants sur sa pertinence et sa faisabilité sur le terrain. Malheureusement, étant donnée la durée d'étude nécessaire, ces retours seront longs à obtenir.

Enfin, il se peut que d'autres outils et approches soient pertinents voire plus adaptés pour l'étude de mesures anti-ICU. Il s'agit par exemple d'utiliser un réseau de stations témoins réparties sur un certain espace pour compenser l'utilisation de stations mal appariées, des outils d'analyse financiers pour désaisonaliser les données ou encore des outils d'extraction de données et d'apprentissage automatique (réseaux neuronaux par exemple).

Ayant étudié les effets microclimatiques de l'arrosage urbain, nous nous intéressons à présent à ses effets thermiques.

Effets thermiques

Pour déterminer les effets thermiques de l'arrosage les mesures de température de surface ainsi que de flux et de température dans la chaussée à 5 cm de profondeur enregistrées rue du Louvre pendant l'été 2013 ont été étudiées.

Premièrement, il a été trouvé que le flux de chaleur à 5 cm de profondeur dans la chaussée était divisé par deux par l'arrosage urbain, réduit de jusqu'à 50 et 150 W/m^2 le matin et l'après-midi, respectivement. La restitution de chaleur pendant la nuit suivant l'arrosage est également réduite.

Deuxièmement, il a été montré que les températures de surface sont réduites de plusieurs degrés, à la fois pendant l'arrosage et jusqu'à plusieurs heures après sa fin. Le matin, les températures sont réduites de jusqu'à 4°C et l'après-midi de 13°C en moyenne. Il a été constaté que les effets sur la chaussée sont plus importants que sur le trottoir.

Troisièmement, la température à 5 cm de profondeur est réduite de 5,9°C l'après-midi. Les températures minimales du matin, atteintes vers 8h les journées de référence, sont maintenues pendant plusieurs heures jusqu'à l'ensoleillement direct de la chaussée les jours arrosés et sont réduites de 2,3°C compte tenu des températures observées à 6h. Par ailleurs, l'amplitude min-max de la température est divisée par deux par l'arrosage.

Des pics de flux de chaleur et de température de surface sont visibles les jours arrosés et témoignent du séchage de la chaussée. Aucun pic n'a été observé pour les températures mesurées à 5 cm de profondeur.

Ces observations sont en accord entre elles et avec la littérature. Nos résultats confirment que l'arrosage atténue les phénomènes physiques responsables du stress thermique des piétons et de la formation des ICU. En effet, l'absorption et le stockage de chaleur par la chaussée sont sensiblement réduits par l'arrosage qui réintroduit artificiellement de l'évapotranspiration dans le milieu urbain. Cela a été montré par les mesures de flux et de température dans la chaussée. Cela entraîne une réduction de la chaleur restituée la nuit longtemps après la fin de l'arrosage. Par ailleurs, l'absorption plus faible de chaleur entraîne une réduction de la température de surface jour et nuit ce qui a deux conséquences positives.

La première est la réduction de l'échauffement par convection de l'atmosphère par la chaussée. Puisque ce transfert de chaleur sensible dépend directement de la température de surface, celui-ci est réduit voire inversé dans les zones arrosées. Ainsi, plus les zones arrosées sont étendues, plus le rafraîchissement obtenu sera important. Cela est confirmé par la comparaison du rafraîchissement observé pour Louvre par rapport à celui de Belleville.

La deuxième conséquence de températures de surface plus faibles est la réduction du rayonnement grande longueur d'onde (GLO) issu de la chaussée, allégeant ainsi le bilan radiatif des piétons. Par ailleurs, alors que l'utilisation de matériaux réfléchissants entraîne une augmentation du flux CLO réfléchi vers les piétons, l'arrosage urbain le réduit. En effet, le mouillage de la chaussée en réduit la réflectivité, venant renforcé l'effet positif de la réduction du rayonnement GLO. Ces effets combinés réduisent ainsi la radiosité totale des surfaces arrosées. Le bilan radiatif des piétons est donc amélioré à la fois au soleil et à l'ombre. Les observations précédentes de la température moyenne de rayonnement en témoignent.

En revanche, l'augmentation de l'humidité entraînée par l'évaporation du film d'eau arrosé a tendance à accentuer le stress thermique des piétons. Cependant,

vu que l'arrosage a vocation à être mis en œuvre par temps particulièrement sec (humidité relative inférieure à 50 %), cette augmentation pourrait être négligeable du point de vue du confort thermique, ce qui est confirmé par nos observations microclimatiques précédentes. Cet effet négatif n'est donc pas d'ampleur suffisante pour compenser les autres effets positifs de l'arrosage.

Ces résultats et analyses nous confèrent une meilleure compréhension des mécanismes mis en jeu par l'arrosage urbain et qui expliquent les observations microclimatiques effectuées à la partie précédente. Les données et tendances discutées ici peuvent être utiles pour la validation d'études numériques ou expérimentales à différentes échelles (cf. Annexes A, B, C). Afin de pouvoir proposer des améliorations pour la méthode d'arrosage, nous nous intéressons à présent aux coûts de l'arrosage urbain. Nous chercherons à les minimiser tout en maximisant ses effets positifs.

Avec ce but en tête, on s'intéresse à présent aux pics de flux et de température de surface observés afin d'affiner la durée et la fréquence d'arrosage. Par ailleurs, le devenir des volumes arrosés sera également étudié et des propositions seront formulées pour réduire la consommation d'eau sans trop impacter le rafraîchissement final.

Amélioration de la consommation d'eau de l'arrosage urbain

Les effets thermiques de l'arrosage identifiés précédemment sont utilisés pour améliorer la méthode d'arrosage et sa consommation d'eau. On s'appuie donc sur les mesures réalisées rue du Louvre.

L'analyse montre que le protocole d'arrosage de la chaussée devrait chercher à déposer 0,16-0,20 mm/cycle (soit la capacité de rétention du revêtement) à la fréquence la plus faible possible pour empêcher le séchage de la surface. L'après-midi, un arrosage toutes les 30 minutes est recommandé jusqu'à la fin de l'ensoleillement, mais n'est pas suffisant pour le trottoir asphalte qui nécessite une fréquence d'un arrosage toutes les 10-20 minutes. Le matin, l'arrosage de 0,16-0,20 mm d'eau toutes les heures est suffisant, mais cette fréquence pourrait être réduite de 50 % comme l'indiquent les pics de flux et de température de surface observés 2h-2h30 après la fin de l'arrosage le soir. Enfin, la période d'arrosage devrait être prolongée pour inclure les quelques minutes précédants le début de l'ensoleillement de la rue, alors que l'arrosage du matin pourrait être décalé jusqu'à 9h30 environ.

De manière générale, la méthode d'arrosage la plus rentable vise à aligner son débit moyen d'arrosage sur le débit évaporé. Ayant ainsi fixé le débit arrosé, c'est la capacité de rétention d'eau de la surface ciblée qui détermine la fréquence d'arrosage adéquate. Bien entendu, la vitesse d'évaporation d'eau dépendra de la surface ciblée et dépend donc de certaines de ses propriétés.

Des essais ont été réalisés pendant l'été 2014 afin de confirmer ces recommandations, bien que le volume déposé par les laveuses n'ait pas pu être réduit à moins de 0,5 mm/cycle. Malheureusement, les mesures du capteur de chaussée se sont révélées être très différentes de celles de l'été 2013 pour des conditions météorologiques très similaires. Le capteur a donc été considéré comme étant tombé en panne. La cause soupçonnée de cette panne est le fluage de l'enrobé à froid utilisé lors de sa pose. Par ailleurs, seuls deux journées ont été arrosées pendant l'été 2014, pendant lesquels la caméra thermique posée en toiture a elle aussi connu une panne d'alimentation électrique. Il n'a donc pas été possible de déterminer l'impact de la réduction du débit arrosé rue du Louvre pendant cette campagne. Une nouvelle campagne est prévue pendant l'été 2015, malheureusement elle ne s'achèvera pas avant la fin de la rédaction du présent manuscrit.

Afin de réduire la fréquence d'arrosage et donc limiter les désagréments associés à la méthode d'arrosage et la simplifier, il faudrait augmenter la capacité de rétention d'eau de la chaussée. En effet, si celle-ci atteignait seulement 1 mm d'eau, l'arrosage de 1 mm/cycle serait nécessaire seulement une fois toutes les 2h30-3h pendant l'ensoleillement.

Toutefois, les rues parisiennes sont actuellement conçues pour retenir le moins d'eau possible. Une nouvelle conception serait donc nécessaire afin d'atteindre cet objectif. Une alternative envisageable consisterait à utiliser des matériaux perméables à rétention d'eau. Ces derniers devraient retenir l'eau à leur surface ou à très faible profondeur afin de ne pas gêner l'évaporation de l'eau retenue, grâce à des matériaux à forte capillarité par exemple. Cette solution limiterait la formation de flaques d'eau et éviterait donc les problèmes que cela pose pour la circulation et les piétons.

Ce type de matériau permettrait de déposer de plus grandes quantités d'eau par arrosage sans ruissellement grâce à sa capacité de rétention accrue et limiterait donc la fréquence d'arrosage nécessaire. Cette nouvelle conception de rue pourrait également permettre des économies d'eau supplémentaires si elle est en mesure de retenir l'eau apportée par les orages estivaux ou encore l'eau déjà mobilisée pour le nettoyage des rues. De plus, elle participerait à limiter le ruissellement par temps pluvieux, permettant ainsi de limiter les déversements au milieu naturel, objectif mis en avant par le Zonage Pluvial de la Ville de Paris et la Loi Cadre sur l'Eau de l'Union Européenne.

Quels que soient les résultats de la campagne 2015, notre analyse nous permet de faire une première estimation de la consommation d'eau nécessaire pour arroser une rue parisienne au mois de juillet. Effectué de 9h30 à 18h30, l'arrosage optimisé, c'est-à-dire moins de 0,20 mm/cycle toutes les deux heures avant 13h30 et toutes les 30 minutes après, consommerait moins de 2,2 mm/j.

Généralisé à l'ensemble des 2 550 ha de rues parisiennes, cela reviendrait à 56 100 m^3/j ou 25 L par jour et par habitant, soit un peu mois d'une demi-douche. Ce volume représente moins de 30 % de la production actuelle d'eau non potable à Paris et est largement compatible avec les capacités de production existantes (de l'ordre de 500 000 m^3/j). On peut comparer cet ordre de grandeur à celui

de l'évapotranspiration potentielle observée à Paris en été, représentative de la consommation d'eau d'un gazon. En juillet, celle-ci atteint souvent 7-8 mm/j et jusqu'à 9 mm/j par temps caniculaire, soit plus de trois plus d'eau que pour l'arrosage urbain. Etant donné la crédibilité attribuée à la végétalisation pour lutter contre les ICU, la consommation d'eau de l'arrosage urbain est jugée suffisamment raisonnable pour que l'arrosage soit considéré comme une technique viable pour Paris. Ceci est renforcé par les opportunités offertes par le réseau d'eau non potable et la diversification de son approvisionnement, mais dépendra également de l'évolution des ressources hydriques de la région au cours des prochaines décennies.

Etant donné que les rues dans une même ville ont généralement des configurations ou utilisent des matériaux différents, les conclusions tirées de nos deux sites ne peuvent pas être généralisées à la ville entière. En effet, le débit évaporé sur une surface arrosée dépendra notamment des propriétés de ses matériaux de surface. Il est donc recommandé d'étudier plusieurs sites caractéristiques avant de mettre au point une stratégie d'arrosage étendue à une ville entière. Cependant, l'utilisation d'un capteur de chaussée couplé à des mesures du rayonnement solaire sur de longues périodes est coûteuse et compliquée et nécessite une bonne coordination avec les services municipaux concernés. Il est donc difficile d'installer un grand nombre de ces capteurs en milieu urbain dense. Heureusement, il a été montré que des mesures de la température de surface à l'aide d'une caméra thermique est une alternative intéressante. Combinée avec une mesure indépendante de la capacité de rétention des surfaces arrosées, la consommation d'eau et la fréquence d'arrosage optimales peuvent être déterminées simultanément.

Les pyromètres, qui mesurent la température en un point fixe et sont bien moins coûteux, pourraient également être utilisés, mais contrairement aux caméras infrarouges ils ne peuvent pas faire de mesure sur plusieurs zones en même temps. Etant donné leur prix plus faible, il pourrait quand même être plus intéressant d'en utiliser plusieurs pour compenser ce désavantage. Les caméras thermiques et les pyromètres sont particulièrement adaptés au milieu urbain vu la simplicité de leur pose comparée à celle des capteurs de chaussée. Les lampadaires urbains sont de bons candidats pour leur alimentation électrique, mais de nombreux points lumineux parisiens sont posés en console sur façade d'immeuble et ne peuvent généralement pas accueillir de poids supplémentaire. Par ailleurs, afin de tenir compte des piétons et véhicules qui peuvent entrée dans la ligne de mesure de ces appareils, il est recommandé d'inclure une webcam synchronisée. Enfin, comme c'était le cas pour notre site d'étude, de nombreuses pollutions thermiques sont présentes en milieu urbain et doivent être clairement identifiées avant de choisir les zones à surveiller afin d'éviter de fausses interprétations. L'imagerie thermique peut être d'une grande aide à cet égard.

Au-delà de la configuration des rues, l'impact des matériaux ne devrait pas être négligé. En effet, les surfaces sombres ne réagiront pas de la même façon qu'une surface claire à l'arrosage, ni des matériaux de texture différentes qui pourraient avoir des capacités de rétention différentes. De nombreux matériaux

sont actuellement mis en œuvre dans l'espace public parisien, dont des dalles de granite, des pavés de granite ou de grès, des chaussées en enrobé bitumineux ou des trottoirs en asphalte. La diversité des revêtements urbains rend très difficile la conception d'une stratégie d'arrosage de la ville si elle doit s'appuyer sur des études de terrain.

Une solution possible consiste à étudier le comportement thermique de ces revêtements en laboratoire. Le dispositif nécessaire doit pouvoir soumettre les échantillons à un même cycle climatique, permettant des comparaisons de comportement plus précises que sur le terrain. Par ailleurs, les conditions de laboratoire permettent d'instrumenter les échantillons à plusieurs profondeur facilement, donnant accès à des informations plus vastes que sur le terrain.

Une expérimentation de ce type a été mise en place et a permis de comparer le comportement thermique de cinq revêtements parisiens sans arrosage. Des échantillons de chaussée et trottoir classiques, de stabilisé, de trottoir dalle granite et de gazon ont ainsi été comparés. Bien que d'autres essais complémentaires soient nécessaires, des résultats préliminaires ont été communiqués dans le cadre de trois conférences. Les articles correspondant (un en anglais) se trouvent aux Annexes A, B et C.

Conclusions et perspectives

Des éléments de réponses ont donc été apportés aux questions de recherches définies. En effet notre recherche apporte une meilleure connaissance de ses effets rafraîchissants, à la fois microclimatiques et thermiques, de l'arrosage. De plus, sa consommation d'eau a été étudiée et des propositions pour l'améliorer davantage ont été formulées. Ces informations permettront d'éclairer le choix des villes qui envisagent de faire appel à l'arrosage urbain pour leur stratégie de rafraîchissement et d'adaptation au changement climatique, notamment pour les quartiers les plus denses et minéraux. Cependant, d'autres aspects qui mériteraient investigation à leur tour ont également pu être identifiés au cours de ce travail.

La méthode d'analyse statistique développée à la Partie 1 soulève un certain nombre de questions concernant ses limites et sa fiabilité. D'autres interrogations concernent la méthode expérimentale utilisée pour estimer les effets microclimatiques de l'arrosage. Ces nouvelles questions sont les suivantes :

- Quel serait le bénéfice d'abris à convection forcée pour réduire le bruit de fond des mesures de la température et de l'humidité de l'air, notamment pour des sites témoin et expérimental éloignés ?
- Quel est l'impact de la cage de mesure ?
- Quelle est la faisabilité de notre méthode d'analyse statistique lorsqu'elle est utilisée avec d'autres techniques plus permanentes de lutte contre les ICU ?

- Quelles améliorations pourraient apporter d'autres outils d'analyse statistiques, issus de l'analyse des séries temporelles par exemple ?

L'usage d'un abri à convection forcée pour les thermo-hygromètres vise à réduire le bruit observé pendant les périodes d'ensoleillement direct. En effet, les différences d'ensoleillement d'un site à un autre peuvent avoir un impact sur les mesures qui brouilleraient le signal de rafraîchissement créé par l'arrosage. Le potentiel pour les abris ventilés d'améliorer cette situation devrait donc être étudié.

Par ailleurs, une cage de mesure a été utilisée pour protéger les instruments de mesure positionnés à hauteur d'homme. Ce dispositif est essentiel pour des stations de mesure installées en milieu urbain pendant de longues périodes. Cependant, bien qu'elle ait été conçue pour minimiser leur impact sur les mesures effectuées en leur sein, elle crée inévitablement de l'ombrage. L'importance de cet impact et d'éventuelles corrections permettant d'en tenir compte devraient être étudiées afin que ces cages puissent être utilisées pour d'autres études de long terme en milieu urbain. L'impact des cages sur des mesures de vent effectuées en leur sein devrait notamment être inclus dans cette analyse et comparé avec les mêmes mesures réalisées hors de la cage, à 4 m de hauteur.

Les difficultés potentielles liées à l'application de la méthode d'analyse développée à d'autres méthodes d'atténuation des ICU ont été décrites. Etant donné que la période de référence doit être étudiée suffisamment longtemps pour être comparée avec la période expérimentale, les campagnes de mesure peuvent durer quelques années. La faisabilité de la méthode doit donc être évaluée, surtout compte tenu des remodelages permanents que connaissent les villes. D'autres études utilisant notre méthode devraient apporter des retours d'expérience intéressants mais qui seront longs à obtenir.

En attendant, d'autres méthodes devraient être envisagées. Etant donné la périodicité quotidienne des paramètres météorologiques, l'analyse des séries temporelles pourrait apporter des outils pertinents, notamment pour décomposer les séries étudiées en leurs composantes de tendance, saisonnière et résiduelle. L'étude de ces composantes pourrait apporter d'autres informations sur les effets rafraîchissants des méthodes étudiées. D'autres outils issus des domaines de l'extraction de données ou de l'apprentissage automatique pourraient également s'avérer utiles.

Par ailleurs, bien que les effets microclimatiques de l'arrosage urbain ont pu être quantifiés pour deux sites parisiens, plusieurs autres éléments doivent être déterminés avant qu'une stratégie d'arrosage municipale puisse être définie :

- Quels effets cumulés peuvent être obtenus grâce à un arrosage de plus grande échelle (quartier, ville, ...) ?
- Quel est l'impact de l'orientation de la rue sur les performances de l'arrosage ?
- Qu'en est-il du ratio d'aspect de la rue ?

- Comment réagissent d'autres matériaux à l'arrosage ?
- Quelles propriétés des matériaux influencent l'efficacité de l'arrosage ?

La première question rend compte du fait que les effets déterminés ici ont été obtenu pour des sites arrosés isolés. A priori, un arrosage plus étendu devrait avoir un impact plus important. Aucune étude qui nous est connue n'a cherché à quantifier les effets cumulés qui peuvent ainsi être obtenus.

Les deux questions suivantes correspondent à un manque de connaissance identifié dans notre recherche sur l'impact de la morphologie urbaine. Bien que des sites d'orientation différente aient été étudiés, les différences de méthode d'arrosage étaient trop importantes pour isoler leur impact. Cela vaut également pour le ratio d'aspect. Etant donnée la diversité des orientations et formes de rue dans une ville donnée, il est essentiel de quantifier l'influence de ces paramètres sur l'efficacité de l'arrosage urbain. Vu le rôle important de l'ensoleillement sur les effets thermiques observés rue du Louvre, il se peut que l'influence de ces paramètres morphologiques se limite à leur impact sur les conditions d'ensoleillement du sol.

Pareillement, notre expérimentation n'a pas permis d'étudier l'influence des matériaux malgré les différences entre les sites de Louvre et de Belleville. Parmi les propriétés des matériaux, l'impact de la capacité de rétention d'eau de la surface arrosée a déjà été identifié. Vue la grande diversité des matériaux utilisés à Paris et ailleurs, cet aspect a une grande importance. Comprendre leur influence et quelles propriétés en sont responsables permettrait de mieux cibler les stratégies d'arrosage ainsi que de concevoir des rues plus performantes d'un point de vue climatique. Ce dernier aspect présente des synergies intéressantes avec les objectifs de gestion alternative des eaux pluviales à Paris si la capacité de rétention d'eau est augmentée.

Comme indiqué, nous avons commencé la conception d'une expérimentation de laboratoire pour étudié le rôle des matériaux. A l'heure actuelle, des essais préliminaires ont été réalisés et les résultats sont satisfaisants au regard des observations de terrain décrites auparavant. Ces résultats initiaux donnent une première impression des performances thermo-climatiques de cinq revêtements parisiens. D'autres essais avec arrosage devraient nous permettre de déterminer son efficacité sur ces structures de revêtement et de proposer des modifications et des compositions nouvelles plus adaptées à l'amélioration du climat urbain. Les nouvelles structures pourraient permettre des économies d'eau importantes en stockant l'eau de pluie ou de nettoyage déjà utilisée et qui ruisselle actuellement à l'égout. Ce travail est réalisé en partenariat avec la Direction de la Voirie et des Déplacements (DVD) de la Ville de Paris et l'Atelier Parisien d'Urbanisme (APUR).

Enfin, notre recherche n'a pas pris en compte les impacts de l'arrosage autres que ses effets rafraîchissants ou sa consommation d'eau.

Parmi ceux-ci, nous avons parlé des améliorations de la qualité de l'air en introduction. Les particules fines sont une des principales causes de la pollution de l'air

à Paris. Le nettoyage de rues est soupçonné réduire la remise en suspension des particules fines par lessivage et a déjà été étudié par certains auteurs. L'arrosage urbain pourrait également lessiver les particules déposées au sol et donc participer à une amélioration de la qualité de l'air. Par ailleurs, la pollution à l'ozone est en augmentation à Paris et dans d'autres villes et pourrait également être réduite par l'arrosage urbain. En effet, cette pollution est fortement thermosensible et pourrait donc bénéficier du rafraîchissement provoqué par l'arrosage urbain. Ces effets potentiels de l'arrosage urbain n'ont pas encore été étudiés par la littérature scientifique.

Par ailleurs, les coûts financiers et environnementaux de l'arrosage devraient également être quantifiés avant que les villes ne puissent l'inclure dans leur stratégie d'atténuation des ICU et d'adaptation au changement climatique. Ces analyses doivent tenir compte des retombées négatives et positives de l'arrosage, par exemple les bénéfices tirés d'économies d'énergie de climatisation sont à comparer à l'énergie nécessaire à l'arrosage et son prix. L'estimation de ces paramètres implique toutefois qu'une méthode d'arrosage et une infrastructure à l'échelle de la ville soient déjà connues ou proposées. Etant donné le niveau de développement de l'arrosage urbain et des autres méthodes d'atténuation, il serait prématuré d'étudier ces paramètres dès à présent.